Jorge Lawrence Marquez
Jorge.marquez1204@gmail.com

EDUCATION:

Ph.D. Pharmaceutical Sciences Fall 2023

University of Maryland Baltimore

Bachelor of Science Molecular Biology, Biochemistry, and Bioinformatics

Minor in Chemistry Spring 2013

Towson University, Towson, MD

RESEARCH EXPERIENCE

Graduate Research Assistant **2017-2023**

Advisor: Dr. Ginette Serrero, A&G Pharmaceutical, Columbia, MD

Dr. Maureen Kane, University of Maryland Baltimore, Pharmaceutical Sciences

***Dissertation Topic*: PTGFRN as a Target for Antibody-Drug Conjugate (ADC) Development in Mesothelioma and Medulloblastoma**

Mesothelioma and Pediatric Medulloblastoma are two cancers that the NIH classify as rare and aggressive cancers, and which currently do not have any specialized or tailored therapies available for treatment. We have found that both cancers also express elevated levels of a cell-surface protein called Prostaglandin F2 Receptor Negative, or PTGFRN. This protein's expression level has previously been linked to a more aggressive, metastatic-like phenotype in cancers. Here, we attempt to further characterize PTGFRN's effect on cancer cell lines derived from epidermoid carcinoma (A431), mesothelioma (MSTO-211H), and pediatric medulloblastoma (DAOY). From the results of these experiments, we posit a potential mechanism by which PTGFRN expression is contributing to a more aggressive, metastatic-like phenotype after our discovery of a previously unreported binding partner of PTGFRN. In addition to this, we have developed a PTGFRN-specific human monoclonal antibody whose binding induces endocytosis of PTGFRN to the cell interior. Using this capability, we develop a potent Antibody-Drug Conjugate (ADC) by conjugating our antibody to the cytotoxic compound Duocarmycin with a cleavable valine-citrulline linker. The resultant ADC shows high potency against the PTGFRN-positive cell lines *in vitro*, as well as in *in vivo* models with tumor-bearing mice, whereas the ADC shows no activity in a PTGFRN-negative cancer cell line. These results highlight the importance of PTGFRN in cancer progression, as well as provide a new potential drug target for ADC development for use treating mesothelioma and pediatric medulloblastoma.

- Characterize PTGFRN's effect on cancer using functional *in vitro* assays

- Generation and screening of anti-PTGFRN monoclonal human antibodies for specific, internalizing antibodies
- Generation of a potent Antibody-Drug Conjugate (ADC) to treat PTGFRN-positive cancers in both *in vitro* and *in vivo* models

SOURCE(S) OF SUPPORT

Meyerhoff Graduate Fellowship (2017-2018)

GRANT APPLICATION(S) WRITTEN FOR PRE-DOCTORAL FUNDING:

2019 F-31 Diversity Fellowship, not awarded
2022 Cancer Biology T32 Training Grant, not awarded

RESEARCH EXPERIENCE (prior to entering graduate program):

May 2012-December 2012: Intern- Johns Hopkins University- Department of Genetic Medicine, Advisor: Dr. Aravinda Chakavarti, Baltimore, MD.

October 2013-August 2017: Research Associate- A&G Pharmaceutical, R&D Division, Columbia, MD.

SKILLS & TECHNIQUES:

Cell Biology and Proteomics: Protein extraction and purification by immunoprecipitation, immunofluorescent microscopy, flow cytometry, immunohistochemistry, immunoblot, enzyme-linked immunoassay (EIA), Hydrophobic Interaction Chromatography (HIC), reduction and conjugation of proteins, total protein quantitation assays (Bradford, BCA), bacterial and mammalian cell culture, *in vivo* nude mouse models

Instruments: 1) Intellicyt High Throughput Flow Cytometry unit. 2) Bio-Rad NGC Medium Pressure Liquid Chromatography Systeme. 3) Nikon A1 Laser Scanning Confocal Microscope. 4) Namocell Hana Single-Cell Dispenser. 5) Azure Biosystems 280 Western Blot system. Software: Azure Biosystems Analysis, ImageJ, NIS Elements, Chrom Lab, Labworks, TSView

PUBLICATIONS

1. Marquez J, Dong J, Dong C, Tian C, Serrero G. Identification of Prostaglandin F2 Receptor Negative Regulator (PTGFRN) as an internalizable target in cancer cells for antibody-drug conjugate development. PLoS One. 2021 Jan 27;16(1):e0246197. doi: 10.1371/journal.pone.0246197. PMID: 33503070; PMCID: PMC7840024.

2. Marquez J, Dong J, Hayahi J, Serrero G. **8C7: A Fully-Human Monoclonal Antibody-Drug Conjugate Capable of Tumor Growth Inhibition in Mesothelioma and Pediatric Medulloblastoma.** Submitted for Publication to Molecular Cancer Therapeutics. Review Pending.

3. Marquez J, Dong J, Weldemariam M, Hayashi J, Kane M, Serrero G. **Prostaglandin F2 Receptor Negative (PTGFRN) Expression Correlates with an Aggressive, Metastatic-like Phenotype in Epidermoid Carcinoma, Pediatric Medulloblastoma, and Mesothelioma.** Submitted for Publication to Clinical Cancer Research. Review Pending.

ABSTRACTS and PRESENTATIONS:

Prostaglandin F2 Receptor Negative Regulator (PTGFRN) is a novel target to inhibit tumor growth via antibody drug conjugate

- AACR Annual Meeting 2021 Philadelphia, PA. Virtual. April 2021

HONORS

PROFESSIONAL MEMBERSHIPS
2020-2023: Member, Rho Chi Honor Society, Omicron Chapter
2017-2023 Meyerhoff Graduate Fellowship

Abstract

Title of dissertation: PTGFRN as a Target for Antibody-Drug Conjugate (ADC) Development in Mesothelioma and Medulloblastoma

Author: Jorge L. Marquez, Doctor of Philosophy, 2023

Dissertation directed by: Dr. Ginette Serrero, Ph.D., President/CEO/Founder of A&G Pharmaceutical, Columbia, MD and

Dr. Maureen Kane, Ph.D., Professor in the Department of Pharmaceutical Sciences, University of Maryland, Baltimore, Baltimore, MD

Cancer is a disease that afflicts millions of people each year. While there are many drugs available to treat certain subsets of cancer, there still remain many types of cancer that do not have tailored therapy available to treat them. Mesothelioma and Pediatric Medulloblastoma are two such cancers that the NIH classifies as rare and aggressive neoplasms. As such, both cancers display unmet needs, and are the subject of much research to improve the chemotherapy available for treatment.

Our laboratory has found that both cancers express a protein called Prostaglandin F2 Receptor Negative, or PTGFRN. PTGFRN is a member of the Tetraspanin family, which are transmembrane proteins. Previously, PTGFRN expression has been found to correlate with a more aggressive phenotype. Additionally, when its expression is inhibited, cellular processes essential for cancer metastasis were also found to be impacted. To better understand how PTGFRN affects cancer progression, we looked at the effects of PTGFRN with various *in vitro* functional assays to assess phenotypic changes. We also performed a global proteome and pathway analysis using mass spectrometric methods to better

understand what pathways were most affected by PTGFRN expression, and identify proteins that are complexed, or in direct interaction, with PTGFRN.

In parallel to these studies, we also developed monoclonal antibodies that are capable of binding cell-surface PTGFRN, and inducing endocytosis to the cytoplasm. Conjugation of our prototype antibody, the mouse mAb 33B7, to the ribosome-inactivating protein Saporin results in an Antibody-Drug Conjugate (ADC) of moderate efficacy. Due to the success of this first ADC attempt, we then developed a fully human antibody, denoted as 8C7, and conjugated it to the payload Duocarmycin via a cleavable linker, resulting in our second generation ADC. This new ADC exhibits improved, highly potent *in vitro* anti-cancer effect, as well as in *in vivo* models with mice bearing mesothelioma and medulloblastoma tumors. The work detailed here lays the groundwork for a tailored therapy to treat the aforementioned cancers, and expands our knowledge of proteins and protein interactions involved in cancer metastasis.

PTGFRN as a Target for Antibody-Drug Conjugate (ADC) Development in Mesothelioma and Medulloblastoma

by
Jorge Marquez

Dissertation submitted to the Faculty of the Graduate School of the
University of Maryland, Baltimore in partial fulfillment
of the requirements for the degree of
Doctor of Philosophy
2023

Dedication

To my amazing, future wife,
Caitlin Marie Long
Buzz buzz!

Acknowledgments

I would first like to thank my family. To my mother, Pamela Bolton, who always pushed me to exceed even my own expectations, and held me to a standard that made me appreciate the spoils of hard work. Thank you for providing support in all the various ways you have over the years. To my grandparents, Larry and Susan Burkins, who constantly motivated me in my endeavors, and shared with me the experiences and lessons learned from their personal and professional lives. I hope I've made you proud. To my sister Natalie, my brother-in-law Enrique, and their children Cora, Emmanuel, and Daphne, you've provided me with so many moments of joy over these last five and a half years. I am so proud to call myself your brother and uncle, and I look forward to watching you kids grow up.

I would also like to give thanks to my mentor, Dr. Ginette Serrero. You took a chance on a new college graduate with very little experience, and eventually pushed me to pursue this doctorate degree, without which I may not have had the self-confidence to take the leap. Your support these last 10 years has made me the scientist I am today, and I will be eternally grateful for that.

I would also like to thank my colleagues at A&G Pharmaceutical, specifically Jianping Dong and Binbin Yue. You both trained me when I first started at A&G, and the work presented here would not have been possible without the foundations you helped me build. The attention to detail that you taught me has had a tremendous impact on the quality of my work, and does not end in the lab. Also, an extra thanks to Jianping for her help with terminating all of my mice for me. I just couldn't bring myself to do it. So. Many. Mice…

To my high school biology teacher, Mr. Richard Kincaid, and high school math

teacher Mrs. Joy Phillipi, who both had a tremendous impact on me, and changed the trajectory of my life with their instruction. I wouldn't have the passion for biology I currently possess if it weren't for Mr. Kincaid's enthusiastic instruction of the subject, and his willingness to answer every random question that popped into my head while he was trying to teach 25 other students. Mrs. Phillipi completely changed how I learned, instilling in me the value and ability of actually understanding what I am being taught, and not just memorizing a sequence of steps for tests. That was truly a "lightbulb" moment for me, without which I may not have succeeded in the classes required for me to reach this point in my quest for higher education.

I would also like to extend my gratitude to my committee members: Dr. Maureen Kane, Dr. Hongbing Wang, Dr. Paul Shapiro, Dr. Yan Shu, and Dr. Stuart Martin. Thank you for your support and advice on my project. The suggestions and questions you provided during our committee meetings provided me with perspectives that I needed to turn my original project proposal into a thesis that I believe can withstand any critique or question thrown at it.

A huge thank you to the friends I made during the time I spent in the PSC program. To Danté Johnson, Sydney Stern, Matthew Hursey, Jordan Pritts, Lizzy Robinson, and Garrick Centola. I will always look back fondly on the weekends spent commiserating and supporting each other during our tenures here at UMB. There will always be a little part of each one of you in my work.

Last, but certainly not least, the biggest thanks of all to my fianceé, and soon to be wife, Caitlin Long. You are the love of my life, and I cannot wait to spend the rest of our lives together. I cherish what we've built over these last 11 years, and I look forward to

what our futures have in store for us. You've seen me at some of my lowest moments during these past 6 years, and not once did you blink. You've been the best sugar momma a guy could ask for, and I can't wait to return the favor. You deserve the world, and it's my personal mission to give it to you. I love you, bee-bee.

Table of Contents

Dedication iii
Acknowledgments iv
List of Tables xi
List of Figures xii
List of Abbreviations xiv

Chapter 1 1
Overview and Objectives 1
1.1 The Need for Targeted Therapy in Oncology 1
1.2 Mesothelioma 2
1.3 Pediatric Medulloblastoma 5
1.4 Cancer Metastasis 7
1.5 Prostaglandin F2 Receptor Negative and Tetraspanins in Cancer 11
1.6 Antibody-Drug Conjugates as Cancer Therapy 16
1.7 Brief History of Antibody-Drug Conjugates 22

Chapter 2 31
PTGFRN and Cancer 31
2.1 Introduction 31
2.2 Materials and Methods 33
2.2.1 Cell Culture 33
2.2.2 Immunohistochemistry 33
2.2.3 Silencing/Overexpression of PTGFRN and Screening 34
2.2.4 Immunoblotting 35
2.2.5 Proliferation Assay 35
2.2.6 Migration Assay 36
2.2.7 Clonogenic Assay 36
2.2.8 3D Spheroid Culture 37
2.2.9 Immunofluorescence 37
2.2.10 Co-Immunoprecipitation 38

2.2.11 Proteomic analysis via liquid chromatography-tandem mass spectrometry .. 40
2.2.12. Statistical Analysis 42
2.3 Results 42
2.3.1 PTGFRN is highly expressed in cancerous tissue, but not in healthy tissue 42
2.3.2 Progression of Mesothelioma from Benign to Malignant phenotype correlated with a significant increase in PTGFRN Expression 43
2.3.3 PTGFRN Expression is Positively Correlated with Characteristics Associated with a Metastatic-like Profile 44
2.3.4 PTGFRN Knockdown Cells Grown in Spheroid Conditions Show Decreased Levels of Integrin β1 and E-Cadherin 50
2.3.5 PTGFRN, Integrin β1, and E-Cadherin All Co-Localize to Cell-Cell Junctions, and Are Capable of Directly Binding to Each Other 51
2.3.6 Loss of PTGFRN Expression Results in an Increase in LC3B Accumulation, Indicating an Increase in Autophagy 53
2.3.7 Effect of PTGFRN on Cellular Proteome 55
2.3.8 Mass Spectrometric Analysis of 8C7 Co-IP Pull-down Products 59
2.4 Discussion 62

Chapter 3 72
PTGFRN as a Target for ADC Development 72
3.1 Introduction 72
3.2 Materials and Methods 73
3.2.1 Cell Culture 73
3.2.2 PTGFRN Immunoblot 73
3.2.3 Production of 33B7 and 8C7 mAb 74
3.2.4 Purification of Antibody Target Protein and Identification by Mass Spectrometry 74
3.2.5 Measurement of Cell Surface Binding by Flow Analysis 76
3.2.6 Examination of 33B7 by Immunofluorescence (IF) Assay 77
3.2.7 PTGFRN cDNA Transfection into HEK-293A Cells 79
3.2.8 Inhibition of Proliferation with 33B7 and Fab-ZAP Secondary Antibodies 80
3.2.9 Direct Conjugation of Antibodies 81
3.2.10 Purification of 8C7 ADC by HIC 82
3.2.11 In Vivo Mouse Studies 82

3.3 Results 84
3.3.1 Binding and Internalization of 33B7 Monoclonal Antibody to Cancer Cells .. 84
3.3.2 Purification of 33B7 Cell Surface Target 86
3.3.3 Mass Spectrometric Identification of the Cell Surface Target 87
3.3.4 HEK-293A Cells Transiently Transfected with Human PTGFRN cDNA Can Bind 33B7 Antibody 88
3.3.5 33B7 induces internalization of PTGFRN 89
3.3.6 Inhibition of Proliferation of PTGFRN-Transfected HEK-293A Cells, Natural Cancer Cells, by Internalization of 33B7 91
3.3.7 *In Vivo* Growth Inhibitory Effect of Saporin-Conjugated 33B7 96
3.3.8 8C7 is a Fully-Human Antibody That is Capable of Binding Cell-Surface PTGFRN, and Internalizing the Transmembrane Protein to the Cell Interior 97
3.3.9 8C7 Conjugation with Mc-Vc-Duocarmycin Results in a Potent, Fully Human Antibody-Drug Conjugate (ADC) in In Vitro and In Vivo Models 100
3.4 Discussion 104

Chapter 4 107
Conclusions and Future Discussions 107

Appendix 1: Supplementary Figures……...111
Figure 1A.1. Migration of A431 Cells After siRNA Transfection……111
Figure 1A.2. A431 Spheroid Growth After siRNA Transfection……111
Figure 1A.3. Immunoblot of 2D A431 Protein Expression…….112
Figure 1A.4. Immunofluorescence on Stable A431 shRNA Cells……..112

Appendix 2. Additional Tables……113
Table 2A.1. Pathway analysis of all genes found to be upregulated after PTGFRN knockdown by shRNA in A431……...113
Table 2A.2. Pathway analysis of all genes found to be downregulated after PTGFRN knockdown by shRNA in A431……...138
Table 2A.3. Pathway analysis of all proteins found to be present in the co-IP of PTGFRN with 8C7 monoclonal antibody in A431 cells……..157

Appendix 3. Additional Author Contributions……199

References……200

List of Tables

Table 1.1 List of All Non-PTGFRN Tetraspanins……12

Table 1.2 List of all FDA-approved Antibody-Drug Conjugates……..……25

Table 2.1 Table of PTGFRN shRNA sequences……..…….34

Table 2.2 Antibodies used in immunofluorescence assays……..……..38

Table 2.3 Antibodies Used in Immunoprecipitation Assays……...…..39

Table 2.4 Antibodies Used in Immunoblotting……..….....40

Table 2.5 Top 10 Most Upregulated Proteins After PTGFRN Knockdown…..……57

Table 2.6 Top 10 Most Upregulated Cellular Pathways After PTGFRN Knockdown……..….....57

Table 2.7 Top 10 Most Downregulated Proteins After PTGFRN Knockdown……..……..58

Table 2.8 Top 10 Most Downregulated Cellular Pathways After PTGFRN Knockdown……....58

Table 2.9 Top 10 Most Abundant Proteins in PTGFRN Co-Immunoprecipitation with 8C7……...……..60

Table 2.10 Top 10 Cellular Pathways Represented in PTGFRN Co-Immunoprecipitation with 8C7…….61

Table 3.1 Mass spectrometric analysis of 33B7 immunoprecipitation elution……..88

List of Figures

Figure 2.1 Immunohistological analysis of PTGFRN expression in healthy and cancerous tissue sections…….43

Figure 2.2 Immunohistological analysis of PTGFRN expression in mesothelioma tissue sections……...44

Figure 2.3 PTGFRN expression level after transfection of shRNA or PTGFRN cDNA..45

Figure 2.4 Comparing proliferative capability of cells after PTGFRN silencing/overexpression……46

Figure 2.5 Effect of PTGFRN expression on migration capability……...47

Figure 2.6 PTGFRN expression affects cells ability to grow in colonies……..48

Figure 2.7 Knockdown of PTGFRN expression inhibits spheroid formation……...49

Figure 2.8 Effect of PTGFRN Knockdown on Proteins Involved in Spheroid Formation……...51

Figure 2.9 Co-localization of PTGFRN, E-Cadherin, and Integrin β1…….52

Figure 2.10 Direct Interaction between PTGFRN, E-Cadherin, and Integrin β1…….53

Figure 2.11 PTGFRN Knockdown Influences Autophagy……54

Figure 2.12 Mass Spectrometric Proteome Analysis after PTGFRN Knockdown……56

Figure 2.13 Mass Spectrometric Analysis of PTGFRN Co-IP Products……...60

Figure 2.14 Major Pathways Affected by PTGFRN Knockdown…….....62

Figure 3.1 33B7 binding and internalization in cancer cells…….85

Figure 3.2 Immunoprecipitation with 33B7 pulls down a unique 130kDa protein……...87

Figure 3.3 Transfection of human PTGFRN cDNA in HEK-293A cells results in a significant increase in 33B7 binding……..89

Figure 3.4 Binding of 33B7 causes the internalization of PTGFRN…….91

Figure 3.5 Incubation of PTGFRN-overexpressing HEK-293A cells with 33B7 and anti-mouse secondary antibody-saporin conjugate……...93

Figure 3.6 PTGFRN expression and effect of 33B7 on various cancer lines……95

Figure 3.7 Effect of 33B7-saporin on tumor growth of A431 cells and ASGCC3 cells in athymic nude mice…….96

Figure 3.8 Fully human 8C7 antibody binding is specific to PTGFRN……99
Figure 3.9 Internalization of PTGFRN by 8C7……100
Figure 3.10 In Vitro Activity of 8C7-Duocarmycin ADC……102
Figure 3.11 In Vivo Treatment of PTGFRN-Positive Tumors in Nude Mice…….103
Figure 3.12 In Vivo Treatment of PTGFRN-Negative Tumors in Nude Mice……...104

List of Abbreviations

AAALAC	Association for Assessment and Accreditation of Laboratory Animal Care
ADC	Antibody-Drug Conjugate
CSC	Cancer Stem Cells
DMA	Dimethyl Acetamide
DMEM	Dulbecco's Modified Eagle Medium
DTNB	5,5′-dithiobis-(2-nitrobenzoic) acid
DTT	Dithiothreitol
EDTA	ethylenediamine tetraacetic acid
ERM	Ezrin-Radixin-Moesin
EtOH	Ethanol
FBS	Fetal Bovine Serum
H_2O_2	Hydrogen Peroxide
HEK	Human Embryonic Kidney
HIC	Hydrophobic Interaction Chromatography
HTFC	High-Throughput Flow Cytometry
HPLC	High Performance Liquid Chromatography
IACUC	Institutional Animal Care and Use Committee
Ig	Immunoglobulin
IND	Investigational New Drug
OLAW	Office of Laboratory Animal Welfare
PBS	Phosphate-buffered Solution
PTGFRN	Prostaglandin F2 Receptor Negative

PVDF	Polyvinylidene fluoride
SMO	Smoothening Protein
SMRP	Soluble Mesothelin-Related Peptides
RIPA	Radio-Immunoprecipitation Assay
TME	Tumor Microenvironment
VEGF	Vascular Endothelial Growth Factor

Chapter 1
Overview and Objectives

1.1 The Need for Targeted Therapy in Oncology

Cancer is a disease that has plagued mankind for millennia, first documented with recommended treatment being described on a papyrus writing dating back to 1600BC, although some believe this was a copy of an even older recording, stretching as far back as 2500-3000BC (1). The introduction of anesthesia in the 19th century during surgical procedures led to surgery becoming the preferred method of cancer treatment up through the 1950s. However, with the discovery of X-rays by W.C. Röntgen in 1895, radiation therapy was gradually incorporated into cancer treatment, with results of radiation therapy in leukemia and lymphoma first published in 1902 and 1903 (2–4). Despite advancements over the years in both of these methods, neither was completely sufficient to combat advanced, metastatic cancers. The use of chemotherapeutic agents to treat cancer began its ascent in the later decades of the 20th century. Since then, many types of chemotherapeutic agents have been investigated, some having more success than others depending on the cancer type (5).

General, systemic chemotherapy has an innate drawback in its use, in that while it can certainly kill cancer cells, it is also quite effective at killing normal, non-cancerous cells, resulting in off-target toxicity to the patient, and adverse side-effects. A drug that can selectively target cancerous cells and exert its anti-cancer effect with minimal effect on non-cancerous cells has resulted in a massive improvement for patient quality of life. The introduction of small-molecule inhibitors and monoclonal antibodies to target and neutralize growth factors takes advantage of cancer cell's elevated rate of growth and

division (6,7). The inhibition of endogenous angiogenesis acts as a way to cutoff a tumor's nutrient supply by preventing blood vessel formation (8). But a targeted therapy is only as good as the drug target itself, which generally are preferentially expressed, significantly overexpressed, or mutated in cancer tissue compared to healthy tissue. As such, researchers are continually looking for novel drug targets, especially in rare and aggressive cancers that have no targeted therapy currently available. With each new drug target discovered, a new option for treatment becomes available to patients, increasing their odds of survival, and improving their quality of life.

1.2 Mesothelioma

Mesothelioma are rare, aggressive cancers that currently have no tailored therapies available on the market (9,10). Occupational exposure to asbestos is the leading cause of mesothelioma cases (11). This cancer typically arises in the pleura of the lungs, although it can also be found in the peritoneum, as well as the pericardium and testes in some rare cases. Diagnosis of mesothelioma can be difficult, as there is a long latency period between the onset of tumorigenesis, and the presentation of symptoms, with some studies estimating that this latency period could last anywhere between 20-50 years (12). Further complicating diagnosis is the fact that routine blood tests are not sufficient to detect mesothelioma. However, the introduction of the MESOMARK® assay now allows doctors to measure levels of soluble mesothelin-related peptides (SMRP) in the blood, which have been found to increase with mesothelioma, and decrease with treatment (13). These limitations result in most patients presenting with advanced disease at the time of diagnosis (14–16).

Treatment of mesothelioma typically relies on systemic chemotherapy, as not all mesothelioma patients are candidates for surgery due to the complicated location of the tumor (17). Pleural effusions are common in patients presenting with mesothelioma, which require frequent drainage for symptom relief. Surgery, for those who qualify, is almost always incomplete, and therefore considered to be palliative in nature, as opposed to curative (18). The most extreme surgery available to patients, referred to as an extrapleural pneumonectomy, only extends the median survival to 18 months, with a 5-year survival rate of 14% (19). However, due to how aggressive this procedure tends to be, and the late age of patients at time of diagnosis, many patients are considered to be at higher risk of complications from surgery than the mesothelioma.

The low number of cases diagnosed per year, along with the limited survival time make it difficult to compile statistically relevant information about treatment outcomes. In the only reported randomized trial to determine the effect of surgery on overall survival, while just over 300 patients were screened for the study, all but 50 participants dropped out. Of the half that were placed in the surgery group, only 16 of them actually went through with the surgery. Further complicating this study was the fact that the patients selected for the “no surgery” group were considered to have a more favorable stage of disease. In the end, the “no surgery” group displayed longer median overall survival compared to those few who underwent surgery (19.5 vs 14.4 months). However, the low statistical power of this study casts significant doubt on these results (20,21).

Disappointingly, a large randomized study found that treatment with the standard regimens of mitomycin, vinblastine, and cisplatin did not provide substantial benefit in survival compared to mesothelioma patients who received solely symptom abatement

treatments consisting of combinations of steroids, analgesic drugs, bronchodilators, palliative radiotherapy (22). Subsequent research has since shown combination therapy with platinum-based drugs and next generation anti-folate compounds, as well as the anti-VEGF monoclonal antibody Bevacizumab, all variably increase overall survival (23–25). With all current treatments being non-specific, median survival time varies from only 5-12 months, even with the improvement from combination therapies (11). Additionally, the drugs tested in these trials all have high rates of toxicity in tested patients, with 37% showing grade 4 hematologic or grade 3/4 non-hematologic toxicity, making some patients incapable of tolerating chemotherapy (26). On average, the 5-year survival rate after initial diagnosis still remains in the range of 5-10% (27).

To date, there has been no data that show radiation therapy having any effect on survival times. In one study comparing radiation in patients who underwent the aforementioned extrapleural pneumonectomy and chemotherapy, their primary endpoint, locoregional relapse-free survival, was never reached. Similarly to the study comparing surgery outcomes, this study was also plagued by low statistical power, as well as inadequate macroscopic clearance of the cancer, which was a starting requirement of the study (28). Hope for better data may be on the horizon though, as a phase III trial looking at the effect of intensity-modulated radiotherapy on malignant mesothelioma is currently underway (29). This may even be an even more beneficial form of radiation therapy compared to traditional radiation, with less off-target side effects, as the oblong, elliptical shape of the entire pleura requires a large radiation field to treat completely. This large field also increases adverse radiation toxicity to neighboring organs (30).

Recently, investigations into the protein mesothelin, which is expressed in 30% of cancers, including, but not limited to, mesothelioma, has led to generation of an anti-mesothelin monoclonal antibody (Amatuximab), as well as an ADC (BMS-986148) that are currently undergoing clinical trials, although the former has not shown great efficacy in late-stage trials (31–33). While the identification of mesothelin as a potential druggable target is a step in the right direction, there is yet to be an approved tailored therapy that can treat mesothelioma.

1.3 Pediatric Medulloblastoma

Medulloblastoma is a central nervous system cancer that represents 25% of all pediatric brain neoplasms, but paradoxically, is only diagnosed at a rate of 4-4.9 per 1,000,000 people a year, awarding it the status of rare cancer (34). Medulloblastoma tumors are thought to arise in the cerebellum, but the medulloblastoma classification can also be extended to tumors found in the brainstem and cerebrum. (35) On average, the 5-year survival rate of pediatric medulloblastoma is 72.1% (9). Medulloblastoma is also an aggressive cancer that tends to metastasize quickly, with around 33% of patients showing evidence of metastasis at time of diagnosis (36,37).

In children younger than 3 years old, medulloblastoma is twice as likely to progress into metastasis. Some of this can be attributed to the fact that young patients are ineligible for radiation therapy, as radiation has been shown to have an extremely detrimental effect on brain development (38,39). As such, young children treatments are limited to surgery and systemic chemotherapy, although this regimen only slows the median overall time to progression to less than 9 months (40).

Current treatment of medulloblastoma is dependent on the classification of disease risk. In patients whose medulloblastoma is considered average-risk, treatment typically relies on surgery to remove as much of the tumor as possible, followed by postoperative radiation, as well as general chemotherapy (41–43). While this trimodal treatment method has shown moderately improved progression-free survival (PFS) in patients compared to just surgery and radiation alone, no specific chemotherapeutic agent has demonstrated superiority in treating medulloblastoma (44). For those patients whose medulloblastoma is considered high-risk, progression-free survival remains around 50% (45). However, trials to further optimize the combination therapy of radiation and high-dose chemotherapy are currently ongoing. While preliminary data looking at short-term survival seem to be promising, and the treatment seems to be well-tolerated, more time is needed to complete these investigations, and follow-up studies will also need to be performed afterwards (43).

The typical chemotherapeutic regimen for this cancer consists of combination cycles of cisplatin and etoposide, which can have unacceptable toxicities such as thrombocytopenia, myelodysplastic syndrome, ossifying fibromas, and/or neutropenia when given in combination (46). These negative treatment side-effects further restrict children who are healthy enough to undertake this chemotherapy. Therefore, the development of new drugs that can specifically target these cancers, while reducing the risk of off-target toxicity, is of upmost importance in today's cancer research.

Efforts to develop tailored therapies for medulloblastoma are currently undergoing. Recently, the hedgehog signaling pathway has been identified as being elevated in medulloblastoma, which is partially attributed to the activity of the

smoothening protein (SMO) (47). While not currently approved for treatment of pediatric medulloblastoma, the SMO-antagonist Vismodegib has begun to report favorable results in clinical trials against medulloblastoma. Numerous other pathway inhibitors, such as Bromodomain (BET) inhibitors, tyrosine kinase inhibitors (TKI), and PI3K/AKT/mTOR inhibitors are currently undergoing clinical trials to evaluate their efficacy in treating medulloblastoma (48).

1.4 Cancer Metastasis

While surgical procedures and chemotherapeutic agents have seen vast improvements over the years, metastasis still makes up >90% of all cancer deaths (49,50). Because of this, our understanding of the mechanics of metastasis, as well as the proteins involved in the process, must also evolve.

Cancer metastasis is a remarkably complex process in cancer progression with numerous molecular pathways and key drivers that is intensely studied and characterized. Metastasis can be divided into 5 distinct cellular processes: 1) Cell migration from the primary tumor, invading the basement membrane; 2) Intravasation into the circulatory vasculature or lymph nodes; 3) Systemic circulation; 4) Extravasation out of the circulatory system into secondary tissue; and 5) Colonization and establishment of a new tumor in a secondary organ site (51). Typically, when a cell migrates from a primary tumor, local stressors and immune surveillance are able to halt the cell from colonizing secondary sites (52). However, tumors are a heterogeneous population of cancer cells, and because of this, these same stressors exert a selective pressure against cancer cells, which can ultimately lead to the development of a population of cells that can evade and survive anti-cancer immune responses (49). Once such a cell or cell population exists,

they eventually gain the ability to migrate from the tumor, and invade nearby blood vessels and/or lymph nodes, where they then circulate in the body until a suitable secondary organ site is established (53). This initial migration can be done by single cells, or collective cell clusters, and is generally considered the differentiating factor between benign and malignant classification of cancer (54). In order to navigate through the basement membrane, cancer cells must degrade and remodel the extracellular matrix (ECM) via matrix metalloprotease secretions, as well as mechanically contract and protrude their own membranes (55).

In order to enter the vasculature of the circulatory system, tumor cells can initiate a process known as angiogenesis, in which it undergoes cellular signaling that results in the formation of incipient blood vessels (56). This process is critical for overall survival of the tumor, as it facilitates the steady supply of oxygen and nutrients for tumor growth, and allows for cellular waste to be carried away from the tumor (51). By secreting multiple various growth factors, predominantly vascular endothelial growth factor (VEGF) and angiopoietin (ANG), pre-existing vasculature begins sprouting in the direction of the tumor (57). These newly formed tumor vessels are structurally abnormal, as they are not comprised solely of endothelial cells, but rather a mixture of cancer cells and endothelial cells (58,59).

Once these migratory cells intravasate into circulation, very few cancer cells actually survive the journey due to immune surveillance, collisions with red blood cells (RBC), and the hydrodynamic pressure of circulation (60). The circulating tumor cells (CTC) that manage to survive these conditions are further limited to where they can travel based on their diameter compared to the width of blood vessels they travel in.

Physical arrest during blood flow based on this size disparity can account for the location of secondary tumor site (61). Cell adhesion can also direct the location where a CTC ends up. CTCs can roll along the endothelial wall through the selective binding of E-Selectin and P-Selectin, eventually arresting in position from binding of intercellular adhesion molecule-1 (ICAM-1) or vascular cell adhesion molecule-1 (VCAM-1) (62,63).

Upon arrest during circulation, tumor cells must extravasate through the endothelium upon which they are arrested. This process is more difficult than intravasation, as these vessels are fully formed, as opposed to the structurally abnormal ones formed in the early steps of tumor angiogenesis. In addition, cancer cells are experiencing fluid shearing stress, which leads to a small percentage of cells actually surviving this step of metastasis (64). Nevertheless, cells that make it to this point, and are able to bind to the epithelium, begin to undergo transendothelial migration, causing an inflammation response through the secretion of cytokines, angiopoietin-like 4 (ANGPTL4), and the inhibition of RhoA GTPase, which in turn leads to the junctions of the endothelial cells loosening, and allowing the cancer cells to navigate out of the vasculature in their new secondary organ site (65). Any cells that are able to survive to this point have one last step to take: colonization. During this stage, the cells are now in an unfamiliar tissue environment, devoid of any stromal support cells, ECM proteins, or growth factors that would normally support them in their primary site (66). As such, these cells may enter into a dormancy state, in which they remain until certain signals switch them into an indolent state, where proliferation begins. While the exact cause of this switch into a proliferative state is not known, the cancer cells that are able to colonize secondary organs have been found to have upregulated levels of certain proteins that are

associated with stem cells such as CD44, CD22, as well as SOX2 and SOX9 transcription factors. These cancer stem cells (CSC) exhibit a much more proliferative phenotype, perhaps explaining why they are able to grow without the usual support system (67).

Due to the many steps required in the metastasis pathway, there have been many genes and proteins that influence the cancer cell phenotype identified. Rearrangement of cytoskeletal proteins, matrix metalloproteinases (MMP), and cathepsins have proved to influence invasion and migration through stroma. The proteins Transforming Growth Factor β (TGF-β), Slug, Snail, Twist, and Zeb-1 have all been found to initiate a process known as Epithelial-to-Mesenchymal transition (EMT), which is a key morphological change in cells that helps facilitate migration and intravasation in the early steps of cancer metastasis. The reversal of EMT, known as MET, has also been implicated in secondary site colonization (66,68,69). The discovery and characterization of proteins that contribute to a metastatic-like phenotype is an ongoing iterative process, both to understand how they may contribute to the metastatic transition, as well as if they can be targeted in drug development.

When comparing cells from a secondary metastatic tumor to cells from its progenitor primary tumors, there are many differences in phenotypic characteristics which can be tested via *in vitro* functional assays. This includes characteristics of metastatic cells such as their high rates of proliferation, increased ability to migrate through a transwell membrane, increased ability to grow in colonies at low cell densities, and ability to grow in 3D spheroid culture conditions (70–75). Cancer cells that have undergone malignant transformation typically present altered expression of proteins that are increased if oncogenic, or decreased if they are oncosuppressors.

1.5 Prostaglandin F2 Receptor Negative and Tetraspanins in Cancer

Prostaglandin F2 Receptor Negative Regulator (PTGFRN), also known as FPRP/CD9P-1/EWI-F/KIAA1436, is a member of the family of proteins called Tetraspanins. This family of proteins consist of 33 unique proteins, which are all capable of binding to other tetraspanins, as well as proteins outside the tetraspanin family (76). The identity of PTGFRN in particular was first discovered and published in 1996, in which its direct interaction with the Prostaglandin $F_{2\alpha}$ Receptor was detailed (77). As such, one of the first processes PTGFRN was implicated in was mediation of inflammation through binding of the Prostaglandin $F_{2\alpha}$ Receptor and blocking the binding of Prostaglandin $F_{2\alpha}$ ($PGF_{2\alpha}$), the main binding partner of Prostaglandin $F_{2\alpha}$ Receptor. Subsequent investigations have found that not only can PTGFRN associate with itself in homodimers, but the main binding partners of PTGFRN are fellow tetraspanins CD9 and CD81 (78–80). PTGFRN has been found to also bind the tetraspanin CD151. However, this direct binding takes place exclusively when PTGFRN is also bound to CD9. This ability of tetraspanins to bind each other in various configurations, both dependent and independent of other binding partners, eventually came to be referred to as the "Tetraspanin Web" (81,82). Due to the numerous binding partners of tetraspanins, this family of proteins has been found to be involved in numerous biological processes, including adhesion, migration, cancer metastasis, invasion, fertilization, and exosome function (76,83–86), and PTGFRN specifically has also been found to be involved with lipid accumulation in preadipocytes, and directly interacts with ezrin-radixin-moesin proteins (78,87). Table 1.1 contains a list of all non-PTGFRN tetraspanins, as well as functions that have been reported for each one.

Table 1.1 List of All Non-PTGFRN Tetraspanins

Tetraspanin Name	Aliases	Function	Reference
TSPAN1	NET-1	Migration, Autophagy flux	(88,89)
TSPAN2	FLJ12082	regulation of cell development, activation, growth and motility	(90)
TSPAN3	TM4-A	regulates expression of ADAM10, presenilin, and amyloid precursor protein	(91)
TSPAN4	NAG-2	mediates signal transduction events in the regulation of cell development, activation, growth and motility.	(92)
TSPAN5	NET-4	Adhesion, proliferation, osteoclastogenesis	(93,94)
TSPAN6	T245	regulator of carcinogenesis in colorectal cancer, suppressor of Ras-driven cancer progression	(95,96)
TSPAN7	DXS1692E, TALLA-1, A15, CD231	Maturation of dendritic cells, regulated postendocytic trafficking	(97,98)
TSPAN8	CO-029	Angiogenesis, wound healing, leukocyte trafficking	(99)
TSPAN9	NET-5	Migration and invasion, platelet function regulation	(100,101)
TSPAN10	OCSP	Facilitates ADAM10 binding	(102)
TSPAN11	N/A	Exact function unknown, predicted to be involved in migration	(103)
TSPAN12	NET-2	inhibits degradation of Beta-catenin, regulates miR-405 to promote chemoresistance and proliferation of small cell lung carcinoma	(104,105)
TSPAN13	NET-6	involved in proliferation, found to be tumor suppressor	(106,107)
TSPAN14	DC-TM4F2, MGC11352	Regulates trafficking and activity of ADAM10	(108)
TSPAN15	NET-7	regulates activity of ADAM10, expression positively correlates with proliferation	(109,110)
TSPAN16	TM4-B, TM-8	Exact Function unknown	(111)
TSPAN17	FBX23	regulates inflammation via interaction with VE-Cadherin and ADAM10	(112)
TSPAN18	N/A	regulates thrombo-inflammation via Orai1/Ca2+ signaling	(113)

Table 1.1 List of All Non-PTGFRN Tetraspanins, Continued

TSPAN19	N/A	Exact Function unknown	(114)
UPK1B	TSPAN20	RegulatesWnt/β-catenin pathway to promote the invasion and metastasis of bladder cancer	(115)
UPK1A	TSPAN21	promotes proliferation and protect from apoptosis in bladder carcinoma	(116)
PRPH2	TSPAN22, rd2, CACD2	essential for the development of rod and cone outer segments in retinal development	(117)
ROM1	TSPAN23	maintains retinal outer nuclear layer	(118)
CD151	TSPAN24, SFA-1, PETA-3, RAPH	Regulates cytoskeletal reorganization, invasion and cell-adhesion functions of endothelial cells during pathological angiogenesis	(119)
CD53	TSPAN25	regulate kinase and phosphatase activity in immune cells	(120)
CD37	TSPAN26	Exact function unknown, found to be a tumor suppressor	(121)
CD82	TSPAN27, R2, IA4	involved in Beta cell maturation, key role in endometriosis development	(122,123)
CD81	TSPAN28, TAPA-1, S5.7	invovlved in formation of actin membrane protrusions after RAC1 activation in migration, sorted into extracellular vesicles	(124,125)
CD9	TSPAN29, BA2, P24, MRP-1	Fusion, adhesion, proliferation, migration/invasion, apoptosis, cell motility, fertilization, extravasation	(126,127)
CD63	TSPAN30, ME491, HOP-26, Pltgp40, AD1	Binds TIMP1 to regulate cell polarization and survival, sorted into extracellular vesicles	(128,129)
TSPAN31	N/A	suppresses cell proliferation through down-regulation of antisense pairing with CDK4	(130)
TSPAN32	IL2	regulates cell-mediated immune response, downregulated upon T-Cell Activation	(131)
TSPAN33	MGC50844, Penumbra	modulates plasma membrane tension to regulate endocytosis and migration	(132)

PTGFRN has also been found to be highly packaged into extracellular vesicles (EV), which are lipid bi-layered secretions of cytoplasmic materials used by cells to communicate in a paracrine fashion with other cells nearby (85,133). These EVs can contain proteins, mRNA, lipids, and other cellular components, and can be hijacked by cancer cells to corrupt the population of cells surrounding the tumor made up of many cell types, such as fibroblasts, adipocytes, and lymphocytes. This collection of supportive cells makes up what is referred to as the Tumor Microenvironment (TME). These cells are often recruited by the tumor to provide them nutrients, extracellular matrix secretions, and other tumor-promoting factors, and secretion of extracellular vesicles (EV) from the tumor to the surrounding stromal cells are one method by which this recruitment takes place. (134–137). In these studies of EVs, it was found that PTGFRN could be used as a fusion scaffold to deliver toxic compounds to tumor cells, as well as surrounding TME cells, in *in vivo* mouse models, and that the efficacy of the anti-tumor response positively correlated with the expression level of PTGFRN in the EVs (138).

While research investigating the role of PTGFRN in cancer is still in its infancy, studies on other members of the tetraspanin family have shown that tetraspanins can act as both metastasis promoters, as in the case of CD151, as well as metastasis suppressors, such as CD82 (139,140). Cell type may play a role in determining the metastatic influence of tetraspanins. For instance, CD9, the primary binding partner of PTGFRN, has been shown to both promote, as well as suppress, migration ability depending on the cell type studied. CD9 seems to inhibit migration and metastasis in small-cell lung cancer (122,141). However, in melanoma and breast cancer-derived cell lines, CD9 can have quite opposite effects, promoting migration and metastasis in cutaneous melanoma, and

collagen-induced migration in triple negative breast cancer, a phenotype characterized for its aggressive phenotype, while suppressing migration and metastasis in these same cancers when in response to fibronectin (142–145).

Previous research has indicated that PTGFRN is associated with a metastatic-like profile. Colin et al. showed that PTGFRN was integral in the occurrence of tumor angiogenesis, the process of blood vessel and capillary formation previously detailed that is required for tumor cells to enter the larger circulatory system during metastasis (146). Notably, mice bearing tumors that expressed a mutant, truncated form of PTGFRN showed decreased formation of capillary tube-like structures, as well as a significant decrease in hemoglobin in said tumors, indicating that angiogenesis was indeed inhibited by the non-functioning PTGFRN. In lung cancer, PTGFRN expression positively correlated with the status of lung cancer metastasis through the downregulation of its binding partner CD9 (147). Karhemo et al. also discovered that when comparing metastatic triple negative breast cancer to their non-metastatic counterparts, the expression of PTGFRN mRNA and protein was increased sevenfold (148).

PTGFRN has also been found to possibly have value as a prognostic factor when predicting overall survival in Glioblastoma (GBM) patients. Aguila et al. showed that patients whose glioblastoma was categorized as a high PTGFRN expresser had much lower rates of overall survival compared to patients whose glioblastoma expressed PTGFRN in low abundance. Their investigations showed that (1) a reduction of PTGFRN expression in GBM led to radiation sensitivity, due to decreased sensing of DNA-damage and repair, (2) increased PTGFRN expression results in increased signaling of the PI3K/AKT pathway, and (3) increased PTGFRN expression resulted in an increase in the

stability of the PI3K subunit p110β, potentially explaining its relationship with DNA-damage sensing (149). The data generated by all of these experiments indicates that not only is PTGFRN involved in processes associated with a metastatic profile, but may also have some use as a prognostic factor, serving as a potentially valuable target for drug development. However, the specific function of PTGFRN remains unclear and deserves further investigation. This will be carried out here as part of this thesis research.

1.6 Antibody-Drug Conjugates as Cancer Therapy

In the ever-expanding field of anti-cancer therapy, Antibody-Drug Conjugates (ADCs) represent a class of drugs gaining academic, regulatory, and industry attention due to their highly selective targeting capability, high tissue specificity, low off-target effects, and ability to be conjugated to a variety of potent payloads (150). ADCs are comprised of a monoclonal antibody that specifically recognizes a unique cell-surface antigen, a bridging chemical linker, and a cytotoxic drug payload. Each component has diverse variations, which has the potential to be mixed and matched to optimize efficacy and minimize off-target toxicity of the resulting ADC (151).

Today, modern biotechnology has allowed for the large-scale generation and production of monoclonal antibodies. Monoclonal antibodies are large, Y-shaped immunoglobulins produced by B lymphoid cells (152). Antibodies consist of two heavy chains and two light chains, held together by disulfide bonds. Antibodies can be further divided into two main regions, the antigen-binding fragment (Fab), and the fragment crystallisable (Fc). It is the variable Fab region that is responsible for the direct interaction and binding to an antibody's specific epitope on the antigen, with the Fc region being conserved within the species from which it is produced (153). Antibodies

can belong to one of five isotypes: IgG, IgA, IgE, IgM, and IgD. The IgG isotype can be further divided into 4 subclasses: IgG1, IgG2, IgG3, and IgG4. IgA antibodies have two additional subclasses as well, being IgA1 and IgA2 (154,155).

For the purpose of ADC development, the IgG isotype, specifically IgG1, is typically preferred for a variety of reasons, although IgG4 antibodies have recently seen increased attention as ADC candidates due to their lack of antibody effector functions that would normally cause antibody-mediated cytotoxicity (156,157). First, IgG antibodies are often capable of activating immune responses that can lead to antibody-dependent cellular toxicity (ADCC) or complement-dependent toxicity (158). These antibody-mediated responses help amplify the anti-cancer effect of the conjugated payload by enlisting the host immune system in the fight. However, immune responses can also sometimes be detrimental, reaching levels too toxic, and can sometimes occlude the internalization of an ADC (159). Secondly, the half-life of IgG in serum is approximately 23 days, which is much longer than those of other isotypes, which can be anywhere from 2-6 days (160,161). This pharmacokinetic property can also be influenced by the level of glycosylation of an antibody. Glycosylation, which is the addition of carbohydrate sugar chains to a protein, can also help improve resistance to proteolytic degradation, reduce rate of aggregation, and improved thermal stability (162).

Antibodies used as the basis of an ADC typically recognize cell-surface antigens that are cancer specific (neoantigen) or become overexpressed after oncogenesis. While the first generation ADCs were generated using murine antibodies, this led to challenges with immunogenicity and accompanying toxicities. Through advancements in protein bioengineering, most ADCs currently developed are either humanized (complementarity-

determining regions of the Fab region being transferred onto a human IgG framework), chimerized (mouse Fc region of the antibody is swapped with a human Fc region), or developed as fully human IgG in origin (163–165). In most instances, the binding of the antibody to its target induces endocytosis to the cell interior. However, in some ADC designs, this internalization step is not required for its mechanism of action (166).

The chemical linker that attaches the toxic payload to the antibody adds an additional layer of complexity to the compound, as these linkers can be either cleavable or non-cleavable, and carry their own metabolic implications for half-life, efficacy, and toxicity. Non-cleavable linkers offer the highest level of stability in plasma, and lower the potential for off-target toxicity due to the lack of "bystander effect", which is when premature cleavage of the payload outside the target cell allows it to diffuse into neighboring, non-target cells (167). However, the inability to separate the linker from the payload required it to be physically embedded in the structure of said payload. This severely limits the types of payloads that are compatible with non-cleavable linkers, as this can negatively alter the structure, and thus activity of the payload compound (168).

Cleavable linkers can be further divided into enzymatic, chemical, or physiochemical linkers, with chemically cleavable linkers accounting for the widest range of options available. Acid-labile linkers rely on lysosomal trafficking of the ADC, where lysosomal acidification during digestion cleaves the payload from the monoclonal antibody (169). ADCs employing this type of linker have shown instability in plasma, which can result in premature payload cleavage and systemic toxicity.

Enzymatically cleavable linkers typically consist of dipeptide unit that can be targeted and degraded by proteases, such as Cathepsin B or β-Glucuronide, whose

increased expression is commonly found in tumor cell environments (170–172). Roughly 70% of all ADCs employ this type of linker, with the most common form being a Valine-Citrulline linker, although other dipeptide-based linkers do exist (151). Similar to their acid-cleavable counterparts, premature cleavage and systemic toxicity are a main concern, and can therefore result in dose-limiting toxicities. However, advancements in improving these enzymatically cleavable linkers have been made, such as the glutamic acid-valine-citrulline tripeptide linker detailed in a 2022 paper published by Ha et al. Their addition of a glutamic acid at the P3 position reduced the susceptibility of the linker to premature cleavage by extra cellular carboxylesterase 1c, thus increasing plasma stability of the ADC, improving anti-cancer efficacy, and reducing negative side-effects. (173).

A lesser-used type of linker being investigated are physiochemical linkers. These unique linkers require an external activator for cleavage, such as near-infrared (NIR) light. Internalization of the antibody is typically not required with these linkers, as the NIR photocleavage both releases the payload, as well as disrupts the membrane of the cancer cell, which allows the payload to enter the cells (174).

Addition of a linker species to an antibody is typically accomplished by targeting lysine or cysteine residues present in the antibody, owing to their ability to be chemically reduced in order to expose a free thiol group. The average IgG1 molecule has roughly 90 lysine residues, with approximately 30 of them exposed for chemical modification (175). Because of diversity in chemical modification lysine sites, there is typically large heterogeneity in ADC species produced. On the other hand, cysteine conjugation shows a much lower amount of heterogeneity, due to the fact that there are only about 8 possible

interchain conjugation sites (176). Site-specific mutagenesis has increasingly been used to engineer cysteines into antibodies, thus resulting in a much more homogenous species of ADC. By controlling the exact site of the conjugatable residues, lot-to-lot consistency in pharmacokinetics, stability, solubility, and potency is achievable (175,177). While cysteine conjugation offers slightly better control over location and potential number of conjugation sites, it should be noted that lysine conjugation has shown to be slightly more stable, likely due to some cysteine residues being located in the hinge region of the antibody, and thus being more prone to protein accumulation (178). This improved stability can lead to better efficacy from lysine conjugation in *in vivo* experiments.

Selection of the cytotoxic payload is a crucial factor in successful generation of a potent ADC. The original payloads investigated in the first generation of ADCs were anti-metabolites, DNA-crosslinking agents, and microtubule inhibitors, with toxicity profiles which had previously been well-studied and characterized (179). However, challenges such as low antigen expression, low potency, or instability/over-stability of the linker have been difficult to overcome. It is described that the majority of ADCs are only capable of delivering 1-2% of the administered dose, further highlighting the importance of the payload and its required potency (180). The payloads of ADCs that have been approved by the FDA can be classified into one of two groups: 1) DNA-damaging agents, or 2) microtubule inhibitors, with the latter being the most-commonly used. Auristatins (e.g. MMAE), Maytansinoids (e.g. DM-1), and tubulysins all inhibit assembly of tubulin, leading to G2/M cell-cycle arrest and death (181). While not as plentiful as microtubule inhibitors, the utility of DNA-damaging payloads, such as Duocarmycin, pyrrolobenzodiazepines, calicheamicin, and various analogues of

Irinotecan, offer an alternative method of inducing cell death. These exert their anticancer effects through disruption of DNA via chain breaks, or direct binding to DNA, which inhibits various polymerases and/or topoisomerases, and initiates apoptosis (169). There have been investigations into alternative payloads, such as Amatoxins, which inhibit transcription by targeting RNA polymerase, and enzyme payloads, which when administered as an ADC in conjunction with a prodrug, can convert the prodrug into its active form at or nearby the targeted cancer cells, allowing it to diffuse past the cancer cell membrane, and induce apoptosis (182,183). However, these are still in preclinical and clinical investigations.

The use of radionuclides as a payload also provides a novel alternative to traditional chemotherapy and radiation by combining them to create the resultant radioimmunoconjugate (RIC). RICs offer an attractive strategy to overcome the requirement of internalization for the anti-cancer effect, as the distance of decay of the radionuclide is often much larger than the diameter of the cell, leading to deeper penetration of the tumor. And since internalization is not required for RICs, a non-cleavable linker can be used for conjugation, preventing premature cleavage of the radionuclide in plasma and subsequent systemic toxicity (184,185).

The mechanism of action of most ADCs is fairly straightforward. During systemic circulation, the Fab region of the monoclonal antibody will recognize its respective antigen, typically a protein preferentially expressed on the cell surface of a cancer cell. This antibody binding begins a cascade that signals for the cell to initiate endocytosis of the bound protein and antibody. While a fraction of these internalizing proteins get recycled back to the cell surface (186), many more of these endosomes end up fusing

with a lysosome, and the contents of the newly formed endolysosome get degraded by a combination of acidity and various proteases, including the bound receptor, as well as the monoclonal antibody (187). Depending on the linker used, the payload will either be cleaved at this stage, and diffuse out of the endolysosome, or, in the case of non-cleavable linkers, the payload will remain inside until the endolysosome naturally degrades, at which point the payload is free to cause cell death in whatever manner it acts in (DNA damaging, microtubule inhibition, etc.) (188).

1.7 Brief History of Antibody-Drug Conjugates

The idea of using monoclonal antibodies as a method for delivery of toxic drugs was first proposed in the 1970s, when the publication of methodology for large-scale production of monoclonal antibodies was initially released (189). However, it would not be until the late 1990s when a full-formed ADC was submitted for FDA approval, with the introduction of Gemtuzumab ozogamicin (Mylotarg). Mylotarg was originally approved by the FDA in 2000 for treatment of Acute Myeloid Leukemia (AML) by its targeting of CD33 on the surface of AML cells (190). Unfortunately, due to serious liver toxicity and elevated numbers of patient deaths Mylotarg was withdrawn from the market upon request from the FDA (191). As of 2017, Mylotarg has gained re-approval by the FDA after studies showed its value in a different subset of patients, as well as its use in combination therapy (192)

The second ADC to be approved by the FDA was Brentuximab vedotin (Adcetris) in 2011, which targeted the protein CD30 in order to treat Hodgkin Lymphoma, as well as Systemic Anaplastic Large Cell Lymphoma (193). With the approval of these two ADCs, there was still the need for an ADC that could be used to treat solid tumors, as

opposed to the hematological ones that Mylotarg and Adcetris were found to be effective with. The next ADC approved to treat a solid tumor was Trastuzumab emtansine (T-DM1, or Kadcyla), which was approved in 2013 to treat HER2-positive metastatic breast cancer (194). This ADC was unique because the antibody moiety of this ADC had already been approved for treatment in its unconjugated form (sold as Herceptin) for HER-2 positive (HER-2 3+ or HER-2 amplified) breast cancer (195).

In the years following Kadcyla's FDA approval, there was a surge in approved ADCs from 2017-2019. Inotuzumab ozogamicin (Besponsa) was approved to treat B-cell precursor acute lymphoblastic leukemia in 2017, and Moxetumomab pasudotox (Lumoxiti) was approved to treat Hairy Cell Leukemia in 2018, with both of these ADCs targeting CD22 (196,197). 2019 saw the approval of three new ADCs: Polatuzumab vedotin-piiq (Polivy) to treat large B-cell lymphoma, Enfortumab vedotin (Padcev) to treat metastatic urothelial cancer, and Trastuzumab deruxtecan (Enhertu) to treat metastatic HER2+ breast cancer, which target CD79, Nectin, and HER2, respectively (198–200). The latter ADC is another example of using the Trastuzumab antibody as the targeting agent, but with the conjugation of a different payload. The ability to achieve a clinically significant ADC by just switching the conjugated payload to a pre-approved antibody highlights the flexibility of ADCs, and how they may be more advantageous in cancer treatment than systemic chemotherapy.

In 2020, the new ADC Sacituzumab govitecan (Trodelvy) was approved by the FDA. This was the first approved ADC that was designed to treat triple negative breast cancer by targeting the protein Trop-2 (201). In this same year, the FDA also approved Belantamab mafodotin-blmf (Blenrep) to treat multiple myeloma through its targeting of

the protein BCMA (202). 2 years later however, this ADC was withdrawn from the market upon request by the FDA after it failed to meet its endpoint in a DREAMM-3 phase III confirmatory trial (203). Two additional ADCs gained FDA approval in 2021, Loncastuximab tesirine-lpyl (Zynlonta), which targets CD19 to treat Large B-cell lymphoma, and Tisotumab vedotin-tftv (Tivdak), targeting TF-011 for treatment of cervical cancer (204,205). The most recent ADC to gain FDA approval was mirvetuximab soravtansine-gynx (Elahere), which received accelerated approved in 2022 for treatment of ovarian, fallopian tube, and peritoneal cancers that are FRα-positive (206). Table 1.1 summarizes all FDA-approved ADCs.

Antibody-Drug Conjugate	Commercial Market Name	Targeted Cancer	Target	Approval Year
Gemtuzumab Ozogamicin	Mylotarg	Acute Myelogenous Leukemia (AML)	CD33	2000, re-approved in 2017
Brentuximab Vedotin	Adcetris	Hodgkin Lymphoma and Systemic Anaplastic Large Cell Lymphoma	CD30	2011
Trastuzumab Emtansine	Kadcyla	HER2+ Metastatic Breast Cancer	HER2	2013
Inotuzumab Ozogamicin	Besponsa	B-cell Precursor Acute Lymphoblastic Leukemia	CD22	2017
Moxetumomab Pasudotox	Lumoxiti	Hairy Cell Leukemia	CD22	2018
Polatuzumab Vedotin-piiq	Polivy	Diffuse Large B-cell Lymphoma	CD79	2019
Enfortumab Vedotin	Padcev	Urothelial Cancer	Nectin-4	2019
Trastuzumab Deruxtecan	Enhertu	HER2+ Metastatic Breast Cancer	HER2	2019
Sacituzumab Govitecan	Trodelvy	Metastatic Triple-Negative Breast Cancer	Trop-2	2020
Belantamab Mafodotin-blmf	Blenrep	Multiple Myeloma	BCMA	2020, withdrawn in 2022
Loncastuximab Tesirine-lpyl	Zynlonta	Large B-cell Lymphoma	CD19	2021
Tisotumab Vedotin-tftv	Tivdak	Cervical cancer	Tissue factor (TF-011)	2021
Mirvetuximab Soravtansine	Elahere	Platinum-Resistant Ovarian Cancer	FRα	2022

Table 1.2 List of all FDA-approved Antibody-Drug Conjugates

1.8 Advantages of Antibody-Drug Conjugate in Cancer Therapy

The aforementioned ADC Kadcyla (T-DM1) presents a perfect example of how an ADC can be used to improve the therapeutic effect of the original unconjugated monoclonal antibody. In its ADC form, T-DM1 has been reported to be more potent than Trastuzumab alone. HER2-positive cancer patients treated with T-DM1 show an improved 3-year disease-free survival rate of 88.3%, compared to 77% in patients treated with Trastuzumab (152). Only 10.5% of T-DM1 patients suffered distant or metastatic recurrence, compared to 15.9% of patients treated with Trastuzumab, and breast cancer recurrence or death occurred in 12.2% of patients who underwent T-DM1 treatment, as opposed to 22.2% of patients who had Trastuzumab therapy. In addition, patients whose HER-2 expression was immunohistologically scored as lower than 3+ and considered "HER-2 negative" and ineligible for Trastuzumab therapy, were able to benefit from Kadcyla therapeutic effects. In this case, the anti-HER2 monoclonal antibody is capable of binding to HER-2 and blocking its dimerization, which interferes with the receptor's signaling for increased proliferation. By conjugating the maytansinoid DM-1 to this antibody, the therapeutic effect is further propagated by triggering apoptosis via mitotic arrest (153). The clinical benefits obtained with T-DM1 further illustrates a core advantage of ADC therapy compared to treatment with its respective monoclonal antibody alone. They emphasize that coupling the high specificity and activity of the antibody with a potent cytotoxic compound may result in a drug with improved efficacy and enhanced therapeutic window compared to each component separately (154).

One common issue in treating cancer, especially when cancer becomes metastatic, is the problem of drug resistance. Drug resistance in tumors typically arises from the

upregulation of efflux pumps, which work to decrease intercellular concentration of compatible drug substrates. The most common and widely studied of these pumps are P-Glycoprotein (Pgp), as well as the adenosine triphosphate-(ATP) binding cassette (ABC) superfamily of proteins (128,155). The use of an ADC represents a great tool to overcome this drug resistance. If a cancer becomes unresponsive to current treatment due to efflux pump upregulation, then an alternate payload that does not share the same pump can be substituted onto the monoclonal antibody, thus re-sensitizing the cancer to the new ADC.

While the tumor is the primary target of anti-cancer therapies, the cells that make up the tumor microenvironment (TME) are also a potential target in combating cancer. By targeting a cell surface antigen that also gets packaged into EVs with a high-affinity ADC, some of the delivered ADC can be packaged as cargo in these EVs, and could be delivered to the surrounding TME cells, leading to cell death not just confined to the tumor, but to the cells surrounding it as well. (156) While killing of the tumor is the main goal of any anti-cancer therapy, a drug having an anti-proliferative influence on TME cells can result in an additive anti-cancer effect (157). In fact, many FDA-approved ADCs, as well as numerous ADCs currently in development, show sorting into EVs (158). As discussed earlier, PTGFRN happens to be an EV protein, with high levels of expression in EVs secreted by the cells. As such, an ADC targeting PTGFRN would be beneficial in cancer therapy, as its effect could be targeted to the tumor, as well as to the surrounding support cells.

1.9 Conclusion

Mesothelioma and Pediatric Medulloblastoma are two examples of rare and aggressive cancers that display poor prognosis in diagnosed patients. These two cancers currently have unmet needs for tailored therapy to help improve progression-free and overall survival. We have found that both cancers express the cell-surface protein PTGFRN in variable amounts. While this protein has been found to be "associated with" cancer aggressiveness and metastasis, the exact manner in which it is involved has yet to be fully understood. This is investigated further in Chapter 2.

The upregulation of PTGFRN expression in cancer, its cell-surface localization, and packaging into extracellular vesicles make it an attractive target for drug development. Specifically, these features can be taken advantage of through targeting by an Antibody-Drug Conjugate. Advancements in monoclonal antibody production make it relatively easy and cost-effective to produce hundreds of high-affinity antibodies, which can be screened for the requisite properties, providing a good foundation for the development of a targeted ADC. The resultant ADC would be a highly valuable tool to develop new targeted treatment for mesothelioma and medulloblastoma, and potentially reduce the need for harsh systemic chemotherapy, surgeries, and/or radiation.

1.10 Research Objectives

This PhD dissertation project is aimed at investigating the role of PTGFRN and examine its effect on a cancer cell's phenotype using various in vitro assays commonly used to characterize a cell's proliferative and metastatic potential. By identifying the cellular pathways that PTGFRN expression modulation influences, we can then use prior

research on other proteins involved in these same pathways to identify potential binding partners and mechanisms through which PTGFRN could be influencing cancer progression and aggressiveness. In parallel to these studies, we also aimed to develop a fully human monoclonal antibody-drug conjugate that can target PTGFRN on the surface of cancer cells, and deliver a cytotoxic compound to cause cell death, both in vitro and in vivo. Furthermore, such an ADC would provide the foundation for a biological drug that could be carried forward to IND-enabling studies.

In Chapter 2, we utilized immunohistological techniques to assess the level of PTGFRN expression in non-cancerous tissues, as well as multiple different patient-derived cancer tissue samples. Additionally, we employed shRNA and plasmid vector transfection technology to modulate the expression of PTGFRN in mesothelioma and medulloblastoma, as well as in epidermoid carcinoma, in order to assess if alteration of PTGFRN expression influences the cells ability to migrate, proliferate, grow in colonies, and grow in 3D spheroids. We found that PTGFRN expression positively correlated with all of these characteristics, and that inhibition of PTGFRN expression negatively affected a cell's metastatic-like phenotype. From this data, we then investigated how PTGFRN was directly influencing this phenotype. By utilizing fluorescent confocal microscopy and immunoprecipitation assays, we identified the cell-surface adhesion protein E-Cadherin and Integrin B1 as being co-localized to the same cellular location as PTGFRN, and indicated that E-Cadherin and PTGFRN may potentially be binding partners, although mass spectrometric proteome analysis carried out provided us with conflicting results, warranting further investigation. We also found evidence that PTGFRN expression is involved in the cellular process of autophagy, providing another avenue by

which PTGFRN may be influencing a cancer cell's metastatic phenotype. This was also confirmed by mass spectrometric proteome analysis.

In Chapter 3, we detail our discovery of PTGFRN as a potential drug target, and describe our efforts to produce a fully human monoclonal antibody that recognizes cell surface PTGFRN, which can then be used to create a novel antibody-drug conjugate for treatment of mesothelioma and medulloblastoma in both in vitro and in vivo studies. We first develop a proof-of-concept murine antibody that we conjugate to the ribosome-inhibiting compound saporin in order to prove that PTGFRN can indeed be internalized by antibody binding, and can serve as a valid target for ADC development. This prototype ADC shows moderate efficacy in all cell lines tested. We then detail the production of a new, fully human monoclonal antibody which was conjugated to the cytotoxic compound duocarmycin using a cleavable valine-citrulline peptide linker. This second-generation anti-PTGFRN ADC shows markedly high efficacy, in both in vitro assays, as well as in in vivo tumor-bearing mice, with no observable off-target toxicities. These studies lend additional evidence to support that PTGFRN is an important protein that modulates a cancer cell's ability to progress to a more aggressive, metastatic-like phenotype.

Chapter 2
PTGFRN and Cancer

2.1 Introduction

The previously cited work by Colin et al. has demonstrated the effect of a truncated mutant form of PTGFRN on angiogenesis (146). This mutant acted as a dominant negative, leading to a reduction in proliferation of human endothelial cells when administered exogenously both *in vitro* and *in* vivo. In particular, these experiments showed that treatment of mice injected with tumour-enriched Matrigel plugs with this mutant form of PTGFRN resulted in decreased tumor size, as well as decreased vascular formation in said tumors, and less hemoglobin present in tumor samples. These findings demonstrate a causal inhibition of angiogenesis by PTGFRN inactivation, demonstrating the requirement of functioning PTGFRN in a major cellular process required for cancer metastasis (146). We then investigated whether PTGFRN was involved in other processes involved in cancer metastasis. Namely, we examined the effect of PTGFRN expression on a cell's ability to proliferate at low cell densities in low-serum concentrations, ability to migrate through a porous membrane, ability to grow in colonies, and ability to grow in 3D spheroid culture. If we find that PTGFRN is involved in any of these processes, then such a protein would be of great interest for potential drug development.

In this chapter, two experimental approaches were used to study this possibility. In the first approach, the phenotype of cells where PTGFRN expression had been inhibited by transient siRNA expression, or stable expression of PTGFRN shRNA was examined. In particular, we were able to significantly and stably decrease the expression of PTGFRN in epidermoid carcinoma (A431) and pediatric medulloblastoma (DAOY), two cell lines with high PTGFRN expression, by using shRNA specific to PTGFRN.

Inversely, the mesothelioma cell line (MSTO-211H) was found to be a relatively low PTGFRN-expressing cell line. As such, we significantly increased PTGFRN expression in mesothelioma using DNA plasmid vector transfection. After isolation of stable single-cell clones from each cancer line, the clones were then assessed in various *in vitro* functional assays. We found PTGFRN expression to positively correlate with the cell's ability to proliferate, migrate, grow in colonies, and form 3D spheroids.

Based on these results, we then looked at any potential protein interactions between PTGFRN and other proteins that have been well-described in colony and spheroid formation. These experiments indicated that PTGFRN and its binding partner Integrin β1 may also be directly complexing with the adhesion molecule E-Cadherin, a trimer of proteins that has not been previously reported. The discovery of this interaction may offer a potential explanation on how PTGFRN influences the progression of cancer. PTGFRN was also found to influence the conversion of LC3 into LC3B, a marker of autophagy, one method of programmed cell death, suggesting yet another method by which PTGFRN may be regulating the progression of cancer, thus making PTGFRN an ideal candidate for drug development.

In parallel to these functional assays, mass spectrometric proteome analysis was carried out on A431 cells and their PTGFRN-knockdown counterparts, as well as the PTGFRN co-IP products, for a more comprehensive look at the effect of PTGFRN expression, and the proteins and cellular pathways involved/affected. These mass spectrometric results verified much of what we observed in the phenotypic assays, with the exception of the PTGFRN-E-Cadherin interaction, which must be further investigated.

2.2 Materials and Methods

2.2.1 Cell Culture

All cell lines used in this study were obtained from the American Type Culture Collection (ATCC, Manassas, VA). All cell cultures were maintained in a 5% CO_2 incubator at 37°C. A431 (CRL-1555), DAOY (HTB-186), and MSTO-211H (CRL-2081) cells were cultured in DMEM/F12 medium (1:1 mixture) supplemented with 50µg/ml Gentamicin and 5% FBS. All reagents were purchased from Thermo Fisher (Waltham, MA).

2.2.2 Immunohistochemistry

The anti-PTGFRN mouse monoclonal antibody 1B4 was generated and validated in our laboratory. Mesothelioma Tissue Array slides (TissueArray.com LLC, T392b) were deparaffinized by three incubations in Xylene, and rehydrated by successive washes with 100% and 95% ethanol (three each), finished by incubation in distilled water (three times). Antigen Retrieval was not required. Slides were blocked with Background Terminator (Biocare Medical, BT967) for 40 minutes at room temperature, then incubated with 1B4 antibody (1µg/mL) diluted in Antibody Enhancer Solution (5% Goat Serum, 10mM Glycine, 0.05% Tween20, 0.1% Triton X-100, 0.1% H_2O_2) for 30 minutes at room temperature. Slides were washed three times in PBS containing 0.2% Tween-20 (PBS-T) for 5 minutes each, then covered with a drop of ImmPRESS anti-Mouse Polymer solution (Vector Laboratories, MP-7452), and incubated for 30 minutes at room temperature. The slides were washed with 0.2% PBS-T for 5 minutes three times before adding a drop of ImmPACT Chromogen Substrate (Vector Laboratories, SK-4105) and

incubating for 5 minutes. After washing with water for 5 minutes, the slides were counterstained with Mayer's Hematoxylin (Millipore Sigma, MHS16). The slides were dehydrated using ethanol and xylene and mounted with a coverslip. Images were captured using an Olympus BX40 microscope using TSView Version 7 software.

2.2.3 Silencing/Overexpression of PTGFRN and Screening

A431 and DAOY cells were transfected with two different human PTGFRN shRNAs (Fenics Bio, Halethorpe, MD), as well as one scrambled control shRNA (Sequences can be found in Table 2.1).

	Sequence
Control shRNA	Scrambled
PTGFRN shRNA #1	TAGCCTTAAGAATGAATATGAA
PTGFRN shRNA #2	GTGGTATGTTTTGCTTTCCTAA

Table 2.1 Table of PTGFRN shRNA sequences

To overexpress PTGFRN, MSTO-211H cells were transfected with pcDNA3.1 plasmid vector (Thermo Fisher) containing a human PTGFRN cDNA insert. Empty vector was used as negative control. All transfections were carried out with Lipofectamine 3000 reagent (Thermo Fisher), according to the manufacturer's instructions.

After transfection, the pooled cells were sorted and dispensed as single cells into a 96-well plate by the Hana Single Cell Dispenser (Namocell, San Jose, CA). These single

cell clones were then expanded and screened via flow cytometry and immunoblot to select for the lowest and highest PTGFRN-expressing clones for each cell line.

2.2.4 Immunoblotting

Cells at ~80% confluency were lysed in RIPA buffer containing protease inhibitor cocktail. 20µg samples of total cell lysate were prepared, and diluted with reducing SDS+DTT sample buffer. After heating to 100^{o}C for 5 minutes, and cooling on ice, all samples were run on 4-12% Bis Tris gels (Genscript, Piscataway, NJ). After separation, proteins were transferred to a PVDF membrane, and blocked in 5% milk-PBST for 1 hour at room temperature. Following blocking, membranes were incubated with the anti-PTGFRN primary antibody (Bio-techne, Minneapolis, MN) at a concentration of 0.2µg/mL in 5% milk-PBST overnight at 4^{o}C. The next day, membranes were washed in PBST, then incubated in Rabbit-anti-Sheep-HRP (Jackson ImmunoResearch,West Grove, PA) antibody in 5% milk-PBST (1:2000) for 1 hour at room temperature. Membranes were then developed with ECL solution in an Azure Biosystems 280 chemiluminescent unit (Azure, Dublin, CA).

2.2.5 Proliferation Assay

All clones selected for functional assays were detached and collected with PBS-5mM EDTA. 250 cells /well (done in triplicate) were then plated in multiple 96-well plates in DMEM/F12 + gentamycin containing 0.2% FBS. These plates were then incubated in a 5% CO2 incubator at 37°C. At each time point, a plate was removed, and ATP levels were measured with the CellTiter-Glo assay reagent (Promega, Madison, WI) using a Molecular Devices LMaxII luminometer (San Jose, CA).

2.2.6 Migration Assay

Transwell inserts and a 96-well plate (Corning Inc., Corning, KY) were coated overnight at 4ºC with Type II Rat Collagen (40µg/mL) in sterile DI water. Coating solution was aspirated the next morning, and allowed to completely air dry. For MSTO-211H cells, a 24-hour serum-starvation step was performed before cell collection. Cells were detached via 5mM EDTA, and washed and re-suspended with DMEM/F12 + 0.1% BSA. $7.5x10^4$ cells (A431 and MSTO-211H) or $5x10^4$ cells (DAOY) were seeded inside the inner chamber of the insert. The outer chamber was filled with DMEM/F12 + 5% FBS. A431 cells were allowed to migrate for 18 hours, DAOY cells for 6 hours, and MSTO-211H cells for 48 hours. A standard curve of cell numbers for each cell line was plated in the 96-well plate, and allowed to attach for 5 hours. All incubations were done in a humidified, 5% CO2, 37ºC incubator.

After respective incubation times, the inserts were removed from their chamber, and non-migratory cells were removed with a cotton swab. Standard curve and inserts were fixed for 10 minutes in 4% paraformaldehyde, then placed in a 0.05% Crystal Violet solution (Fisher Scientific, Hampden, NH), and allowed to stain overnight at room temperature. Images of the inserts were taken, and stain was eluted via a citric acid solution for quantification of cell number migrated compared to the standard curve of cell number described above.

2.2.7 Clonogenic Assay

All A431, DAOY, and MSTO-211H clones were plated in duplicate at 200, 100, and 50cells/well in a 6 well plate in DMEM/F12+ 5% FBS. These plates were incubated at 37ºC for 10 days, at which point the cell culture media was aspirated, the wells were

washed with PBS, and the cells were fixed for 10 minutes in 4% Paraformaldehyde. After fixation, paraformaldehyde was removed, and the cells were stained in a 0.005% Crystal Violet solution for 20 minutes. Wells were washed 3 times with H_2O, and images were captured, and colony numbers were counted.

2.2.8 3D Spheroid Culture

2.2.9 Immunofluorescence

The anti-PTGFRN human antibody 8C7 was generated in-house. Conjugation of 8C7 to Alexa Fluor 555 was performed with Zip Alexa Fluor™ Rapid Antibody Labeling Kits (Thermo Fisher), following manufacturer instructions.

Chambered coverslips (Thermo Fisher) were coated overnight at 4°C in 50µg/mL Poly-D-Lysine (Millipore Sigma, Rockville, MD) in sterile deionized water. Next day, aspirated coating solution from the coverslips, and allowed the coverslips to air-dry for 2 hours. $8x10^4$ cells were seeded in each chamber, and allowed to attach overnight in a 37°C humidified 5% CO_2 incubator. The next day, cells were washed once with PBS and fixed with 100% methanol chilled to -20°C for 10 minutes. After three washes in PBS, cells were incubated with 1µg/mL 8C7-Alexa Fluor 555, 1:200 Anti-E-Cadherin-Alexa Fluor 488 (rabbit polyclonal; Cell Signaling, Danvers, MA), 1:100 anti-Integrin β1-Alexa Fluor 647 (mouse monoclonal; Abcam, Boston, MA), and 1µg/mL Hoechst 33342 (Thermo Fisher) diluted in 0.2% PBST + 1% BSA overnight at 4°C. The next day, coverslips were washed three times with 0.2% PBST, then mounted in ProLong™ Glass Antifade Mountant solution (Thermo Fisher Scientific). Slides were allowed to cure overnight at 4°C, then viewed using a Nikon A1 point-scanning laser confocal microscope (NIS-Elements, 100X).

For autophagy immunofluorescence, coverslips and cells were prepared in the same method, with the exception of the fixation step. The cells were fixed in 4% Paraformaldehyde for 10 minutes, then permeabilized in 0.2% TritonX-100, followed by three PBS washes. Incubation with 1µg/mL anti-LC3B antibody (rabbit polyclonal; Abcam) and Hoechst 33342 was performed overnight at 4°C. After three washes in PBST, incubation with 5µg/mL Goat-anti-Rabbit-Alexa Fluor 555 (Abcam) was done at 4°C for 2 hours. Washing, mounting, and visualization was performed as outlined above. Table 2.2 summarizes the antibodies used in the immunofluorescence assay.

Antibody	Supplier	Catalog Number
PTGFRN (8C7)	Generated In-House	N/A
E-Cadherin	Cell Signaling Technology	3195S
Integrin β1	Abcam	ab214706
LC3B	Abcam	ab48394

Table 2.2 Antibodies used in immunofluorescence assays

2.2.10 Co-Immunoprecipitation

Cells were lysed in 1% Brij-O10 lysis buffer containing protease inhibitor cocktail, and precleared with protein G agarose beads (Protein Mods, Madison, WI) overnight at 4°C. The next day, aliquots of lysates (250µg) were incubated with 10µg of either control human IgG, 8C7, anti-E-Cadherin (rabbit polyclonal; Novus Biologicals, Centennial, CO), or anti-Integrin β1 (mouse monoclonal; Bio-techne) overnight at 4°C.

The next day, Protein G agarose beads were added to the lysates, and mixed constantly for 2 hours. After 5 washes with 1% Brij-O10 lysis buffer, 2X SDS+DTT sample buffer was added, and the beads were heated to 100^{o}C for 5 minutes, then cooled on ice. The elutions were then run on multiple gels and analyzed by immunoblot as outlined above with their respective antibodies. Table 2.3 summarizes the immunoprecipitation antibodies used in this section.

Antibody	Supplier	Catalog Number
PTGFRN (8C7)	Generated In-House	N/A
E-Cadherin	Novus Biologicals	NBP3-14687
Integrin β1	Bio-Techne	MAB1778

Table 2.3 Antibodies Used in Immunoprecipitation Assays

The anti-E-Cadherin immunoblot antibody was purchased from Cell Signaling. The anti-Integrin β1 immunoblot antibody was purchased from Fortis Life Sciences. The anti-GAPDH immunoblot antibody was purchased from Cell Signaling. The Goat-anti-Rabbit-HRP antibody was purchased from Jackson ImmunoResearch Laboratories. Table 2.4 summarizes the immunoblot antibodies used.

Antibody	Supplier	Catalog Number	WB dilution
PTGFRN	Bio-Techne	AF4495	0.2µg/mL
E-Cadherin	Cell Signaling Technology	3195S	1:1000
Integrin β1	Fortis Life Sciences	A303-735A	1:4000
LC3B	Abcam	ab48394	1:1000
GAPDH	Cell Signaling Technology	2118S	1:4000
horseradish peroxidase goat anti-Rabbit	Jackson ImmunoResearch	111-035-144	1:2000
Horseradish peroxidase anti-Sheep	Jackson ImmunoResearch	313-035-045	1:2000

Table 2.4 Antibodies Used in Immunoblotting

2.2.11 Proteomic analysis via liquid chromatography-tandem mass spectrometry

Cell lysis and protein digestion were performed as previously described (207). Briefly, samples were lysed in a lysis buffer containing 5% sodium dodecyl sulfate (Sigma, L4509), 50 mM triethylammonium bicarbonate (1 M, pH 8.0) (Sigma, 7408). Proteins were extracted, and separated on a nanoACQUITY Ultra-Performance Liquid Chromatography analytical column (BEH130 C18, 1.7 µm, 75 µm x 200 mm; Waters Corporation, Milford, MA, USA) over a 185-min linear acetonitrile gradient (3–40%) with 0.1% formic acid on a nanoACQUITY Ultra-Performance Liquid Chromatography system (Waters Corporation, Milford, MA USA) and analyzed on a coupled Orbitrap Fusion Lumos Tribrid mass spectrometer (Thermo Scientific, San Jose, CA USA). Full

scans were acquired at a resolution of 240,000m/z, and precursors were selected for fragmentation by high-energy collisional dissociation of 35% for a maximum 3-s cycle. The MS/MS raw files were processed with Proteome Discoverer (PD, version 2.5.0.400, Thermo Fisher Scientific) using Sequest HT search engine against a UniProt human reference proteome (release 2022.04, 20292 entries). Searches were configured with static modifications for carbamidomethyl on cysteines (+57.021 Da), dynamic modifications for oxidation of methionine residues (+15.995 Da), precursor mass tolerance of 20 ppm, fragment mass tolerance of 0.5 Da. Trypsin was used as digestion enzyme with maximum of two missed cleavages. The minimum and maximum peptide lengths were set as 6 and 144, respectively. Label-free quantification was performed using Minora feature detector, a tool embedded in the PD bioinformatics platform (208). For high confidence results, protein identification was filtered to 1% false discovery rate (FDR) in peptide spectra match (PSM), peptide, and protein levels. The FDR was calculated using the Percolator algorithm embedded in PD. Next, the exported protein abundance values were analyzed and visualized using Perseus software (version 1.6.14.0) (209). To ensure high confidence in statistical analysis, data were further filtered to include only proteins identified without any missing values in all the biological samples. The quantitative protein data were $\log_2$ transformed and further normalized using median centering. Two-tailed student's t-test was applied for comparisons between two conditions ($p < 0.05$) to determine if each treatment group was significantly different from the control group. Enrichment of functions and signaling pathways of the differentially expressed proteins (DEPs) identified from different conditions was performed using Metascape (http://metascape.org) as described previously (207,210).

2.2.12. Statistical Analysis

All statistical analyses were performed using GraphPad Prism's (v.7). Significance across the mean values of each triplicate group was done using two-tailed t-test for two experimental groups. For comparison of two groups, Student's t-test was used. Results are shown as mean ± SD. Significance was determined at $P < 0.05$ (*), $P < 0.01$ (**), $P < 0.001$ (***).

2.3 Results

2.3.1 PTGFRN is highly expressed in cancerous tissue, but not in healthy tissue

Surface-protein expression that differs based on malignancy offers an attractive strategy for targeting cancers in a tissue-specific manner. Thus, we set out to determine if PTGFRN expression is differentially expressed in cancerous tissue compared to healthy, non-cancerous tissue. Using our anti-PTGFRN antibody 1B4 (generated in-house), we can detect and grade PTGFRN expression in FFPE tissue sections. Looking at the staining patterns in the numerous healthy tissue sections screened (Figure 2.1**)**, PTGFRN expression was undetectable, depicting no significant differences in 1B4 staining compared to a non-immune mouse IgG control antibody. However, when screening various head & neck, lung, pancreas, and kidney cancer tissue samples, Squamous Cell Carcinoma, Melanoma, Papillary Renal Cell Carcinoma, Clear Cell Carcinoma, and Pancreatic Duct Adenocarcinoma all demonstrated an increased expression of PTGFRN to a strongly detectable level.

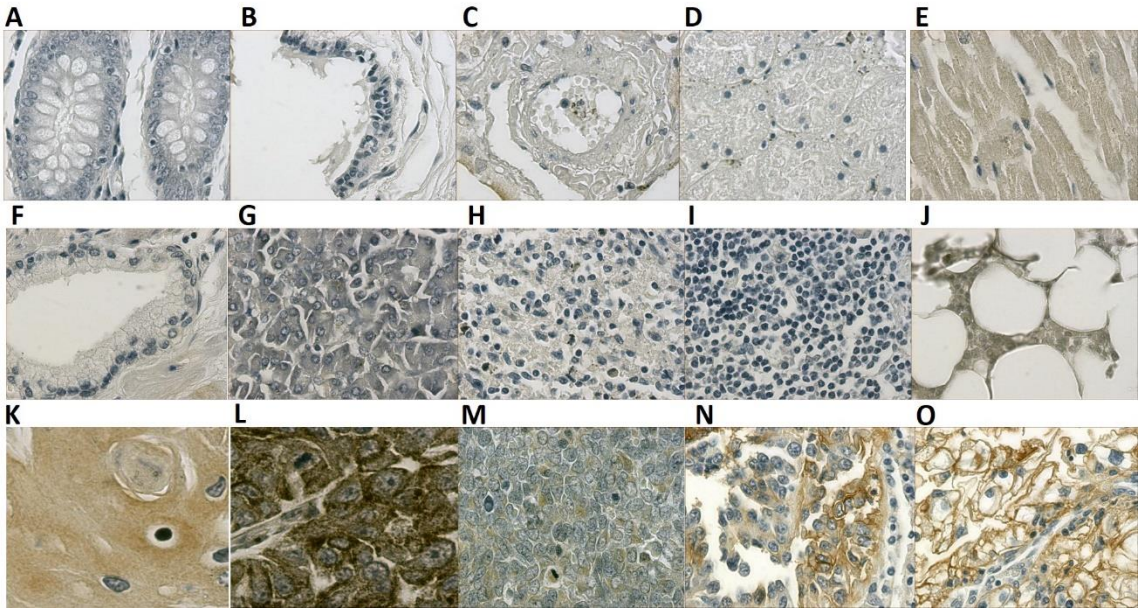

Figure 2.1 Immunohistological analysis of PTGFRN expression in healthy and cancerous tissue sections. Tissue microarrays were stained using the IHC antibody 1B4 to assess expression level of PTGFRN. Healthy non-cancerous tissue, such as (A) Colon, (B) Breast, (C) Lung, (D) Kidney, (E) Cardiac, (F) Prostate, (G) Pancreas, (H) Spleen, (I) Tonsil, and (J) Bone Marrow show little to no PTGFRN. Cancerous tissue samples from (K) Squamous Cell Carcinoma, (L) Melanoma, (M) Pancreatic Duct Adenocarcinoma, (N) Papillary Renal Cell Carcinoma, and (O) Clear Cell Carcinoma all show elevated expression levels of PTGFRN.

2.3.2 Progression of Mesothelioma from Benign to Malignant phenotype correlated with a significant increase in PTGFRN Expression

When determining the relative level of protein expression in tissue, histopathologic scoring is a commonly used semi-quantitative tool that can be used to grade expression level on a 0-3 scale (159). Using patient-derived mesothelioma tissue arrays, normal lung tissue has undetectable PTGFRN expression, while benign mesothelioma tissue shows a modest increase in PTGFRN, being graded as a 1+ score. Malignant mesothelioma tissue shows a significant increase in PTGFRN staining, with its expression level reaching a 3+ score (Figure 2.2). This observation remains consistent

with previous findings, which show PTGFRN expression correlating with cancer aggressiveness and metastatic potential.

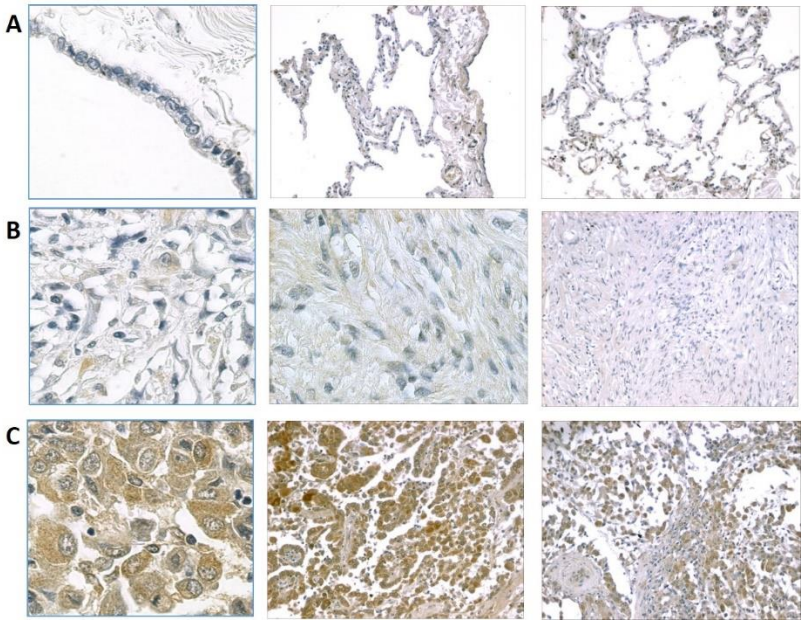

Figure 2.2 Immunohistological analysis of PTGFRN expression in mesothelioma tissue sections. Mesothelioma tissue microarray was stained using the IHC antibody 1B4 to assess expression level of PTGFRN in different stages of mesothelioma, including (A) non-cancerous lung pleural tissue, (B) Benign mesothelioma, and (C) Malignant mesothelioma. PTGFRN expression increases drastically when mesothelioma becomes its most aggressive.

2.3.3 PTGFRN Expression is Positively Correlated with Characteristics Associated with a Metastatic-like Profile

In order to compare physical characteristics of cells after PTGFRN expression modulation, stable knockdown clones of A431 and DAOY cells were generated after transient PTGFRN shRNA transfection. Likewise, a stable PTGFRN-overexpressing clone of MSTO-211H was created by transient transfection of human PTGFRN cDNA. Immunoblots in figure 2.3 indicate the relative PTGFRN expression level of each of these resulting clones.

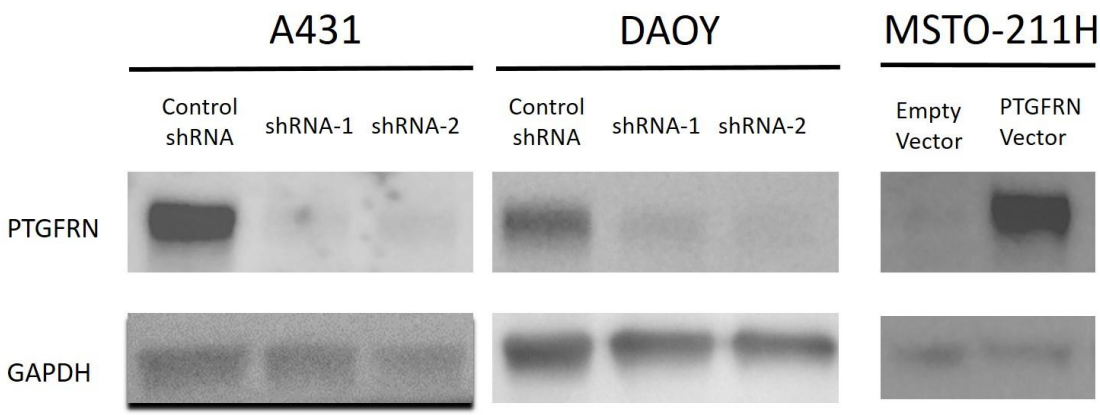

Figure 2.3 PTGFRN expression level after transfection of shRNA or PTGFRN cDNA. Western Blot analysis shows that PTGFRN expression was significantly decreased after shRNA transfection in A431 and DAOY cells, and significantly increased after cDNA transfection in MSTO-211H cells.

When comparing proliferative capability, A431 and DAOY clones whose PTGFRN expression was silenced by shRNA showed markedly lower levels of proliferation in low-serum conditions (0.2% FBS) compared to the control shRNA clones. In the MSTO-211H clone whose PTGFRN expression was increased by stable plasmid transfection, proliferation levels were significantly higher compared to the empty vector clone that did not show any proliferation (Figure 2.4).

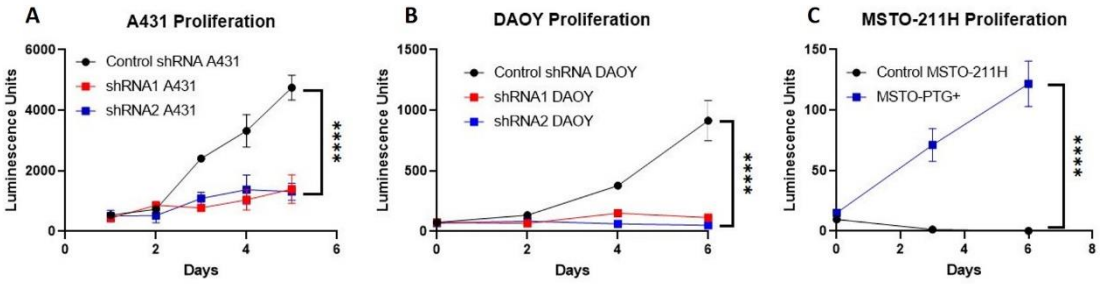

Figure 2.4 Comparing proliferative capability of cells after PTGFRN silencing/overexpression. Ability to proliferate at low serum levels (0.2% FBS) was severely decreased after PTGFRN silencing by shRNA in (A) A431 and (B) DAOY cells, while PTGFRN overexpression in (C) MSTO-211H resulted in a significant increase in proliferation.

We next examined the migration capabilities of cells where PTGFRN expression had been silenced or overexpressed. As shown in Figure 2.5, cell migration capability was severely inhibited after PTGFRN silencing by shRNA in A431 and DAOY cells. This effect was not as strong in DAOY cells as it was in A431 cells. However, DAOY cells seem to have much higher innate migratory capability, as an incubation time of only 6 hours in our control shRNA clone showed high numbers of cell migrated. Nonetheless, PTGFRN knockdown significantly reduced migration in both of these cells lines. In contrast, PTGFRN overexpression in MSTO-211H cells showed a significant increase in migration levels compared to the empty vector control clone. This experiment was carried out with A431 cells transfected with PTGFRN siRNA as well, and we saw the same decrease in migration after knockdown by this method. These results can be found in Appendix 1, as Figure 1A.1.

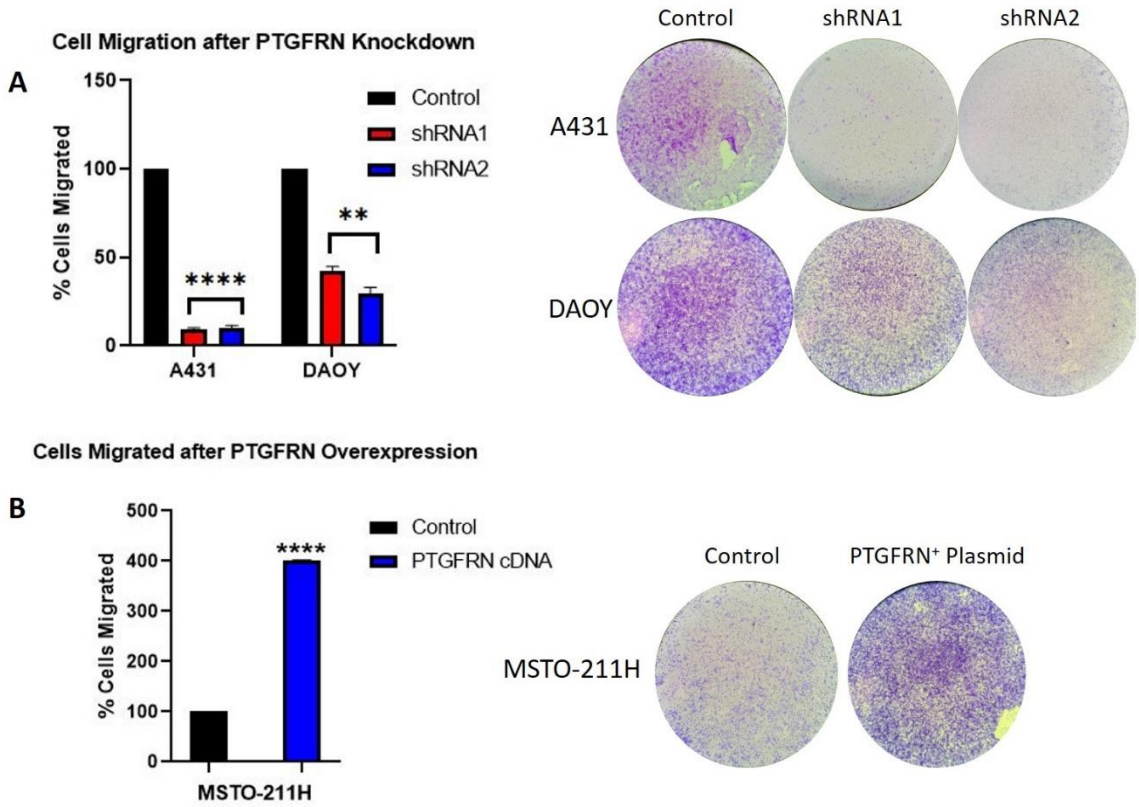

Figure 2.5 Effect of PTGFRN expression on migration capability. (A) PTGFRN silencing via shRNA in A431 and DAOY cells results in a significant reduction in cell migration, while (B) overexpressing PTGFRN in MSTO-211H cells resulted in a significant increase in migration levels.

We also examined whether PTGFRN expression had an effect on clonogenic ability of the cells. The shRNA knockdown clones in both A431 and DAOY showed a significant decrease in the number of colonies formed, whereas PTGFRN overexpression in MSTO-211H cells significantly increased the number of colonies formed, even at cell numbers as low as 50 cells/well. In the MSTO-211H control cell line, no colonies were formed at all, even at the highest cell number tested of 200 cells/well (Figure 2.6).

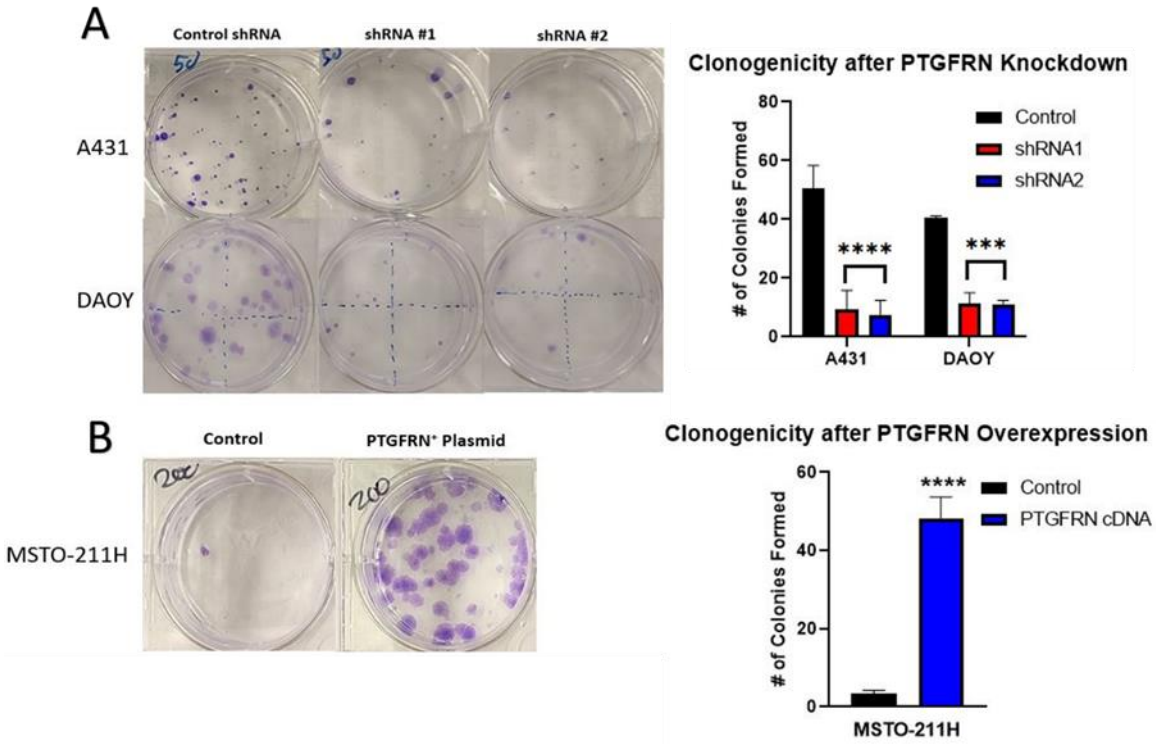

Figure 2.6 PTGFRN expression affects cells ability to grow in colonies. Reduction in PTGFRN expression in A431 and DAOY (A) results in less colonies formed when plated at low cell density, while PTGFRN overexpression in MSTO-211H (B) shows a significant increase in colonies under these same conditions.

Spheroid formation in three-dimensional culture (3D) is a hallmark of cancers that contain higher populations of cancer stem cells (CSC), which express increased levels of various stemness genes, such as SOX2, OCT4, C-MYC, etc. (211). It is these CSCs that metastasize and that may be responsible for cancer relapse. Based on the results above, we determined the ability of cells to form 3D-spheroids when PTGFRN level had been altered. After PTGFRN knockdown, A431 and DAOY shRNA clones were unable to form spheroids of the same size, shape, and/or number compared to the control shRNA clones (Figure 2.7). In the case of DAOY PTGFRN shRNA cells, while cell aggregates did form, and appear spheroidal in shape, the moment the plates were disturbed, or we attempted to collect the aggregates, they immediately deteriorated into single cells. In

contrast to these, the control shRNA clone spheroids could be manipulated repeatedly without the breakdown of the spheroids into single cells. Spheroid assays were carried out with A431 cells transfected with PTGFRN siRNA as well, and we saw the same inability to grow as spheroids after PTGFRN knockdown by this method. These results can be found in Appendix 1, as Figure 1A.2.

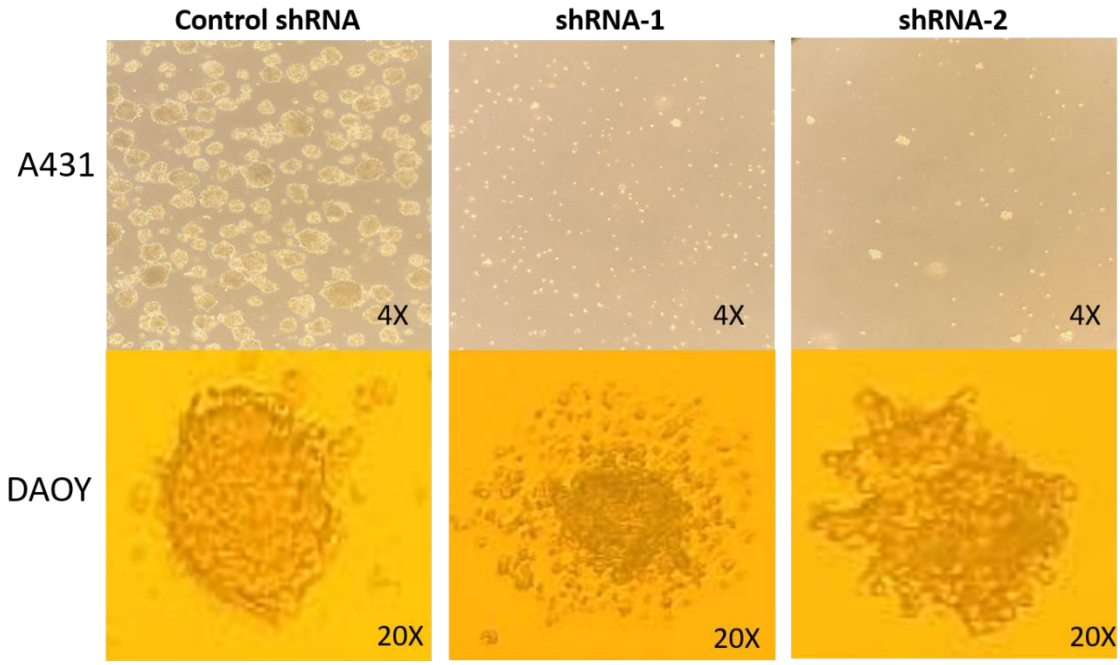

Figure 2.7 Knockdown of PTGFRN expression inhibits spheroid formation. Loss of PTGFRN via shRNA knockdown prevented A431 and DAOY cells from being able to grown in 3D spheroid conditions. Any aggregates that did form in the shRNA clones broke apart when disturbed, whereas the control cell spheroids could be easily manipulated without losing their 3D shape.

All of the assays detailed above measure characteristics that are commonly associated with metastatic cells. Thus, it is concluded that PTGFRN expression in cancer cells appears to contribute to a more proliferative, aggressive, and metastatic-like phenotype.

2.3.4 PTGFRN Knockdown Cells Grown in Spheroid Conditions Show Decreased Levels of Integrin β1 and E-Cadherin

Much attention has been paid to two main drivers of spheroid formation; specifically, E-Cadherin and Integrin β1. The work done by Lin et al. showed that the binding of Integrin β1 to extracellular matrix (ECM) proteins triggered what they referred to as a "lag phase", where cells began to upregulate the expression of p, which was essential for spheroid compaction and growth (212). Because of this, we compared the expression of integrin β1 and E-Cadherin in the A431 PTGFRN shRNA knockdown cells grown in 3D spheroid conditions compared to shRNA control cells. We observed that the expression level of Integrin β1was reduced by approximately 30% compared to the control spheroids, and E-Cadherin expression was reduced almost 90% compared to the control spheroids (Figure 2.8). This decrease in Integrin β1 and E-Cadherin expression was not seen in PTGFRN shRNA cells grown in 2D monolayer (Figure 1A.3 in Appendix 1), which leads us to believe that PTGFRN expression is required for expression increases in Integrin β1 in spheroids, which then triggers the accumulation of E-Cadherin responsible for spheroid compaction and growth, as outlined by Lin et al (212). By knocking down PTGFRN expression via shRNA, Integrin β1 levels do not reach the threshold required to trigger E-Cadherin accumulation, reducing the cell aggregates seen in the knockdown clones that did not retain their spheroidal integrity during manipulation.

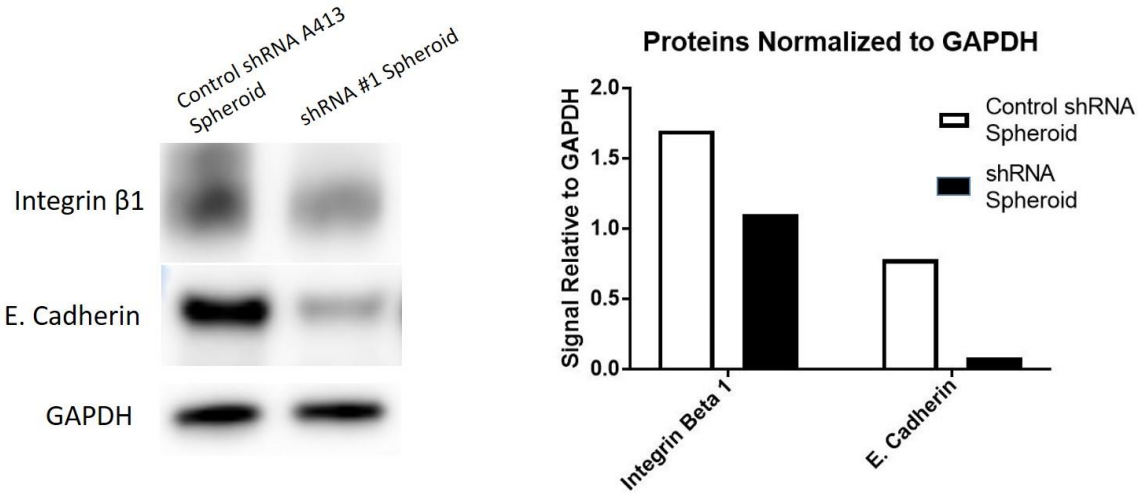

Figure 2.8 Effect of PTGFRN Knockdown on Proteins Involved in Spheroid Formation. PTGFRN shRNA-transfected A431 cells grown in spheroid culture conditions did not show the increase in Integrin β1 and E-Cadherin levels seen in control shRNA spheroids

2.3.5 PTGFRN, Integrin β1, and E-Cadherin All Co-Localize to Cell-Cell Junctions, and Are Capable of Directly Binding to Each Other

To evaluate the association between PTGFRN, Integrin β1, and E-Cadherin, fluorescent microscopy was used to determine if these three proteins were present in the same subcellular area, which would be the first step in determining if they could possibly be directly bound to each other. Using confocal fluorescent microscopy, we observed that fluorescent antibodies raised against PTGFRN, Integrin β1, and E-Cadherin all seemed to co-localize in the cell junctions (Figure 2.9).

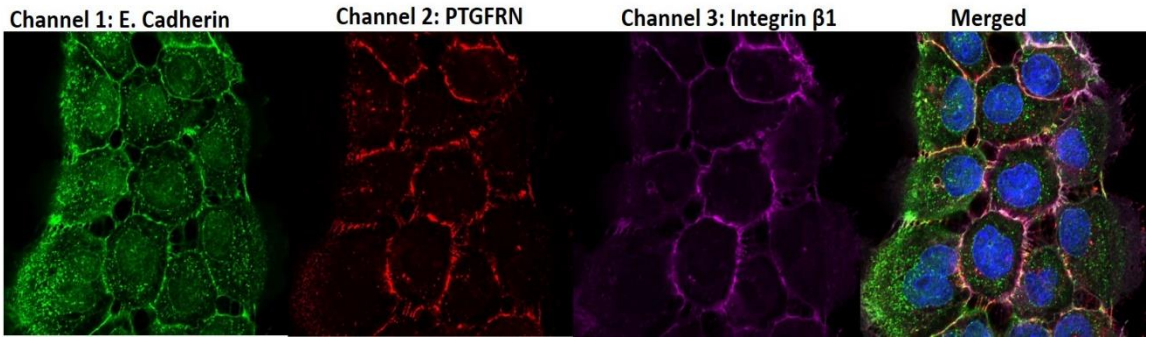

Figure 2.9 Co-localization of PTGFRN, E-Cadherin, and Integrin β1.
A431 Immunofluorescence using specific antibodies show that PTGFRN (Red), E-Cadherin (Green), and Integrin β1 (Purple) all co-localize together in the cell junction areas (Pink). Nucleus counterstained with Hoechst 33342 (Blue).

However, in order to determine if this is true co-localization, or just signal overlap, co-immunoprecipitation assays were also carried out in tandem. By lysing cells in a weak detergent lysis buffer such as Brij O10, direct protein-protein interactions were uninterrupted. Immunoprecipitation using our anti-PTGFRN antibody 8C7 showed the presence of both Integrin β1 and E-Cadherin in the IP elution. IP using an anti-Integrin β1 antibody showed the presence of PTGFRN and E-Cadherin, and IP using an anti-E-Cadherin antibody showed the presence of PTGFRN and Integrin β1 (Figure 2.10).

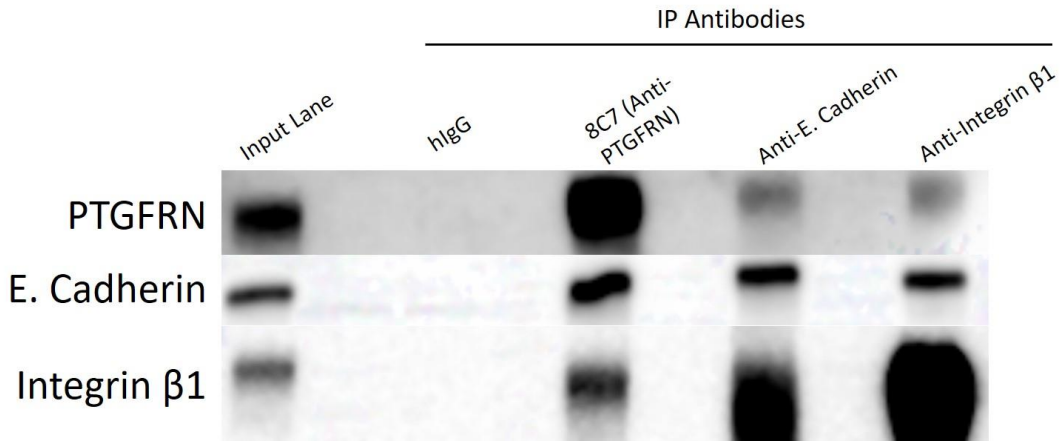

Figure 2.10 Direct Interaction between PTGFRN, E-Cadherin, and Integrin β1. Co-immunoprecipitation using specific antibodies show that PTGFRN, E-Cadherin, Integrin β1 are all directly interacting with each other, and thus can co-IP with each other.

This experiment seems to demonstrate that these three proteins are indeed directly associated with each other and confirms the co-localization observed with the imaging study. However, this does not help us determine if they are in a 3-protein complex, part of an even larger complex with other protein members, or three distinct binding configurations, with only two proteins associated at one time. Of note, immunofluorescence experiments looking at Integrin β1 and E-Cadherin on A431 PTGFRN shRNA cells was carried out, and the co-localization of these two proteins was not affected in any obvious way (Figure 1A.4 in Appendix 1).

2.3.6 Loss of PTGFRN Expression Results in an Increase in LC3B Accumulation, Indicating an Increase in Autophagy

After PTGFRN knockdown in A431 cells, we observed changes in the cell's morphology compared to the control clone; namely, an increase in large vacuole-like structures. Such structures are commonly viewed as an indicator of the cellular process

known as autophagy. To determine if this was the case, expression levels of LC3B, a marker of autophagy, were measured using immunofluorescence, as well as western blot analysis. In both cases, LC3B expression was increased in our PTGFRN shRNA knockdown clones compared to the control shRNA clone (Figure 2.11). As a positive control, we treated A431 with the compound Metformin, a known autophagy inducer.

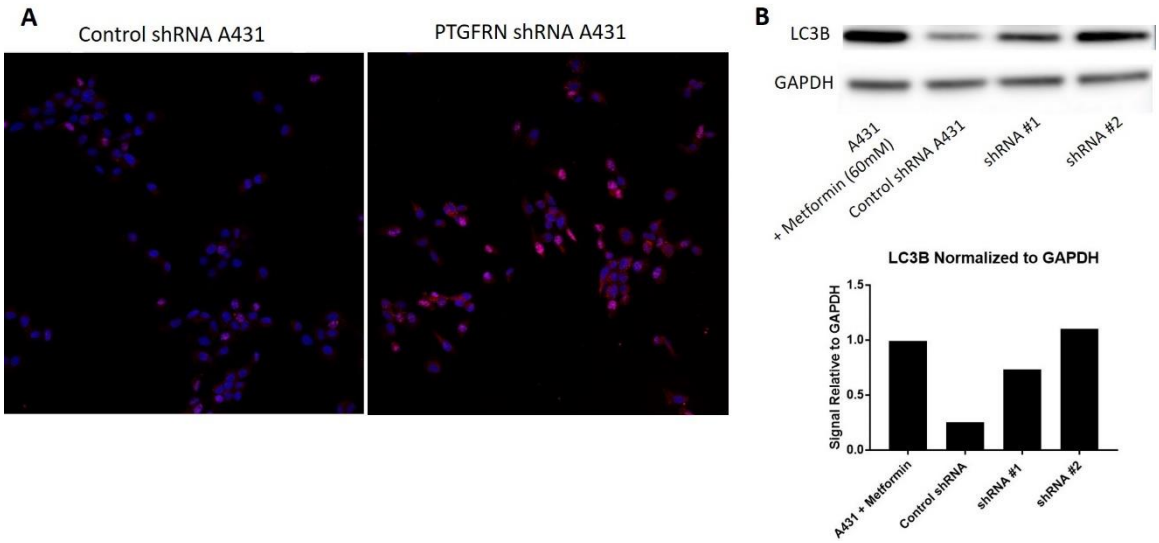

Figure 2.11 PTGFRN Knockdown Influences Autophagy. Knockdown of PTGFRN in A431 results in an increase in LC3B accumulation. This is visible via (A) fluorescent microscopy where higher levels of LC3B (red) can be seen in the shRNA cells, compared to the control cells, as well as (B) immunoblot, including the positive control of A431 cells treated with metformin, which functions by inducing autophagy in cells.

This provides another pathway by which PTGFRN is influencing a cells phenotype. It is possible that loss of PTGFRN expression acts as a stress or starvation factor that causes the cell to undergo autophagy for survival. This “pro-survival” mechanism of autophagy has been observed in cancer cells before (213). However, further investigation is needed to better elucidate exactly how PTGFRN is influencing autophagy, and whether it is “pro-cell death” or “pro-cell survival” in nature.

2.3.7 Effect of PTGFRN on Cellular Proteome

In order to further characterize the effect of PTGFRN expression on cancer cells phenotype and gain some insight on the molecular drivers of the phenotypic changes observed, we performed mass spectrometric analysis on control shRNA A431 cells vs. PTGFRN shRNA A431 cells, and assessed proteins whose expression was significantly increased or decreased in response to PTGFRN knockdown. Using this extensive list of modulated proteins, we performed pathway analysis in order to determine what cellular functions and pathways were most affected by the attenuation of PTGFRN.

After PTGFRN knockdown, three of the top four pathways that were most downregulated involve the synthesis of various metabolites, metabolic precursors, and energy, especially those involved in the Respiratory Electron Transport Chain. In addition to this, other significantly inhibited pathways include ER to Golgi Anterograde Transport, Ribosome Biogenesis, Exosome Function, NADH Oxidation, and VEGFA-VEGFR2 signaling. PTGFRN knockdown also resulted in increases of other pathways, with many of them involved in immune system signaling, such as Cytokine Signaling, Interferon Signaling, and Neutrophil Degranulation. The heatmap in Figure 2.12 outlines the top 20 cellular processes that were increased or decreased after PTGFRN knockdown by shRNA transfection. Table 2.5 contains the top 10 proteins found to be upregulated after PTGFRN, and Table 2.6 outlines the top 10 pathways whose proteins were upregulated after PTGFRN knockdown. Table 2.7 is comprised of the top 10 proteins whose expression was downregulated after PTGFRN knockdown, followed by Table 2.8, which contains the pathways most impacted by those downregulated proteins. Tables 1A.1 and 1A.2 in Appendix 1 are the complete list of all pathways and gene expressions found to

be upregulated and downregulated, respectively, after PTGFRN knockdown in A431 cells.

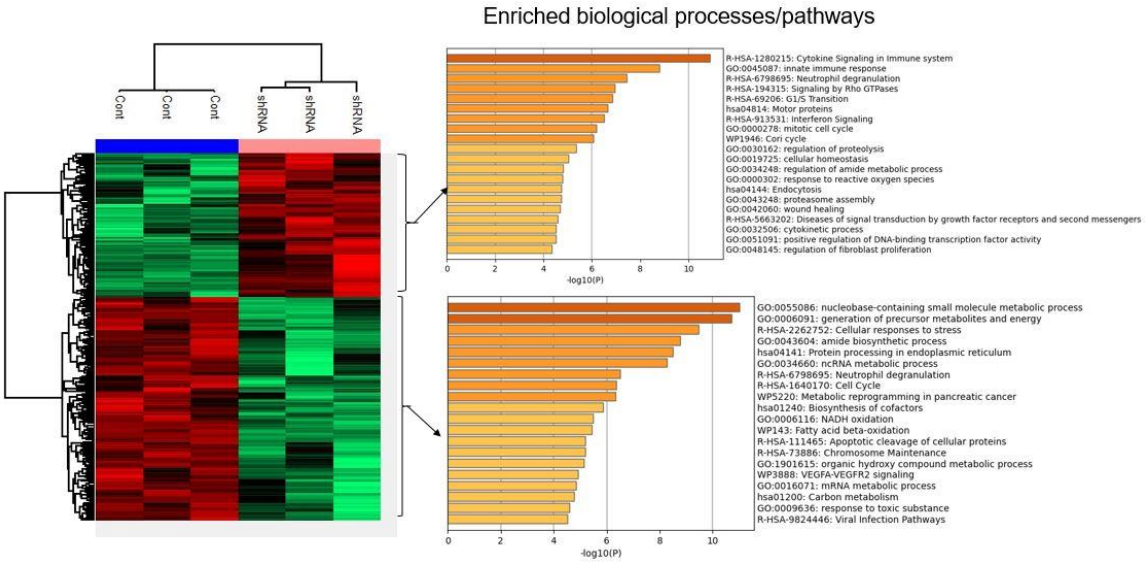

Figure 2.12 Mass Spectrometric Proteome Analysis after PTGFRN Knockdown. Heat map displaying the top 20 cellular processes impacted by PTGFRN knockdown based on Student T-test analysis.

Accession Number	Gene Name	Protein Description
Q92817	EVPL	Component of desmosome and epidermal cornified envelope
P06702	S100A9	Calcium-binding protein
O95786	RIGI	RNA Helicase-DEAD Box Protein
P01583	IL1A	Interleukin 1 Alpha; Cytokine
O95999	BCL10	Immune Signaling Adaptor
P01833	PIGR	IgA/IgM Transport Receptor
P29966	MARCKS	Substrate for Protein Kinase C
P80188	LCN2	Hydrophobic Molecule Transporter
Q9Y316	MEMO1	Regulator of cell motility
P14317	HCLS1	Actin-binding protein

Table 2.5 Top 10 Most Upregulated Proteins After PTGFRN Knockdown

Pathway	Adjusted p-value
Cytokine Signaling in Immune system	2.87E-07
Innate immune response	1.78E-05
Neutrophil degranulation	2.02E-04
Signaling by Rho GTPases	4.98E-04
G1/S Transition	4.98E-04
Motor proteins	6.35E-04
Interferon Signaling	6.44E-04
Mitotic cell cycle	8.65E-04
Cori cycle	1.06E-03
Regulation of proteolysis	3.15E-03

Table 2.6 Top 10 Most Upregulated Cellular Pathways After PTGFRN Knockdown

Accession Number	Gene Name	Protein Description
Q8IVL5	P3H2	Post-translational 3-hydroxylation enzyme
Q14155	ARHGEF7	Rho protein activator
Q8NHV4	NEDD1	Centrosome interactor with γ-tubulin
P54652	HSPA2	Heat-shock protein, protein folding chaperone
P13646	KRT13	Keratin 13
Q8N1T3	MYO1H	Microfilament binding and organization
Q9UK22	FBXO2	Ubiquitin protein transferase enzyme
P13647	KRT5	Keratin 5
Q16658	FSCN1	F-actin organization
O95260	ATE1	Arginyl-tRNA-protein transferase

Table 2.7 Top 10 Most Downregulated Proteins After PTGFRN Knockdown

Pathway	Adjusted p-value
Nucleobase-containing small molecule metabolic process	2.15E-07
Generation of precursor metabolites and energy	2.18E-07
Cellular responses to stress	1.87E-06
Amide biosynthetic process	7.71E-06
Protein processing in endoplasmic reticulum	9.02E-06
ncRNA metabolic process	1.18E-05
Neutrophil degranulation	2.82E-04
Cell Cycle	3.19E-04
Metabolic reprogramming in pancreatic cancer	3.19E-04
Biosynthesis of cofactors	8.11E-04

Table 2.8 Top 10 Most Downregulated Cellular Pathways After PTGFRN Knockdown

2.3.8 Mass Spectrometric Analysis of 8C7 Co-IP Pull-down Products

While we were able to show that both Integrin β1 and E-Cadherin were able to co-immunoprecipitate with PTGFRN using our 8C7, we also wanted to determine other potential direct binding or complex partners. Therefore we chose to perform mass spectrometric analysis of the A431 cell lysate immunoprecipitated with 8C7 antibody to identify the proteins in 8C7 sample compared to control IgG IP. From this list of proteins, pathway analysis was also performed, indicating which processes had proteins members who were either directly bound to, or complexed with PTGFRN.

The cellular process which had by far the most members found to be associated with PTGFRN was the Metabolism of RNA. VEGFA-VEGFR2 signaling, Regulation of Translation, and Ribonucleoprotein Complex Biogenesis also had many protein constituents pulled down along with PTGFRN. Figure 2.13 displays the heatmap that outlines the top 20 processes whose protein members were found to co-IP with PTGFRN, indicating protein interactions. Table 2.9 displays the top 10 proteins that were the most abundantly present besides PTGFRN after co-IP with 8C7, while Table 2.10 contains the top 10 pathways associated with these proteins. Table 1A.3 in Appendix 1 contains the list of all pathways and proteins and their respective pathways whose presence was found to be significantly increased in our 8C7 IP sample compared to our control IgG IP. Figure 2.14 highlights some of the pathway and co-IP analysis after PTGFRN knockdown.

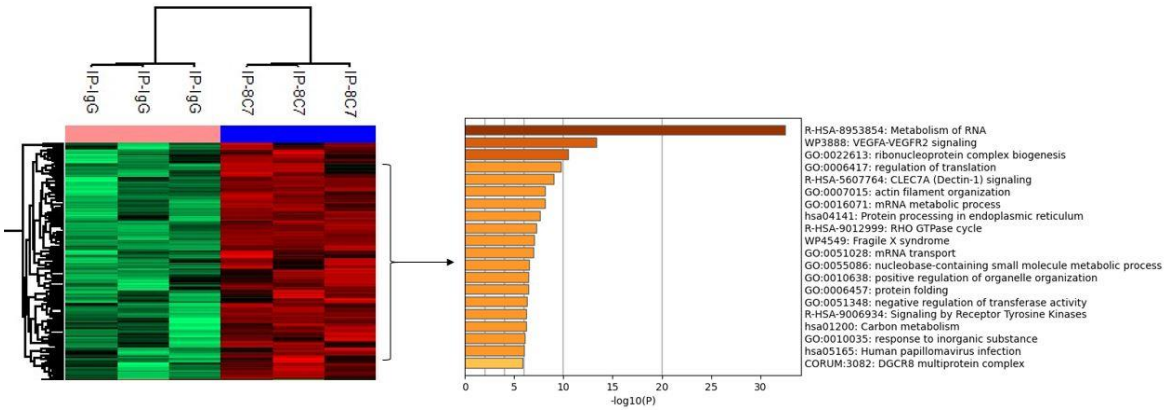

Figure 2.13 Mass Spectrometric Analysis of PTGFRN Co-IP Products. Heatmap displaying the top 20 cellular processes whose members were found to co-IP along with PTGFRN using our 8C7 antibody compared to an IgG control antibody. Statistical significance was determined by Student T-test analysis.

Accession Number	Gene Name	Protein Description
P08579	SNRPB2	Ribonuclear protein
P50851	LRBA	Cellular component recycler in autophagy
O60294	LCMT2	Leucine carboxyl methyltransferase 2
Q8IWA5	SLC44A2	Choline Transporter
Q9ULC3	RAB23	Vesicle trafficking protein
Q02878	RPL6	Ribosomal protein
Q13685	AAMP	Angio-associated migratory cell protein
Q8N573	OXR1	Oxidation resistance protein
Q9Y5V0	ZNF706	Zinc-finger protein
Q9HCU5	PREB	Transcription factor that regulates prolactin (PRL) gene expression

Table 2.9 Top 10 Most Abundant Proteins in PTGFRN Co-Immunoprecipitation with 8C7

Pathway	Adjusted p-value
Metabolism of RNA	6.20E-29
VEGFA-VEGFR2 signaling	2.60E-11
ribonucleoprotein complex biogenesis	1.66E-08
regulation of translation	8.59E-08
CLEC7A (Dectin-1) signaling	4.49E-07
actin filament organization	2.76E-06
mRNA metabolic process	3.12E-06
Protein processing in endoplasmic reticulum	8.79E-06
RHO GTPase cycle	1.74E-05
Fragile X syndrome	2.52E-05

Table 2.10 Top 10 Cellular Pathways Represented in PTGFRN Co-Immunoprecipitation with 8C7

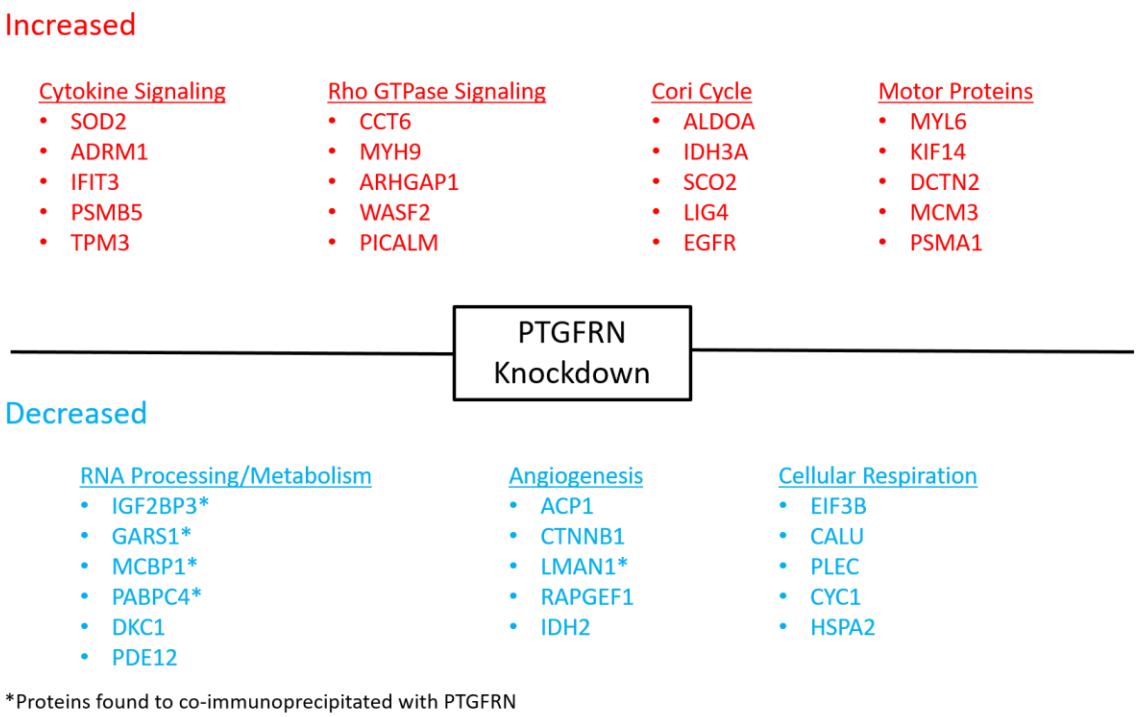

Figure 2.14 Major Pathways Affected by PTGFRN knockdown. This figure highlights some major pathways whose protein member's expression were increased or decreased following PTGFRN knockdown. Proteins followed by an asterisk (*) were also found to co-IP with PTGFRN, indicating association with PTGFRN.

2.4 Discussion

While surgical procedures and chemotherapeutic agents have seen vast improvements over the years, metastasis still makes up >90% of all cancer deaths (49,50). Because of this, our understanding of the mechanics of metastasis, as well as the proteins involved in the process, must also evolve. As such, we have further characterized the protein Prostaglandin F2 Receptor Negative Regulator, or PTGFRN, and its potential role in contributing to a metastatic-like profile. We have shown a positive correlation between PTGFRN expression level, and a cells ability to proliferate, migrate, grow in colonies at low cell number, and form multicellular 3D spheroids in three different cell types, characteristics which are hallmarks of a metastatic cancer cell. From these

investigations, we identified the adhesion molecule E-Cadherin as a potential direct binding partner to PTGFRN, although this was not verified in the mass spectrometric analysis, which is discussed in more detail below.

Additionally, we demonstrated that loss of PTGFRN expression coincides with the increase in the conversion of LC3B, a key marker of a cellular process called Autophagy, which may be another contributing factor to PTGFRNs effect on cancer metastasis. With this data, we hypothesize that PTGFRN could be a player in the latter steps of cancer metastasis, when the cell has already detached from its primary tumor, and has begun to settle in a secondary organ site. PTGFRN could be involved in the binding to extracellular matrix proteins of this secondary site and facilitates the increase in expression levels of E-Cadherin and Integrin β1 needed to establish the multicellular secondary tumor.

Previous research has been undertaken to understand how PTGFRN influences a cells proliferative capability. Recently, Mala et al. published their results in investigating the effect of PTGFRN expression in glioblastoma cells, and found very similar results to ours, with PTGFRN silencing resulting in decreased proliferation, migration, and colony formation in GBM cells, among other features tested. With regards to proliferation, they found that the attenuation of PTGFRN was found to lower signaling of the ERK, AKT, and mTOR pathways (214). A decrease in ERK and AKT phosphorylation was not seen in the three cells lines we tested (data not shown). As discussed previously, tetraspanin function can have opposing effects based on cell type.

The published results of Mala et al. not only support the results presented here, but also add to the list of cell types in which PTGFRN expression correlates to a

metastatic-like phenotype. And like their GBM cell type, two of the cell lines tested here are derived from rare and aggressive cancers (Pediatric Medulloblastoma and Mesothelioma). Unlike Mala et al., our work here also looks at the effect of increasing PTGFRN expression in a naturally low-expressing cell line, as opposed to solely looking at PTGFRN silencing.

PTGFRN's primary binding partner, the tetraspanin CD9, has also been found to promote proliferation of certain cell types, but is still generally categorized as a metastasis suppressor, whereas CD151, a secondary partner of PTGFRN, is classified as a metastasis promoter (215,216). Interestingly, PTGFRN has been found to downregulate the expression of both CD9 and CD151 at the cell surface (146). While on the one hand, the downregulation of a metastasis suppressor would support PTGFRN contributing to a metastatic-like profile, the downregulation of a proliferation promoter and a metastasis promoter such as CD151 would theoretically be contrary to the observed effect of PTGFRN overexpression outlined above. This perhaps points to the involvement of other binding partners and/or signaling molecules being required to determine the final effect of tetraspanins on a cells phenotype.

Previous research has indicated that both the transmembrane domains, as well as the cytoplasmic domain of PTGFRN regulates the effect on cell motility (217). In leukocytes, PTGFRN has been found to interact with ERM (Ezrin-Radixin-Moesin) proteins, which act as intermediaries between the cell membrane and cytoskeletal components (78). The rearrangement of cytoskeletal proteins is a requirement for cell motility, and has been found to be partially driven by not only ERM, but by the suppression of E-Cadherin expression, which leads to decreased cell junction tightness,

as well as altered membrane protrusion activity (218). Somewhat perplexing is the reported observation of collective migration in breast cancer, where rather than a single cell migrating individually, groups or clusters of cells migrate as a unit. In these units, the leading invading cells retain their E-Cadherin expression in order to stay connected to the other cells within the migrating cluster, while still being able to migrate (219). While this seems to contradict the idea that less E-Cadherin is required for cell migration, it perhaps highlights the importance of expression level, where falling below a certain threshold is sufficient, and not necessarily complete silencing of E-Cadherin, or perhaps modulation by binding partners such as PTGFRN and/or other tetraspanin partners.

As discussed previously, one of the last stages of metastasis after systemic circulation and extravasation is the colonization of a secondary organ site. The ability of a single cancer cell to be able to proliferate and form a secondary tumor is a property that can be empirically measured *in vitro* through the use of the Clonogenic Assay. Clonogenicity is considered a hallmark property of malignant cancer cells, or cells transforming from benign to malignant type (220,221). Cells that exhibit enhanced clonogenicity have also been found to express higher amounts of stem-cell markers, such as ALDH, CD31, and OCT4 (222–224). We have looked at the effect of PTGFRN overexpression on multiple stem cell-like markers through the use of Microarrays and the Aldefluor Assay, and found a negligible effect on the expression of any tested stemness markers after PTGFRN knockdown or overexpression (Data not shown). Because of this, we can surmise that the effect of PTGFRN on clonogenesis may not be through promoting a stem cell-like phenotype.

Similar to clonogenic ability, the ability to form spheroids have previously been linked to the increased expression of stemness makers (225). Our discovery that E-Cadherin and PTGFRN directly interact with each other, and that silencing of PTGFRN inhibits both Integrin β1 and E-Cadherin accumulation in 3D culture lends further evidence that PTGFRN can perhaps modulate the activity of multiple protein and protein complexes involved in cell migration and spheroid growth.

Stable knockdown of PTGFRN by shRNA in A431 cells showed a significant increase in the conversion of LC3I into LC3B, a well-studied marker of the process known as autophagy (226). Autophagy is a category of cell death by which a cell selectively sequesters protein aggregates, lipids, and organelles, and delivers them for lysosomal degradation in response to stress or starvation, after which the degraded material is then recycled by the cell (227–229). This process has been found to play a pivotal role in cancer suppression, as demonstrated in liver carcinogenesis (230,231). However, the role of autophagy in survival during periods of starvation also mean that it can be used as a protective mechanism by cancer cells (232). Curiously, in a breast cancer model, autophagy was found to be supportive of the growth of primary tumors, yet inhibit metastatic outgrowth to a secondary site (233).

Integrin β1, a known regulator of autophagy, exerts its suppressive effect by disrupting mTORC2/Akt phosphorylation (234). Furthermore, it directly interacts with the Receptor Tyrosine Kinase (RTK) c-Met, facilitating survival signaling from the autophagosome membrane (235). Integrins play a crucial role in cell attachment to the extracellular matrix (ECM), and their disruption can trigger anoikis, a form of cell death (236). Autophagy, activated as a survival mechanism during detachment-induced anoikis,

has been observed in such conditions (237). E-Cadherin is also linked to autophagy, as it gets sequestered into the autophagosome in breast and lung cancers (238,239). This autophagy-driven degradation of E-Cadherin is believed to regulate tumor progression, as the loss of E-Cadherin is commonly observed in migratory cells, breast cancers with poor prognosis, and dormant cancer cells (226,240). Determining whether the autophagy observed after PTGFRN knockdown is protective or pro-cell death would provide valuable insight. If this autophagy is determined to be pro-death, this would further support the positive correlation between PTGFRN expression and a metastatic-like phenotype.

The mass spectrometric analysis performed here provided a copious amount of data for us to learn about the binding/complex partners of PTGFRN, and the overall effect of PTGFRN expression modulation in cancer. Firstly, the cellular processes whose members were decreased in expression after PTGFRN knockdown appear to validate some of our phenotypic findings described above. The inability to biosynthesize metabolic precursors, transport proteins for appropriate post-translational modification, or even produce normal levels of ATP from NADH oxidation would certainly likely result in diminished ability to proliferate in low-serum conditions, and would severely limit how many cells could grow into colonies from a single cell if said cell has lower proliferative capability. Secondly, while migration was not a pathway listed in the database these results were analyzed within, there are indeed proteins found to be involved in migration and invasion whose expression is decreased after PTGFRN knockdown. The proteins NUDT1, DKC1, RBBP7, and RSF-1 (all contained within the Chromosome Maintenance pathway), as well as LRRC59 (VEGFA-VEGFR2 signaling

pathway), have all been found to be involved in, and influence, migration in cancer cells (241–245). Likewise, while spheroid formation does not appear to be a listed pathway in the Metascape database, several proteins, such as Beta Catenin, CYC1, Plectin, and PRDX2 were found to be downregulated after PTGFRN knockdown, and studies have shown that downregulation of each of these proteins have been found to be detrimental to spheroid formation (246–248).

Our observations on autophagy also seem to be supported with this analysis, with proteins such as RILPL2 and TRIM65 being upregulated after PTGFRN knockdown. Both of these proteins have been found to positively regulate autophagy (249,250). In addition to multiple autophagy-related proteins being increased after PTGFRN knockdown, we also discovered that proteins involved in the pathway of apoptotic cleavage of cellular proteins were also significantly decreased. This seemingly confirms that the autophagy observed after PTGFRN knockdown is protective, and a mechanism to prevent apoptosis of the cancer cell. Thus, loss of PTGFRN exhibits a stress to the cell, which in turn causes the cell to turn to autophagy to stave off apoptosis. The upregulation of numerous immune system signaling and cell cycle pathways after PTGFRN knockdown seem to indicate that PTGFRN typically functions as a negative regulator of these processes, although further research will need to be done to elucidate the exact mechanism by which PTGFRN performs said negative regulation.

When analyzing the proteins that are directly bound/complexed with PTGFRN, and can immunoprecipitate using an anti-PTGFRN antibody, the pathway whose members showed the most interaction with PTGFRN was Metabolism of RNA. In fact, of the top 20 pathways whose proteins were found to be bound to PTGFRN, 9 of them are

involved or associated with RNA processing and/or translation. Proteins involved in the formation of the ribosome subunits (RPL3, RPS8), RNA polymerase (POLR2H), removal of introns from pre-mRNA (SNRPB2), and translation initiation factors (EIF2a) were among the most abundantly co-immunoprecipitated along with PTGFRN. This is quite interesting, as these proteins are typically found in the cytoplasm, located nearby the endoplasmic reticulum (251), whereas PTGFRN is most commonly found in the plasma membrane. This result could mean that PTGFRN serves as a membrane anchor, working as a part of a large scaffold to stabilize the ribosome, as well as the various polymerases and translation factors, so that they can properly process RNA. PTGFRN could also be functioning as a trafficking protein, making sure that these components reach their required subcellular locations from the Golgi Apparatus, but not actually contributing to their overall function. Regardless, these results show that there seems to be intracellular PTGFRN whose functions differ from those associated with its plasma membrane form. It is unclear at this time if these differing functions are due to distinct isoforms through alternative splicing, different glycosylation patterns, or if the subcellular location of PTGFRN determines their overall functions.

Another pathway whose protein members were found to co-IP with PTGFRN was that of VEGFA-VEGFR2 signaling, which is a pathway that was also found to be significantly attenuated following PTGFRN knockdown. Notably, the only protein that was found to be both downregulated after PTGFRN knockdown, as well as bound to PTGFRN in our co-IP was LMAN1, a protein found to regulate protein folding, transport to the Golgi from the Endoplasmic Reticulum, and other organelle organization, lending further support to the hypothesis that PTGFRN seems to be highly involved in RNA

processing and translation, and the trafficking of the newly-translated protein to the Golgi and further cellular locations.

The co-immunoprecipitation analysis also verified some of our above immunoblot data, confirming that PTGFRN was able to also pulldown Integrin β1. However, E-Cadherin, while indeed found to be present in the pulled-down proteins, was not found to be statistically significantly present in quantities higher than those seen in the control IP samples. This is concerning, and warrants more exploration to determine if our immunoblot data was a fluke, or where this discrepancy may have originated from. We have verified that our anti-E-Cadherin immunoblot antibody is specific to E-Cadherin by transfecting E-Cadherin siRNA into these cells, and confirming that the western blot band attributed to E-Cadherin decreased after transient knockdown. Regardless, more work will need to be undertaken in order to definitively conclude that PTGFRN is a direct binding partner of E-Cadherin.

To conclude, we have found elevated PTGFRN expression to be associated with a metastatic-like phenotype in three different cancer cell lines. The proliferative, migratory, and clonogenic capability of these cancer cells, as well as their ability to form 3D spheroids, drastically decreased following PTGFRN abrogation, and increased in PTGFRN-overexpressing cells. Using previous knowledge of the proteins that drive spheroid formation, we found evidence of direct protein-protein interactions between PTGFRN and the proteins Integrin β1 and E-Cadherin using co-immunoprecipitation methods. In parallel to these assays, mass spectrometric analysis was carried out on A431 cells and their PTGFRN-knockdown counterparts, as well as the PTGFRN co-immunoprecipitation products, for a more comprehensive look at the effect of PTGFRN

expression, and the proteins and cellular pathways involved/affected. These mass spectrometric results verified much of what we observed in the phenotypic assays, with the exception of the PTGFRN-E-Cadherin interaction, which needs to be further explored. The results in total reported in this chapter point to a role of PTGFRN in cancer progression and offer the possibility that it could also be a target for drug development.

Chapter 3
PTGFRN as a Target for ADC Development

3.1 Introduction

The studies described in Chapter 2 support the hypothesis that PTGFRN expression directly or indirectly controls several characteristics of a cancer cell's phenotype, and thus could be involved in cancer metastasis. Also of note was the fact that healthy tissue samples screened for their expression of PTGFRN did not show significant levels of PTGFRN, while various cancerous tissues examined showed elevated PTGFRN expression. This would suggest that PTGFRN has therapeutic potential and that PTGFRN could be targeted by an internalizing monoclonal antibody in the form of an Antibody-Drug Conjugate, which could deliver to PTGFRN positive cancer cells a toxic payload, which could be tested by *in vitro* and *in vivo* animal studies.

In this chapter, we describe how we originally identified PTGFRN as a potential antibody target using mass spectrometric analysis. After confirming PTGFRN's identity, we then conjugated the ribosome-inactivating compound Saporin to our first-generation murine antibody 33B7 as a proof-of-concept ADC. Initial testing of this 33B7-based ADC showed moderate activity, both in vitro and in vivo.

From this data, we then developed and characterized a second-generation, fully human anti-PTGFRN antibody, referred to as 8C7. This human antibody displayed improved physical and binding characteristics compared to the 33B7 mouse antibody. In addition, we opted to use the alternative payload Duocarmycin for this new ADC, as this

compound was found to be more efficacious, and ADCs using this payload have previously been carried further into clinical trials, although to date, none have been granted approval. This second-generation ADC showed remarkedly higher activity, and no obvious signs of off-target toxicity in tumor-bearing mice. This data indicates that PTGFRN could very well be a valid target for ADC development, and that our 8C7-Duocarmycin-based ADC should be further developed and investigated in potential IND-enabling studies.

3.2 Materials and Methods

3.2.1 Cell Culture

All cell lines were obtained from the American Type Culture Collection (ATCC, Manassas, VA). The hamster spindle cell carcinoma cell line AGSCC-3 was isolated in our laboratory. All cell cultures were incubated in a 5% CO2 incubator at 37°C. HEK-293A cells, as well as all transfected clones derived from HEK-293A cells, were cultured in Dulbecco's Modified Eagle's Medium (DMEM; HyClone, Cat. SH30022.02) with 5% fetal bovine serum (FBS). Culture medium for the PTGFRN-transfected HEK-293A cells also contained 600μg/mL of G418. AGSCC-3, A431 (CRL-1555), DAOY (HTB-186), and MSTO-211H (CRL-2081), MDA-231 (CRM-HTB-26), and TOV-21G (CRL-11730) cells were cultured in DMEM/F12 medium (1:1 mixture) supplemented with 50μg/ml Gentamicin and 5% FBS.

3.2.2 PTGFRN Immunoblot

For Western Blot analysis, cells were lysed in RIPA buffer containing protease inhibitors. 30μg of total cell lysate proteins were prepared, and diluted with reducing

SDS+DTT sample buffer. After heating to 100^{o}C for 5 minutes, and cooling on ice, all samples were run on 4-12% Bis Tris gels (Genscript, M00653). After separation, proteins were transferred to a PVDF membrane, and blocked in 5% milk-PBST for 1 hour at room temperature. Following blocking, membranes were incubated with the anti-PTGFRN sheep antibody (Bio-techne, AF4495) at a concentration of 0.2µg/mL, overnight at 4^{o}C. The next day, membranes were washed in PBST, then incubated in Rabbit-anti-Sheep-HRP conjugated antibody (Jackson ImmunoResearch, 313-035-045) in 5% milk-PBST (1:2000) for 1 hour at room temperature. Membranes were then developed with ECL chemiluminescent solution in an Azure Biosystems 280 chemiluminescent unit.

3.2.3 Production of 33B7 and 8C7 mAb

33B7 and 8C7 hybridomas were cultured in static bioreactor bag in serum-free medium for 14 days. Both antibodies were purified from the culture medium by affinity purification through a 10 ml protein-A sepharose column using an FPLC NGC machine (Bio-rad, Hercules, CA) at a flow rate of 5mL/min. The captured antibody was eluted with pH 2.5 Glycine (50mM), and neutralized with pH 8.5 Tris (1M) to a final pH of 7.4. The antibody was then buffer exchanged by dialysis into PBS pH: 7.4. Antibody purity was checked by SDS-PAGE electrophoresis in reduced and non-reduced conditions.

3.2.4 Purification of Antibody Target Protein and Identification by Mass Spectrometry

AGSCC-3 spindle cell carcinoma cells were cultured in 2 Roller Bottles in DMEM/F12 medium supplemented with 5% FBS. After reaching confluency, the cells were detached by incubation with 5mM EDTA in PBS. $5.0x10^{7}$ cells were then washed

twice with 10mL of PBS, and finally re-suspended in 2mL of PBS. 4mg of Thermo Fisher EZ-Link™ Sulfo-NHS-Biotin (Thermo Fisher) was added to the cell suspension, and the cells were allowed to mix for 2 hours at 4°C.

After 2 hours, the biotinylation reaction was quenched by spinning down the cells, aspirating the biotin-containing supernatant from the pellet, and washing the pellet 3 times with 10mL of PBS containing 100mM Glycine. Cells were then incubated with a hypotonic solution (10mM HEPES, 15mM MgCl2, 10mM KCl, 0.2mM Sodium Orthovanadate, 0.5mM PMSF) for 20 minutes on ice. After hypotonic shock, cell material was homogenized by Teflon pestle to promote cell rupture.

Differential centrifugation was then carried out, starting first with a 15-minute centrifugation at 700G in a Sorvall RT6000 Refrigerated Centrifuge to remove the nuclei. The supernatant was then centrifuged at 10,000G for 25 minutes in a Fisher Scientific accuSpin Micro R tabletop centrifuge for organelle removal. Finally, a 60-minute centrifugation at 114,000G in a Beckman J2-21 centrifuge was carried out to isolate the membrane fraction. This pellet was then solubilized in RIPA buffer (Millipore Sigma) containing Roche cOmpleteTM, EDTA-free protease inhibitor cocktail (Millipore Sigma). After initial solubilization, the solution was sonicated for 20 seconds on ice, with 40 seconds rest on ice. This cycle was repeated three times.

After determining the total protein concentration by MicroBCA, samples containing 1mg each of solubilized membrane protein fraction were immunoprecipitated by incubation with either 40µg of 33B7 antibody, 40µg of non-immune mouse IgG (BioXCell, Lebanon, NH), or 40µg of unrelated control antibody called 21F2 overnight at 4°C. 25µL of protein G agarose beads (Protein Mods) were then added to bind the

antibody and any antibody-bound proteins. The beads were subsequently centrifuged and washed 5 times with 1mL cold RIPA buffer. Protein G agarose-bound proteins were eluted with pH 1.9 Glycine buffer (50mM Glycine, 25mM NaCl), and neutralized to pH 7.4 with a Tris neutralization buffer (1M Tris, 1.5M NaCl). 25µL of Streptavidin agarose beads (Millipore Sigma) were added to this elution, and incubated for 1.5 hours at 4°C. After washing the beads 5 times with PBS, the beads were treated with 50µL of 2X SDS sample buffer solution containing 200mM DTT (Grainger, Lake Forest, IL) and heated to 95°C for 5 minutes.

To confirm the presence of protein, 10µL of the eluted material was analyzed by SDS-PAGE on two 1mm 4–12% Bis-Tris Bolt gels (Invitrogen). With one of the gels, proteins were transferred onto a PVDF membrane, followed by Western Blot with Streptavidin-HRP to visualize biotinylated proteins pulled down by our antibodies. The second gel was incubated in a colloidal blue staining solution (Thermo Fisher) for 3 hours to stain the proteins. After being de-stained, a prominent 130kDa band was apparent in the gel. This band, and the same area of the gel in the mouse IgG lane, was excised for Mass Spec analysis. In-gel trypsin digestion, followed by HPLC and mass spectrometry using a Quadrupole-Orbitrap mass spectrometer was performed at the Proteomics and Mass Spectrometry Facility of the University of Massachusetts Medical School (Shrewsbury, MA). Data was analyzed using Scaffold software.

3.2.5 Measurement of Cell Surface Binding by Flow Analysis

For 33B7 flow binding analysis, cells were collected with PBS-5mM EDTA. $5x10^5$ cells were incubated in 10µg/mL mouse IgG or 33B7 mAb in DMEM + 1% FBS for 1-hour at 4°C. Cells were then washed in 200µL cold PBS, and incubated with

10µg/mL Rabbit-anti-Mouse IgG (Jackson ImmunoResearch Laboratories) in DMEM + 1%FBS for 1-hour at 4°C. Cells were then washed in 200µL cold PBS, and incubated in 20µg/mL Goat-anti-Rabbit-Alexa 647 in DMEM + 1% FBS for 1-hour at 4°C (Jackson ImmunoResearch Laboratories).

For 8C7 flow binding analysis, $5x10^5$ cells were incubated in 0.1 and 1.0µg/mL human IgG or 8C7 mAb in DMEM + 1% FBS for 1-hour at 4°C. Cells were then washed in 200µL cold PBS, and incubated with 10µg/mL Rabbit-anti-Human-Alexa 647 in DMEM + 1% FBS for 1-hour at 4°C (Jackson ImmunoResearch Laboratories).

All cells were washed in 200µL cold PBS, then re-suspended in 160µL PBS, and binding was measured using an HTFC Screening Flow Cytometer (Sartorius).

3.2.6 Examination of 33B7 by Immunofluorescence (IF) Assay

AGSCC-3 IF

Sterile glass coverslips (Thermo Fisher) were placed in 35mm dishes (Corning), and coated with 33µg/mL Rat Collagen Type 1 (Corning) in sterile H2O overnight at 4°C. The collagen solution was aspirated the next day, and the dishes and coverslips were air-dried. $1x10^5$ cells were seeded into these dishes and cultured for 2 days. On Day 2, cells were incubated in 1.5mL of 5µg/mL mouse IgG or 33B7 in DMEM + 1% FBS for 1-hour at 4°C. This antibody solution also contained 10µg/mL of DAPI (4′,6-diamidino-2-phenylindole; Thermo Fisher, Cat. D1306) for nuclear counter-staining. Cells were then washed with 2mL cold PBS, and incubated with 10µg/mL rabbit-anti-mouse IgG in DMEM + 1%FBS for 1-hour at 4°C. Cells were washed with 2mL cold PBS, and incubated with 20µg/mL goat-anti-rabbit-rhodamine conjugate (Thermo Fisher, Cat. R-

6394) in DMEM + 1% FBS for 1-hour at 4°C. Cells were washed in 2mL cold PBS. For time = 0, the coverslips were immediately removed from the 35mm dishes, and placed on a microscope slide (Thermo Fisher, Cat. 3400), and viewed with an Olympus BX40 fluorescence microscope, through the TRITC filter. The t = 1-hour at 37°C and t = 1-hour at 4°C dishes were placed in their respective incubator/fridge, and incubated for 1-hour, at which point the cells were washed once more with cold PBS. The coverslips were removed, placed on a slide, and viewed in our fluorescent microscope.

PTGFRN- and Mock-Transfected HEK-293A Immunofluorescence (IF)

HEK-293A cells were transiently transfected with either human PTGFRN cDNA expression vector, or empty expression vector as described below. After 48 hours transient transfection, cells were collected with PBS-5mM EDTA. $5x10^5$ cells were incubated in 100µL of 5µg/mL mouse IgG or 33B7 in DMEM + 1% FBS for 1-hour at 4°C. This antibody solution also contained 10µg/mL of DAPI (4′,6-diamidino-2-phenylindole) for nuclear counter-staining. Cells were then washed in 200µL cold PBS, and incubated with 10µg/mL rabbit-anti-mouse IgG in DMEM + 1%FBS for 1-hour at 4°C. Cells were then washed in 200µL cold PBS, and incubated in 20µg/mL goat-anti-rabbit-rhodamine conjugate in DMEM + 1% FBS for 1-hour at 4°C. Cells were washed in 200µL cold PBS. At time 0, the cells were then re-suspended in 10µL of PBS, pipetted onto a microscope slide with coverslip, and viewed with an Olympus BX40 fluorescence microscope, through the TRITC filter. In parallel, one aliquot of the cell suspension was placed for 1-hour in a 37°C incubator, and a second aliquot was placed for 1-hour in a 4°C fridge. At the end of the incubation, the cells were washed with cold PBS, re-suspended in 10µL of PBS, pipetted onto a microscope slide with coverslip, and viewed

with an Olympus BX40 fluorescence microscope, through the TRITC filter. All images were taken with TSView software (Version 7), and composite images were generated using ImageJ software.

A431 Immunofluorescence (IF)

Chambered coverslips were coated overnight at 4^{o}C in 50µg/mL Poly-D-Lysine in sterile deionized water. Next day, aspirated solution from the coverslips, and allowed the coverslips to air dry for 2 hours. 7.5x10^{4} A431 cells were seeded on coverslips and allowed to attach overnight in a 37^{o}C humidified 5% CO2 incubator. The next day, cells were washed once with PBS, and incubated with 1mg/mL 8C7 directly conjugated to Alexa Fluor647 at 4^{o}C for 1 hour (Diluted in 1% BSA in DMEM). After binding incubation, one coverslip was placed back into the 37^{o}C incubator for 1.5 hours. Upon time point completion, coverslips were washed three times with cold PBS and fixed in 4% paraformaldehyde for 10 minutes at room temperature. After three more washes in PBS, cells were mounted and viewed using a Nikon A1 point-scanning laser confocal microscope (NIS-Elements, 60X).

3.2.7 PTGFRN cDNA Transfection into HEK-293A Cells

Full-length human PTGFRN cDNA was synthesized into pcDNA3.1 (+) vector (Invitrogen). The PTGFRN cDNA expression vector plasmid (1µg) was transiently transfected into HEK-293A cells with a Lipofectamine transfection kit (Thermo Fisher). 4x10^{5} HEK-293A cells were plated in a 6-well plate. 24 hours later, 3 wells were transfected with an empty pcDNA 3.1 vector as a mock transfection negative control, while the other 3 wells received the PTGFRN plasmid. After 5 hours incubation with

Lipofectamine and plasmid DNA, the mixture was aspirated from the cells, and replaced with complete serum-supplemented medium. For transient transfection, the cells were collected after 48 hours, with one well used to collect lysate (100μL RIPA lysis buffer with protease inhibitor cocktail), while the remaining cells were harvested with 5mM EDTA, and Flow Cytometry and Immunofluorescence were performed as described above.

3.2.8 Inhibition of Proliferation with 33B7 and Fab-ZAP Secondary Antibodies

In a 96-well plate, 2000 cells/well were plated in triplicate in 100μL of DMEM/F12 medium supplemented with 5% FBS, 0.4ug/ml 33B7 antibody, and 0.9ug/ml of anti-mouse Fab-conjugated with Saporin (Fab-ZAP, Advanced Targeting Systems, Cat. IT-48). As an isotype control, cells were incubated with mouse IgG (instead of 33B7) and Fab-ZAP. Cells incubated with 33B7 and mouse IgG without Fab-ZAP were also used as experimental negative controls. After 72 hours, cell proliferation was measured by CellTiter-Glo® Luminescent Cell Viability Assay reagent (Promega) according to manufacturer's instructions. The luminescence levels were measured with a SpectraMax M2 (Molecular Devices, San Jose, CA).

After testing the antibody with the secondary antibody-saporin conjugation, we then tested our 33B7 directly conjugated to saporin in the same assay at various concentrations up to 10nM. 8C7 directly conjugated to Duocarmycin was also tested via this same method.

3.2.9 Direct Conjugation of Antibodies

Purified 33B7 antibody was sent to Advanced Targeting Systems (Carlsbad, CA), where saporin was directly conjugated to the Fc region of 33B7 using their proprietary cleavable linker.

The human IgG control antibody was generated in-house and purified in identical manner as 8C7, but raised against an unrelated antigen. TCEP, L-cysteine hydrochloride, Ellman's Assay reagents, and Dimethylacetamide (DMA) were all purchased from Thermo Fisher. The duocarmycin payload and valine-citrulline linker moiety were purchased pre-synthesized from MedChem Express in the form of MC-Val-Cit-PAB-Duocarmycin chloride. The G-25 gel filtration columns were purchased from Cytiva.

8C7 and IgG control antibodies were buffer exchanged into a conjugation buffer (pH 8) consisting of 25mM Borate, 25mM NaCl, and 1mM Diethylenetriaminepentaacetic acid (DTPA), and concentrated until >5mg/mL. 2.5 molar equivalents of TCEP were added to the antibody solution and incubated for 40 minutes at 37^{o}C. After this incubation, the antibody solution was immediately chilled on ice and Ellman's Assay analysis showed an average free thiol/IgG ratio of 4-5.

Dimethylacetamide (DMA) was added to the antibody solution at a final concentration of 10%. The pre-synthesized duocarmycin payload and valine-citrulline linker in the form of MC-Val-Cit-PAB-Duocarmycin was added at a 1.2-fold molar excess of the free thiol concentration and incubated at room temperature for 45 minutes. The reaction was quenched by adding a 20X excess of Cysteine-HCl. After 30 minutes incubation with cysteine at room temperature, the ADC solution was run through two

G25 columns equilibrated in a 50% HIC Mobile Phase A/50% H2O solution to completely remove unreacted Linker-payload and free cysteine.

3.2.10 Purification of 8C7 ADC by HIC

8C7-Duocarmycin, as well as the IgG-duocarmycin control, were purified on a pre-packed HiScreen Butyl HP HIC column (7.7 X 100mm, 4.7mL, Cytiva, Cat. 28978242) attached to a Bio-Rad NGC Medium Pressure Chromatography System at room temperature. Before injection of the sample, the column was equilibrated with 3 column volumes of Mobile Phase A buffer (1.5M Ammonium Sulphate, 25mM Na3PO4, pH 8). The ADC sample in 50% mobile phase A buffer was loaded onto the column and eluted using a linear gradient from 0% Mobile Phase B to 100% Mobile Phase B (25% Isopropanol, 25mM Na_3PO_4, pH 8). The flow rate was 0.8ml/min, and elution was performed over 18 minutes, or three column volumes. Only the conjugated ADC fraction was collected, buffer exchanged to PBS (pH 7.4), and then sterilized by syringe filtration. Concentration was determined using Nanodrop measuring absorbance at OD280.

3.2.11 In Vivo Mouse Studies

These studies were carried out in strict accordance with the recommendations of the Guide for the Care and Use of Laboratory Animals from the National Institutes of Health. The protocol used for these studies was approved by the Institutional Animal Care and Use Committee (IACUC) of A&G Pharmaceutical (Protocol number: GS-01). All animal procedures were performed under isoflurane anesthesia and all efforts were made to minimize animal suffering.

Animals were housed in the Institution's AAALAC-accredited and OLAW certified animal facility, (OLAW D16-00700). Experiments were carried out following A&G's IACUC-approved procedures. Animal rooms were humidity and temperature controlled with a 12-hour light/dark cycle. 6 to 8-week-old female Athymic nude mice (Charles River Laboratories, Wilmington, MA) were housed with no more than 5 mice/cage aseptically in autoclaved plastic cages with filter top containing autoclaved 1/8" corncob bedding, 18% protein, 9% fat, extruded rodent pellets, and sterile tap water. Cages, food, and water were replaced once a week, using aseptic techniques.

For each cell line investigated, 30 Athymic nude mice (Charles River) were subcutaneously injected with 10^6 cells in serum-free DMEM/F12. For A431 cells, only $5x10^5$ cells were injected per mouse. The mice were monitored until the subcutaneous tumor reached approximately 50-100mm3. After measuring tumor size as described below, mice were randomized into 2-3 experimental groups, and ear-marked for individual identification. Animals with tumors that were too large or too small at the time of randomization were not included in the experiments. The number of mice per group was determined by power calculation based on the hypothesis of an at least 50% difference in tumor volume between the test and control groups (183).

Mice were monitored daily for general health, sign of distress, and/or tumor necrosis. If a mouse within a cage showed any signs of illness, the mouse was isolated in a new cage with enrichment objects and monitored for any change in health. Humane endpoints were incorporated into animal procedures. Mice were euthanized once tumor volume exceed 3000mm3, whenever tumor ulceration/necrosis became severe, or if mice were persistently ill, even after isolation and monitoring. Any tumor ulcerations typically

coincided with other humane endpoints, or occurred at the end of the experiment, so termination of the mice was prompt in order to reduce potential pain and distress.

Tumor measurements were taken twice a week aseptically with a caliper, and volume was calculated using the formula ($L \times (W^2)/2$). For each mouse, tumor growth rate was measured as the tumor volume on day of measurement divided by the initial tumor volume on Day 1. At the end of the experiments, the mice were euthanized following approved guidelines by isoflurane anesthesia, exsanguination by cardiac puncture, followed by cervical dislocation. Both experiments were repeated twice.

3.2.12 Statistical Analysis

Statistical analyses were carried out using GraphPad Prism version 8.3. All in vitro assays were carried out in triplicates and repeated three times. Results were analyzed for statistical significance using a Welsh's T-test.

Animal studies were analyzed at each time point between the groups using Two-Way Analysis of Variance (ANOVA) utilizing post-hoc Bonferroni analysis, and/or Mixed Effects analysis wherever necessary. For all statistical analysis, results are shown as mean ± SD. Significance was determined at $P < 0.05$ (*), $P < 0.01$ (**), $P < 0.001$ (***).

3.3 Results

3.3.1 Binding and Internalization of 33B7 Monoclonal Antibody to Cancer Cells

Flow binding assay to examine 33B7 binding on cell surface identified the spindle cell carcinoma cell line AGSCC-3 as highly positive for 33B7 binding. In addition to the

binding to the cell surface of AGSCC-3 cells, 33B7 was internalized when cells were placed at 37°C for 1 hour. These results are presented in Figure 3.1.

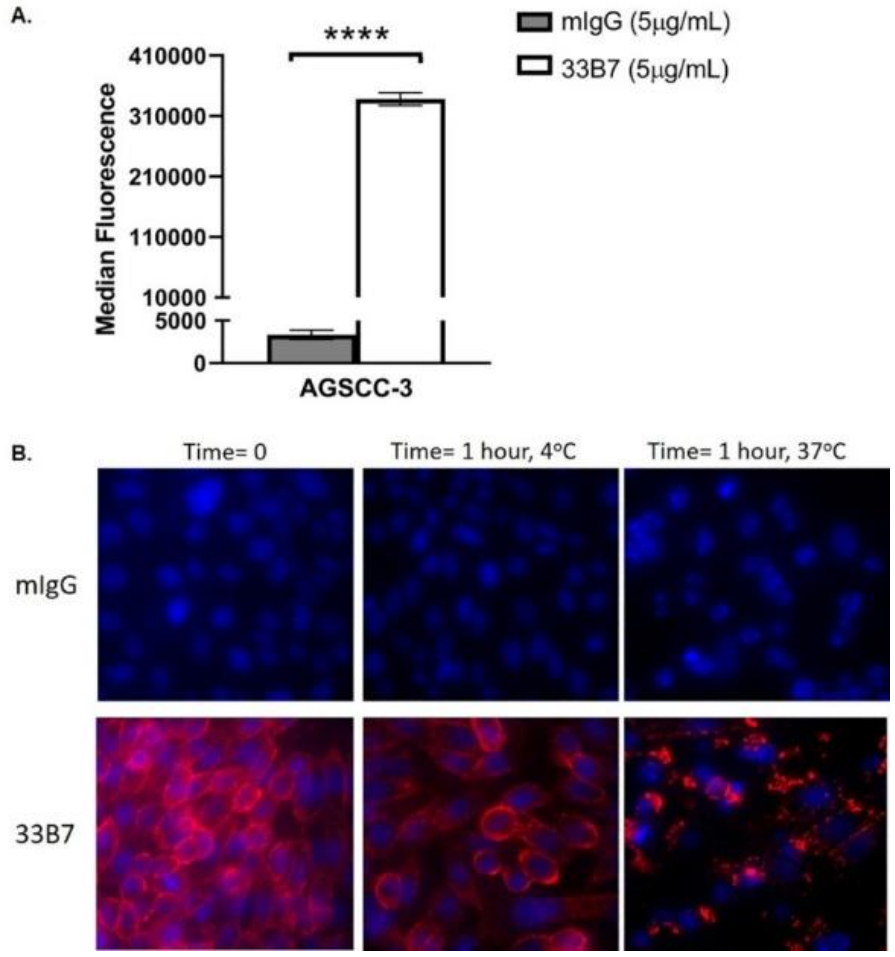

Figure 3.1 33B7 binding and internalization in cancer cells. (A) The spindle cell carcinoma cell line AGSCC-3 was tested for 33B7 binding by Flow Cytometry and showed high levels of binding. (B) AGSCC-3 cells show immunofluorescence binding of 33B7 (red), and not mouse IgG. Cells allowed to incubate at 37C for an hour show a punctate appearance, signifying internalization of the fluorescent-labelled antibody. Cells incubated at 4^0C did not show this internalization. DAPI (blue) was used to counterstain nuclei.

3.3.2 Purification of 33B7 Cell Surface Target

AGSCC-3 cells, which showed a high level of 33B7 binding by flow assay, was used for purification and identification of the 33B7 cell surface target. Details of the purification procedures are provided in the Material and Method section. Briefly, the cell-surface proteins were biotinylated, followed by plasma membrane preparation, solubilization, and immunoprecipitation by incubation with 33B7 antibody, or with unrelated antibodies used as negative controls, followed by protein G beads capture as described in the method section. Proteins bound to the 33B7-protein G beads or control antibody-protein G beads were eluted by acidic pH and the resulting supernatants were neutralized and incubated with streptavidin beads to bind the biotinylated proteins eluted from the antibodies protein G beads. After incubation, beads were washed, mixed with SDS-sample buffer and the bound proteins were resolved by SDS-polyacrylamide gel electrophoresis on a 4–12% Bis-Tris polyacrylamide gel.

This gel was then transferred to a PVDF membrane for western blot analysis to detect biotinylated proteins with Streptavidin-HRP incubation as described in the method section. As shown in Figure 3.2A, a major protein band with an apparent molecular weight of 130kDa was detected by HRP-streptavidin western blot analysis. At this point, the remaining IP elution was run on an additional gel, and this time was stained with Coomassie Blue stain. A major band with a similar apparent molecular weight was also detected on the gel stained with Coomassie Blue (Figure 3.2B). This band was not present in samples from the same cell extract that had been immunoprecipitated with non-immune mouse IgG, or an unrelated antibody control 21F2.

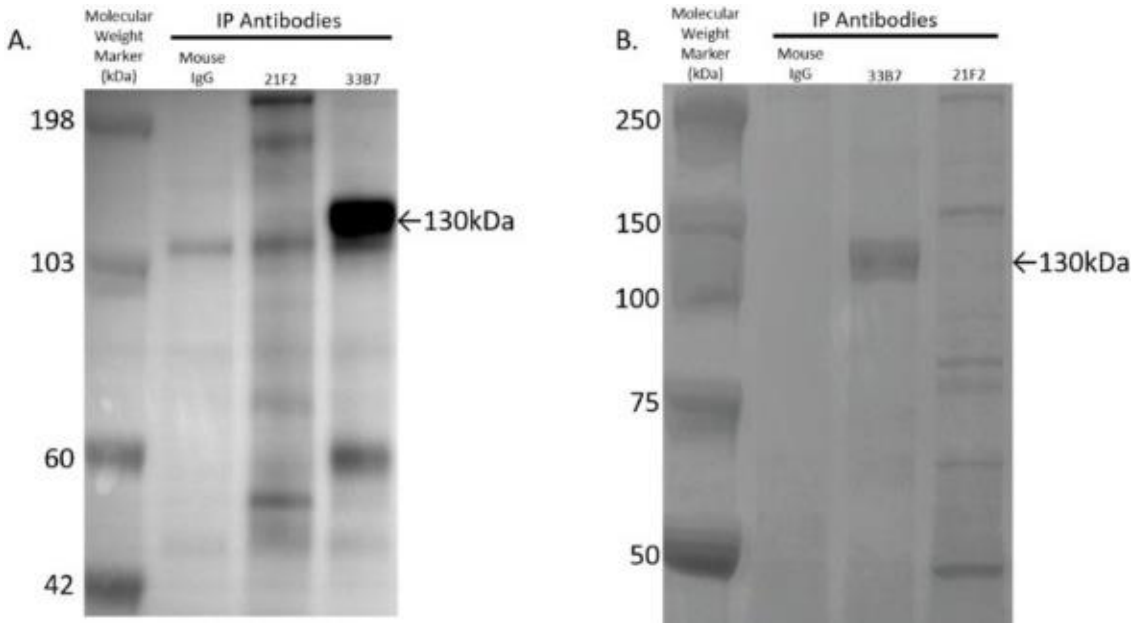

Figure 3.2 Immunoprecipitation with 33B7 pulls down a unique 130kDa protein. 33B7 and two negative control antibodies were used to immunoprecipitate (IP) the biotinylated membrane fraction of AGSSC-3 cells. (A) Western Blot using Streptavidin-HRP on IP elutions of biotinylated membrane fraction. (B) Coomassie gel staining of IP elutions. A 130kDa band was visible in both assays, and only seen in the fraction immunoprecipitated with the 33B7 mAb.

The gel fragments corresponding to the position of the 130kDa band detected by Coomassie Blue were excised from the 33B7 lane and from the mIgG lane and sent to the Proteomics and Mass Spectrometry Facility of the University of Massachusetts Medical School for in-gel trypsin digestion, HPLC, and Mass Spectrometric analysis.

3.3.3 Mass Spectrometric Identification of the Cell Surface Target

After analyzing the data received from the mass spectrometry facility, the protein with the highest number of identified peptides in the 33B7 lane was identified as

Prostaglandin F2 Receptor Negative Regulator, or PTGFRN (ID number Q9P2B2). Table 3.1 shows the top 5 most abundant proteins identified. We can see that the band excised from the 33B7 IP lane contained 246 PTGFRN-unique peptides, compared to just 53 in the corresponding excised mIgG portion, with PTGFRN being by far the most abundant protein identified.

Protein Name	Accession Number	Molecular Weight (kDa)	33B7 Unique Peptide Number	mIgG Unique Peptide Number
Prostaglandin F2 Receptor Negative Regulator	Q9P2B2	94	246	53
Keratin, Type II cytoskeletal	P04264	94	80	41
Desmoplakin	P15924	328	39	5
Vimentin	P08670	54	15	16
Junction Plakoglobin	P14923	128	15	4

Table 3.1 Mass spectrometric analysis of 33B7 immunoprecipitation elution. This table shows the 5 most abundant proteins detected in the mass spectrometric analysis of the 33B7 IP. PTGFRN is the most abundant protein immunoprecipitated by 33B7 and is most likely to be the 33B7 antigen.

3.3.4 HEK-293A Cells Transiently Transfected with Human PTGFRN cDNA Can Bind 33B7 Antibody

Experiments were carried out to verify that PTGFRN identified by mass spectrometry was the target protein binding to the 33B7 antibody. For this purpose, as described in the methods section, we inserted human PTGFRN cDNA into a pcDNA3.1

vector, and transiently transfected it into HEK-293A cells, which are negative for PTGFRN, as shown by western blot analysis. The resulting PTGFRN expressing cells were used to examine 33B7 binding by flow cytometry, comparing mock transfected HEK-293A cells vs. PTGFRN transfected cells (HEK-PTG). As presented in Figure 3.3, the HEK-PTG cells showed a large increase in binding by 33B7 while mock transfected HEK-293A cells showed no 33B7 binding, confirming the mass spectrometry results identifying PTGFRN as the 33B7 binding protein.

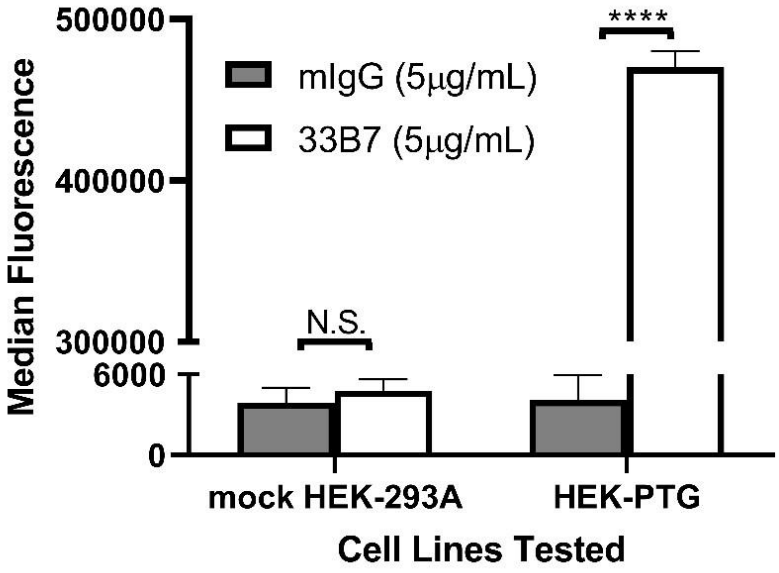

Figure 3.3 Transfection of human PTGFRN cDNA in HEK-293A cells results in a significant increase in 33B7 binding. 33B7 cannot bind to the surface of HEK-293A cells. However, after transfection of human PTGFRN cDNA, 33B7 binding increases almost 100X.

3.3.5 33B7 induces internalization of PTGFRN

Since 33B7 was binding on the cell surface of PTGFRN-transfected (HEK-PTG) cells, we then tested by immunofluorescence whether the transfected PTGFRN protein was also internalized by 33B7. After antibody binding at 4^{o}C, the cells were placed in a

37^{o}C incubator for 1-hour followed by observation under a fluorescent microscope. Figure 3.4 shows strong cell surface binding of 33B7 on the PTGFRN-transfected HEK-PTG cells maintained at 4^{o}C, with no visible binding on the mock-transfected HEK-293A cells. After 1-hour incubation at 37^{o}C, the immunofluorescence (red) was intracellular and had a punctate appearance, indicating internalization of PTGFRN had occurred at 37^{o}C upon binding of the 33B7 antibody. The 33B7 binding remained on the cell surface for the cells maintained at 4^{o}C for 1 hour, instead of 37^{o}C indicating that no internalization had occurred at 4^{o}C.

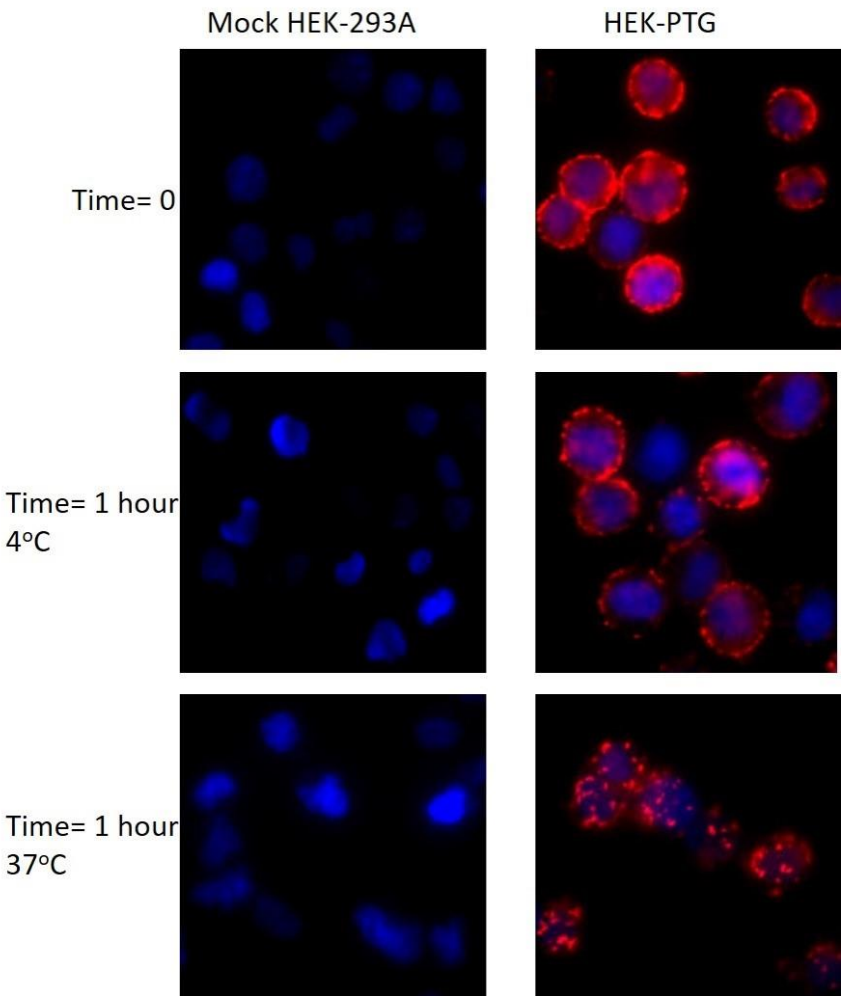

Figure 3.4 Binding of 33B7 causes the internalization of PTGFRN. Mock HEK-293A cells and HEK-PTG cells were used to visualize 33B7 binding and internalization by immunofluorescence as described in the method section. DAPI was used to counterstain the cell nuclei (Blue).

3.3.6 Inhibition of Proliferation of PTGFRN-Transfected HEK-293A Cells, Natural Cancer Cells, by Internalization of 33B7

After confirming that 33B7 could bind and internalize cell-surface PTGFRN on the HEK-PTG cells, we next examined whether it could be used to deliver a toxic payload to cells expressing this target. As a proof-of-concept, we chose to use a saporin-conjugated Fab fragment anti-mouse IgG antibody, which is commercially available, and is widely used for internalization studies (252). Saporin is a 30kDa Ribosome-

inactivating protein purified from the seeds of the Soapwort plant (*Saponaria officinalis)*. It acts as an N-glycosidase and cleaves RNA that codes for the 28S subunit of the ribosome. This results in inactive ribosomes, and thus, cell death. However, saporin is unable to pass through the cell membrane by itself (253). The only way it can reach the ribosomal RNA is by conjugation to an internalizing antibody, or other agent able to enter the cell. This makes it a great tool to demonstrate proof of concept for payload delivery via 33B7 antibody. Treatment with the internalizing anti-PTGFRN 33B7 antibody either directly conjugated to saporin, or in combination with an anti-mouse secondary antibody conjugated to saporin (Fab-ZAP), should result in inhibition of cell proliferation of 33B7-positive cells.

As shown in figure 3.5, HEK-PTG proliferation was inhibited by 80% ± 5% by treatment with 33B7 antibody and Fab-ZAP, as described in the methods section. We also tested the sensitivity of the cell lines under investigation to unconjugated saporin alone and found that the lowest concentration that we saw toxicity was 1μM (data not shown). This concentration greatly exceeds the working concentration of saporin that would be used with our conjugates, which is approximately 25nM for our *in vitro* assays, and approximately 100nM in our *in vivo* assays.

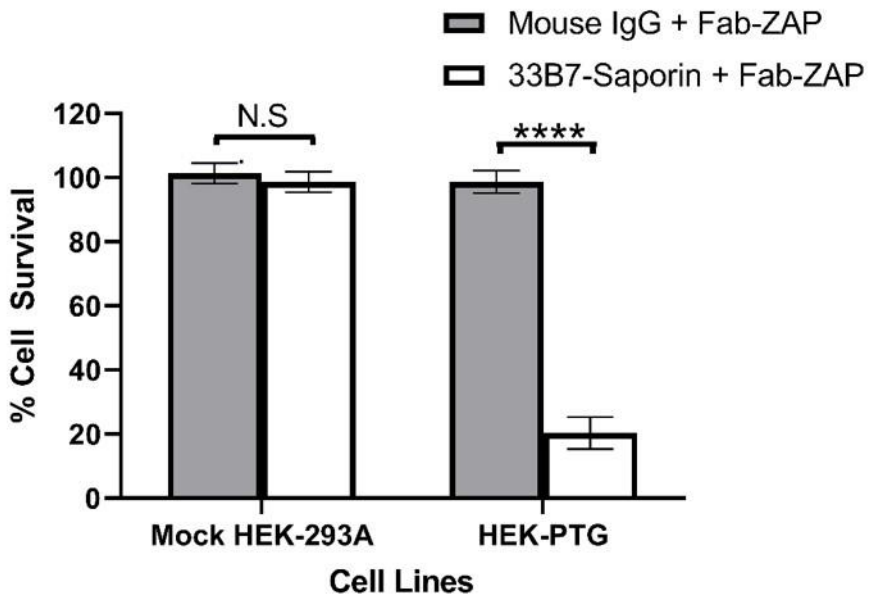

Figure 3.5 Incubation of PTGFRN-overexpressing HEK-293A cells with 33B7 and anti-mouse secondary antibody-saporin conjugate. Cells that overexpress PTGFRN were killed when incubated in the presence of 33B7 and an anti-mouse secondary antibody conjugated to the cytotoxic payload Saporin.

At this point, we had the 33B7 antibody custom conjugated directly to saporin, resulting in our proof-of-concept ADC. Mouse IgG conjugated with saporin was used as a negative isotype control.

Western blot analysis using an anti-PTGFRN antibody was used to examine PTGFRN expression in several cancer cell lines. Among the human cell lines investigated, A431, DAOY, and MSTO-211H cells were positive for PTGFRN, with the highest expression being in A431 cells. JEG-3, TOV-21G, and MDA-231 cells were found to be PTGFRN negative. We then looked at levels of 33B7 binding to these cells by flow cytometry, and found that 33B7 binding occurred at levels that reflected their respective PTGFRN expression level.

These cell lines were then used to examine the effect of the 33B7-saporin ADC on *in* vitro cell proliferation. When compared to the saporin IgG negative control, PTGFRN-positive human cancer cells treated with the 33B7-ADC resulted in a 61% ± 2% reduction of proliferation in A431 cells, and a 51% ± 6% reduction on proliferation in DAOY cells. No growth inhibitory effect of the 33B7-saporin ADC was observed for the PTGFRN-negative cell lines (TOV-21G, MDA-MB-231). Figure 3.6 illustrates the results of these western blot, flow cytometry, and proliferation inhibition assays.

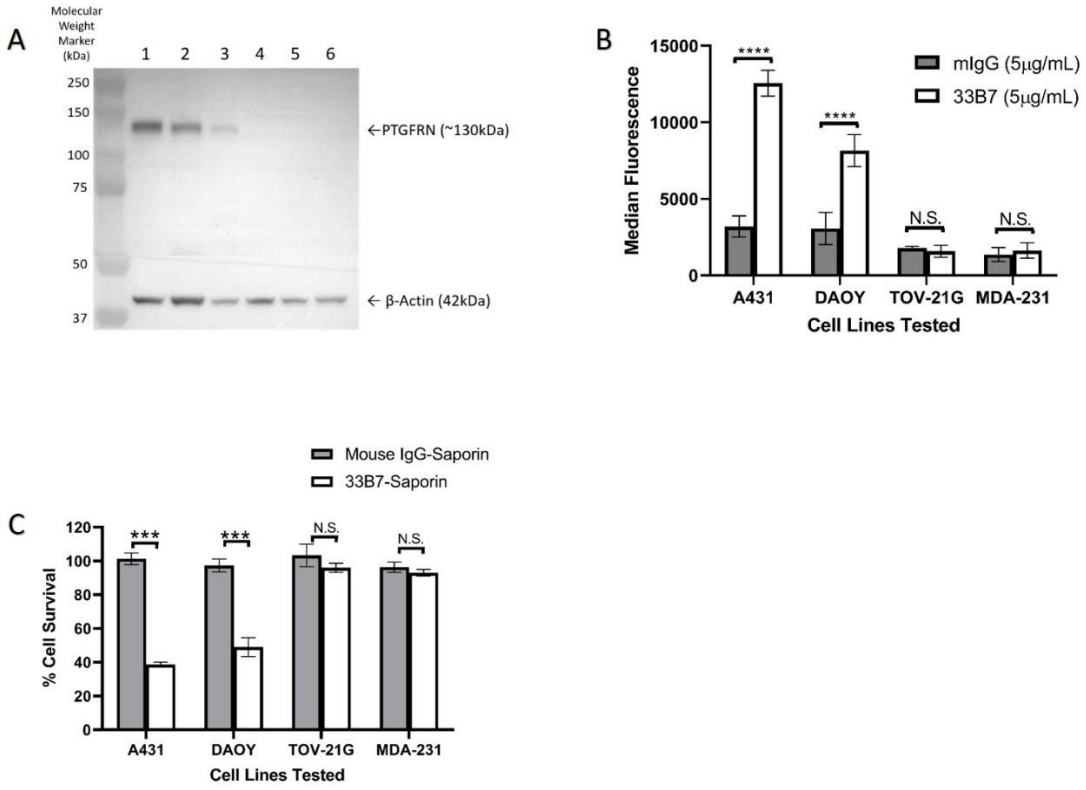

Figure 3.6 PTGFRN expression and effect of 33B7 on various cancer lines.
(A) PTGFRN expression by Western Blot with anti-PTGFRN antibody in 1. A431 (40μg), 2. DAOY (40μg), 3. MSTO-211H (40μg), 4. JEG-3 (40μg), 5. TOV-21G (40μg), and 6. MDA-231 (40μg) cell lysates. (B) Several cancer cells were screened for 33B7 cell surface binding by flow assay. A431, DAOY showed 33B7 binding compared to a mouse IgG control while TOV-21G and MDA-MB-231 showed no 33B7 binding. (C) Effect of 33B7-ADC on various cancer cell lines. Treatment with 33B7-Saporin conjugate (10nM) over 3 days shows decrease in proliferation compared Mouse IgG-Saporin conjugate (10nM). Cancer cells with undetectable PTGFRN expression levels (TOV-21G, MDA-231) showed no growth inhibitory response. Statistical analysis was shown via a Welch's t-test between control (Mouse IgG-Saporin) and 33B7-Saporin (**, $P < 0.01$; ***, $P < 0.001$; ****, $P < 0.0001$).

3.3.7 *In Vivo* Growth Inhibitory Effect of Saporin-Conjugated 33B7

Since the AGSCC3 and A431 cell lines showed the highest level of PTGFRN expression, as well as the highest response to 33B7-ADC, these cell lines were selected to examine the effect of 33B7-ADC on *in vivo* tumor growth in mouse xenograft model when compared to isotype control ADC.

As shown in Figure 3.7, the treatment of athymic nude mice bearing A431 tumors with weekly intravenous (i.v.) administration of 33B7-saporin ADC (10μg/mouse) resulted in a reduction of tumor growth by at least 50% when compared to mice treated with vehicle control or with isotype control 21F2-ADC. 80% Tumor inhibitory effect of 33B7-ADC was also observed with ASGCC3 cells when compared to IgG-saporin antibody control.

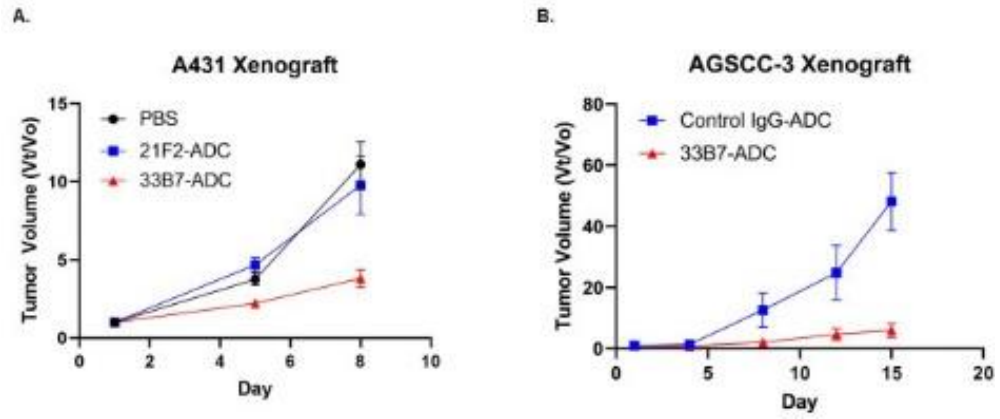

Figure 3.7 Effect of 33B7-saporin on tumor growth of A431 cells and ASGCC3 cells in athymic nude mice. *In vivo* effect of treatment with 33B7-Saporin in athymic nude mice xenografts with (A) A431 cells, and (B) AGSCC-3 cells. Isotype control (Blue Square; 10μg/mouse of saporin-conjugated isotype control) or 33B7-Saporin (Red Triangle;10μg/mouse) were administered once weekly via tail vein injection. PBS (Black Circle) volume equivalent was used as vehicle control. Tumor sizes were measured biweekly with calipers. Statistical analysis showed significance (at least *, $P < 0.05$) between the Isotype/Vehicle control and 33B7-Saporin for each time point after start of treatment.

While the 33B7 antibody directly conjugated to saporin demonstrated an anti-tumor growth effect, we wondered if a more potent ADC could be developed towards PTGFRN. 33B7 was identified as an IgG2b antibody, and found to have moderate binding affinity (KD= 10^{-9}M; Data not shown). We hypothesized that by switching to an IgG1 antibody with higher binding affinity, we could potentially improve the potency of our ADC. Additionally, while saporin was a good payload to test if PTGFRN could be a valid target for ADC development, it has not been used as a payload with any FDA-approved ADCs. Because of this, we decided to switch our payload to Duocarmycin, a compound that is being investigated with ADCs currently in clinical trials. Duocarmycin is a highly toxic compound with an IC50 in the nano- and picomolar range, capable of binding to the minor groove of DNA, leading to DNA-damage accumulation, and subsequent apoptosis. Due to this mechanism, it can act on dividing cells, as well as non-dividing cells. Finally, duocarmycin also shows superb activity in cancer cells that are hypoxic, chemoresistant, and stem-cell like (254–257). By generating an antibody with better physical characteristics, and switching to a more potent duocarmycin payload, we then determined if we could produce an overall more potent ADC.

3.3.8 8C7 is a Fully-Human Antibody That is Capable of Binding Cell-Surface PTGFRN, and Internalizing the Transmembrane Protein to the Cell Interior

Following the initial success of our murine antibody 33B7, we developed a fully human anti-PTGFRN antibody capable of internalizing the target as described in the method section. The advantage of directly developing fully human antibodies allows us to skip the humanization process that would need to occur for antibodies of mouse origin. By immunizing transgenic humanized TC mice (258) against the extracellular domain of PTGFRN, a library of single clone hybridomas was generated and screened to produce

fully human antibodies which bind to cell-surface PTGFRN, are internalizing, and have a high affinity. After screening these antibodies and comparing various criteria, the hybridoma designated 8C7 was identified to have a high antibody production level, was a singular clone, and was found to produce an IgG1, the ideal isotype for ADC development (259). Notably, the binding affinity (Kd) of 8C7 to PTGFRN was found to be $<10^{-12}$M, 1000X stronger than that of 33B7 (Data not shown).

Figure 3.8 depicts that 8C7 is capable of binding to the cell surface of A431, DAOY, and MSTO-211H cells. To further confirm that binding is occurring specifically to PTGFRN, flow analysis was also carried out on the shRNA clones of A431 and DAOY, as well as the PTGFRN-overexpressing MSTO-211H clone previously described in Chapter 2. Cell-surface binding of the 8C7 antibody was significantly reduced in the shRNA knockdown cells, and significantly increased after PTGFRN transfection and overexpression in the MSTO-211H clone (Figure 3.8). Finally, flow analysis of 8C7 binding to MDA-231 cells, which are negative for PTGFRN, show no difference in binding profile between negative control antibody, and 8C7 at both concentrations.

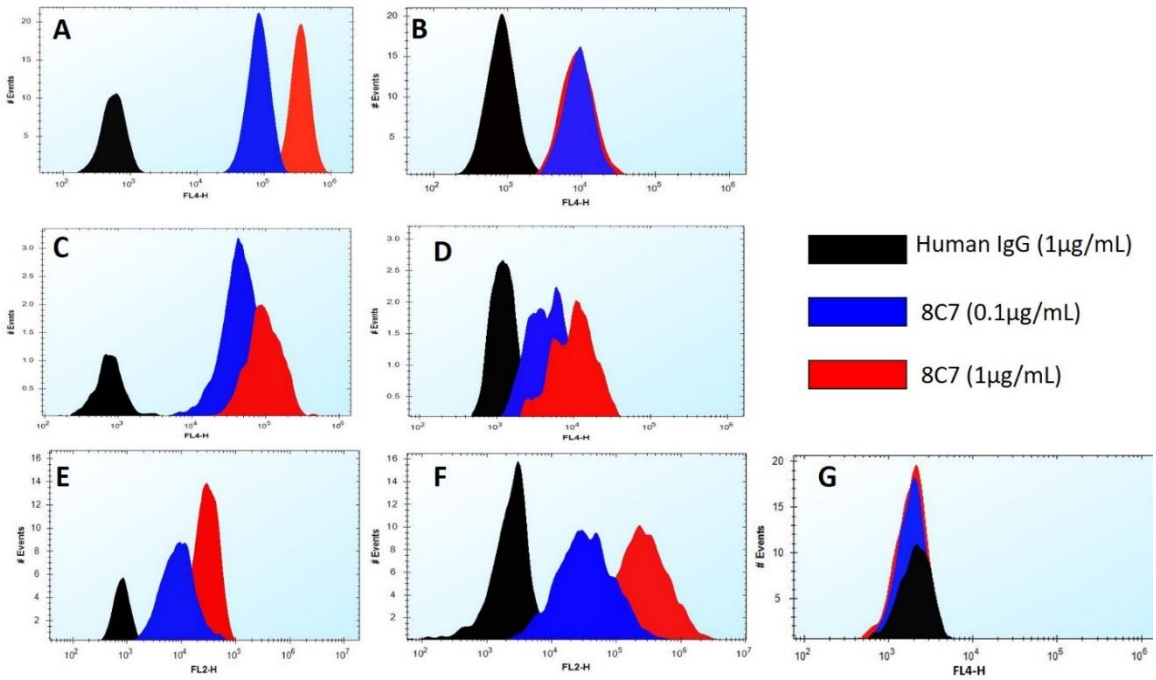

Figure 3.8 Fully human 8C7 antibody binding is specific to PTGFRN. 8C7 Flow Cytometry Binding results on (A) Control shRNA A431, (B) PTGFRN shRNA A431 Clones, (C) Control shRNA DAOY, (D) PTGFRN shRNA DAOY Clones, (E) Control MSTO-211H, (F) PTGFRN-Overexpressing MSTO-211H Clone, and (G) MDA-231

Immunofluorescence analysis was also conducted to confirm endocytosis of PTGFRN following 8C7 binding. As seen in Figure 3.9, the majority of 8C7 fluorescence was localized to the cell membrane and cell-cell junctions at time=0. After 3 hours of incubation at 37^{o}C, the 8C7 immunofluorescence was observed intracellularly with some of the signal still residing on the cell membranes. After 5 hours incubation, 8C7 fluorescence was seen primarily inside the cell, with little to no signal seen on the cell surface, confirming that PTGFRN was internalized following 8C7 antibody binding.

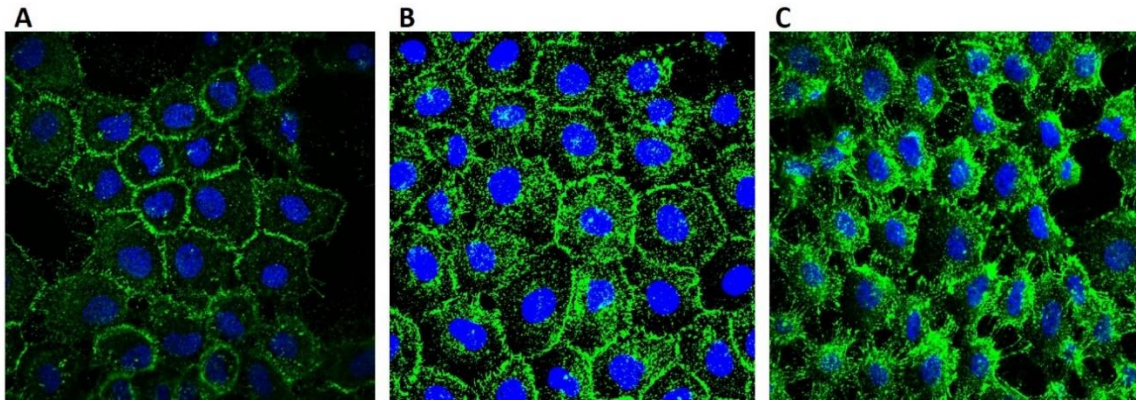

Figure 3.9 Internalization of PTGFRN by 8C7. Binding of 8C7 antibody to PTGFRN induces endocytosis of the receptor. Incubation with 8C7 (Green) at 37ºC for (A) Time 0, (B) 3 hours, and (C) 5 hours. Hoechst 33342used to counterstain nuclei (Blue).

Following this result, the toxic payload Duocarmycin was conjugated to the 8C7 antibody to verify internalization and delivery of payload to the cells.

3.3.9 8C7 Conjugation with Mc-Vc-Duocarmycin Results in a Potent, Fully Human Antibody-Drug Conjugate (ADC) in In Vitro and In Vivo Models

Duocarmycin is an anti-cancer agent that exerts its effect by binding to the minor groove of the DNA double-helix and alkylating the nucleotide adenine (254). This binding and alkylation trigger tumor cell death. Conjugation of duocarmycin to 8C7 and control antibody was performed as described in the method section. Briefly, 8C7 was partially reduced with TCEP, then re-alkylated using a pre-synthesized cleavable linker-duocarmycin moiety commercially available from MedChem Express. After conjugation, and reaction quenching, the fully conjugated IgG species was separated and purified using Hydrophobic Interaction Chromatography (HIC). After fraction collection, ADC was buffer exchanged into PBS, and sterilized via 0.22µm filtration.

After conjugating Duocarmycin to the 8C7 antibody, the resulting ADC was tested first *in vitro* for its ability to inhibit the proliferation of PTGFRN-expressing cell

lines epidermoid carcinoma (A431), biphasic mesothelioma (MSTO-211H), and medulloblastoma (DAOY). In addition to these PTGFRN-positive cancers, we also tested the ADC with the triple-negative breast cancer cell line MDA-MB-231, previously found to be negative for PTGFRN (260). As shown in Figure 3.10, treatment with the 8C7-ADC showed a dose-dependent inhibition of cell proliferation in all cell lines expressing PTGFRN. Specifically, at the highest ADC dose tested (10nM), A431 proliferation was reduced by 95%, DAOY proliferation was reduced by 80%, and MSTO-211H proliferation was reduced by approximately 40%. The degree of inhibition followed the level of expression of PTGFRN in these three cell lines. The low PTGFRN-expressing MSTO-211H cells still demonstrated a reduced yet significant inhibition of proliferation, even though PTGFRN expression was lower than that of A431 and DAOY. However, the PTGFRN-negative cancer line, MDA-MB-231, showed no growth inhibition when treated with 8C7-ADC, even at the highest concentration tested, showing the specificity of the 8C7 ADC for PTGFRN.

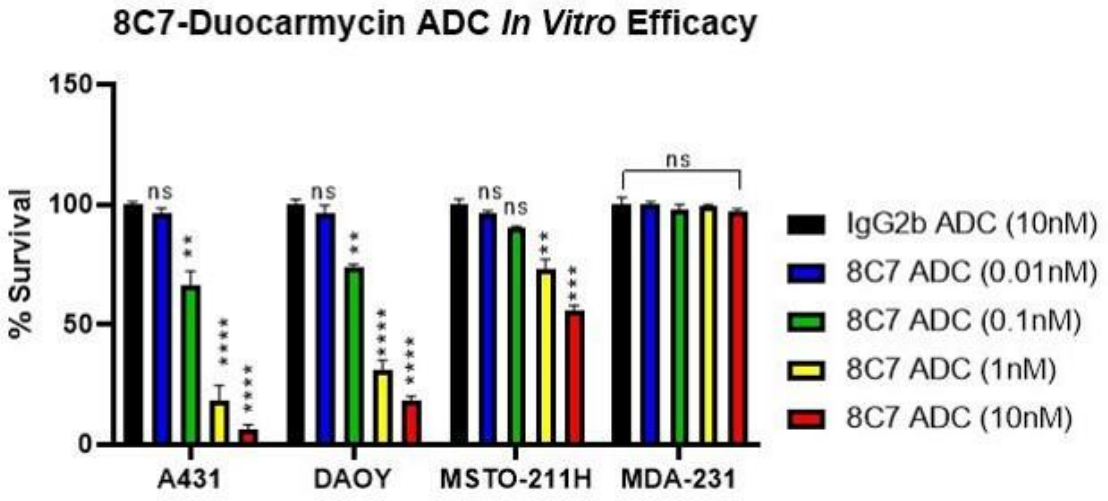

Figure 3.10 *In Vitro* Activity of 8C7-Duocarmycin ADC. Incubation of 8C7-Duocarmycin with PTGFRN-positive cancer cell lines results in potent anti-cancer effect. No effect is seen in a cancer cell line that is PTGFRN-negative (MDA-231).

We next examined the effect of 8C7-ADC on tumor growth using an *in vivo* xenograft models. The same cell lines used in the in vitro assays were subcutaneously injected into athymic nude mice as described in the method section. For each cell line, once the mice developed tumors, they were randomized into control and treatment groups as described in the method section. When compared to the Control ADC, we observed a dose-dependent and significant reduction in tumor growth rate, as well as tumor volume for the three PTGFRN expressing cell lines treated with the 8C7 ADC. Treatment with the highest dose of ADC resulted in tumor growth reduction by 90% in A431, 80% in DAOY, and 62% in MSTO-211H (Figure 3.11). No visible off-target toxicity was observed in any mice as shown by the fact that there was no change in body and organ weights. Even the mesothelioma cell line, which displays lower PTGFRN expression, still displayed tumor growth inhibition when treated with the 8C7-ADC, whereas the PTGFRN-negative cell line, MDA-MB-231, showed no response to the 8C7 ADC, and

no difference in tumor growth was observed between IgG negative control ADC and the 8C7 ADC groups (Figure 3.12).

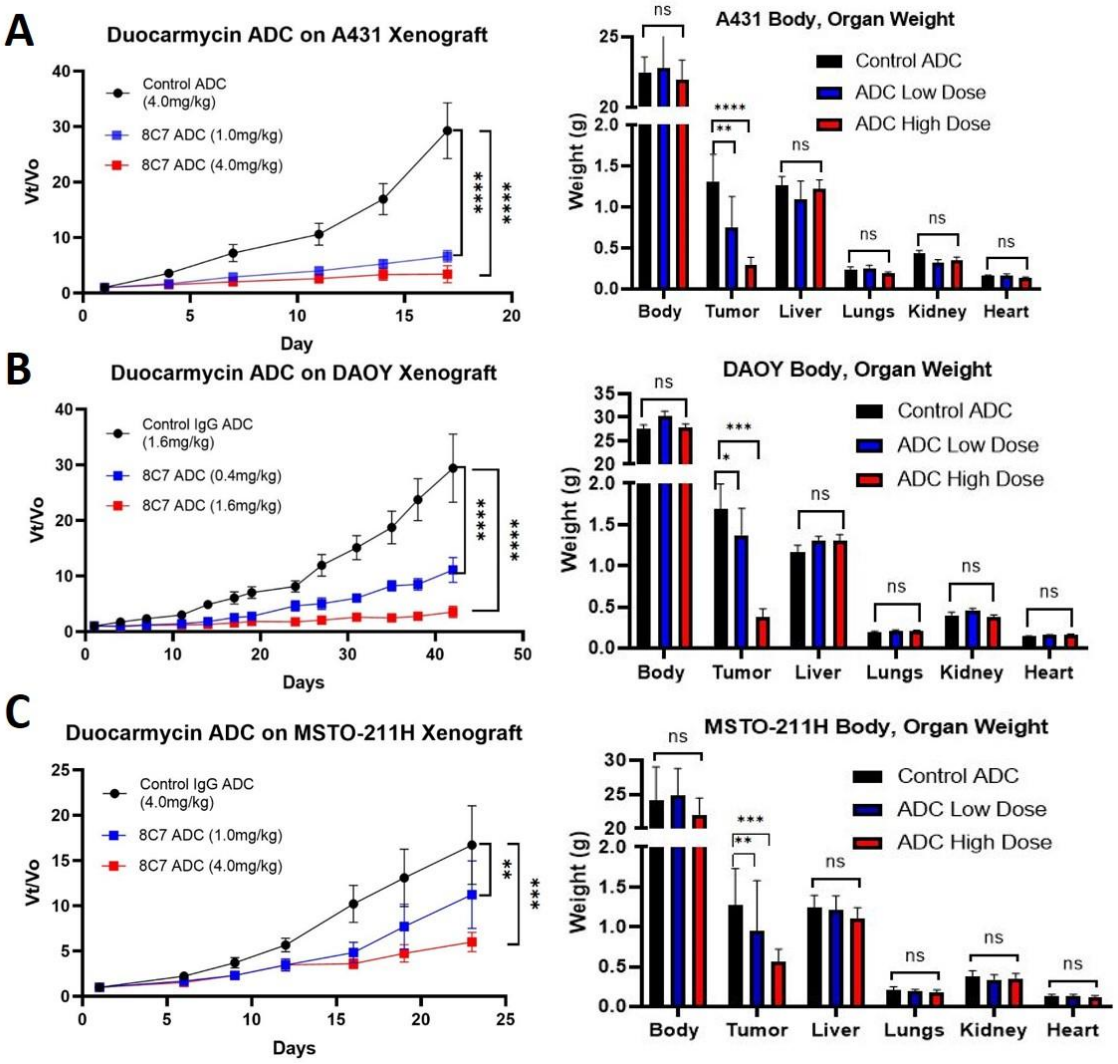

Figure 3.11 *In Vivo* Treatment of PTGFRN-Positive Tumors in Nude Mice. Treatment of nude mice bearing PTGFRN-positive (A) A431, (B) DAOY, and (C) MSTO-211H tumors with our 8C7-Duocarmycin antibody shows significant reduction in tumor growth compared to Isotype Control ADC, with no obvious signs of toxicity at time of necropsy.

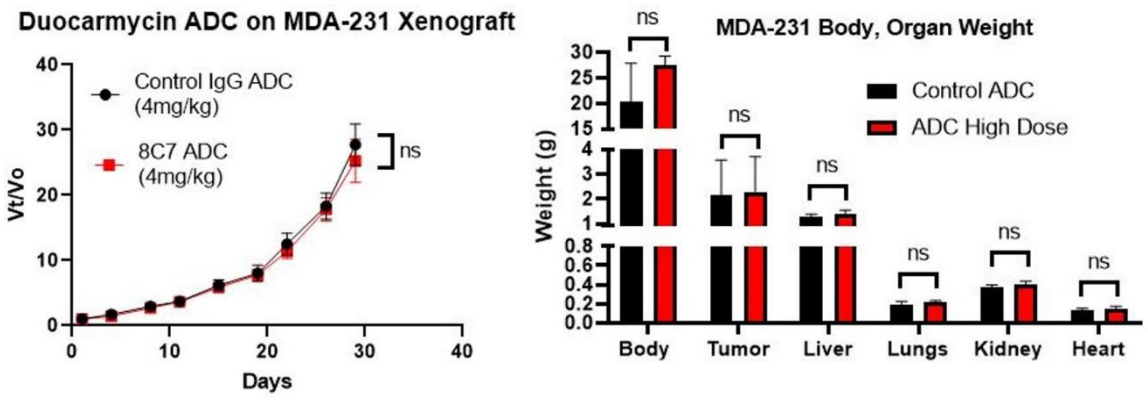

Figure 3.12 *In Vivo* Treatment of PTGFRN-Negative Tumors in Nude Mice. Treatment of nude mice bearing PTGFRN-negative MDA-231 tumors with our 8C7-Duocarmycin antibody shows no difference in tumor growth compared to Isotype Control ADC, with no obvious signs of toxicity, indicating high specificity of our 8C7 antibody.

3.4 Discussion

Using the selected mouse monoclonal antibody 33B7 to carry out immunoprecipitation, followed by mass spectrometry analysis, our laboratory has identified Prostaglandin F2 Receptor Negative Regulator (PTGFRN) as an internalizable cell-surface target expressed on several cancer cells. The identification of PTGFRN carried out with spindle cell carcinoma cells was confirmed in human head and neck cancer A431 and medulloblastoma DAOY cells by immunoprecipitation with the 33B7 antibody followed by mass spectrometry analysis.

The validation of PTGFRN as the target for 33B7 antibody was performed by showing that HEK-293A cells, which cannot bind the 33B7 antibody, and do not express PTGFRN, were able to bind 33B7 when the cells were transfected with human PTGFRN cDNA, as shown by flow binding assay and by immunofluorescence staining. 33B7 was also able to internalize PTGFRN as shown by immunofluorescence, as well as inhibit cell proliferation of PTGFRN-expressing cell lines by toxic payload delivery, either directly

via a 33B7-ADC, or indirectly via an anti-mouse secondary antibody saporin conjugate. We have demonstrated a statistically significant and dose-dependent efficacy of the 33B7 ADC in inhibiting the proliferation of several cancer cell lines that express PTGFRN, when compared to control ADC antibody. Using A431 cells and AGSCC-3 cells as mouse xenografts models, we show that 33B7-ADC inhibited tumor growth when compared to control-ADC antibody.

Using this preliminary data, we were able to generate a second-generation, fully human monoclonal antibody with improved binding characteristics. This antibody was also able to bind specifically to PTGFRN, internalize the receptor, and deliver a toxic payload that would kill PTGFRN-positive cancer cells, and not PTGFRN-negative cells. This improved antibody served as the basis for a new ADC. This time, when conjugated to the DNA-alkylating compound duocarmycin, this human ADC displayed significantly improved anti-cancer effect, in both *in vitro* and *in vivo* assays. The efficacy of this ADC in mesothelioma and pediatric medulloblastoma is of particular interest, because, as covered extensively in chapter 1, these two cancers display unmet needs in tailored therapy, and affect a vulnerable population of patients who would highly benefit from the approval of an ADC therapy. Our work here validates PTGFRN as a potential ADC target, and our human antibody 8C7 is a great starting point for further ADC optimization.

Previous studies in optimizing payload delivery to cellular interiors by ADCs have identified multiple factors that determine the efficacy of ADC internalization. Receptor recycling of the target protein can re-release an ADC back to the cell exterior, and the presence of the neonatal Fc receptor (FcRn) can also shuttle the ADC back to the

cell surface, both of which lower the payload concentration inside the cell. Importantly, rate of internalization can differ between antibodies based on their biochemical properties, so analysis of the binding affinity and rate of internalization should be considered when developing or selecting prospective antibodies. As covered earlier, once an ADC actually gets inside the cell, and begins to be trafficked to the lysosome, the chemistry of a given linker may also affect how well the payload dissociates from the antibody, and how much can accumulate inside the cell (261). Cleavable linkers typically result in slightly higher amounts of free payload inside the cell, and these linkers can be designed to cleave at various acidic pH levels. Doing so can allow one to control at which point a payload is cleaved after internalization, whether this will occur in the early endosome, late endosome, or in the lysosome itself (262). All these factors should be considered when trying to develop an ADC, and will be taken into consideration in further optimization of our anti-PTGFRN antibodies.

Chapter 4

Conclusions and Future Discussions

PTGFRN is a cell-surface transmembrane protein that is upregulated in certain solid tumor cancers, such as the rare and hard-to-treat medulloblastoma and mesothelioma, but is undetectable in many healthy tissues. This upregulation can be used to specifically target these cancers through the use of an Antibody-Drug Conjugate, which can deliver cytotoxic payloads directly to the cancer, without affecting healthy, non-cancerous tissue. Our identification of PTGFRN as a validated ADC target is the first step in developing specific therapy for several solid tumor cancers (melanoma, kidney carcinomas, etc.), including Pediatric Medulloblastoma and Mesothelioma, two cancers that are classified as rare and aggressive, with no tailored therapy currently on the market. Our research highlights that by conjugating our fully human anti-PTGFRN antibody 8C7 to the payload Duocarmycin using a cleavable valine-citrulline linker, superior anti-cancer response in reducing tumor growth rate, as well as tumor volume, was accomplished, with no appreciable signs of off-target toxicity.

Our research here also reinforces a potential correlation between PTGFRN and cancer metastasis. PTGFRN expression has been linked to poor prognosis and lower survival rates in patients with glioblastoma (149,263). PTGFRN has also been reported to be upregulated in many different types of cancer, increasingly so in metastatic cancer cells, compared to their non-metastatic counterparts (146,148,217). The performed immunohistochemistry described here indicates that PTGFRN expression is undetectable in various healthy tissues such as cardiac, lung, kidney, brain, breast, and colon tissue, whereas PTGFRN expression is significantly elevated in melanoma, squamous cell

carcinoma, papillary renal cell carcinoma, clear cell carcinoma, pancreatic ductal adenocarcinoma, and mesothelioma tissues.

We also found that PTGFRN expression is drastically increased in mesothelioma malignant lesions when compared to benign lesions, depicting PTGFRN as a potential novel biomarker. This upregulation may provide an opportunity for exploitation in treating cancers that have transformed from benign to malignant. Tumor metastasis is a prognostic factor for aggressive features, and a marked increase in drug resistance. Thus, an ADC that targets increased expression of any biomarker during this stage would be an invaluable tool to develop novel therapeutic approaches to treat patients suffering from these advanced cancers (264).

While our ADC in its current form shows remarkably improved therapeutic efficacy compared to its first-generation counterpart, there is still plenty of room for improvement. The duocarmycin payload analogue (Duocarmycin SA) we use in this design is biologically active in its standard form. *Seco*-DUBA is a newer analogue that is in prodrug form, which only becomes active when it is cleaved from the antibody, and undergoes spontaneous spirocyclization (265). This step further reduces off-target toxicity due to the bystander effect. Switching to this analogue of duocarmycin would also require us to switch to a Val-Cit-PABC linker moiety, which includes a polyethylene glycol (PEG) element to improve solubility, as well as a self-immolative component for the aforementioned prodrug conversion (266). Our monoclonal antibody, 8C7, could also be further modified via cysteine engineering. As previously discussed, this process consists of genetically mutating additional cysteines into the genetic sequence of the antibody. Reduction and conjugation to these non-natural cysteines both preserves the

internal disulfide bonds of the antibody heavy and light chains, as well as allows for more control over the homogeneity of our resultant ADC. These changes would likely have a cumulative effect of improved pharmacokinetic/pharmacodynamic properties, and therapeutic efficacy, although a baseline for these properties with our current design still needs to be established (267,268). Regardless, our ADC strategy and the results reported here provide a novel therapeutic opportunity to treat aggressive cancers, such as pediatric medulloblastoma and mesothelioma, an area of unmet need.

While our ADC relies on the overexpression of PTGFRN for its effect, it is possible for cancers to overcome drug treatment by downregulating the expression of the drug target, as in the case of EGFR downregulation in non-small cell lung cancer (269). In this example, treatment of non-small cell lung cancer with tyrosine kinase inhibitors led to acquired drug resistance, as the cancer eventually began to downregulate the expression of EGFR, significantly reducing the effectiveness of the RTK inhibitors. While further research will need to be carried out to see if PTGFRN downregulation could be one method cancers utilize to resist ADC therapy, in this case, the downregulation of PTGFRN could, in theory, result in an increase in autophagy, as seen in our *in vitro* culture and confirmed by mass spectrometry. If this is the case, inhibition of said autophagy could be an avenue for combination targeting of cancer, even after initial drug resistance (270).

In chapter 2, we investigated the effect of PTGFRN expression on a cancer cell's phenotype. By doing so, we observed that its overexpression correlated with properties also reported in metastatic cells, further validating PTGFRN's relationship to metastasis. This also supports our argument that an ADC targeting PTGFRN would be valuable, as

metastatic cancers are among the hardest to treat, and have limited effective chemotherapies. The expression of the cell-surface tetraspanin PTGFRN has a significant effect on all three cancer cell phenotypes, demonstrating a positive correlation with a cells ability to proliferate in reduced serum conditions, migrate, grow in colonies, and form 3D spheroids, specifically in the case of epidermoid carcinoma (A431) and pediatric medulloblastoma (DAOY). The loss of PTGFRN expression also coincides with an increase in the occurrence of autophagy, a mechanism of controlled cell death. In mesothelioma specifically, immunohistological staining of patient-derived tissue samples demonstrate that progression of mesothelioma from benign to malignant results in a significant increase in PTGFRN expression, reinforcing the trends we observed in our *in vitro* functional assays.

Also reinforcing our functional assay results was the mass spectrometry pathway analysis. By using a global approach in comparing control A431 with their PTGFRN shRNA knockdown counterparts, we found that the biggest impact from PTGFRN knockdown was the downregulation of proteins involved in metabolite precursor synthesis, the electron transport chain, and anterograde transport from the Endoplasmic Reticulum (ER) to the Golgi Apparatus. Also downregulated after PTGFRN knockdown were pathways involving VEGFA-VEGFR2 signaling, mRNA metabolic processing, chromosome maintenance, and NADH oxidation. Obviously, a cell with deficiencies in getting proteins to their correct subcellular location, the production of metabolic substrates, and cellular respiration would likely not be able to proliferate, especially in low-serum conditions. These impacted pathways would also explain the knockdown cell's inability to form and grow in single-cell colonies, or in spheroid conditions. And

while cell migration was not specifically a pathway flagged in the analysis, we have indicated that numerous downregulated proteins have been previously found to regulate cell migration, such as NUDT1, DKC1, and RBBP7 among others. Regardless, the mass spectrometry analysis carried out seemingly corroborates everything we observed in our functional assays.

When analyzing the pathways that saw an upregulation of protein members after PTGFRN knockdown, the most significantly increased pathways are that of cytokine signaling in the immune system, the innate immune response, and neutrophil degranulation. This observation perhaps provides the largest potential for future investigation, as it indicates the role of PTGFRN as a negative regulator of this process in natural conditions, although it would have to be determined experimentally if this negative regulation of the immune response is due to binding and inactivation of specific proteins by PTGFRN, or perhaps by PTGFRN regulating upstream transcription factors. Regardless, PTGFRN''s specific role in the immune system could help us better understand the various roles this tetraspanin plays.

The discovery that PTGFRN silencing in A431 results in an increase in autophagy certainly merits more investigation as well. As highlighted earlier, this process can be either pro-cancer or pro-death, and future work probing the various signaling molecules recruited with the process would help determine which of the two outcomes is occurring. This would be an additional valuable tool to further combat cancer, as if this autophagy is pro-cancer, targeted inhibition of this autophagy can provide an additional treatment. Our observation that PTGFRN knockdown resulted in an increase in cellular autophagy was one that is at least indirectly confirmed in the mass spectrometric analysis. Several

proteins involved in the positive regulation of autophagy were found to be increased after PTGFRN knockdown, and the process of apoptotic cleavage of cellular proteins was decreased after PTGFRN knockdown. Since one main purpose of autophagy is to stave off apoptosis in conditions of stress, it would seem as if the autophagy observed in A431 after PTGFRN knockdown is achieving its goal.

The global mass spectrometric analysis of proteins that co-immunoprecipitated with PTGFRN using the anti-PTGFRN antibody 8C7 also sheds new light on the proteins that directly associate, or complex with, PTGFRN, and the pathways in which these proteins are involved. Overwhelmingly, PTGFRN was found to be associated with proteins that regulate RNA metabolism and translation, including subunits of the ribosome itself, RNA polymerase, and pre-mRNA-processing proteins. The second-most represented pathway is that of VEGFA-VEGFR2 signaling. The reported upregulation of PTGFRN in cancers that become malignant and/or metastatic makes perfect sense with this information. In this advanced stage of cancer progression, cancer cells have to heavily modify the expression of numerous proteins to evade immune detection, increase proliferation signaling, and secrete various proteases which allow them to alter and navigate through the ECM during migration from the primary tumor (271–273). In order to fulfill the needs of the rapidly proliferating and/or migrating cells, there is a requirement for increase in the transcription, processing, and translation of RNA into proteins. Therefore, PTGFRN would also need to be upregulated to help support this increase in cellular transcription and translation.

One concerning point of this co-IP mass spectrometric analysis is the fact that E-Cadherin was not found to be significantly enriched in our PTGFRN IP samples

compared to the negative IgG control IP samples. This is not in agreement with what was observed in our co-IP and immunoblot, where E-Cadherin appears to be found to be co-immunoprecipitated with PTGFRN. The specificty of the antibody for E-cadherin used in the co-IP experiments was verified by showing that the E-Cadherin immunoblot band intensity was decreased when E-Cadherin expression was inhibited by siRNA indicating that the co-IP western blot findings are valid. Resolving this apparent contradiction will require further investigation as stated previously. One possibility would be that the threshold of adjusted statistical significance may have been too high for the purposes of our analysis. We may be able to adjust our IP wash conditions in order to minimize non-specific binding to non-immune IgG negative control, or inversely, develop gentle conditions which would better maintain protein interaction within the anti-PTGFRN IP so that more E-Cadherin could then be detected by mass spectrometric analysis.

Taken together, we hypothesize that PTGFRN does impact a cell's overall phenotype, and results in a metastatic-like profile. The data presented here points to PTGFRN's potential importance in the later steps of metastasis, when a cell has detached from a primary tumor, and needs to migrate through stromal cells, colonize a secondary organ site, and proliferate into a secondary multicellular tumor. The increase in PTGFRN reported in some metastatic cancers falls in line with the increase in cellular metabolism that these advanced-staged cancers require. The upregulation of oncogenes and downregulation of onco-suppressors is achieved through the regulation of gene transcription and translation. The discovery that PTGFRN directly associates with proteins involved in this RNA regulation further supports the idea that PTGFRN is a key player that helps maintain the elevated metabolism and protein production required by

cancer cells. Therefore, loss of PTGFRN expression acts as a cellular stressor, hampering the cell's metabolism and precluding normal protein translation and intracellular shuttling. In response to this stress, the cell initiates autophagy in an attempt to prevent apopotosis. This dissertation aims to further characterize PTGFRN's potential role in cancer metastasis, and that it is a valid target for ADC development, which could be used to treat mesothelioma and pediatric medulloblastoma, two rare and aggressive cancers which have no tailored therapy available at this time.

Appendix 1: Supplementary Figures

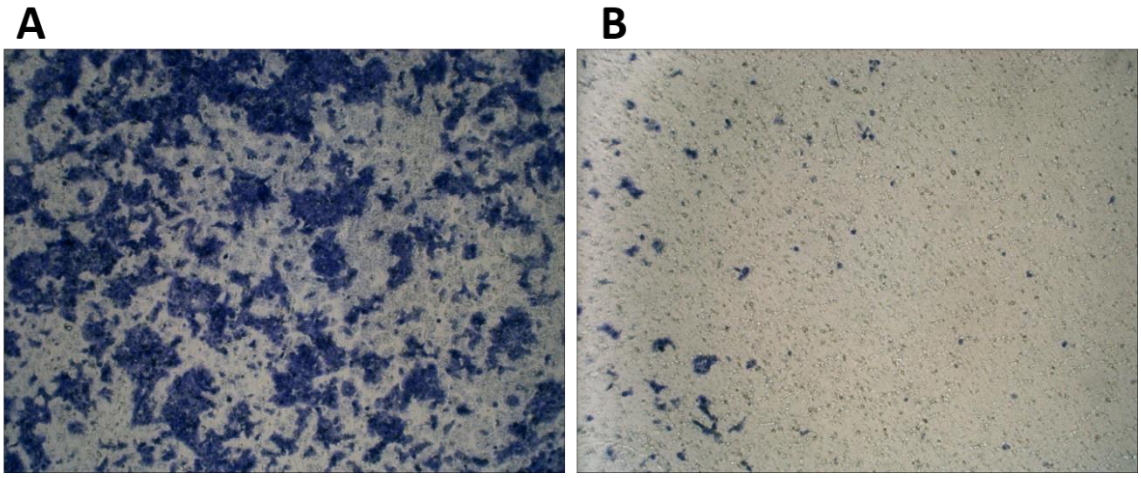

Figure 1A.1. Migration of A431 Cells After siRNA Transfection. A431 cells transfected with either (A) scrambled siRNA or (B) PTGFRN siRNA shows that knockdown of PTGFRN by siRNA results in a significant decrease of migrated cells

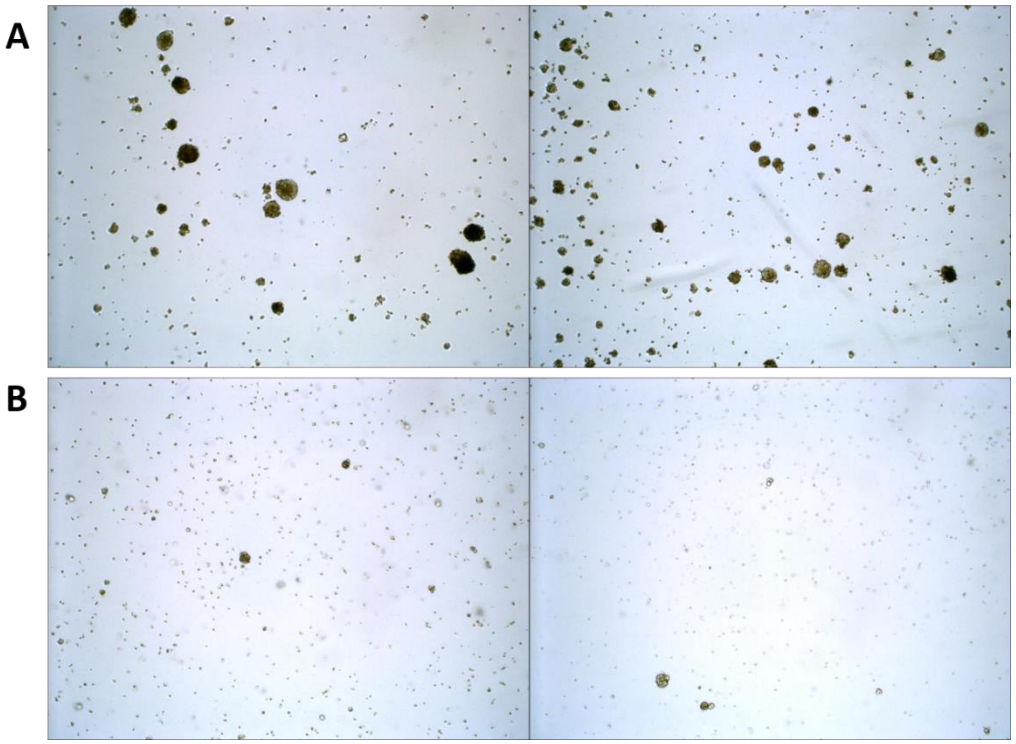

Figure 1A.2. A431 Spheroid Growth After siRNA Transfection. A431 cells transfected with either (A) scrambled siRNA or (B) PTGFRN siRNA shows that knockdown of PTGFRN by siRNA results in a significant decrease of 3D spheroids formed.

Figure 1A.3. Immunoblot of 2D A431 Protein Expression. Stable knockdown of PTGFRN had no significant effect on the expression of E-Cadherin or Integrin β1in A431 cells grown in 2D culture.

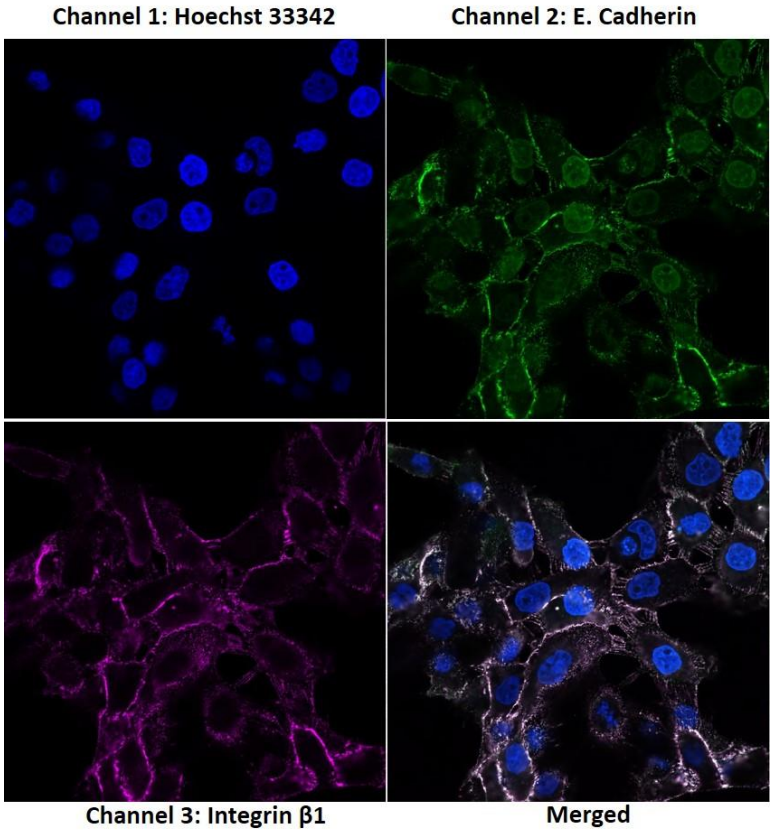

Figure 1A.4. Immunofluorescence on Stable A431 shRNA Cells. Knockdown of PTGFRN in A431 by shRNA had no effect on the localization of E-Cadherin and Integrin β1.

Appendix 2. Additional Tables

Table 2A.1. Pathway analysis of all genes found to be upregulated after PTGFRN knockdown by shRNA in A431. Statistical significance determined at p <0.05.

Pathway Description	adj. p-value	Genes Upregulated after PTGFRN Knockdown
Cytokine Signaling in Immune system	2.87E-07	BST2,CASP3,EIF4A2,ICAM1,IFI35,IFIT3,IL1A,LCN2,MX1,SERPINB2,PML,PSMA1,PSMB5,PSMB7,SDC1,SOD2,STAT, IKBKG,AIP,N4BP1,RIGI
innate immune response	1.78E-05	ATP1B1,BST2,GAPDH,IFI35,IFIT3,LCN2,MX1,PRDX1,PML,S100A9,STAT1,IKBKG,BCL10,N4BP1,TUBB4B,RIGI, PPP1R14B,NLRP2,TUBB,EVPL,LDLR,PSMA1
Neutrophil degranulation	2.02E-04	ALDOA,BST2,EEF2,FTL,LCN2,PA2G4,PGAM1, PIGR,PSMB7,S100A9,HUWE1, TUBB4B,CCT8,TUBB
Signaling by Rho GTPases	4.98E-04	ARHGAP1,CCT6A,MYH9,MYL6,S100A9,TPM3, TPM4,ARHGEF5,PICALM,KIF14,WASF2,TUBB4B,SH3BP1,ANLN,NDE1,MRTFA,ALDOA,HCLS1,MARCKS,PDCD6IP, PALLD,SERPINH1,KRT17,HOOK1
G1/S Transition	4.98E-04	CCNB1,MCM3,MCM6,PRIM1,PSMA1,PSMB5,PSMB7,RBL1,ARAF,CASP3,GAPDH,IL1A,TUBB4B,ADRM1,TUBB,LDLR,PML,PPT1,SGTA,UBE2L3,UCHL3,KIF14,PDCD6IP,UBXN1,CHMP5,RNF123,SOD2,DCTN2,DCTN4,IKBKG,ICAM1,S100A9,THOP1,BCL10,HUWE1,N4BP1,RIGI,STAT1,PRDX1,SCO2,NDE1,LIG4,ANP32A,ATP6V1C1,EGFR,PEA15
Motor proteins	6.35E-04	MYH9,MYL6,TPM3,TPM4,KIF14,TUBB4B,DCTN2,DCTN4,TUBB,CCNB1,ENSA,MCM3,MCM6, PRIM1,PSMA1,PSMB5,PSMB7,RBL1,NDE1,CASP3,GAPDH,HCLS1,IKBKG,WASF2,SOD2,CCT8,TFB2M,ANXA3,ICAM1,IFI35,LIG4,PRDX1,BCL10,HOOK1,RSPH9,UBE2L3,ATP6V1C1,STX7,EGFR
Interferon Signaling	6.44E-04	BST2,EIF4A2,ICAM1,IFI35,IFIT3,MX1,PML,STAT1,RIGI,ATP1B1,EGFR,LIG4,PSMA1,PSMB5,PSMB7,SDC1,IKBKG,PDCD6IP,TUBB4B,CHMP5,TUBB,ARAF,CASP3,LDLR,CCNB1,IL1A,ADRM1,N4BP1,GAPDH,ZNF573

Table 2A.1. Pathway analysis of all genes found to be upregulated after PTGFRN knockdown by shRNA in A431, continued

mitotic cell cycle	8.65E-04	CCNB1,ENSA,MCM3,MCM6,PML,KIF14,PDCD6IP,TUBB4B,DCTN2,CHMP5,ANLN,NDE1,PSMG2,TUBB,LIG4,MYH9,NASP,SMC6,PICALM,IKBKG,STX7
Cori cycle	1.06E-03	ALDOA,GAPDH,PFKP,PGAM1,FH,IDH3A,GNPDA1,EGFR,SCO2,SDC1,CASP3,IL1A,LIG4
regulation of proteolysis	3.15E-03	ARAF,SERPINH1,GAPDH,MYH9,SERPINB2,PML,S100A9,SGTA,PICALM,BCL10,N4BP1,BCL2L13,UBXN1,NLRP2,ICAM1,IL1A,PEA15,EGFR,ARHGEF5,SH3BP1,SOD2
cellular homeostasis	6.27E-03	ALDOA,ATP1B1,ATP6V1C1,FTL,IL1A,PRDX1,PML,PPT1,RBM4,S100A9,SOD2,PICALM,SCO2
regulation of amide metabolic process	8.86E-03	CASP3,EEF2,EIF4A2,GAPDH,KRT17,PA2G4,PGAM1,RBM4,PICALM,CNOT11,NIBAN1,MTPN
response to reactive oxygen species	8.89E-03	CASP3,EGFR,IL1A,PRDX1,SDC1,SOD2,STAT1,EEF1D,LIG4,PML,PSMB5,RBM4,N4BP1,CCNB1,ATIC,S100A9,BCL10,CHMP5,KRT17,SH3BP1,MRTFA,ATP1B1
Endocytosis	8.98E-03	EGFR,LDLR,PML,SNX2,PDCD6IP,EHD4,CHMP5,EPS15L1,FTL,MYH9,PICALM,TUBB4B,DCTN2,DCTN4,ANXA3,PPT1,SDC1,WASF2,SH3BP1,ARHGAP1,EHHADH,CASP3
proteasome assembly	9.01E-03	PSMG1,ADRM1,PSMG2
wound healing	9.23E-03	CASP3,CLIC1,EVPL,IL1A,MYH9,SERPINB2,SDC1,CHMP5,MRTFA,SOD2,MBNL1,MYL6,MTPN
Diseases of signal transduction by growth factor receptors and second messengers	1.10E-02	ARAF,ATIC,EGFR,MYH9,PSMA1,PSMB5,PSMB7,STAT1,TPM3,TPM4,MYL6,ALDOA,ATP1B1,SCO2
cytokinetic process	1.22E-02	MYH9,PDCD6IP,CHMP5,ANLN,ATP1B1,EGFR,PPT1,SGTA,PICALM,STX7,SH3BP1,ATP6V1C1,HOOK1

Table 2A.1. Pathway analysis of all genes found to be upregulated after PTGFRN knockdown by shRNA in A431, continued

positive regulation of DNA-binding transcription factor activity	1.22E-02	ANXA3,HCLS1,S100A9,ARHGEF5,IKBKG,BCL10, RIGI,MTPN,BST2,EEF1D,GAPDH,IL1A,STAT1, NLRP2,ICAM1,EGFR,WASF2,EVPL,STX7
regulation of fibroblast proliferation	1.42E-02	CCNB1,EGFR,LIG4,PML,SOD2,IL1A,RBL1,KIF14,PDCD6IP,CHMP5,ANLN,PSMG2,SMC6,CNOT11,ARAF,CASP3,PEA15,PRDX1,SCO2
Cytokine Signaling in Immune system	2.87E-07	BST2,CASP3,EIF4A2,ICAM1,IFI35,IFIT3,IL1A,LCN2,MX1, SERPINB2,PML,PSMA1,PSMB5,PSMB7,SDC1, SOD2,STAT1,IKBKG,AIP,N4BP1,RIGI
Signaling by Interleukins	2.02E-04	CASP3,ICAM1,IL1A,LCN2,SERPINB2,PSMA1,PSMB5,PSMB7,SDC1,SOD2,STAT1,IKBKG,AIP, N4BP1
innate immune response	1.78E-05	ATP1B1,BST2,GAPDH,IFI35,IFIT3,LCN2,MX1,PRDX1,PML, S100A9,STAT1,IKBKG,BCL10,N4BP1,TUBB4B, RIGI,PPP1R14B,NLRP2,TUBB
regulation of defense response	1.84E-01	EVPL,IFI35,LDLR,PSMA1,S100A9, STAT1,BCL10,N4BP1,RIGI,NLRP2
Neutrophil degranulation	2.02E-04	ALDOA,BST2,EEF2,FTL,LCN2,PA2G4,PGAM1, PIGR,PSMB7,S100A9,HUWE1,TUBB4B,CCT8,TUBB
Signaling by Rho GTPases	4.98E-04	ARHGAP1,CCT6A,MYH9,MYL6,S100A9, TPM3,TPM4, ARHGEF5,PICALM,KIF14, WASF2,TUBB4B,SH3BP1,ANLN,NDE1,MRTFA
Signaling by Rho GTPases, Miro GTPases and RHOBTB3	4.98E-04	ARHGAP1,CCT6A,MYH9,MYL6,S100A9,TPM3, TPM4, ARHGEF5,PICALM,KIF14,WASF2,TUBB4B,SH3BP1,ANLN,NDE1,MRTFA
actin filament-based process	7.98E-04	ALDOA,HCLS1,MARCKS,MYH9,MYL6,TPM3, TPM4,ARHGEF5,PDCD6IP,WASF2,PALLD,SH3BP1,ANLN,MRTFA
actin cytoskeleton organization	1.06E-03	ALDOA,HCLS1,MARCKS,MYH9,TPM3,TPM4, ARHGEF5,PDCD6IP,WASF2,PALLD,SH3BP1,ANLN,MRTFA
RHO GTPase cycle	1.29E-02	ARHGAP1,CCT6A,TPM3,TPM4,ARHGEF5,PICALM,KIF14,WASF2,SH3BP1,ANLN

Table 2A.1. Pathway analysis of all genes found to be upregulated after PTGFRN knockdown by shRNA in A431, continued

supramolecular fiber organization	3.84E-02	ALDOA,SERPINH1,HCLS1,KRT17,MARCKS,TPM3,TPM4,SH3BP1,HOOK1,NDE1
actin filament organization	1.01E-01	ALDOA,HCLS1,MARCKS,TPM3,TPM4,SH3BP1
G1/S Transition	4.98E-04	CCNB1,MCM3,MCM6,PRIM1,PSMA1,PSMB5,PSMB7,RBL1
Alzheimer's disease	6.44E-04	ARAF,CASP3,GAPDH,IL1A,PSMA1,PSMB5,PSMB7,TUBB4B,ADRM1,TUBB
protein catabolic process	6.44E-04	CASP3,LDLR,PML,PPT1,PSMA1,PSMB5,PSMB7,SGTA,UBE2L3,UCHL3,KIF14,PDCD6IP,ADRM1,UBXN1,CHMP5,RNF123
Mitotic G1 phase and G1/S transition	6.44E-04	CCNB1,MCM3,MCM6,PRIM1,PSMA1,PSMB5,PSMB7,RBL1
Huntington disease	1.33E-03	CASP3,PSMA1,PSMB5,PSMB7,SOD2,TUBB4B,DCTN2,ADRM1,DCTN4,TUBB
Alzheimer disease	1.33E-03	ARAF,CASP3,GAPDH,IL1A,PSMA1,PSMB5,PSMB7,IKBKG,TUBB4B,ADRM1,TUBB
Pathways of neurodegeneration - multiple diseases	1.51E-03	ARAF,CASP3,IL1A,PSMA1,PSMB5,PSMB7,UBE2L3,TUBB4B,DCTN2,ADRM1,DCTN4,TUBB
Alzheimer's disease and miRNA effects	2.08E-03	ARAF,CASP3,GAPDH,IL1A,PSMA1,PSMB5,PSMB7,TUBB4B,ADRM1,TUBB
proteolysis involved in protein catabolic process	5.14E-03	PML,PSMA1,PSMB5,PSMB7,SGTA,UBE2L3,UCHL3,KIF14,PDCD6IP,ADRM1,UBXN1,CHMP5,RNF123
Adaptive Immune System	6.27E-03	ICAM1,PSMA1,PSMB5,PSMB7,S100A9,THOP1,UBE2L3,IKBKG,BCL10,HUWE1,TUBB4B,DCTN2,DCTN4,RNF123
Activation of NF-kappaB in B cells	8.06E-03	PSMA1,PSMB5,PSMB7,IKBKG,BCL10
Interleukin-1 signaling	8.06E-03	IL1A,PSMA1,PSMB5,PSMB7,IKBKG,N4BP1
Orc1 removal from chromatin	8.98E-03	MCM3,MCM6,PSMA1,PSMB5,PSMB7
Synthesis of DNA	8.98E-03	MCM3,MCM6,PRIM1,PSMA1,PSMB5,PSMB7

Table 2A.1. Pathway analysis of all genes found to be upregulated after PTGFRN knockdown by shRNA in A431, continued

The role of GTSE1 in G2/M progression after G2 checkpoint	1.08E-02	CCNB1,PSMA1,PSMB5,PSMB7,TUBB4B
Parkinson disease	1.13E-02	CASP3,PSMA1,PSMB5,PSMB7,UBE2L3,TUBB4B,ADRM1,TUBB
20S proteasome	1.22E-02	PSMA1,PSMB5,PSMB7
Prion disease	1.26E-02	CASP3,IL1A,PSMA1,PSMB5,PSMB7,TUBB4B,ADRM1,TUBB
FCERI mediated NF-kB activation	1.29E-02	PSMA1,PSMB5,PSMB7,IKBKG,BCL10
Downstream signaling events of B Cell Receptor (BCR)	1.29E-02	PSMA1,PSMB5,PSMB7,IKBKG,BCL10
PA28gamma-20S proteasome	1.29E-02	PSMA1,PSMB5,PSMB7
Amyotrophic lateral sclerosis	1.30E-02	CASP3,PSMA1,PSMB5,PSMB7,TUBB4B,DCTN2,ADRM1,DCTN4,TUBB
PA28-20S proteasome	1.45E-02	PSMA1,PSMB5,PSMB7
ER-Phagosome pathway	1.51E-02	PSMA1,PSMB5,PSMB7,S100A9,IKBKG
Proteasome	1.51E-02	PSMA1,PSMB5,PSMB7,ADRM1
Class I MHC mediated antigen processing & presentation	1.57E-02	PSMA1,PSMB5,PSMB7,S100A9,THOP1,UBE2L3,IKBKG,HUWE1,RNF123
ubiquitin-dependent protein catabolic process	1.61E-02	PML,PSMA1,PSMB5,PSMB7,SGTA,UBE2L3,UCHL3,KIF14,ADRM1,UBXN1,CHMP5
Switching of origins to a post-replicative state	1.61E-02	MCM3,MCM6,PSMA1,PSMB5,PSMB7
Deubiquitination	1.63E-02	PSMA1,PSMB5,PSMB7,UCHL3,IKBKG,ADRM1,RIGI,RNF123
Ub-specific processing proteases	1.64E-02	PSMA1,PSMB5,PSMB7,IKBKG,ADRM1,RIGI,RNF123
Interleukin-1 family signaling	1.73E-02	IL1A,PSMA1,PSMB5,PSMB7,IKBKG,N4BP1

Table 2A.1. Pathway analysis of all genes found to be upregulated after PTGFRN knockdown by shRNA in A431, continued

modification-dependent protein catabolic process	1.76E-02	PML,PSMA1,PSMB5,PSMB7,SGTA,UBE2L3,UCHL3,KIF14,ADRM1,UBXN1,CHMP5
Downstream TCR signaling	2.02E-02	PSMA1,PSMB5,PSMB7,IKBKG,BCL10
modification-dependent macromolecule catabolic process	2.02E-02	PML,PSMA1,PSMB5,PSMB7,SGTA,UBE2L3,UCHL3,KIF14,ADRM1,UBXN1,CHMP5
DNA Replication Pre-Initiation	2.02E-02	MCM3,MCM6,PRIM1,PSMA1,PSMB5,PSMB7
CLEC7A (Dectin-1) signaling	2.20E-02	PSMA1,PSMB5,PSMB7,IKBKG,BCL10
S Phase	2.20E-02	MCM3,MCM6,PRIM1,PSMA1,PSMB5,PSMB7
UCH proteinases	2.23E-02	PSMA1,PSMB5,PSMB7,UCHL3,ADRM1
G2/M Checkpoints	2.37E-02	CCNB1,MCM3,MCM6,PSMA1,PSMB5,PSMB7
Antigen processing-Cross presentation	2.40E-02	PSMA1,PSMB5,PSMB7,S100A9,IKBKG
26S proteasome	2.53E-02	PSMA1,PSMB5,PSMB7
Signaling by the B Cell Receptor (BCR)	2.85E-02	PSMA1,PSMB5,PSMB7,IKBKG,BCL10
proteasome-mediated ubiquitin-dependent protein catabolic process	2.86E-02	PML,PSMA1,PSMB5,PSMB7,SGTA,KIF14,ADRM1,UBXN1
Proteasome degradation	3.14E-02	PSMA1,PSMB5,PSMB7,UCHL3
DNA Replication	3.44E-02	MCM3,MCM6,PRIM1,PSMA1,PSMB5,PSMB7
TCR signaling	3.52E-02	PSMA1,PSMB5,PSMB7,IKBKG,BCL10
Transcriptional regulation by RUNX2	3.60E-02	CCNB1,PSMA1,PSMB5,PSMB7,STAT1

Table 2A.1. Pathway analysis of all genes found to be upregulated after PTGFRN knockdown by shRNA in A431, continued

proteasomal protein catabolic process	4.02E-02	PML,PSMA1,PSMB5,PSMB7,SGTA,KIF14,ADRM1,UBXN1
Cellular response to chemical stress	4.03E-02	PRDX1,PSMA1,PSMB5,PSMB7,SOD2,SCO2
Regulation of RUNX2 expression and activity	4.51E-02	PSMA1,PSMB5,PSMB7,STAT1
Fc epsilon receptor (FCERI) signaling	4.76E-02	PSMA1,PSMB5,PSMB7,IKBKG,BCL10
Cell Cycle Checkpoints	4.88E-02	CCNB1,MCM3,MCM6,PSMA1,PSMB5,PSMB7,NDE1
Activation of APC/C and APC/C:Cdc20 mediated degradation of mitotic proteins	5.12E-02	CCNB1,PSMA1,PSMB5,PSMB7
Nuclear events mediated by NFE2L2	5.40E-02	PRDX1,PSMA1,PSMB5,PSMB7
C-type lectin receptors (CLRs)	5.48E-02	PSMA1,PSMB5,PSMB7,IKBKG,BCL10
Assembly of the pre-replicative complex	5.48E-02	MCM3,MCM6,PSMA1,PSMB5,PSMB7
Regulation of APC/C activators between G1/S and early anaphase	5.67E-02	CCNB1,PSMA1,PSMB5,PSMB7
Antigen processing: Ubiquitination & Proteasome degradation	5.73E-02	PSMA1,PSMB5,PSMB7,THOP1,UBE2L3,HUWE1,RNF123

Table 2A.1. Pathway analysis of all genes found to be upregulated after PTGFRN knockdown by shRNA in A431, continued

PA700-20S-PA28 complex	6.13E-02	PSMA1,PSMB5,PSMB7
HIV Infection	6.48E-02	LIG4,PSMA1,PSMB5,PSMB7,PDCD6IP,CHMP5
APC/C-mediated degradation of cell cycle proteins	6.69E-02	CCNB1,PSMA1,PSMB5,PSMB7
Regulation of mRNA stability by proteins that bind AU-rich elements	6.69E-02	PSMA1,PSMB5,PSMB7,ANP32A
Regulation of mitotic cell cycle	6.69E-02	CCNB1,PSMA1,PSMB5,PSMB7
Mitotic Anaphase	6.85E-02	CCNB1,PSMA1,PSMB5,PSMB7,TUBB4B,NDE1
Mitotic Metaphase and Anaphase	6.95E-02	CCNB1,PSMA1,PSMB5,PSMB7,TUBB4B,NDE1
Cellular responses to stress	7.92E-02	ATP6V1C1,IL1A,PRDX1,PSMA1,PSMB5,PSMB7,SOD2,SCO2,TUBB4B,DCTN2,DCTN4
KEAP1-NFE2L2 pathway	1.14E-01	PRDX1,PSMA1,PSMB5,PSMB7
Cross-presentation of soluble exogenous antigens (endosomes)	1.14E-01	PSMA1,PSMB5,PSMB7
Regulation of activated PAK-2p34 by proteasome mediated degradation	1.19E-01	PSMA1,PSMB5,PSMB7
Regulation of ornithine decarboxylase (ODC)	1.22E-01	PSMA1,PSMB5,PSMB7

Table 2A.1. Pathway analysis of all genes found to be upregulated after PTGFRN knockdown by shRNA in A431, continued

Vpu mediated degradation of CD4	1.24E-01	PSMA1,PSMB5,PSMB7
Autodegradation of the E3 ubiquitin ligase COP1	1.24E-01	PSMA1,PSMB5,PSMB7
Ubiquitin Mediated Degradation of Phosphorylated Cdc25A	1.24E-01	PSMA1,PSMB5,PSMB7
p53-Independent DNA Damage Response	1.24E-01	PSMA1,PSMB5,PSMB7
p53-Independent G1/S DNA damage checkpoint	1.24E-01	PSMA1,PSMB5,PSMB7
Ubiquitin-dependent degradation of Cyclin D	1.24E-01	PSMA1,PSMB5,PSMB7
GSK3B and BTRC:CUL1-mediated-degradation of NFE2L2	1.24E-01	PSMA1,PSMB5,PSMB7
RAF/MAP kinase cascade	1.25E-01	ARAF,EGFR,PSMA1,PSMB5,PSMB7,PEA15
Hedgehog 'off' state	1.25E-01	PSMA1,PSMB5,PSMB7,TUBB4B
Separation of Sister Chromatids	1.26E-01	PSMA1,PSMB5,PSMB7,TUBB4B,NDE1
Regulation of Apoptosis	1.27E-01	PSMA1,PSMB5,PSMB7
Vif-mediated degradation of APOBEC3G	1.32E-01	PSMA1,PSMB5,PSMB7
FBXL7 down-regulates AURKA during mitotic entry and in early mitosis	1.32E-01	PSMA1,PSMB5,PSMB7
Negative regulation of NOTCH4 signaling	1.32E-01	PSMA1,PSMB5,PSMB7
MAPK1/MAPK3 signaling	1.33E-01	ARAF,EGFR,PSMA1,PSMB5,PSMB7,PEA15

Table 2A.1. Pathway analysis of all genes found to be upregulated after PTGFRN knockdown by shRNA in A431, continued

SCF-beta-TrCP mediated degradation of Emi1	1.35E-01	PSMA1,PSMB5,PSMB7
Degradation of AXIN	1.35E-01	PSMA1,PSMB5,PSMB7
Regulation of RUNX3 expression and activity	1.35E-01	PSMA1,PSMB5,PSMB7
AUF1 (hnRNP D0) binds and destabilizes mRNA	1.39E-01	PSMA1,PSMB5,PSMB7
Hh mutants are degraded by ERAD	1.39E-01	PSMA1,PSMB5,PSMB7
Degradation of DVL	1.44E-01	PSMA1,PSMB5,PSMB7
Stabilization of p53	1.44E-01	PSMA1,PSMB5,PSMB7
Metabolism of polyamines	1.53E-01	PSMA1,PSMB5,PSMB7
Hh mutants abrogate ligand secretion	1.53E-01	PSMA1,PSMB5,PSMB7
NIK-->noncanonical NF-kB signaling	1.53E-01	PSMA1,PSMB5,PSMB7
SCF(Skp2)-mediated degradation of p27/p21	1.58E-01	PSMA1,PSMB5,PSMB7
Dectin-1 mediated noncanonical NF-kB signaling	1.58E-01	PSMA1,PSMB5,PSMB7
Degradation of GLI1 by the proteasome	1.58E-01	PSMA1,PSMB5,PSMB7
Degradation of GLI2 by the proteasome	1.58E-01	PSMA1,PSMB5,PSMB7
GLI3 is processed to GLI3R by the proteasome	1.58E-01	PSMA1,PSMB5,PSMB7
Defective CFTR causes cystic fibrosis	1.64E-01	PSMA1,PSMB5,PSMB7
Autodegradation of Cdh1 by Cdh1:APC/C	1.83E-01	PSMA1,PSMB5,PSMB7

Table 2A.1. Pathway analysis of all genes found to be upregulated after PTGFRN knockdown by shRNA in A431, continued

Asymmetric localization of PCP proteins	1.83E-01	PSMA1,PSMB5,PSMB7
Hedgehog ligand biogenesis	1.90E-01	PSMA1,PSMB5,PSMB7
Oxygen-dependent proline hydroxylation of Hypoxia-inducible Factor Alpha	1.94E-01	PSMA1,PSMB5,PSMB7
p53-Dependent G1 DNA Damage Response	1.94E-01	PSMA1,PSMB5,PSMB7
p53-Dependent G1/S DNA damage checkpoint	1.94E-01	PSMA1,PSMB5,PSMB7
MAPK family signaling cascades	2.04E-01	ARAF,EGFR,PSMA1,PSMB5, PSMB7,PEA15
APC/C:Cdc20 mediated degradation of Securin	2.05E-01	PSMA1,PSMB5,PSMB7
Regulation of RAS by GAPs	2.05E-01	PSMA1,PSMB5,PSMB7
G1/S DNA Damage Checkpoints	2.05E-01	PSMA1,PSMB5,PSMB7
PTEN Regulation	2.08E-01	PML,PSMA1,PSMB5,PSMB7
Regulation of PTEN stability and activity	2.09E-01	PSMA1,PSMB5,PSMB7
Spinocerebellar ataxia	2.17E-01	PSMA1,PSMB5,PSMB7,ADRM1
Signaling by NOTCH	2.25E-01	EGFR,PSMA1,PSMB5,PSMB7,STAT1
Cdc20:Phospho-APC/C mediated degradation of Cyclin A	2.30E-01	PSMA1,PSMB5,PSMB7
CDK-mediated phosphorylation and removal of Cdc6	2.30E-01	PSMA1,PSMB5,PSMB7
APC/C:Cdh1 mediated degradation of Cdc20 and other APC/C:Cdh1 targeted proteins in late mitosis/early G1	2.38E-01	PSMA1,PSMB5,PSMB7
APC:Cdc20 mediated degradation of cell cycle proteins prior to satisfation of the cell cycle checkpoint	2.38E-01	PSMA1,PSMB5,PSMB7

Table 2A.1. Pathway analysis of all genes found to be upregulated after PTGFRN knockdown by shRNA in A431, continued

Signaling by Hedgehog	2.39E-01	PSMA1,PSMB5,PSMB7,TUBB4B
Cellular response to hypoxia	2.43E-01	PSMA1,PSMB5,PSMB7
ABC transporter disorders	2.64E-01	PSMA1,PSMB5,PSMB7
Signaling by NOTCH4	2.87E-01	PSMA1,PSMB5,PSMB7
Degradation of beta-catenin by the destruction complex	2.93E-01	PSMA1,PSMB5,PSMB7
Cyclin E associated events during G1/S transition	2.93E-01	PSMA1,PSMB5,PSMB7
Hedgehog 'on' state	3.06E-01	PSMA1,PSMB5,PSMB7
Cyclin A:Cdk2-associated events at S phase entry	3.06E-01	PSMA1,PSMB5,PSMB7
PIP3 activates AKT signaling	3.23E-01	EGFR,PML,PSMA1,PSMB5,PSMB7
MAPK6/MAPK4 signaling	3.39E-01	PSMA1,PSMB5,PSMB7
PCP/CE pathway	3.61E-01	PSMA1,PSMB5,PSMB7
Apoptosis	3.80E-01	CASP3,PSMA1,PSMB5,PSMB7
Transcriptional regulation by RUNX3	3.93E-01	PSMA1,PSMB5,PSMB7
Motor proteins	6.35E-04	MYH9,MYL6,TPM3,TPM4,KIF14,TUBB4B,DCTN2,DCTN4,TUBB
Cell Cycle, Mitotic	1.42E-03	CCNB1,ENSA,MCM3,MCM6,PRIM1,PSMA1,PSMB5,PSMB7,RBL1,TUBB4B,DCTN2,NDE1,TUBB
G2/M Transition	2.45E-03	CCNB1,PSMA1,PSMB5,PSMB7,TUBB4B,DCTN2,NDE1,TUBB
Pathogenic Escherichia coli infection	2.45E-03	CASP3,GAPDH,HCLS1,MYH9,IKBKG, WASF2,TUBB4B,TUBB
Mitotic G2-G2/M phases	2.45E-03	CCNB1,PSMA1,PSMB5,PSMB7,TUBB4B,DCTN2,NDE1,TUBB
Cell Cycle	8.27E-03	CCNB1,ENSA,MCM3,MCM6,PRIM1,PSMA1,PSMB5,PSMB7,RBL1,TUBB4B,DCTN2,NDE1,TUBB

Table 2A.1. Pathway analysis of all genes found to be upregulated after PTGFRN knockdown by shRNA in A431, continued

Regulation of PLK1 Activity at G2/M Transition	1.46E-02	CCNB1,TUBB4B,DCTN2,NDE1,TUBB
M Phase	2.40E-02	CCNB1,ENSA,PSMA1,PSMB5,PSMB7,TUBB4B,DCTN2,NDE1,TUBB
Salmonella infection	2.61E-02	CASP3,GAPDH,IKBKG,TUBB4B,DCTN2,DCTN4,TUBB
Loss of Nlp from mitotic centrosomes	4.02E-02	TUBB4B,DCTN2,NDE1,TUBB
Loss of proteins required for interphase microtubule organization from the centrosome	4.02E-02	TUBB4B,DCTN2,NDE1,TUBB
AURKA Activation by TPX2	4.51E-02	TUBB4B,DCTN2,NDE1,TUBB
Organelle biogenesis and maintenance	5.04E-02	SOD2,TUBB4B,DCTN2,CCT8,NDE1,TFB2M,TUBB
immune effector process	5.32E-02	ANXA3,ICAM1,IFI35,LIG4,PRDX1,BCL10,TUBB4B,TUBB
natural killer cell mediated cytotoxicity	5.61E-02	PRDX1,TUBB4B,TUBB
Recruitment of mitotic centrosome proteins and complexes	5.83E-02	TUBB4B,DCTN2,NDE1,TUBB
Centrosome maturation	5.83E-02	TUBB4B,DCTN2,NDE1,TUBB
natural killer cell mediated immunity	6.13E-02	PRDX1,TUBB4B,TUBB
leukocyte mediated immunity	6.29E-02	ANXA3,LIG4,PRDX1,BCL10,TUBB4B,TUBB
Recruitment of NuMA to mitotic centrosomes	7.92E-02	TUBB4B,DCTN2,NDE1,TUBB

Table 2A.1. Pathway analysis of all genes found to be upregulated after PTGFRN knockdown by shRNA in A431, continued

microtubule cytoskeleton organization	8.02E-02	CCNB1,GAPDH,MYH9,TUBB4B,DCTN2,HOOK1,NDE1,TUBB,RSPH9
Anchoring of the basal body to the plasma membrane	8.99E-02	TUBB4B,DCTN2,NDE1,TUBB
lymphocyte mediated immunity	9.96E-02	LIG4,PRDX1,BCL10,TUBB4B,TUBB
COPI-independent Golgi-to-ER retrograde traffic	1.22E-01	TUBB4B,DCTN2,DCTN4
HSP90 chaperone cycle for steroid hormone receptors (SHR) in the presence of ligand	1.35E-01	TUBB4B,DCTN2,DCTN4
Pathogenic Escherichia coli infection	1.35E-01	HCLS1,TUBB4B,TUBB
Cilium Assembly	1.44E-01	TUBB4B,DCTN2,CCT8,NDE1,TUBB
Mitotic Prometaphase	1.51E-01	CCNB1,TUBB4B,DCTN2,NDE1,TUBB
cell killing	1.51E-01	GAPDH,PRDX1,TUBB4B,TUBB
leukocyte mediated cytotoxicity	1.64E-01	PRDX1,TUBB4B,TUBB
Parkin-ubiquitin proteasomal system pathway	2.18E-01	UBE2L3,TUBB4B,TUBB
Phagosome	2.52E-01	ATP6V1C1,STX7,TUBB4B,TUBB
spindle organization	2.92E-01	CCNB1,MYH9,DCTN2,TUBB
Gap junction	3.30E-01	EGFR,TUBB4B,TUBB
Interferon Signaling	6.44E-04	BST2,EIF4A2,ICAM1,IFI35,IFIT3,MX1,PML,STAT1,RIGI
Viral Infection Pathways	6.44E-04	ATP1B1,BST2,EGFR,LIG4,PML,PSMA1,PSMB5,PSMB7,SDC1,STAT1,IKBKG,PDCD6IP,TUBB4B,RIGI,CHMP5,TUBB
Hepatitis C	8.32E-04	ARAF,CASP3,EGFR,LDLR,MX1,STAT1,IKBKG,RIGI

Table 2A.1. Pathway analysis of all genes found to be upregulated after PTGFRN knockdown by shRNA in A431, continued

Network map of SARS-CoV-2 signaling pathway	8.65E-04	BST2,CASP3,CCNB1,EIF4A2,IL1A,MX1,STAT1,IKBKG,RIGI
Influenza A	1.19E-03	CASP3,ICAM1,IL1A,MX1,PML,STAT1,IKBKG,RIGI
Immune response to tuberculosis	2.45E-03	IFI35,IFIT3,MX1,STAT1
Interferon alpha/beta signaling	8.98E-03	BST2,IFI35,IFIT3,MX1,STAT1
Measles virus infection	1.29E-02	CASP3,IL1A,MX1,STAT1,IKBKG,RIGI
Measles	1.30E-02	CASP3,IL1A,MX1,STAT1,IKBKG,RIGI
Epstein-Barr virus infection	4.31E-02	CASP3,ICAM1,STAT1,IKBKG,ADRM1,RIGI
ISG15 antiviral mechanism	4.36E-02	EIF4A2,MX1,STAT1,RIGI
Host-pathogen interaction of human coronaviruses - interferon induction	5.36E-02	STAT1,IKBKG,RIGI
Antiviral mechanism by IFN-stimulated genes	5.57E-02	EIF4A2,MX1,STAT1,RIGI
Hepatitis B infection	6.43E-02	ARAF,CASP3,STAT1,IKBKG,RIGI
negative regulation of viral process	7.20E-02	BST2,MX1,STAT1,N4BP1
Hepatitis B	7.76E-02	ARAF,CASP3,STAT1,IKBKG,RIGI
antiviral innate immune response	1.10E-01	IFIT3,MX1,RIGI
defense response to virus	1.13E-01	BST2,IFIT3,MX1,PML,STAT1,RIGI
defense response to symbiont	1.14E-01	BST2,IFIT3,MX1,PML,STAT1,RIGI
response to virus	1.24E-01	BST2,IFIT3,MX1,PML,STAT1,IKBKG,RIGI
negative regulation of viral genome replication	1.39E-01	BST2,MX1,N4BP1

Table 2A.1. Pathway analysis of all genes found to be upregulated after PTGFRN knockdown by shRNA in A431, continued

SARS-CoV Infections	1.67E-01	ATP1B1,BST2,SDC1,STAT1, IKBKG,RIGI,TUBB
Ebola virus infection in host	1.71E-01	BST2,EGFR,STAT1,RIGI
Viral life cycle - HIV-1	1.77E-01	BST2,MX1,PDCD6IP
SARS-CoV-2 innate immunity evasion and cell-specific immune response	1.94E-01	MX1,STAT1,RIGI
positive regulation of type I interferon production	2.14E-01	GAPDH,STAT1,RIGI
Coronavirus disease - COVID-19	2.17E-01	EGFR,MX1,STAT1,IKBKG,RIGI
Cytosolic DNA-sensing pathway	2.43E-01	CASP3,IKBKG,RIGI
regulation of viral process	3.04E-01	BST2,MX1,STAT1,N4BP1
regulation of viral genome replication	3.14E-01	BST2,MX1,N4BP1
Herpes simplex virus 1 infection	3.64E-01	BST2,CASP3,PML,STAT1,IKBKG,RIGI,ZNF573
mitotic cell cycle	8.65E-04	CCNB1,ENSA,MCM3,MCM6,PML,KIF14,PDCD6IP,TUBB4B,DCTN2,CHMP5,ANLN,NDE1,PSMG2,TUBB
mitotic cell cycle process	2.87E-03	CCNB1,ENSA,MCM3,MCM6,PML,KIF14,PDCD6IP,DCTN2,CHMP5,ANLN,NDE1,PSMG2
establishment of chromosome localization	1.03E-02	CCNB1,KIF14,DCTN2,CHMP5,NDE1
chromosome localization	1.29E-02	CCNB1,KIF14,DCTN2,CHMP5,NDE1
mitotic metaphase plate congression	2.02E-02	CCNB1,KIF14,DCTN2,CHMP5
cell division	2.37E-02	CCNB1,ENSA,LIG4,MYH9,KIF14,PDCD6IP,CHMP5,ANLN,NDE1,TUBB
metaphase plate congression	3.27E-02	CCNB1,KIF14,DCTN2,CHMP5

Table 2A.1. Pathway analysis of all genes found to be upregulated after PTGFRN knockdown by shRNA in A431, continued

chromosome organization	4.31E-02	CCNB1,LIG4,MCM3,MCM6, NASP,KIF14,DCTN2,CHMP5 ,SMC6
establishment of organelle localization	5.06E-02	CCNB1,MYH9,PICALM,IKB KG,KIF14, DCTN2,CHMP5,NDE1
organelle localization	6.43E-02	CCNB1,MYH9,PICALM,STX 7,IKBKG, KIF14,DCTN2,CHMP5,NDE1
mitotic nuclear division	7.76E-02	CCNB1,KIF14,DCTN2,CHMP 5,NDE1
mitotic sister chromatid segregation	1.96E-01	CCNB1,KIF14,DCTN2,CHMP 5
sister chromatid segregation	2.08E-01	CCNB1,KIF14,DCTN2,CHMP 5
chromosome segregation	2.14E-01	CCNB1,KIF14,DCTN2,CHMP 5,NDE1,TUBB
establishment of vesicle localization	3.29E-01	PICALM,IKBKG,DCTN2,ND E1
vesicle localization	3.96E-01	PICALM,IKBKG,DCTN2,ND E1
Cori cycle	1.06E-03	ALDOA,GAPDH,PFKP,PGA M1
Carbon metabolism	8.06E-03	ALDOA,FH,GAPDH,IDH3A, PFKP,PGAM1
Glycolysis	9.01E-03	ALDOA,GAPDH,PFKP,PGA M1,GNPDA1
Biosynthesis of amino acids	9.86E-03	ALDOA,GAPDH,IDH3A,PFK P,PGAM1
Metabolic reprogramming in colon cancer	1.29E-02	FH,GAPDH,IDH3A,PGAM1
glycolytic process	1.42E-02	ALDOA,GAPDH,PFKP,PGA M1
Glycolysis and gluconeogenesis	1.48E-02	ALDOA,GAPDH,PFKP,PGA M1
Glucose metabolism	1.64E-02	ALDOA,GAPDH,PFKP,PGA M1,GNPDA1
Glycolysis / Gluconeogenesis	3.72E-02	ALDOA,GAPDH,PFKP,PGA M1
pyruvate metabolic process	3.96E-02	ALDOA,GAPDH,PFKP,PGA M1

Table 2A.1. Pathway analysis of all genes found to be upregulated after PTGFRN knockdown by shRNA in A431, continued

Central carbon metabolism in cancer	4.02E-02	EGFR,PFKP,PGAM1,SCO2
Gluconeogenesis	5.84E-02	ALDOA,GAPDH,PGAM1
Clear cell renal cell carcinoma pathways	6.44E-02	ALDOA,EGFR,GAPDH,PFKP
HIF-1 signaling pathway	1.19E-01	ALDOA,EGFR,GAPDH,PFKP
carbohydrate catabolic process	1.22E-01	ALDOA,GAPDH,PFKP,PGAM1
Metabolism of carbohydrates	1.49E-01	ALDOA,GAPDH,PFKP,PGAM1,SDC1,GNPDA1
hexose metabolic process	2.81E-01	ALDOA,GAPDH,PFKP,PGAM1
Sudden infant death syndrome (SIDS) susceptibility pathways	2.85E-01	ALDOA,CASP3,GAPDH,IL1A
neuron apoptotic process	4.07E-01	CASP3,GAPDH,LIG4
regulation of proteolysis	3.15E-03	ARAF,SERPINH1,GAPDH,MYH9,SERPINB2,PML,S100A9,SGTA,PICALM,BCL10,N4BP1,BCL2L13,UBXN1,NLRP2
regulation of endopeptidase activity	8.89E-03	SERPINH1,GAPDH,SERPINB2,PML, S100A9,PICALM,BCL10,BCL2L13,NLRP2
regulation of peptidase activity	9.01E-03	SERPINH1,GAPDH,SERPINB2,PML,S100A9,PICALM,BCL10,BCL2L13,UBXN1,NLRP2
positive regulation of endopeptidase activity	2.49E-02	PML,S100A9,PICALM,BCL10,BCL2L13,NLRP2
positive regulation of peptidase activity	3.29E-02	PML,S100A9,PICALM,BCL10,BCL2L13,NLRP2
positive regulation of cysteine-type endopeptidase activity involved in apoptotic process	3.72E-02	PML,S100A9,BCL10,BCL2L13,NLRP2

Table 2A.1. Pathway analysis of all genes found to be upregulated after PTGFRN knockdown by shRNA in A431, continued

positive regulation of proteolysis	3.72E-02	MYH9,PML,S100A9,SGTA,PICALM, BCL10,BCL2L13,NLRP2
positive regulation of cysteine-type endopeptidase activity	5.40E-02	PML,S100A9,BCL10,BCL2L13,NLRP2
regulation of extrinsic apoptotic signaling pathway	7.15E-02	ICAM1,IL1A,PML,PEA15,BCL10
positive regulation of hydrolase activity	9.63E-02	EGFR,PML,S100A9,ARHGEF5,PICALM, BCL10,SH3BP1,BCL2L13,NLRP2
defense response to fungus	1.22E-01	GAPDH,S100A9,BCL10
regulation of cysteine-type endopeptidase activity involved in apoptotic process	1.25E-01	PML,S100A9,BCL10,BCL2L13,NLRP2
positive regulation of extrinsic apoptotic signaling pathway	1.27E-01	PML,PEA15,BCL10
regulation of apoptotic signaling pathway	1.27E-01	ICAM1,IL1A,PML,S100A9,SOD2,PEA15,BCL10
response to fungus	1.71E-01	GAPDH,S100A9,BCL10
regulation of cysteine-type endopeptidase activity	1.97E-01	PML,S100A9,BCL10,BCL2L13,NLRP2
positive regulation of apoptotic signaling pathway	2.14E-01	PML,S100A9,PEA15,BCL10
activation of cysteine-type endopeptidase activity involved in apoptotic process	2.43E-01	PML,S100A9,BCL2L13
cellular homeostasis	6.27E-03	ALDOA,ATP1B1,ATP6V1C1, FTL,IL1A,PRDX1,PML,PPT1, RBM4,S100A9,SOD2,PICALM,SCO2

Table 2A.1. Pathway analysis of all genes found to be upregulated after PTGFRN knockdown by shRNA in A431, continued

intracellular chemical homeostasis	3.55E-02	ATP1B1,FTL,IL1A,PML,PPT1,RBM4,S100A9,SOD2,PICALM,SCO2
monoatomic cation homeostasis	4.76E-02	ATP1B1,FTL,IL1A,PML,PPT1,S100A9,SOD2,PICALM,SCO2
monoatomic ion homeostasis	5.13E-02	ATP1B1,FTL,IL1A,PML,PPT1,S100A9,SOD2,PICALM,SCO2
intracellular monoatomic cation homeostasis	6.12E-02	ATP1B1,FTL,IL1A,PML,PPT1,S100A9,PICALM,SCO2
inorganic ion homeostasis	6.42E-02	ATP1B1,FTL,IL1A,PML,S100A9,SOD2,PICALM,SCO2
intracellular monoatomic ion homeostasis	6.68E-02	ATP1B1,FTL,IL1A,PML,PPT1,S100A9,PICALM,SCO2
regulation of amide metabolic process	8.86E-03	CASP3,EEF2,EIF4A2,GAPDH,KRT17,PA2G4,PGAM1,RBM4,PICALM,CNOT11,NIBAN1,MTPN
positive regulation of amide metabolic process	2.53E-02	CASP3,EEF2,KRT17,RBM4,PICALM,NIBAN1
regulation of translation	6.69E-02	EEF2,EIF4A2,GAPDH,KRT17,PA2G4,RBM4,CNOT11,NIBAN1,MTPN
positive regulation of translation	2.17E-01	EEF2,KRT17,RBM4,NIBAN1
response to reactive oxygen species	8.89E-03	CASP3,EGFR,IL1A,PRDX1,SDC1,SOD2,STAT1
response to ionizing radiation	1.42E-02	CASP3,EEF1D,IL1A,LIG4,PML,SOD2
response to oxidative stress	1.48E-02	CASP3,EGFR,IL1A,PRDX1,PML,PSMB5,SDC1,SOD2,STAT1
response to gamma radiation	2.45E-02	IL1A,LIG4,PML,SOD2
response to radiation	3.14E-02	CASP3,EEF1D,EGFR,IL1A,LIG4,PML,RBM4,SOD2,N4BP1
CKAP4 signaling pathway map	3.19E-02	CASP3,CCNB1,EGFR,SDC1,STAT1
response to inorganic substance	7.14E-02	ATIC,CASP3,EGFR,IL1A,LIG4,PRDX1,SDC1,SOD2,STAT1

Table 2A.1. Pathway analysis of all genes found to be upregulated after PTGFRN knockdown by shRNA in A431, continued

response to hydrogen peroxide	1.07E-01	CASP3,SDC1,SOD2,STAT1
AGE/RAGE pathway	1.94E-01	CASP3,EGFR,STAT1
response to lipopolysaccharide	2.22E-01	CASP3,IL1A,S100A9,SOD2,BCL10,CHMP5
morphogenesis of an epithelium	2.30E-01	CASP3,EGFR,KRT17,PML,BCL10,SH3BP1,MRTFA
response to UV	2.48E-01	CASP3,EGFR,PML,N4BP1
response to molecule of bacterial origin	2.73E-01	CASP3,IL1A,S100A9,SOD2,BCL10,CHMP5
response to monosaccharide	2.92E-01	CASP3,IL1A,RBM4,SOD2
response to metal ion	3.00E-01	CASP3,EGFR,IL1A,LIG4,SDC1,SOD2
cellular response to chemical stress	3.75E-01	CASP3,EGFR,PRDX1,PML,SOD2
response to hypoxia	3.78E-01	ATP1B1,CASP3,IL1A,PML,SOD2
Endocytosis	8.98E-03	EGFR,LDLR,PML,SNX2,PDCD6IP,EHD4,CHMP5,EPS15L1
Membrane Trafficking	2.62E-02	EGFR,FTL,LDLR,MYH9,SNX2,PICALM,TUBB4B,DCTN2,DCTN4,CHMP5,EPS15L1
endocytosis	2.65E-02	ANXA3,LDLR,MYH9,PPT1,SDC1,PICALM,WASF2,SH3BP1,EHD4,EPS15L1
Vesicle-mediated transport	3.68E-02	EGFR,FTL,LDLR,MYH9,SNX2,PICALM,TUBB4B,DCTN2,DCTN4,CHMP5,EPS15L1
endosomal transport	6.69E-02	ARHGAP1,SNX2,PICALM,EHD4,CHMP5,EPS15L1
Cargo recognition for clathrin-mediated endocytosis	1.12E-01	EGFR,LDLR,PICALM,EPS15L1
Fatty Acids and Lipoproteins Transport in Hepatocytes	1.25E-01	EHHADH,LDLR,SNX2,PICALM,WASF2,EHD4,EPS15L1
Clathrin-mediated endocytosis	2.29E-01	EGFR,LDLR,PICALM,EPS15L1
receptor-mediated endocytosis	3.00E-01	LDLR,PPT1,SDC1,PICALM
learning or memory	3.61E-01	CASP3,EGFR,LDLR,PPT1,PICALM

Table 2A.1. Pathway analysis of all genes found to be upregulated after PTGFRN knockdown by shRNA in A431, continued

proteasome assembly	9.01E-03	PSMG1,ADRM1,PSMG2
wound healing	9.23E-03	CASP3,CLIC1,EVPL,IL1A,MYH9,SERPINB2,SDC1,CHMP5,MRTFA
response to wounding	1.29E-02	CASP3,CLIC1,EVPL,IL1A,MYH9,SERPINB2,SDC1,SOD2,CHMP5,MRTFA
muscle structure development	3.50E-01	CASP3,MBNL1,MYH9,MYL6,SDC1,MRTFA,MTPN
muscle cell differentiation	3.54E-01	CASP3,MYH9,SDC1,MRTFA,MTPN
Diseases of signal transduction by growth factor receptors and second messengers	1.10E-02	ARAF,ATIC,EGFR,MYH9,PSMA1,PSMB5,PSMB7,STAT1,TPM3,TPM4
Signaling by ALK in cancer	2.37E-02	ATIC,MYH9,TPM3,TPM4
Signaling by ALK fusions and activated point mutants	2.37E-02	ATIC,MYH9,TPM3,TPM4
Smooth Muscle Contraction	9.63E-02	MYL6,TPM3,TPM4
muscle system process	1.34E-01	ALDOA,ATP1B1,MYL6,TPM3,TPM4,SCO2
muscle contraction	2.14E-01	ALDOA,ATP1B1,MYL6,TPM3,TPM4
Cardiac muscle contraction	3.21E-01	ATP1B1,TPM3,TPM4
cytokinetic process	1.22E-02	MYH9,PDCD6IP,CHMP5,ANLN
cytokinesis	1.25E-01	MYH9,PDCD6IP,CHMP5,ANLN
membrane organization	1.48E-01	ATP1B1,EGFR,MYH9,PPT1,SGTA,PICALM,STX7,PDCD6IP,SH3BP1,CHMP5
vesicle organization	2.29E-01	ATP6V1C1,PICALM,STX7,PDCD6IP,HOOK1,CHMP5
mitotic cytokinesis	2.87E-01	PDCD6IP,CHMP5,ANLN
endosome organization	3.54E-01	PDCD6IP,HOOK1,CHMP5
positive regulation of DNA-binding transcription factor activity	1.22E-02	ANXA3,HCLS1,S100A9,ARHGEF5,IKBKG,BCL10,RIGI,MTPN
regulation of I-kappaB kinase/NF-kappaB signaling	3.25E-02	BST2,EEF1D,GAPDH,IL1A,STAT1,IKBKG,BCL10
positive regulation of I-kappaB kinase/NF-kappaB signaling	3.73E-02	BST2,EEF1D,GAPDH,IL1A,IKBKG,BCL10

Table 2A.1. Pathway analysis of all genes found to be upregulated after PTGFRN knockdown by shRNA in A431, continued

regulation of DNA-binding transcription factor activity	3.84E-02	ANXA3,HCLS1,S100A9,ARHGEF5,IKBKG,BCL10,RIGI,NLRP2,MTPN
NF-kappa B signaling pathway	1.07E-01	ICAM1,IKBKG,BCL10,RIGI
Shigellosis	2.62E-01	EGFR,HCLS1,IKBKG,BCL10,WASF2
positive regulation of NF-kappaB transcription factor activity	2.81E-01	S100A9,IKBKG,BCL10,MTPN
T-cell receptor signaling pathway	3.47E-01	IL1A,IKBKG,BCL10
regulation of immune effector process	3.54E-01	BST2,EVPL,ICAM1,STX7,BCL10,RIGI
B cell receptor signaling pathway	4.00E-01	HCLS1,IKBKG,BCL10
regulation of fibroblast proliferation	1.42E-02	CCNB1,EGFR,LIG4,PML,SOD2
positive regulation of fibroblast proliferation	2.20E-02	CCNB1,EGFR,LIG4,PML
regulation of cell cycle process	6.09E-02	CCNB1,EGFR,IL1A,PML,RBL1,KIF14,PDCD6IP,CHMP5,ANLN,PSMG2,SMC6
regulation of mitotic cell cycle phase transition	9.83E-02	CCNB1,EGFR,PML,RBL1,KIF14,ANLN,PSMG2
TP53 Regulates Transcription of Cell Cycle Genes	1.10E-01	CCNB1,RBL1,CNOT11
regulation of mitotic cell cycle	1.53E-01	CCNB1,EGFR,IL1A,PML,RBL1,KIF14,ANLN,PSMG2
FoxO signaling pathway	1.79E-01	ARAF,CCNB1,EGFR,SOD2
DNA damage response	2.09E-01	CASP3,CCNB1,PML
regulation of cell cycle phase transition	2.38E-01	CCNB1,EGFR,PML,RBL1,KIF14,ANLN,PSMG2
PID P73PATHWAY	2.71E-01	CCNB1,PML,PEA15
Transcriptional Regulation by TP53	2.85E-01	CCNB1,PRDX1,PML,RBL1,SCO2,CNOT11
positive regulation of cell cycle process	3.02E-01	CCNB1,EGFR,IL1A,KIF14,SMC6
regulation of G1/S transition of mitotic cell cycle	4.06E-01	EGFR,PML,RBL1,KIF14

Table 2A.2. Pathway analysis of all genes found to be downregulated after PTGFRN knockdown by shRNA in A431. Statistical significance determined at $p < 0.05$.

Pathway Description	adj. p-value	Genes Downregulated after PTGFRN Knockdown
nucleobase-containing small molecule metabolic process	2.15E-07	AK1,AK4,AMPD2,NQO1,DLD,GARS1,GFPT1,GMDS,GNAI3,IDH2,NUDT1,NDUFA10,NDUFB5,RRM2,PAPSS2,PAICS,CLPX,ACOT9,ACSS2,UGGT1,QNG1,NADK2,ALDH1L2,PCYT2,PYGL,PDXK,SPTLC2,GPHN,AKR1A1,CEPT1,INPP5F,PNPO,TMEM258,RPN1,MOGS,ACP1
generation of precursor metabolites and energy	2.18E-07	ACADVL,ASPH,CAT,CYC1,DLD,NIPSNAP2,GFPT1,GPD2,IDH2,ME2,NDUFA10,NDUFB5,PHKG2,PLEC,PYGL,PDIA5,CYCS,ACSS2,ALDH1L2,ACP1,SLC25A6,NQO1,AKR1A1,POLR2E,TGM2,PSMD6,ACTR1B,CAPN1,CTNNB1,GNAI3,CTSD,HSPA2,NCBP1
Cellular responses to stress	1.87E-06	ACADVL,ADD1,ATR,BLVRA,BLVRB,CAT,NQO1,GFPT1,HSPA2,EXOSC9,RBBP7,RHEB,RPL27A,RPL34,ELOB,PRDX2,H4C9,H2BC21,PSMD6,PREB,PDIA5,SEC31A,EXOSC3,EXOSC1,CYCS
amide biosynthetic process	7.71E-06	ASS1,CARS1,DLD,EIF1AX,GARS1,GLUD1,NARS1,NCBP1,RPL27A,RPL34,YARS1,EIF3B,PABPC4,SPTLC2,MRPL19,IGF2BP3,MRPS2,DARS2,IARS2,ACSS2,CTSZ,XPNPEP1,ACOT9,ALDH1L2,RPN1,SRP72,TRMT112,EXOSC9,EXOSC3,THUMPD1,QNG1,GFPT1,PYCR1,PDE12
Protein processing in endoplasmic reticulum	9.02E-06	CAPN1,HSPA2,LMAN1,RPN1,MOGS,SEC24D,PREB,LMAN2,SEC31A,GANAB,FBXO2,UGGT1,CTSZ,GFPT1,GMDS,GOLGB1,COPZ1,RAB1B,RAB6A,TJP1,TPD52L1,KIF23,ACBD3,MYO18A,S100A10,CTSD,ACTR1B
ncRNA metabolic process	1.18E-05	CARS1,DKC1,GARS1,NARS1,NCBP1,EXOSC9,ELOB,YARS1,EXOSC3,EXOSC1,SBDS,DDX47,TRMT112,DARS2,ZCCHC8,THUMPD1,IARS2,INTS9,QNG1,RPL27A,RPL34,GNL3,RBM28,POLR2E,SRSF4,PSMD6,HNRNPR,PRPF8,IGF2BP3,CRNKL1,PRPF40A,BLVRA,BLVRB,NUDT1,PABPC4,PDE12,EIF3B,GNL2,MRPS2

Table 2A.2. Pathway analysis of all genes found to be downregulated after PTGFRN knockdown by shRNA in A431, continued

Neutrophil degranulation	2.82E-04	CAPN1,CAT,CTSD,CTSZ,CYB5R3,SERPINB1,LGALS3,SERPINB6,PYGL,RAB6A,RAP2B,PDXK,IST1,PSMD6,ACTR1B,PRDX4
Cell Cycle	3.19E-04	ATR,DKC1,HSPA2,LYN,POLA1,POLD1,POLR2E,PPP2R5D,RAB2A,RBBP7,RRM2,H4C9,H2BC21,KIF23,IST1,PSMD6,RSF1,RAB1B,NEDD1
Metabolic reprogramming in pancreatic cancer	3.19E-04	DLD,GFPT1,GLUD1,HK1,SOAT1,SLC7A5,CYB5R3,GMDS,UGGT1
Biosynthesis of cofactors	8.11E-04	AK1,AK4,NQO1,DLD,PDXK,GPHN,AKR1A1,PNPO,NADK2,IDH2,ALDH1L2,CYB5R3
NADH oxidation	1.68E-03	NQO1,GPD2,PCK2,CA2,GLUD1
Fatty acid beta-oxidation	1.84E-03	ACADVL,DLD,GPD2,HADHB,ACSS2,GLUD1,HK1,NUDT1,PCK2,ABCD3,AKR1A1,ALDH1L2,IDH2,ME2,OSBPL3,ACOT9,INPP5F,NCEH1
Apoptotic cleavage of cellular proteins	2.92E-03	ADD1,CTNNB1,DSG2,PLEC,TJP1,PSMD6,CYCS,FSCN1,PKP3,RAPGEF1
Chromosome Maintenance	2.92E-03	DKC1,POLA1,POLD1,POLR2E,RBBP7,H4C9,H2BC21,RSF1,ATR,RRM2,BOD1L1,NUDT1,UBE2V1,SWAP70,UFL1,EXOSC3,MYO18A
organic hydroxy compound metabolic process	3.04E-03	CAT,CYB5R3,NQO1,GPD2,IDH2,PCK2,ABCD3,SOAT1,PDXK,SPTLC2,AKR1A1,OSBPL3,PNPO,ACSS2,ASS1,GLUD1,PYCR1,QNG1,ACBD3,PCYT2,CEPT1,INPP5F
VEGFA-VEGFR2 signaling	4.74E-03	ACP1,CALU,CTNNB1,FLNB,GLUD1,RAPGEF1,IDH2,LMAN1,FSCN1,PRDX2,ACOT9,CYCS,LRRC59

Table 2A.2. Pathway analysis of all genes found to be downregulated after PTGFRN knockdown by shRNA in A431, continued

mRNA metabolic process	5.61E-03	DKC1,LGALS3,NCBP1,EXOSC9,S100A10,SRSF4,HNRNPR,PRPF8,HNRNPA0,EXOSC3,DDX47,CRNKL1,RBM28,ZCCHC8,PRPF40A,PDE12,IGF2BP3,POLR2E,HSPA2
Carbon metabolism	6.27E-03	CAT,DLD,GLUD1,HK1,IDH2,ME2,ACSS2,PCK2,AKR1A1,CYCS,PAPSS2,ACOT9
response to toxic substance	8.22E-03	ASS1,CAT,NQO1,LYN,PRDX2,AKR1A1,PRDX4,KDM5B,NXN,BLVRA,BLVRB,PSMD6,CYCS,PNPO
Viral Infection Pathways	9.33E-03	SLC25A6,HLA-A,NCBP1,POLR2E,RBBP7,RPL27A,RPL34,RPN1,ELOB,TJP1,UBE2V1,MOGS,H4C9,H2BC21,PSMD6,SEC24D,GANAB,TMEM258,GFPT1,UGGT1
nucleobase-containing small molecule metabolic process	2.15E-07	AK1,AK4,AMPD2,NQO1,DLD,GARS1,GFPT1,GMDS,GNAI3,IDH2,NUDT1,NDUFA10,NDUFB5,RRM2,PAPSS2,PAICS,CLPX,ACOT9,ACSS2,UGGT1,QNG1,NADK2,ALDH1L2
organophosphate biosynthetic process	1.87E-06	AK1,AK4,AMPD2,DLD,GARS1,NDUFA10,NDUFB5,PCYT2,PYGL,RRM2,PDXK,PAPSS2,SPTLC2,GPHN,AKR1A1,CEPT1,PAICS,INPP5F,PNPO,ACSS2,NADK2
nucleotide metabolic process	1.59E-05	AK1,AK4,AMPD2,NQO1,DLD,GARS1,GNAI3,IDH2,NDUFA10,NDUFB5,RRM2,PAPSS2,PAICS,CLPX,ACOT9,ACSS2,NADK2,ALDH1L2
nucleoside phosphate metabolic process	1.95E-05	AK1,AK4,AMPD2,NQO1,DLD,GARS1,GNAI3,IDH2,NDUFA10,NDUFB5,RRM2,PAPSS2,PAICS,CLPX,ACOT9,ACSS2,NADK2,ALDH1L2
purine-containing compound metabolic process	3.19E-05	AK1,AK4,AMPD2,NQO1,DLD,GNAI3,IDH2,NUDT1,NDUFA10,NDUFB5,PAPSS2,PAICS,CLPX,ACOT9,ACSS2,NADK2,ALDH1L2

Table 2A.2. Pathway analysis of all genes found to be downregulated after PTGFRN knockdown by shRNA in A431, continued

carbohydrate derivative biosynthetic process	6.11E-05	AK1,AK4,AMPD2,TMEM258,DLD,GFPT1,GMDS,NDUFA10,NDUFB5,PYGL,RPN1,RRM2,MOGS,PAPSS2,AKR1A1,PAICS,ACSS2,UGGT1,QNG1
purine nucleotide metabolic process	6.61E-05	AK1,AK4,AMPD2,NQO1,DLD,GNAI3,IDH2,NDUFA10,NDUFB5,PAPSS2,PAICS,CLPX,ACOT9,ACSS2,NADK2,ALDH1L2
nucleotide biosynthetic process	3.08E-04	AK1,AK4,AMPD2,DLD,GARS1,NDUFA10,NDUFB5,RRM2,PAPSS2,PAICS,ACSS2,NADK2
nucleoside phosphate biosynthetic process	3.11E-04	AK1,AK4,AMPD2,DLD,GARS1,NDUFA10,NDUFB5,RRM2,PAPSS2,PAICS,ACSS2,NADK2
ribose phosphate metabolic process	1.21E-03	AK1,AK4,AMPD2,DLD,GNAI3,NDUFA10,NDUFB5,PYGL,PAPSS2,PAICS,CLPX,ACOT9,ACSS2
ribose phosphate biosynthetic process	1.59E-03	AK1,AK4,AMPD2,DLD,NDUFA10,NDUFB5,PYGL,PAPSS2,PAICS,ACSS2
purine nucleotide biosynthetic process	2.49E-03	AK1,AK4,AMPD2,DLD,NDUFA10,NDUFB5,PAPSS2,PAICS,ACSS2,NADK2
purine ribonucleotide metabolic process	2.58E-03	AK1,AK4,AMPD2,DLD,GNAI3,NDUFA10,NDUFB5,PAPSS2,PAICS,CLPX,ACOT9,ACSS2
purine-containing compound biosynthetic process	3.04E-03	AK1,AK4,AMPD2,DLD,NDUFA10,NDUFB5,PAPSS2,PAICS,ACSS2,NADK2
ribonucleotide metabolic process	3.84E-03	AK1,AK4,AMPD2,DLD,GNAI3,NDUFA10,NDUFB5,PAPSS2,PAICS,CLPX,ACOT9,ACSS2
purine ribonucleotide biosynthetic process	3.84E-03	AK1,AK4,AMPD2,DLD,NDUFA10,NDUFB5,PAPSS2,PAICS,ACSS2
ribonucleotide biosynthetic process	6.27E-03	AK1,AK4,AMPD2,DLD,NDUFA10,NDUFB5,PAPSS2,PAICS,ACSS2
AMP metabolic process	8.22E-03	AK1,AK4,AMPD2,PAICS

Table 2A.2. Pathway analysis of all genes found to be downregulated after PTGFRN knockdown by shRNA in A431, continued

Metabolism of nucleotides	1.78E-02	AK1,AK4,AMPD2,NUDT1,RRM2,PAICS
Thiamine metabolism	3.13E-02	ACP1,AK1,AK4
purine ribonucleoside monophosphate metabolic process	3.81E-02	AK1,AK4,AMPD2,PAICS
purine nucleoside monophosphate metabolic process	4.24E-02	AK1,AK4,AMPD2,PAICS
Purine metabolism	4.68E-02	AK1,AK4,AMPD2,RRM2,PAPSS2,PAICS
purine ribonucleoside triphosphate metabolic process	7.20E-02	AK1,AK4,GNAI3,NDUFA10,NDUFB5,CLPX
purine nucleoside triphosphate metabolic process	8.16E-02	AK1,AK4,GNAI3,NDUFA10,NDUFB5,CLPX
ribonucleoside triphosphate metabolic process	8.46E-02	AK1,AK4,GNAI3,NDUFA10,NDUFB5,CLPX
ribonucleoside monophosphate metabolic process	9.46E-02	AK1,AK4,AMPD2,PAICS
nucleoside triphosphate metabolic process	1.28E-01	AK1,AK4,GNAI3,NDUFA10,NDUFB5,CLPX
ribonucleoside diphosphate metabolic process	1.28E-01	AK1,AK4,RRM2
Interconversion of nucleotide di- and triphosphates	1.28E-01	AK1,AK4,RRM2
ATP metabolic process	1.51E-01	AK1,AK4,NDUFA10,NDUFB5,CLPX

Table 2A.2. Pathway analysis of all genes found to be downregulated after PTGFRN knockdown by shRNA in A431, continued

nucleoside monophosphate metabolic process	1.86E-01	AK1,AK4,AMPD2,PAICS
nucleoside diphosphate metabolic process	1.96E-01	AK1,AK4,RRM2
Nucleotide metabolism	2.44E-01	AK1,AK4,AMPD2,RRM2
nucleoside triphosphate biosynthetic process	4.88E-01	AK1,AK4,NDUFA10,NDUFB5
generation of precursor metabolites and energy	2.18E-07	ACADVL,ASPH,CAT,CYC1,DLD,NIPSNAP2,GFPT1,GPD2,IDH2,ME2,NDUFA10,NDUFB5,PHKG2,PLEC,PYGL,PDIA5,CYCS,ACSS2,ALDH1L2
energy derivation by oxidation of organic compounds	1.19E-05	ACADVL,CAT,CYC1,DLD,NIPSNAP2,GFPT1,GPD2,IDH2,NDUFA10,NDUFB5,PHKG2,PLEC,PYGL,CYCS
electron transport chain	3.05E-04	ASPH,CYC1,DLD,GPD2,ME2,NDUFA10,NDUFB5,PLEC,PDIA5,CYCS
cellular respiration	7.73E-04	CAT,CYC1,DLD,NIPSNAP2,GPD2,IDH2,NDUFA10,NDUFB5,PLEC,CYCS
respiratory electron transport chain	6.64E-03	CYC1,DLD,GPD2,NDUFA10,NDUFB5,PLEC,CYCS
aerobic respiration	6.84E-03	CAT,CYC1,DLD,NIPSNAP2,IDH2,NDUFA10,NDUFB5,CYCS
Chemical carcinogenesis - reactive oxygen species	3.54E-02	ACP1,SLC25A6,CAT,CYC1,NQO1,NDUFA10,NDUFB5,AKR1A1
oxidative phosphorylation	3.81E-02	CYC1,DLD,NIPSNAP2,NDUFA10,NDUFB5,CYCS

Table 2A.2. Pathway analysis of all genes found to be downregulated after PTGFRN knockdown by shRNA in A431, continued

The citric acid (TCA) cycle and respiratory electron transport	4.42E-02	CYC1,DLD,IDH2,ME2,NDUFA10,NDUFB5,CYCS
Huntington disease	5.10E-02	SLC25A6,CYC1,NDUFA10,NDUFB5,POLR2E,TGM2,PSMD6,ACTR1B,CYCS
aerobic electron transport chain	6.09E-02	CYC1,DLD,NDUFA10,NDUFB5,CYCS
ATP synthesis coupled electron transport	7.20E-02	CYC1,DLD,NDUFA10,NDUFB5,CYCS
mitochondrial ATP synthesis coupled electron transport	7.20E-02	CYC1,DLD,NDUFA10,NDUFB5,CYCS
Pathways of neurodegeneration - multiple diseases	1.86E-01	SLC25A6,CAPN1,CAT,CTNNB1,CYC1,NDUFA10,NDUFB5,PSMD6,ACTR1B,CYCS
Parkinson disease	2.31E-01	SLC25A6,CYC1,GNAI3,NDUFA10,NDUFB5,PSMD6,CYCS
Diabetic cardiomyopathy	2.50E-01	SLC25A6,CTSD,CYC1,GFPT1,NDUFA10,NDUFB5
Prion disease	2.53E-01	SLC25A6,CYC1,HSPA2,NDUFA10,NDUFB5,PSMD6,CYCS
mitochondrial electron transport, NADH to ubiquinone	2.99E-01	DLD,NDUFA10,NDUFB5
Amyotrophic lateral sclerosis	3.07E-01	CAT,CYC1,NCBP1,NDUFA10,NDUFB5,PSMD6,ACTR1B,CYCS
Alzheimer disease	3.85E-01	SLC25A6,CAPN1,CTNNB1,CYC1,NDUFA10,NDUFB5,PSMD6,CYCS
Respiratory electron transport	3.88E-01	CYC1,NDUFA10,NDUFB5,CYCS

Table 2A.2. Pathway analysis of all genes found to be downregulated after PTGFRN knockdown by shRNA in A431, continued

Cellular responses to stress	1.87E-06	ACADVL,ADD1,ATR,BLVRA,BLVRB,CAT,NQO1,GFPT1,HSPA2,EXOSC9,RBBP7,RHEB,RPL27A,RPL34,ELOB,PRDX2,H4C9,H2BC21,PSMD6,PREB,PDIA5,SEC31A,EXOSC3,EXOSC1,CYCS
Unfolded Protein Response (UPR)	3.19E-05	ACADVL,ADD1,GFPT1,EXOSC9,PREB,PDIA5,SEC31A,EXOSC3,EXOSC1
XBP1(S) activates chaperone genes	7.97E-04	ACADVL,ADD1,GFPT1,PREB,PDIA5,SEC31A
IRE1alpha activates chaperones	9.33E-04	ACADVL,ADD1,GFPT1,PREB,PDIA5,SEC31A
amide biosynthetic process	7.71E-06	ASS1,CARS1,DLD,EIF1AX,GARS1,GLUD1,NARS1,NCBP1,RPL27A,RPL34,YARS1,EIF3B,PABPC4,SPTLC2,MRPL19,IGF2BP3,MRPS2,DARS2,IARS2,ACSS2
amide metabolic process	8.12E-06	ASS1,CARS1,CTSZ,DLD,EIF1AX,GARS1,GLUD1,NARS1,NCBP1,RPL27A,RPL34,XPNPEP1,YARS1,EIF3B,PABPC4,SPTLC2,MRPL19,IGF2BP3,ACOT9,MRPS2,DARS2,IARS2,ACSS2,ALDH1L2
Translation	8.12E-06	CARS1,EIF1AX,GARS1,NARS1,RPL27A,RPL34,RPN1,SRP72,YARS1,EIF3B,MRPL19,MRPS2,TRMT112,DARS2,IARS2
translation	1.42E-04	CARS1,EIF1AX,GARS1,NARS1,NCBP1,RPL27A,RPL34,YARS1,EIF3B,PABPC4,MRPL19,IGF2BP3,MRPS2,DARS2,IARS2
tRNA metabolic process	1.49E-04	CARS1,GARS1,NARS1,EXOSC9,YARS1,EXOSC3,TRMT112,DARS2,THUMPD1,IARS2,QNG1
peptide metabolic process	1.49E-04	CARS1,CTSZ,EIF1AX,GARS1,NARS1,NCBP1,RPL27A,RPL34,XPNPEP1,YARS1,EIF3B,PABPC4,MRPL19,IGF2BP3,MRPS2,DARS2,IARS2
peptide biosynthetic process	2.67E-04	CARS1,EIF1AX,GARS1,NARS1,NCBP1,RPL27A,RPL34,YARS1,EIF3B,PABPC4,MRPL19,IGF2BP3,MRPS2,DARS2,IARS2

Table 2A.2. Pathway analysis of all genes found to be downregulated after PTGFRN knockdown by shRNA in A431, continued

tRNA aminoacylation for protein translation	3.11E-04	CARS1,GARS1,NARS1,YARS1,DARS2,IARS2
tRNA Aminoacylation	3.19E-04	CARS1,GARS1,NARS1,YARS1,DARS2,IARS2
tRNA aminoacylation	3.99E-04	CARS1,GARS1,NARS1,YARS1,DARS2,IARS2
amino acid activation	4.44E-04	CARS1,GARS1,NARS1,YARS1,DARS2,IARS2
amino acid metabolic process	2.45E-03	ASS1,CARS1,DLD,GARS1,GFPT1,GLUD1,NARS1,PYCR1,YARS1,DARS2,IARS2
Aminoacyl-tRNA biosynthesis	2.95E-03	CARS1,GARS1,NARS1,YARS1,DARS2,IARS2
Cytosolic tRNA aminoacylation	7.20E-03	CARS1,GARS1,NARS1,YARS1
Mitochondrial tRNA aminoacylation	6.09E-02	GARS1,DARS2,IARS2
mitochondrial translation	1.19E-01	GARS1,MRPL19,MRPS2,DARS2,IARS2
mitochondrial gene expression	2.59E-01	GARS1,MRPL19,MRPS2,DARS2,IARS2
mitochondrial RNA metabolic process	2.72E-01	GARS1,DARS2,PDE12
Protein processing in endoplasmic reticulum	9.02E-06	CAPN1,HSPA2,LMAN1,RPN1,MOGS,SEC24D,PREB,LMAN2,SEC31A,GANAB,FBXO2,UGGT1
Asparagine N-linked glycosylation	1.09E-05	CTSZ,GFPT1,GMDS,GOLGB1,LMAN1,RPN1,MOGS,SEC24D,PREB,LMAN2,COPZ1,SEC31A,GANAB,UGGT1,RAB1B
COPII-mediated vesicle transport	3.33E-04	CTSZ,LMAN1,SEC24D,PREB,LMAN2,SEC31A,RAB1B
ER to Golgi Anterograde Transport	8.34E-04	CTSZ,GOLGB1,LMAN1,SEC24D,PREB,LMAN2,COPZ1,SEC31A,RAB1B

Table 2A.2. Pathway analysis of all genes found to be downregulated after PTGFRN knockdown by shRNA in A431, continued

Cargo concentration in the ER	1.66E-03	CTSZ,LMAN1,SEC24D,PREB,LMAN2
Transport to the Golgi and subsequent modification	2.92E-03	CTSZ,GOLGB1,LMAN1,SEC24D,PREB,LMAN2,COPZ1,SEC31A,RAB1B
Membrane Trafficking	3.39E-02	CTSZ,GOLGB1,LMAN1,RAB6A,TJP1,TPD52L1,KIF23,SEC24D,PREB,LMAN2,COPZ1,SEC31A,ACBD3,RAB1B
Golgi vesicle transport	3.46E-02	LMAN1,RAB6A,SEC24D,PREB,LMAN2,COPZ1,SEC31A,RAB1B,MYO18A
vesicle budding from membrane	3.81E-02	S100A10,SEC24D,PREB,SEC31A,MYO18A
endoplasmic reticulum to Golgi vesicle-mediated transport	4.24E-02	LMAN1,SEC24D,PREB,LMAN2,SEC31A,RAB1B
Vesicle-mediated transport	4.76E-02	CTSZ,GOLGB1,LMAN1,RAB6A,TJP1,TPD52L1,KIF23,SEC24D,PREB,LMAN2,COPZ1,SEC31A,ACBD3,RAB1B
MHC class II antigen presentation	1.68E-01	CTSD,KIF23,SEC24D,ACTR1B,SEC31A
COPII-coated vesicle budding	2.41E-01	SEC24D,PREB,SEC31A
ncRNA metabolic process	1.18E-05	CARS1,DKC1,GARS1,NARS1,NCBP1,EXOSC9,ELOB,YARS1,EXOSC3,EXOSC1,SBDS,DDX47,TRMT112,DARS2,ZCCHC8,THUMPD1,IARS2,INTS9,QNG1
rRNA processing in the nucleus and cytosol	1.49E-04	DKC1,EXOSC9,RPL27A,RPL34,GNL3,EXOSC3,EXOSC1,DDX47,TRMT112,RBM28,THUMPD1
Metabolism of RNA	1.73E-04	DKC1,NCBP1,EXOSC9,POLR2E,RPL27A,RPL34,SRSF4,PSMD6,HNRNPR,PRPF8,IGF2BP3,GNL3,EXOSC3,EXOSC1,DDX47,CRNKL1,TRMT112,RBM28,THUMPD1,PRPF40A

Table 2A.2. Pathway analysis of all genes found to be downregulated after PTGFRN knockdown by shRNA in A431, continued

rRNA processing	2.24E-04	DKC1,EXOSC9,RPL27A,RPL34,GNL3,EXOSC3,EXOSC1,DDX47,TRMT112,RBM28,THUMPD1
cellular nitrogen compound catabolic process	6.84E-03	BLVRA,BLVRB,NUDT1,NCBP1,EXOSC9,ELOB,PABPC4,EXOSC3,EXOSC1,ZCCHC8,PDE12
heterocycle catabolic process	7.13E-03	BLVRA,BLVRB,NUDT1,NCBP1,EXOSC9,ELOB,PABPC4,EXOSC3,EXOSC1,ZCCHC8,PDE12
RNA catabolic process	7.46E-03	NCBP1,EXOSC9,ELOB,PABPC4,EXOSC3,EXOSC1,ZCCHC8,PDE12
aromatic compound catabolic process	1.01E-02	BLVRA,BLVRB,NUDT1,NCBP1,EXOSC9,ELOB,PABPC4,EXOSC3,EXOSC1,ZCCHC8,PDE12
snRNA metabolic process	1.09E-02	DKC1,EXOSC9,EXOSC3,ZCCHC8,INTS9
Exosome	1.11E-02	EXOSC9,EXOSC3,EXOSC1
ncRNA processing	1.15E-02	DKC1,NCBP1,EXOSC9,EXOSC3,EXOSC1,SBDS,DDX47,TRMT112,ZCCHC8,THUMPD1,INTS9,QNG1
ribonucleoprotein complex biogenesis	1.18E-02	DKC1,NCBP1,EXOSC9,EIF3B,PRPF8,GNL2,EXOSC3,EXOSC1,MRPS2,SBDS,DDX47,CRNKL1,TRMT112
Major pathway of rRNA processing in the nucleolus and cytosol	1.33E-02	EXOSC9,RPL27A,RPL34,GNL3,EXOSC3,EXOSC1,DDX47,RBM28
Exosome	1.38E-02	EXOSC9,EXOSC3,EXOSC1
Exosome	1.78E-02	EXOSC9,EXOSC3,EXOSC1
organic cyclic compound catabolic process	1.84E-02	BLVRA,BLVRB,NUDT1,NCBP1,EXOSC9,ELOB,PABPC4,EXOSC3,EXOSC1,ZCCHC8,PDE12
mRNA decay by 3' to 5' exoribonuclease	3.46E-02	EXOSC9,EXOSC3,EXOSC1

Table 2A.2. Pathway analysis of all genes found to be downregulated after PTGFRN knockdown by shRNA in A431, continued

nucleobase-containing compound catabolic process	3.80E-02	NUDT1,NCBP1,EXOSC9,ELOB,PABPC4,EXOSC3,EXOSC1,ZCCHC8,PDE12
Butyrate Response Factor 1 (BRF1) binds and destabilizes mRNA	3.81E-02	EXOSC9,EXOSC3,EXOSC1
Tristetraprolin (TTP, ZFP36) binds and destabilizes mRNA	3.81E-02	EXOSC9,EXOSC3,EXOSC1
KSRP (KHSRP) binds and destabilizes mRNA	3.81E-02	EXOSC9,EXOSC3,EXOSC1
ncRNA catabolic process	4.03E-02	EXOSC9,ELOB,EXOSC3,ZCCHC8
regulatory ncRNA 3'-end processing	4.80E-02	DKC1,EXOSC9,EXOSC3
ribosome biogenesis	5.65E-02	DKC1,EXOSC9,GNL2,EXOSC3,EXOSC1,MRPS2,SBDS,DDX47,TRMT112
snRNA 3'-end processing	7.26E-02	EXOSC9,EXOSC3,INTS9
RNA 3'-end processing	8.16E-02	DKC1,NCBP1,EXOSC9,EXOSC3,INTS9
rRNA processing	9.93E-02	DKC1,EXOSC9,EXOSC3,EXOSC1,SBDS,DDX47,TRMT112
ATF4 activates genes in response to endoplasmic reticulum stress	1.01E-01	EXOSC9,EXOSC3,EXOSC1
rRNA modification in the nucleus and cytosol	1.01E-01	DKC1,DDX47,TRMT112,THUMPD1
snRNA processing	1.10E-01	EXOSC9,EXOSC3,INTS9

Table 2A.2. Pathway analysis of all genes found to be downregulated after PTGFRN knockdown by shRNA in A431, continued

PERK regulates gene expression	1.49E-01	EXOSC9,EXOSC3,EXOSC1
rRNA metabolic process	1.73E-01	DKC1,EXOSC9,EXOSC3,EXOSC1,SBDS,DDX47,TRMT112
RNA degradation	2.02E-01	EXOSC9,PABPC4,EXOSC3,EXOSC1
RNA phosphodiester bond hydrolysis, exonucleolytic	2.60E-01	EXOSC9,EXOSC3,PDE12
Regulation of mRNA stability by proteins that bind AU-rich elements	2.61E-01	EXOSC9,PSMD6,EXOSC3,EXOSC1
nuclear-transcribed mRNA catabolic process, deadenylation-dependent decay	2.72E-01	EXOSC9,EXOSC3,PDE12
nuclear-transcribed mRNA catabolic process	3.88E-01	NCBP1,EXOSC9,EXOSC3,PDE12
Deadenylation-dependent mRNA decay	4.15E-01	EXOSC9,EXOSC3,EXOSC1
Neutrophil degranulation	2.82E-04	CAPN1,CAT,CTSD,CTSZ,CYB5R3,SERPINB1,LGALS3,SERPINB6,PYGL,RAB6A,RAP2B,PDXK,IST1,PSMD6,ACTR1B,PRDX4
Cell Cycle	3.19E-04	ATR,DKC1,HSPA2,LYN,POLA1,POLD1,POLR2E,PPP2R5D,RAB2A,RBBP7,RRM2,H4C9,H2BC21,KIF23,IST1,PSMD6,RSF1,RAB1B,NEDD1
Cell Cycle, Mitotic	3.46E-02	LYN,POLA1,POLD1,PPP2R5D,RAB2A,RRM2,H4C9,H2BC21,KIF23,IST1,PSMD6,RAB1B,NEDD1
M Phase	2.31E-01	PPP2R5D,RAB2A,H4C9,H2BC21,KIF23,IST1,PSMD6,RAB1B,NEDD1

Table 2A.2. Pathway analysis of all genes found to be downregulated after PTGFRN knockdown by shRNA in A431, continued

Metabolic reprogramming in pancreatic cancer	3.19E-04	DLD,GFPT1,GLUD1,HK1,SOAT1,SLC7A5
Amino sugar and nucleotide sugar metabolism	5.89E-02	CYB5R3,GFPT1,GMDS,HK1
nucleotide-sugar metabolic process	1.87E-01	GFPT1,GMDS,UGGT1
Biosynthesis of nucleotide sugars	1.96E-01	GFPT1,GMDS,HK1
Biosynthesis of cofactors	8.11E-04	AK1,AK4,NQO1,DLD,PDXK,GPHN,AKR1A1,PNPO,NADK2
pyridine-containing compound metabolic process	6.58E-03	NQO1,IDH2,PDXK,PNPO,NADK2,ALDH1L2
water-soluble vitamin biosynthetic process	6.58E-03	PDXK,AKR1A1,PNPO
NADP metabolic process	2.67E-02	NQO1,IDH2,NADK2,ALDH1L2
vitamin biosynthetic process	3.13E-02	PDXK,AKR1A1,PNPO
Metabolism of water-soluble vitamins and cofactors	4.19E-02	CYB5R3,PDXK,GPHN,PNPO,NADK2,ALDH1L2
vitamin metabolic process	8.16E-02	NQO1,PDXK,AKR1A1,PNPO,ALDH1L2
water-soluble vitamin metabolic process	9.02E-02	PDXK,AKR1A1,PNPO,ALDH1L2
cellular aldehyde metabolic process	1.01E-01	IDH2,PDXK,AKR1A1,PNPO

Table 2A.2. Pathway analysis of all genes found to be downregulated after PTGFRN knockdown by shRNA in A431, continued

pyridine-containing compound biosynthetic process	1.40E-01	PDXK,PNPO,NADK2
pyridine nucleotide metabolic process	1.56E-01	NQO1,IDH2,NADK2,ALDH1L2
nicotinamide nucleotide metabolic process	1.56E-01	NQO1,IDH2,NADK2,ALDH1L2
Metabolism of vitamins and cofactors	2.02E-01	CYB5R3,PDXK,GPHN,PNPO,NADK2,ALDH1L2
NADH oxidation	1.68E-03	NQO1,GPD2,PCK2
Proximal tubule bicarbonate reclamation	7.26E-02	CA2,GLUD1,PCK2
Fatty acid beta-oxidation	1.84E-03	ACADVL,DLD,GPD2,HADHB,ACSS2
small molecule catabolic process	1.17E-02	ACADVL,DLD,GLUD1,GPD2,HADHB,HK1,NUDT1,PCK2,ABCD3,AKR1A1,ALDH1L2
monocarboxylic acid catabolic process	3.46E-02	ACADVL,HADHB,PCK2,ABCD3,AKR1A1,ALDH1L2
organic acid catabolic process	4.24E-02	ACADVL,DLD,GLUD1,HADHB,PCK2,ABCD3,AKR1A1,ALDH1L2
carboxylic acid catabolic process	4.24E-02	ACADVL,DLD,GLUD1,HADHB,PCK2,ABCD3,AKR1A1,ALDH1L2
monocarboxylic acid metabolic process	4.57E-02	ACADVL,DLD,HADHB,HK1,IDH2,ME2,PCK2,ABCD3,AKR1A1,OSBPL3,ACSS2,ALDH1L2
fatty acid catabolic process	6.31E-02	ACADVL,HADHB,PCK2,ABCD3,ALDH1L2
fatty acid beta-oxidation	9.82E-02	ACADVL,HADHB,ABCD3,ALDH1L2

Table 2A.2. Pathway analysis of all genes found to be downregulated after PTGFRN knockdown by shRNA in A431, continued

Mitochondrial Fatty Acid Beta-Oxidation	1.96E-01	ACADVL,HADHB,ACOT9
cellular lipid catabolic process	2.11E-01	ACADVL,HADHB,PCK2,ABCD3,INPP5F,ALDH1L2
fatty acid oxidation	2.24E-01	ACADVL,HADHB,ABCD3,ALDH1L2
lipid oxidation	2.61E-01	ACADVL,HADHB,ABCD3,ALDH1L2
lipid catabolic process	3.14E-01	ACADVL,HADHB,PCK2,ABCD3,INPP5F,NCEH1,ALDH1L2
lipid modification	4.02E-01	ACADVL,HADHB,ABCD3,INPP5F,ALDH1L2
Apoptotic cleavage of cellular proteins	2.92E-03	ADD1,CTNNB1,DSG2,PLEC,TJP1
Apoptotic execution phase	9.46E-03	ADD1,CTNNB1,DSG2,PLEC,TJP1
Apoptotic cleavage of cell adhesion proteins	1.38E-02	CTNNB1,DSG2,TJP1
Apoptosis	4.66E-02	ADD1,CTNNB1,DSG2,PLEC,TJP1,PSMD6,CYCS
Programmed Cell Death	9.46E-02	ADD1,CTNNB1,DSG2,PLEC,TJP1,PSMD6,CYCS
cell-cell junction organization	1.65E-01	CTNNB1,DSG2,PLEC,FSCN1,TJP1,PKP3
PID ECADHERIN NASCENT AJ PATHWAY	2.17E-01	CTNNB1,RAPGEF1,TJP1
adherens junction organization	3.84E-01	CTNNB1,PLEC,TJP1
Chromosome Maintenance	2.92E-03	DKC1,POLA1,POLD1,POLR2E,RBBP7,H4C9,H2BC21,RSF1
Telomere Maintenance	3.13E-02	DKC1,POLA1,POLD1,POLR2E,H4C9,H2BC21

Table 2A.2. Pathway analysis of all genes found to be downregulated after PTGFRN knockdown by shRNA in A431, continued

DNA replication	2.31E-01	ATR,POLA1,POLD1,RBBP7,RRM2,BOD1L1
Pyrimidine metabolism	2.38E-01	POLA1,POLD1,POLR2E,RRM2
DNA metabolic process	2.64E-01	ATR,DKC1,NUDT1,POLA1,POLD1,RBBP7,RRM2,UBE2V1,SWAP70,UFL1,EXOSC3,BOD1L1,MYO18A
Extension of Telomeres	3.68E-01	DKC1,POLA1,POLD1
DNA-templated DNA replication maintenance of fidelity	4.15E-01	ATR,POLD1,BOD1L1
organic hydroxy compound metabolic process	3.04E-03	CAT,CYB5R3,NQO1,GPD2,IDH2,PCK2,ABCD3,SOAT1,PDXK,SPTLC2,AKR1A1,OSBPL3,PNPO,ACSS2
small molecule biosynthetic process	2.30E-02	ASS1,CYB5R3,GLUD1,PCK2,ABCD3,PYCR1,PDXK,SPTLC2,AKR1A1,OSBPL3,PNPO,QNG1
organic hydroxy compound biosynthetic process	3.84E-02	CYB5R3,PCK2,ABCD3,PDXK,SPTLC2,OSBPL3,PNPO
alcohol metabolic process	6.92E-02	CAT,CYB5R3,GPD2,IDH2,PCK2,SOAT1,SPTLC2,AKR1A1,ACSS2
Cholesterol biosynthesis pathway in hepatocytes	4.54E-01	CYB5R3,ABCD3,OSBPL3,ACBD3
steroid biosynthetic process	4.88E-01	CYB5R3,ABCD3,OSBPL3,ACBD3
steroid metabolic process	5.23E-01	CAT,CYB5R3,ABCD3,SOAT1,OSBPL3,ACBD3
lipid biosynthetic process	5.30E-01	CYB5R3,PCK2,ABCD3,PCYT2,SPTLC2,CEPT1,INPP5F,OSBPL3,ACSS2,ACBD3

Table 2A.2. Pathway analysis of all genes found to be downregulated after PTGFRN knockdown by shRNA in A431, continued

VEGFA-VEGFR2 signaling	4.74E-03	ACP1,CALU,CTNNB1,FLNB,GLUD1,RAPGEF1,IDH2,LMAN1,FSCN1,PRDX2,ACOT9,CYCS,LRRC59
mRNA metabolic process	5.61E-03	DKC1,LGALS3,NCBP1,EXOSC9,S100A10,SRSF4,HNRNPR,PRPF8,HNRNPA0,EXOSC3,DDX47,CRNKL1,RBM28,ZCCHC8,PRPF40A,PDE12
mRNA processing	3.54E-02	LGALS3,NCBP1,SRSF4,HNRNPR,PRPF8,HNRNPA0,DDX47,CRNKL1,RBM28,ZCCHC8,PRPF40A,PDE12
Spliceosome	6.92E-02	NCBP1,SRSF4,PRPF8,IGF2BP3,CRNKL1,PRPF40A
RNA splicing	8.16E-02	LGALS3,NCBP1,SRSF4,HNRNPR,PRPF8,DDX47,CRNKL1,RBM28,ZCCHC8,PRPF40A
mRNA Splicing - Major Pathway	8.35E-02	NCBP1,POLR2E,SRSF4,HNRNPR,PRPF8,CRNKL1,PRPF40A
mRNA Splicing	9.77E-02	NCBP1,POLR2E,SRSF4,HNRNPR,PRPF8,CRNKL1,PRPF40A
Spliceosome	9.77E-02	HSPA2,NCBP1,SRSF4,PRPF8,CRNKL1,PRPF40A
mRNA processing	1.82E-01	NCBP1,SRSF4,HNRNPR,PRPF8,PRPF40A
C complex spliceosome	2.02E-01	HNRNPR,PRPF8,CRNKL1,ZCCHC8
RNA splicing, via transesterification reactions with bulged adenosine as nucleophile	2.50E-01	NCBP1,SRSF4,HNRNPR,PRPF8,CRNKL1,ZCCHC8,PRPF40A
mRNA splicing, via spliceosome	2.50E-01	NCBP1,SRSF4,HNRNPR,PRPF8,CRNKL1,ZCCHC8,PRPF40A
RNA splicing, via transesterification reactions	2.60E-01	NCBP1,SRSF4,HNRNPR,PRPF8,CRNKL1,ZCCHC8,PRPF40A

Table 2A.2. Pathway analysis of all genes found to be downregulated after PTGFRN knockdown by shRNA in A431, continued

Processing of Capped Intron-Containing Pre-mRNA	2.97E-01	NCBP1,POLR2E,SRSF4,HNRNPR,PRPF8,CRNKL1,PRPF40A
Carbon metabolism	6.27E-03	CAT,DLD,GLUD1,HK1,IDH2,ME2,ACSS2
Pyruvate metabolism	6.64E-03	DLD,ME2,PCK2,AKR1A1,ACSS2
Glycolysis / Gluconeogenesis	2.56E-02	DLD,HK1,PCK2,AKR1A1,ACSS2
Citric acid cycle (TCA cycle)	6.82E-02	DLD,IDH2,ME2
Transcriptional activation of mitochondrial biogenesis	8.16E-02	GLUD1,IDH2,CYCS,ACSS2
Citrate cycle (TCA cycle)	1.28E-01	DLD,IDH2,PCK2
Glyoxylate and dicarboxylate metabolism	1.28E-01	CAT,DLD,ACSS2
pyruvate metabolic process	1.48E-01	DLD,HK1,ME2,PCK2
Mitochondrial biogenesis	3.22E-01	GLUD1,IDH2,CYCS,ACSS2
nucleoside bisphosphate biosynthetic process	3.88E-01	DLD,PAPSS2,ACSS2
ribonucleoside bisphosphate biosynthetic process	3.88E-01	DLD,PAPSS2,ACSS2
purine nucleoside bisphosphate biosynthetic process	3.88E-01	DLD,PAPSS2,ACSS2

Table 2A.2. Pathway analysis of all genes found to be downregulated after PTGFRN knockdown by shRNA in A431, continued

Pyruvate metabolism and Citric Acid (TCA) cycle	4.15E-01	DLD,IDH2,ME2
nucleoside bisphosphate metabolic process	5.25E-01	DLD,PAPSS2,ACOT9,ACSS2
ribonucleoside bisphosphate metabolic process	5.25E-01	DLD,PAPSS2,ACOT9,ACSS2
purine nucleoside bisphosphate metabolic process	5.25E-01	DLD,PAPSS2,ACOT9,ACSS2
response to toxic substance	8.22E-03	ASS1,CAT,NQO1,LYN,PRDX2,AKR1A1,PRDX4,KDM5B,NXN
cellular detoxification	2.56E-02	CAT,NQO1,PRDX2,AKR1A1,PRDX4,NXN
cellular response to toxic substance	3.46E-02	CAT,NQO1,PRDX2,AKR1A1,PRDX4,NXN
detoxification	4.04E-02	CAT,NQO1,PRDX2,AKR1A1,PRDX4,NXN
cellular oxidant detoxification	5.71E-02	CAT,NQO1,PRDX2,PRDX4,NXN
Cellular response to chemical stress	7.20E-02	BLVRA,BLVRB,CAT,NQO1,PRDX2,PSMD6,CYCS
hydrogen peroxide catabolic process	1.01E-01	CAT,PRDX2,PRDX4
Detoxification of Reactive Oxygen Species	1.96E-01	CAT,PRDX2,CYCS
hydrogen peroxide metabolic process	2.17E-01	CAT,PRDX2,PRDX4
cell redox homeostasis	2.31E-01	NQO1,PRDX2,PRDX4

Table 2A.2. Pathway analysis of all genes found to be downregulated after PTGFRN knockdown by shRNA in A431, continued

Selenium micronutrient network	2.50E-01	CAT,PRDX2,PRDX4,PNPO
reactive oxygen species metabolic process	4.16E-01	CAT,NQO1,PRDX2,PRDX4
Viral Infection Pathways	9.33E-03	SLC25A6,HLA-A,NCBP1,POLR2E,RBBP7,RPL27A,RPL34,RPN1,ELOB,TJP1,UBE2V1,MOGS,H4C9,H2BC21,PSMD6,SEC24D,GANAB
protein N-linked glycosylation	3.27E-02	TMEM258,GFPT1,RPN1,MOGS,UGGT1
N-glycan trimming in the ER and Calnexin/Calreticulin cycle	1.76E-01	MOGS,GANAB,UGGT1
Maturation of spike protein	1.96E-01	RPN1,MOGS,GANAB
N-Glycan biosynthesis	3.54E-01	RPN1,MOGS,GANAB
SARS-CoV-2 Infection	3.56E-01	HLA-A,RPN1,TJP1,UBE2V1,MOGS,SEC24D,GANAB
Translation of Structural Proteins	4.42E-01	RPN1,MOGS,GANAB

Table 2A.3. Pathway analysis of all proteins found to be present in the co-IP of PTGFRN with 8C7 monoclonal antibody in A431 cells. Statistical significance determined at $p < 0.05$.

Pathway Description	adj. p-value	Proteins Present in 8C7 IP Elution
Metabolism of RNA	6.20E-29	CLNS1A,EIF4G1,GSPT1,HNRNPU,NCBP1,NCL,POLR2H,PPP2R2A,PSMA4,PSMB5,PSMB7,PSMB8,PSMC1,PSMD3,UPF1,RPL3,RPL6,RPL18A,RPL24,RPL26,RPL32,RPL38,RPLP0,RPS8,RPS15,RPS16,RPS23,RPS24,RPS27A,SRSF3,SNRPB2,SNRPE,PRPF4,RPL23,APOBEC3B,NUP58,LCMT2,POP7,CHERP,IGF2BP3,IGF2BP2,RPP40,NUDT21,CNOT1,PES1,PABPC1,GPKOW,DDX41,RBM28,RBM25,THOC3,EXOSC6,PRKAR2A,SRC,ADAM10,AP2M1,CLTC,CREB1,ITGB1,LAMC1,MSN,MYL6,PLCG1,EZR,EIF2S3,EIF4G2,EIF5A,GARS1,HARS1,LTA4H,PABPC4,LANCL1,MRPL2,ERAP1,QRSL1,IARS2,CARS2,EIF2A,MRPL53,ACAT1,ASNS,DLST,HEXB,OAT,FAR1,ILF2,ILF3,H1-10,GCSH,ETHE1,TXN2,CDK6,G6PD,HSPA5,IL1A,PGD,RHEB,HSP90B1,BAG2,PREB,LRPPRC,PRDX3,FEN1,PPIB,IKBKG,G3BP2,PDCD6IP,AP1M2,TRIM28,MBD3,OAS3,SRFBP1
VEGFA-VEGFR2 signaling	2.60E-11	ADAM10,ALDOA,CLTC,CREB1,CRK,EIF4G1,EIF4G2,ITGB1,LMAN1,MMP14,MYO6,NCL,PGD,PLCG1,PPP3CA,RPL18A,RPL26,FSCN1,SRC,STAT6,TPM3,EZR,PABPC1,EIF2A,CCDC124
ribonucleoprotein complex biogenesis	1.66E-08	CLNS1A,EIF2S3,NCBP1,PA2G4,RPL6,RPL26,RPL38,RPLP0,RPS8,RPS15,RPS16,RPS23,RPS24,SNRPB2,SNRPE,RUVBL1,POP7,RPP40,NUDT21,PES1,EIF2A,EXOSC6,SRFBP1,GARS1,HARS1,SRSF3,LCMT2,TDRKH,QRSL1,IARS2,CARS2,TRUB1
regulation of translation	8.59E-08	EIF4G1,EIF4G2,EIF5A,GSPT1,HNRNPU,ILF3,NCBP1,NCL,PA2G4,UPF1,RPL26,RPL38,BZW1,LRPPRC,SYNCRIP,IGF2BP3,IGF2BP2,CNOT1,LARP4B,CYFIP1,PABPC1,ZNF706,EIF2A,CLNS1A,SRSF3,PABPC4,AHCYL1,NUDT21,TRA2A,RBM25,CAPN1,RHEB,IKBKG,SEC22B,FBXO7,UBQLN1,EXOC1,SLIRP,PCSK9,SNRPB2,SNRPE,DDX41,RPL23

Table 2A.3. Pathway analysis of all proteins found to be present in the co-IP of PTGFRN with 8C7 monoclonal antibody in A431 cells, continued

CLEC7A (Dectin-1) signaling	4.49E-07	PPP3CA,PSMA4,PSMB5,PSMB7,PSMB8,PSMC1,PSMD3,RPS27A,SRC,IKBKG,AHCYL1,EIF4G1,PABPC1,CREB1,CRK,EIF4G2,GBP2,IL1A,ITGB1,MSN,OAS3,PLCG1,RPLP0,FSCN1,STAT6,HSP90B1,OASL,NUP58,EXOSC6,AP2M1,CLTC,SCRIB,FEN1,NCBP1,POLR2H,PDCD6IP,AP1M2,G6PD,PGD,BAK1,PLEC,STK24,BCAP31,PRKAR2A,KIF3A,ADCY10,CDK6,POLE,PPP2R2A,SEC22B,LRPPRC,PRDX3,TXN2,HSPA5,UBE3A,FBXO7,ERAP1,ADAM10,PEBP1,TPM3,RHEB,MBD3,RUVBL1,EIF2S3,ATP5F1D,NDUFS3,SRSF3,MATR3,UBQLN1,LAMC1,TGM2,GUSB,RAD23A,RAD23B,MAEA,PCSK9,NUDC,CAPN1,SMC4,RGL2,DCAF8,AKAP1,GLRX3,LSR,SLC44A2
actin filament organization	2.76E-06	ALDOA,DIAPH1,MYO5A,MYO6,PLEC,FSCN1,SRC,TPM3,HSP90B1,EZR,TAGLN2,CORO1C,CORO1B,INF2,CORO7,CRK,ITGB1,ARHGEF10,PDCD6IP,MYL6,CYFIP1
mRNA metabolic process	3.12E-06	CLNS1A,CREB1,GSPT1,HNRNPU,NCBP1,UPF1,SRSF3,SNRPB2,SNRPE,PRPF4,SYNCRIP,AHCYL1,NUDT21,CNOT1,PABPC1,GPKOW,TRA2A,DDX41,RBM28,RBM25,THOC3,EXOSC6,TRUB1,IGF2BP3,POLR2H,NUP58,CHERP,NCL,AHNAK
Protein processing in endoplasmic reticulum	8.79E-06	BAK1,CAPN1,HSPA5,LMAN1,RAD23A,RAD23B,HSP90B1,BAG2,PREB,BCAP31,HSPBP1,UBQLN1,MSN,PSMC1,SUMO2,EZR,SEC22B,PCSK9,PSMD3,UBE3A,RPL23,UPF1,IKBKG,CNOT1,FBXO7,PABPC1,SERPINC1,MMP14,PEBP1,PSMB8,SRC
RHO GTPase cycle	1.74E-05	ALDH3A2,CCT6A,CLTC,DIAPH1,NIPSNAP2,ITGB1,LMAN1,MYO6,NDUFS3,SRC,TPM3,ARHGAP29,ARHGEF10,BCAP31,NUDC,CYFIP1,SCRIB,LRRC1,MYL6,TAX1BP3
Fragile X syndrome	2.52E-05	ALDH3A2,AP2M1,CLTC,CREB1,EIF4G1,PLCG1,PPP3CA,RHEB,SRC,CYFIP1,PRKAR2A,AHCYL1,AAMP,ADAM10,RPS27A,CRK,STAT6,DIAPH1,IL1A,IKBKG,ILF2,BAK1,APOBEC3B,AP1M2,PEBP1,EZR,CAPN1,HSPA5,HSP90B1
mRNA transport	3.34E-05	NCBP1,UPF1,SRSF3,NUP58,G3BP2,LRPPRC,NUTF2,IGF2BP3,IGF2BP2,THOC3,HNRNPU,PPP3CA,RPS15,RPL23,AHCYL1,SNRPE,NUDT21,SUMO2

Table 2A.3. Pathway analysis of all proteins found to be present in the co-IP of PTGFRN with 8C7 monoclonal antibody in A431 cells, continued

nucleobase-containing small molecule metabolic process	6.21E-05	ACAT1,ADK,ALDOA,ATP5F1D,CTPS1,DLST,DTYMK,G6PD,GARS1,GMDS,HPRT1,MDH2,NDUFS3,PGD,APOBEC3B,RAB23,CMPK1,ADCY10,FAR1,HEXB,SORD,HDHD5,SLC44A2,LCMT2
positive regulation of organelle organization	7.31E-05	BAK1,CCT6A,FEN1,IL1A,LMAN1,MSN,FSCN1,SRC,RUVBL1,MACROH2A1,ARHGEF10,G3BP2,PDCD6IP,SMC4,TRIM28,CNOT1,CYFIP1,FBXO7,HNRNPU,EZR,SEC22B,SCRIB,CRK,ITGB1,CORO7,EIF4G1,GBP2,HSPA5,PREB,SEPTIN8
protein folding	7.74E-05	CCT6A,GAK,HSPA5,LMAN1,PFDN4,PPIB,HSP90B1,BAG2,NUDC,FKBP9,MESD,HSPBP1
negative regulation of transferase activity	9.09E-05	HNRNPU,PLEC,PRKAR2A,SRC,GPRC5A,RPL23,BAG2,MACROH2A1,PRDX3,CORO1C,FBXO7,SMYD3,CEP85,BAK1,EIF4G1,G6PD,RPS15,UBR5,OXR1,SERPINC1,PEBP1
Signaling by Receptor Tyrosine Kinases	1.02E-04	AAMP,ADAM10,AP2M1,CLTC,CREB1,CRK,DIAPH1,ITGA3,ITGB1,LAMC1,NCBP1,PLCG1,POLR2H,RPS27A,SRC,STAT6,AHCYL1,CYFIP1,NCL,MMP14,CAPN1,IKBKG,SEPTIN8,LMAN1,TACSTD2,TGM2,UBQLN1,EZR,HSPA5,IL1A,PPP3CA,RGL2,ARHGAP29,ARHGEF10,MSN,PLEC,PPIB,PRKAR2A,GPRC5A,PCSK9
Carbon metabolism	1.03E-04	ACAT1,ALDOA,ALDOC,CS,DLST,G6PD,GCSH,MDH2,PGD,ATP5F1D,FDXR,NIPSNAP2,NDUFS3,PLEC,ASNS,OAT,LRPPRC
response to inorganic substance	1.32E-04	ATP5F1D,BAK1,CREB1,CRK,G6PD,HSPA5,IL1A,LTA4H,PLEC,PPP3CA,SORD,SRC,STAT6,UBE3A,STK24,AHCYL1,PRDX3,ADCY10,PPP2R2A,TGM2,HSP90B1
Human papillomavirus infection	1.43E-04	BAK1,CDK6,CREB1,ITGA3,ITGB1,LAMC1,PPP2R2A,PSMC1,RHEB,UBE3A,IKBKG,OASL,BCAP31,SCRIB,CKS2,SRC,CRK,PLCG1,STAT6,TPM3,HSP90B1,CCDC6,DSC3,EIF4G1,MMP14,BAG2,TGM2,INF2,LSR,IL1A
DGCR8 multiprotein complex	2.23E-04	HNRNPU,HSPA5,ILF3,NCL,MATR3,UBR5

Table 2A.3. Pathway analysis of all proteins found to be present in the co-IP of PTGFRN with 8C7 monoclonal antibody in A431 cells, continued

Metabolism of RNA	6.20E-29	CLNS1A,EIF4G1,GSPT1,HNRNPU,NCBP1,NCL,POLR2H,PPP2R2A,PSMA4,PSMB5,PSMB7,PSMB8,PSMC1,PSMD3,UPF1,RPL3,RPL6,RPL18A,RPL24,RPL26,RPL32,RPL38,RPLP0,RPS8,RPS15,RPS16,RPS23,RPS24,RPS27A,SRSF3,SNRPB2,SNRPE,PRPF4,RPL23,APOBEC3B,NUP58,LCMT2,POP7,CHERP,IGF2BP3,IGF2BP2,RPP40,NUDT21,CNOT1,PES1,PABPC1,GPKOW,DDX41,RBM28,RBM25,THOC3,EXOSC6
Regulation of expression of SLITs and ROBOs	1.07E-19	EIF4G1,GSPT1,NCBP1,PSMA4,PSMB5,PSMB7,PSMB8,PSMC1,PSMD3,RPL3,RPL6,RPL18A,RPL24,RPL26,RPL32,RPL38,RPLP0,RPS8,RPS15,RPS16,RPS23,RPS24,RPS27A,RPL23,PABPC1
Signaling by ROBO receptors	1.07E-19	EIF4G1,GSPT1,NCBP1,PRKAR2A,PSMA4,PSMB5,PSMB7,PSMB8,PSMC1,PSMD3,RPL3,RPL6,RPL18A,RPL24,RPL26,RPL32,RPL38,RPLP0,RPS8,RPS15,RPS16,RPS23,RPS24,RPS27A,SRC,RPL23,PABPC1
Axon guidance	7.80E-19	ADAM10,AP2M1,CLTC,CREB1,EIF4G1,GSPT1,ITGB1,LAMC1,MSN,MYL6,NCBP1,PLCG1,PRKAR2A,PSMA4,PSMB5,PSMB7,PSMB8,PSMC1,PSMD3,RPL3,RPL6,RPL18A,RPL24,RPL26,RPL32,RPL38,RPLP0,RPS8,RPS15,RPS16,RPS23,RPS24,RPS27A,SRC,EZR,RPL23,PABPC1
Nonsense Mediated Decay (NMD) independent of the Exon Junction Complex (EJC)	7.80E-19	EIF4G1,GSPT1,NCBP1,UPF1,RPL3,RPL6,RPL18A,RPL24,RPL26,RPL32,RPL38,RPLP0,RPS8,RPS15,RPS16,RPS23,RPS24,RPS27A,RPL23,PABPC1
Nonsense-Mediated Decay (NMD)	1.12E-18	EIF4G1,GSPT1,NCBP1,PPP2R2A,UPF1,RPL3,RPL6,RPL18A,RPL24,RPL26,RPL32,RPL38,RPLP0,RPS8,RPS15,RPS16,RPS23,RPS24,RPS27A,RPL23,PABPC1
Nonsense Mediated Decay (NMD) enhanced by the Exon Junction Complex (EJC)	1.12E-18	EIF4G1,GSPT1,NCBP1,PPP2R2A,UPF1,RPL3,RPL6,RPL18A,RPL24,RPL26,RPL32,RPL38,RPLP0,RPS8,RPS15,RPS16,RPS23,RPS24,RPS27A,RPL23,PABPC1

Table 2A.3. Pathway analysis of all proteins found to be present in the co-IP of PTGFRN with 8C7 monoclonal antibody in A431 cells, continued

Nervous system development	2.15E-18	ADAM10,AP2M1,CLTC,CREB1,EIF4G1,GSPT1,ITGB1,LAMC1,MSN,MYL6,NCBP1,PLCG1,PRKAR2A,PSMA4,PSMB5,PSMB7,PSMB8,PSMC1,PSMD3,RPL3,RPL6,RPL18A,RPL24,RPL26,RPL32,RPL38,RPLP0,RPS8,RPS15,RPS16,RPS23,RPS24,RPS27A,SRC,EZR,RPL23,PABPC1
peptide metabolic process	3.38E-18	ADAM10,EIF2S3,EIF4G1,EIF4G2,EIF5A,GARS1,GSPT1,HARS1,LTA4H,NCBP1,RPL3,RPL6,RPL18A,RPL24,RPL26,RPL32,RPL38,RPLP0,RPS8,RPS15,RPS16,RPS23,RPS24,RPS27A,PABPC4,RPL23,LANCL1,IGF2BP3,MRPL2,ERAP1,QRSL1,IARS2,CARS2,EIF2A,MRPL53
translation	7.85E-18	EIF2S3,EIF4G1,EIF4G2,EIF5A,GARS1,GSPT1,HARS1,NCBP1,RPL3,RPL6,RPL18A,RPL24,RPL26,RPL32,RPL38,RPLP0,RPS8,RPS15,RPS16,RPS23,RPS24,RPS27A,PABPC4,RPL23,IGF2BP3,MRPL2,QRSL1,IARS2,CARS2,EIF2A,MRPL53
amide metabolic process	2.85E-17	ACAT1,ADAM10,ASNS,DLST,EIF2S3,EIF4G1,EIF4G2,EIF5A,GARS1,GSPT1,HARS1,HEXB,LTA4H,NCBP1,OAT,RPL3,RPL6,RPL18A,RPL24,RPL26,RPL32,RPL38,RPLP0,RPS8,RPS15,RPS16,RPS23,RPS24,RPS27A,PABPC4,RPL23,LANCL1,IGF2BP3,MRPL2,ERAP1,QRSL1,IARS2,CARS2,EIF2A,FAR1,MRPL53
peptide biosynthetic process	5.01E-17	EIF2S3,EIF4G1,EIF4G2,EIF5A,GARS1,GSPT1,HARS1,NCBP1,RPL3,RPL6,RPL18A,RPL24,RPL26,RPL32,RPL38,RPLP0,RPS8,RPS15,RPS16,RPS23,RPS24,RPS27A,PABPC4,RPL23,IGF2BP3,MRPL2,QRSL1,IARS2,CARS2,EIF2A,MRPL53
Nop56p-associated pre-rRNA complex	5.01E-17	HNRNPU,ILF2,ILF3,NCL,RPL3,RPL6,RPL18A,RPL24,RPL26,RPL32,RPLP0,RPS8,RPS15,RPS16,RPS23,RPS24,H1-10,RPL23,RBM28
amide biosynthetic process	1.07E-15	ACAT1,ASNS,EIF2S3,EIF4G1,EIF4G2,EIF5A,GARS1,GSPT1,HARS1,NCBP1,RPL3,RPL6,RPL18A,RPL24,RPL26,RPL32,RPL38,RPLP0,RPS8,RPS15,RPS16,RPS23,RPS24,RPS27A,PABPC4,RPL23,IGF2BP3,MRPL2,QRSL1,IARS2,CARS2,EIF2A,MRPL53
Metabolism of amino acids and derivatives	2.86E-15	ACAT1,ASNS,DLST,GCSH,OAT,PSMA4,PSMB5,PSMB7,PSMB8,PSMC1,PSMD3,RPL3,RPL6,RPL18A,RPL24,RPL26,RPL32,RPL38,RPLP0,RPS8,RPS15,RPS16,RPS23,RPS24,RPS27A,RPL23,ETHE1,TXN2

Table 2A.3. Pathway analysis of all proteins found to be present in the co-IP of PTGFRN with 8C7 monoclonal antibody in A431 cells, continued

Cellular responses to stress	4.33E-15	ASNS,CDK6,CREB1,EIF2S3,G6PD,HSPA5,IL1A,PGD,PSMA4,PSMB5,PSMB7,PSMB8,PSMC1,PSMD3,RHEB,RPL3,RPL6,RPL18A,RPL24,RPL26,RPL32,RPL38,RPLP0,RPS8,RPS15,RPS16,RPS23,RPS24,RPS27A,HSP90B1,RPL23,BAG2,NUP58,PREB,LRPPRC,PRDX3,TXN2,EXOSC6
L13a-mediated translational silencing of Ceruloplasmin expression	4.33E-15	EIF2S3,EIF4G1,RPL3,RPL6,RPL18A,RPL24,RPL26,RPL32,RPL38,RPLP0,RPS8,RPS15,RPS16,RPS23,RPS24,RPS27A,RPL23,PABPC1
Translation	6.39E-15	EIF2S3,EIF4G1,GARS1,GSPT1,HARS1,RPL3,RPL6,RPL18A,RPL24,RPL26,RPL32,RPL38,RPLP0,RPS8,RPS15,RPS16,RPS23,RPS24,RPS27A,RPL23,PABPC1,MRPL2,IARS2,CARS2,MRPL53
Viral Infection Pathways	1.11E-14	AP2M1,CLTC,CREB1,FEN1,ITGB1,NCBP1,POLR2H,PPIB,PSMA4,PSMB5,PSMB7,PSMB8,PSMC1,PSMD3,RPL3,RPL6,RPL18A,RPL24,RPL26,RPL32,RPL38,RPLP0,RPS8,RPS15,RPS16,RPS23,RPS24,RPS27A,SNRPE,IKBKG,RPL23,NUP58,G3BP2,PDCD6IP,AP1M2,TRIM28,MBD3
Eukaryotic Translation Initiation	1.27E-14	EIF2S3,EIF4G1,RPL3,RPL6,RPL18A,RPL24,RPL26,RPL32,RPL38,RPLP0,RPS8,RPS15,RPS16,RPS23,RPS24,RPS27A,RPL23,PABPC1
Cap-dependent Translation Initiation	1.27E-14	EIF2S3,EIF4G1,RPL3,RPL6,RPL18A,RPL24,RPL26,RPL32,RPL38,RPLP0,RPS8,RPS15,RPS16,RPS23,RPS24,RPS27A,RPL23,PABPC1
Response of EIF2AK4 (GCN2) to amino acid deficiency	1.54E-14	ASNS,EIF2S3,RPL3,RPL6,RPL18A,RPL24,RPL26,RPL32,RPL38,RPLP0,RPS8,RPS15,RPS16,RPS23,RPS24,RPS27A,RPL23
cytoplasmic translation	1.82E-14	EIF2S3,EIF4G1,NCBP1,RPL3,RPL6,RPL18A,RPL24,RPL26,RPL32,RPL38,RPLP0,RPS8,RPS15,RPS16,RPS23,RPS24,RPS27A,RPL23
GTP hydrolysis and joining of the 60S ribosomal subunit	8.59E-14	EIF2S3,EIF4G1,RPL3,RPL6,RPL18A,RPL24,RPL26,RPL32,RPL38,RPLP0,RPS8,RPS15,RPS16,RPS23,RPS24,RPS27A,RPL23
Eukaryotic Translation Termination	8.68E-14	GSPT1,RPL3,RPL6,RPL18A,RPL24,RPL26,RPL32,RPL38,RPLP0,RPS8,RPS15,RPS16,RPS23,RPS24,RPS27A,RPL23

Table 2A.3. Pathway analysis of all proteins found to be present in the co-IP of PTGFRN with 8C7 monoclonal antibody in A431 cells, continued

Major pathway of rRNA processing in the nucleolus and cytosol	1.12E-13	NCL,RPL3,RPL6,RPL18A,RPL24,RPL26,RPL32,RPL38,RPLP0,RPS8,RPS15,RPS16,RPS23,RPS24,RPS27A,RPL23,RPP40,PES1,RBM28,EXOSC6
Ribosome, cytoplasmic	1.62E-13	RPL3,RPL6,RPL18A,RPL24,RPL26,RPL32,RPL38,RPLP0,RPS8,RPS15,RPS16,RPS23,RPS24,RPS27A,RPL23
rRNA processing in the nucleus and cytosol	2.93E-13	NCL,RPL3,RPL6,RPL18A,RPL24,RPL26,RPL32,RPL38,RPLP0,RPS8,RPS15,RPS16,RPS23,RPS24,RPS27A,RPL23,RPP40,PES1,RBM28,EXOSC6
Cytoplasmic ribosomal proteins	6.79E-13	RPL3,RPL6,RPL18A,RPL24,RPL26,RPL32,RPL38,RPLP0,RPS8,RPS15,RPS16,RPS23,RPS24,RPS27A,RPL23
rRNA processing	7.26E-13	NCL,RPL3,RPL6,RPL18A,RPL24,RPL26,RPL32,RPL38,RPLP0,RPS8,RPS15,RPS16,RPS23,RPS24,RPS27A,RPL23,RPP40,PES1,RBM28,EXOSC6
Peptide chain elongation	8.75E-13	RPL3,RPL6,RPL18A,RPL24,RPL26,RPL32,RPL38,RPLP0,RPS8,RPS15,RPS16,RPS23,RPS24,RPS27A,RPL23
Viral mRNA Translation	8.75E-13	RPL3,RPL6,RPL18A,RPL24,RPL26,RPL32,RPL38,RPLP0,RPS8,RPS15,RPS16,RPS23,RPS24,RPS27A,RPL23
Influenza Infection	1.04E-12	CLTC,POLR2H,RPL3,RPL6,RPL18A,RPL24,RPL26,RPL32,RPL38,RPLP0,RPS8,RPS15,RPS16,RPS23,RPS24,RPS27A,RPL23,NUP58
Cellular response to starvation	1.04E-12	ASNS,EIF2S3,RHEB,RPL3,RPL6,RPL18A,RPL24,RPL26,RPL32,RPL38,RPLP0,RPS8,RPS15,RPS16,RPS23,RPS24,RPS27A,RPL23
Influenza Viral RNA Transcription and Replication	1.45E-12	POLR2H,RPL3,RPL6,RPL18A,RPL24,RPL26,RPL32,RPL38,RPLP0,RPS8,RPS15,RPS16,RPS23,RPS24,RPS27A,RPL23,NUP58
Eukaryotic Translation Elongation	1.49E-12	RPL3,RPL6,RPL18A,RPL24,RPL26,RPL32,RPL38,RPLP0,RPS8,RPS15,RPS16,RPS23,RPS24,RPS27A,RPL23
Selenocysteine synthesis	1.49E-12	RPL3,RPL6,RPL18A,RPL24,RPL26,RPL32,RPL38,RPLP0,RPS8,RPS15,RPS16,RPS23,RPS24,RPS27A,RPL23
Formation of a pool of free 40S subunits	5.14E-12	RPL3,RPL6,RPL18A,RPL24,RPL26,RPL32,RPL38,RPLP0,RPS8,RPS15,RPS16,RPS23,RPS24,RPS27A,RPL23

Table 2A.3. Pathway analysis of all proteins found to be present in the co-IP of PTGFRN with 8C7 monoclonal antibody in A431 cells, continued

SRP-dependent cotranslational protein targeting to membrane	2.39E-11	RPL3,RPL6,RPL18A,RPL24,RPL26,RPL32,RPL38, RPLP0,RPS8,RPS15,RPS16,RPS23,RPS24,RPS27A, RPL23
Selenoamino acid metabolism	4.98E-11	RPL3,RPL6,RPL18A,RPL24,RPL26,RPL32,RPL38, RPLP0,RPS8,RPS15,RPS16,RPS23,RPS24,RPS27A, RPL23
Ribosome	5.45E-10	RPL3,RPL6,RPL18A,RPL24,RPL26,RPL32,RPL38, RPLP0,RPS8,RPS15,RPS16,RPS23,RPS24,RPS27A, RPL23,MRPL2
Coronavirus disease - COVID-19	7.44E-10	OAS3,PLCG1,RPL3,RPL6,RPL18A,RPL24,RPL26,R PL32,RPL38,RPLP0,RPS8,RPS15,RPS16,RPS23,RP S24,RPS27A,IKBKG,RPL23
60S ribosomal subunit, cytoplasmic	9.00E-08	RPL3,RPL6,RPL18A,RPL24,RPL26,RPL32,RPL38, RPLP0,RPL23
Translation initiation complex formation	7.00E-07	EIF2S3,EIF4G1,RPS8,RPS15,RPS16,RPS23,RPS24, RPS27A,PABPC1
Activation of the mRNA upon binding of the cap-binding complex and eIFs, and subsequent binding to 43S	8.01E-07	EIF2S3,EIF4G1,RPS8,RPS15,RPS16,RPS23,RPS24, RPS27A,PABPC1
Ribosomal scanning and start codon recognition	1.13E-05	EIF2S3,EIF4G1,RPS8,RPS15,RPS16,RPS23,RPS24, RPS27A
40S ribosomal subunit, cytoplasmic	5.07E-05	RPS8,RPS15,RPS16,RPS23,RPS24,RPS27A
SARS-CoV-2 modulates host translation machinery	5.61E-05	RPS8,RPS15,RPS16,RPS23,RPS24,RPS27A,SNRPE
Formation of the ternary complex, and subsequently, the 43S complex	5.91E-05	EIF2S3,RPS8,RPS15,RPS16,RPS23,RPS24,RPS27A

Table 2A.3. Pathway analysis of all proteins found to be present in the co-IP of PTGFRN with 8C7 monoclonal antibody in A431 cells, continued

40S ribosomal subunit, cytoplasmic	6.48E-05	RPS8,RPS15,RPS16,RPS23,RPS24,RPS27A
SARS-CoV-1 modulates host translation machinery	1.08E-04	RPS8,RPS15,RPS16,RPS23,RPS24,RPS27A
ribosomal small subunit biogenesis	3.81E-04	RPL38,RPS8,RPS15,RPS16,RPS23,RPS24,RPP40,SRFBP1
SARS-CoV-2-host interactions	9.69E-04	RPS8,RPS15,RPS16,RPS23,RPS24,RPS27A,SNRPE,IKBKG,NUP58,G3BP2
SARS-CoV Infections	1.23E-03	AP2M1,ITGB1,PPIB,RPS8,RPS15,RPS16,RPS23,RPS24,RPS27A,SNRPE,IKBKG,NUP58,G3BP2,MBD3
SARS-CoV-1-host interactions	1.59E-03	PPIB,RPS8,RPS15,RPS16,RPS23,RPS24,RPS27A
SARS-CoV-1 Infection	1.22E-02	PPIB,RPS8,RPS15,RPS16,RPS23,RPS24,RPS27A
SARS-CoV-2 Infection	1.37E-02	RPS8,RPS15,RPS16,RPS23,RPS24,RPS27A,SNRPE,IKBKG,NUP58,G3BP2
VEGFA-VEGFR2 signaling	2.60E-11	ADAM10,ALDOA,CLTC,CREB1,CRK,EIF4G1,EIF4G2,ITGB1,LMAN1,MMP14,MYO6,NCL,PGD,PLCG1,PPP3CA,RPL18A,RPL26,FSCN1,SRC,STAT6,TPM3,EZR,PABPC1,EIF2A,CCDC124
ribonucleoprotein complex biogenesis	1.66E-08	CLNS1A,EIF2S3,NCBP1,PA2G4,RPL6,RPL26,RPL38,RPLP0,RPS8,RPS15,RPS16,RPS23,RPS24,SNRPB2,SNRPE,RUVBL1,POP7,RPP40,NUDT21,PES1,EIF2A,EXOSC6,SRFBP1
ncRNA metabolic process	1.59E-06	GARS1,HARS1,NCBP1,PA2G4,RPL26,RPS8,RPS15,RPS16,RPS24,SRSF3,LCMT2,POP7,RPP40,TDRKH,PES1,QRSL1,IARS2,CARS2,EXOSC6,TRUB1,SRFBP1
ribosome biogenesis	3.94E-06	PA2G4,RPL6,RPL26,RPL38,RPLP0,RPS8,RPS15,RPS16,RPS23,RPS24,POP7,RPP40,PES1,EIF2A,EXOSC6,SRFBP1
ncRNA processing	1.03E-04	NCBP1,PA2G4,RPL26,RPS8,RPS15,RPS16,RPS24,SRSF3,LCMT2,POP7,RPP40,TDRKH,PES1,EXOSC6,TRUB1,SRFBP1
rRNA processing	3.22E-04	PA2G4,RPL26,RPS8,RPS15,RPS16,RPS24,POP7,RPP40,PES1,EXOSC6,SRFBP1
rRNA metabolic process	9.15E-04	PA2G4,RPL26,RPS8,RPS15,RPS16,RPS24,POP7,RPP40,PES1,EXOSC6,SRFBP1

Table 2A.3. Pathway analysis of all proteins found to be present in the co-IP of PTGFRN with 8C7 monoclonal antibody in A431 cells, continued

maturation of SSU-rRNA	4.69E-02	RPS8,RPS16,RPP40,SRFBP1
maturation of SSU-rRNA from tricistronic rRNA transcript (SSU-rRNA, 5.8S rRNA, LSU-rRNA)	1.26E-01	RPS8,RPS16,RPP40
regulation of translation	8.59E-08	EIF4G1,EIF4G2,EIF5A,GSPT1,HNRNPU,ILF3,NCBP1,NCL,PA2G4,UPF1,RPL26,RPL38,BZW1,LRPPRC,SYNCRIP,IGF2BP3,IGF2BP2,CNOT1,LARP4B,CYFIP1,PABPC1,ZNF706,EIF2A
regulation of amide metabolic process	7.00E-07	EIF4G1,EIF4G2,EIF5A,GSPT1,HNRNPU,ILF3,NCBP1,NCL,PA2G4,UPF1,RPL26,RPL38,BZW1,LRPPRC,SYNCRIP,IGF2BP3,IGF2BP2,CNOT1,LARP4B,CYFIP1,PABPC1,ZNF706,EIF2A
regulation of mRNA metabolic process	3.38E-06	CLNS1A,HNRNPU,NCBP1,NCL,UPF1,SRSF3,PABPC4,SYNCRIP,IGF2BP3,IGF2BP2,AHCYL1,NUDT21,CNOT1,LARP4B,PABPC1,TRA2A,RBM25
CRD-mediated mRNA stabilization	6.50E-06	HNRNPU,SYNCRIP,IGF2BP3,IGF2BP2,PABPC1
regulation of cellular catabolic process	9.67E-05	CAPN1,EIF4G1,EIF4G2,HNRNPU,UPF1,RHEB,IKBKG,PABPC4,SEC22B,LRPPRC,SYNCRIP,IGF2BP3,IGF2BP2,CNOT1,LARP4B,FBXO7,PABPC1,UBQLN1,EXOC1,SLIRP,PCSK9
negative regulation of RNA catabolic process	8.24E-04	HNRNPU,LRPPRC,SYNCRIP,IGF2BP3,IGF2BP2,PABPC1,SLIRP
negative regulation of cellular catabolic process	9.69E-04	EIF4G1,EIF4G2,HNRNPU,SEC22B,LRPPRC,SYNCRIP,IGF2BP3,IGF2BP2,PABPC1,SLIRP
IGF2BP1 complex	3.75E-03	HNRNPU,RPL26,SYNCRIP
C complex spliceosome	4.24E-03	HNRNPU,SNRPB2,SNRPE,SYNCRIP,PABPC1,DDX41

Table 2A.3. Pathway analysis of all proteins found to be present in the co-IP of PTGFRN with 8C7 monoclonal antibody in A431 cells, continued

regulation of nuclear-transcribed mRNA catabolic process, deadenylation-dependent decay	4.75E-03	HNRNPU,SYNCRIP,CNOT1,PABPC1
regulation of mRNA stability	6.14E-03	HNRNPU,UPF1,PABPC4,SYNCRIP,IGF2BP3,IGF2BP2,CNOT1,LARP4B,PABPC1
negative regulation of nuclear-transcribed mRNA catabolic process, deadenylation-dependent decay	8.07E-03	HNRNPU,SYNCRIP,PABPC1
regulation of RNA stability	8.51E-03	HNRNPU,UPF1,PABPC4,SYNCRIP,IGF2BP3,IGF2BP2,CNOT1,LARP4B,PABPC1
mRNA stabilization	1.02E-02	HNRNPU,SYNCRIP,IGF2BP3,IGF2BP2,PABPC1
negative regulation of catabolic process	1.06E-02	EIF4G1,EIF4G2,HNRNPU,RPL23,SEC22B,LRPPRC,SYNCRIP,IGF2BP3,IGF2BP2,PABPC1,SLIRP
regulation of mRNA catabolic process	1.06E-02	HNRNPU,UPF1,PABPC4,SYNCRIP,IGF2BP3,IGF2BP2,CNOT1,LARP4B,PABPC1
positive regulation of translation	1.27E-02	EIF4G1,EIF5A,HNRNPU,RPL26,SYNCRIP,LARP4B,PABPC1
positive regulation of cytoplasmic translation	1.41E-02	HNRNPU,SYNCRIP,PABPC1
RNA stabilization	1.69E-02	HNRNPU,SYNCRIP,IGF2BP3,IGF2BP2,PABPC1
negative regulation of mRNA catabolic process	1.99E-02	HNRNPU,SYNCRIP,IGF2BP3,IGF2BP2,PABPC1
positive regulation of amide metabolic process	2.96E-02	EIF4G1,EIF5A,HNRNPU,RPL26,SYNCRIP,LARP4B,PABPC1

Table 2A.3. Pathway analysis of all proteins found to be present in the co-IP of PTGFRN with 8C7 monoclonal antibody in A431 cells, continued

negative regulation of mRNA metabolic process	5.32E-02	HNRNPU,SYNCRIP,IGF2BP3,IGF2BP2,PABPC1
regulation of cytoplasmic translation	8.61E-02	HNRNPU,SYNCRIP,PABPC1
negative regulation of translation	1.09E-01	EIF4G1,ILF3,NCL,UPF1,SYNCRIP,IGF2BP3,IGF2BP2,CNOT1
negative regulation of amide metabolic process	1.68E-01	EIF4G1,ILF3,NCL,UPF1,SYNCRIP,IGF2BP3,IGF2BP2,CNOT1
CLEC7A (Dectin-1) signaling	4.49E-07	PPP3CA,PSMA4,PSMB5,PSMB7,PSMB8,PSMC1,PSMD3,RPS27A,SRC,IKBKG,AHCYL1
AUF1 (hnRNP D0) binds and destabilizes mRNA	4.49E-07	EIF4G1,PSMA4,PSMB5,PSMB7,PSMB8,PSMC1,PSMD3,RPS27A,PABPC1
Cytokine Signaling in Immune system	1.47E-06	CREB1,CRK,EIF4G1,EIF4G2,GBP2,IL1A,ITGB1,MSN,OAS3,PLCG1,PSMA4,PSMB5,PSMB7,PSMB8,PSMC1,PSMD3,RPLP0,RPS27A,FSCN1,SRC,STAT6,HSP90B1,IKBKG,OASL,NUP58
Regulation of mRNA stability by proteins that bind AU-rich elements	1.56E-06	EIF4G1,PSMA4,PSMB5,PSMB7,PSMB8,PSMC1,PSMD3,RPS27A,PABPC1,EXOSC6
PCP/CE pathway	2.33E-06	AP2M1,CLTC,PSMA4,PSMB5,PSMB7,PSMB8,PSMC1,PSMD3,RPS27A,SCRIB
HIV Infection	4.23E-06	AP2M1,FEN1,NCBP1,POLR2H,PSMA4,PSMB5,PSMB7,PSMB8,PSMC1,PSMD3,RPS27A,NUP58,PDCD6IP,AP1M2
Regulation of RUNX3 expression and activity	6.89E-06	PSMA4,PSMB5,PSMB7,PSMB8,PSMC1,PSMD3,RPS27A,SRC
Fc epsilon receptor (FCERI) signaling	6.91E-06	PLCG1,PPP3CA,PSMA4,PSMB5,PSMB7,PSMB8,PSMC1,PSMD3,RPS27A,IKBKG,AHCYL1

Table 2A.3. Pathway analysis of all proteins found to be present in the co-IP of PTGFRN with 8C7 monoclonal antibody in A431 cells, continued

Nuclear events mediated by NFE2L2	7.74E-06	G6PD,PGD,PSMA4,PSMB5,PSMB7,PSMB8,PSMC1,PSMD3,RPS27A
Downstream signaling events of B Cell Receptor (BCR)	1.13E-05	PPP3CA,PSMA4,PSMB5,PSMB7,PSMB8,PSMC1,PSMD3,RPS27A,IKBKG
Programmed Cell Death	1.14E-05	BAK1,IL1A,PLEC,PSMA4,PSMB5,PSMB7,PSMB8,PSMC1,PSMD3,RPS27A,STK24,PDCD6IP,BCAP31
C-type lectin receptors (CLRs)	1.14E-05	PPP3CA,PSMA4,PSMB5,PSMB7,PSMB8,PSMC1,PSMD3,RPS27A,SRC,IKBKG,AHCYL1
Signaling by the B Cell Receptor (BCR)	1.22E-05	PPP3CA,PSMA4,PSMB5,PSMB7,PSMB8,PSMC1,PSMD3,RPS27A,IKBKG,AHCYL1
Hedgehog 'off' state	1.32E-05	PRKAR2A,PSMA4,PSMB5,PSMB7,PSMB8,PSMC1,PSMD3,RPS27A,KIF3A,ADCY10
Beta-catenin independent WNT signaling	1.45E-05	AP2M1,CLTC,PPP3CA,PSMA4,PSMB5,PSMB7,PSMB8,PSMC1,PSMD3,RPS27A,SCRIB
Mitotic G1 phase and G1/S transition	1.74E-05	CDK6,POLE,PPP2R2A,PSMA4,PSMB5,PSMB7,PSMB8,PSMC1,PSMD3,RPS27A,SRC
Asymmetric localization of PCP proteins	1.91E-05	PSMA4,PSMB5,PSMB7,PSMB8,PSMC1,PSMD3,RPS27A,SCRIB
ER-Phagosome pathway	2.04E-05	PSMA4,PSMB5,PSMB7,PSMB8,PSMC1,PSMD3,RPS27A,IKBKG,SEC22B
Activation of NF-kappaB in B cells	2.66E-05	PSMA4,PSMB5,PSMB7,PSMB8,PSMC1,PSMD3,RPS27A,IKBKG
Cellular response to chemical stress	3.74E-05	G6PD,PGD,PSMA4,PSMB5,PSMB7,PSMB8,PSMC1,PSMD3,RPS27A,LRPPRC,PRDX3,TXN2
Host Interactions of HIV factors	4.32E-05	AP2M1,PSMA4,PSMB5,PSMB7,PSMB8,PSMC1,PSMD3,RPS27A,NUP58,AP1M2
Adaptive Immune System	4.52E-05	AP2M1,CLTC,HSPA5,ITGB1,PLCG1,PPP3CA,PSMA4,PSMB5,PSMB7,PSMB8,PSMC1,PSMD3,RPS27A,SRC,UBE3A,IKBKG,SEC22B,AP1M2,BCAP31,AHCYL1,KIF3A,FBXO7,ERAP1
Diseases of signal transduction by growth factor receptors and second messengers	4.73E-05	ADAM10,CLTC,CREB1,MSN,NCBP1,PEBP1,PLCG1,POLR2H,PSMA4,PSMB5,PSMB7,PSMB8,PSMC1,PSMD3,RPS27A,SRC,TPM3

Table 2A.3. Pathway analysis of all proteins found to be present in the co-IP of PTGFRN with 8C7 monoclonal antibody in A431 cells, continued

Regulation of activated PAK-2p34 by proteasome mediated degradation	5.04E-05	PSMA4,PSMB5,PSMB7,PSMB8,PSMC1,PSMD3,RPS27A
Vpu mediated degradation of CD4	5.91E-05	PSMA4,PSMB5,PSMB7,PSMB8,PSMC1,PSMD3,RPS27A
Autodegradation of the E3 ubiquitin ligase COP1	5.91E-05	PSMA4,PSMB5,PSMB7,PSMB8,PSMC1,PSMD3,RPS27A
Ubiquitin Mediated Degradation of Phosphorylated Cdc25A	5.91E-05	PSMA4,PSMB5,PSMB7,PSMB8,PSMC1,PSMD3,RPS27A
p53-Independent DNA Damage Response	5.91E-05	PSMA4,PSMB5,PSMB7,PSMB8,PSMC1,PSMD3,RPS27A
p53-Independent G1/S DNA damage checkpoint	5.91E-05	PSMA4,PSMB5,PSMB7,PSMB8,PSMC1,PSMD3,RPS27A
Ubiquitin-dependent degradation of Cyclin D	5.91E-05	PSMA4,PSMB5,PSMB7,PSMB8,PSMC1,PSMD3,RPS27A
GSK3B and BTRC:CUL1-mediated-degradation of NFE2L2	5.91E-05	PSMA4,PSMB5,PSMB7,PSMB8,PSMC1,PSMD3,RPS27A
Antigen processing-Cross presentation	5.98E-05	PSMA4,PSMB5,PSMB7,PSMB8,PSMC1,PSMD3,RPS27A,IKBKG,SEC22B
Regulation of Apoptosis	6.48E-05	PSMA4,PSMB5,PSMB7,PSMB8,PSMC1,PSMD3,RPS27A
KEAP1-NFE2L2 pathway	6.70E-05	G6PD,PGD,PSMA4,PSMB5,PSMB7,PSMB8,PSMC1,PSMD3,RPS27A

Table 2A.3. Pathway analysis of all proteins found to be present in the co-IP of PTGFRN with 8C7 monoclonal antibody in A431 cells, continued

Vif-mediated degradation of APOBEC3G	7.07E-05	PSMA4,PSMB5,PSMB7,PSMB8,PSMC1,PSMD3,RPS27A
FBXL7 down-regulates AURKA during mitotic entry and in early mitosis	7.07E-05	PSMA4,PSMB5,PSMB7,PSMB8,PSMC1,PSMD3,RPS27A
Negative regulation of NOTCH4 signaling	7.07E-05	PSMA4,PSMB5,PSMB7,PSMB8,PSMC1,PSMD3,RPS27A
SCF-beta-TrCP mediated degradation of Emi1	7.76E-05	PSMA4,PSMB5,PSMB7,PSMB8,PSMC1,PSMD3,RPS27A
Degradation of AXIN	7.76E-05	PSMA4,PSMB5,PSMB7,PSMB8,PSMC1,PSMD3,RPS27A
Apoptosis	7.87E-05	BAK1,PLEC,PSMA4,PSMB5,PSMB7,PSMB8,PSMC1,PSMD3,RPS27A,STK24,BCAP31
Intracellular signaling by second messengers	8.12E-05	CREB1,PLCG1,PRKAR2A,PSMA4,PSMB5,PSMB7,PSMB8,PSMC1,PSMD3,RHEB,RPS27A,SRC,AHCYL1,MBD3
Hh mutants are degraded by ERAD	8.58E-05	PSMA4,PSMB5,PSMB7,PSMB8,PSMC1,PSMD3,RPS27A
FCERI mediated NF-kB activation	8.79E-05	PSMA4,PSMB5,PSMB7,PSMB8,PSMC1,PSMD3,RPS27A,IKBKG
Signaling by NOTCH4	8.79E-05	ADAM10,PSMA4,PSMB5,PSMB7,PSMB8,PSMC1,PSMD3,RPS27A
Degradation of DVL	9.30E-05	PSMA4,PSMB5,PSMB7,PSMB8,PSMC1,PSMD3,RPS27A
Stabilization of p53	9.30E-05	PSMA4,PSMB5,PSMB7,PSMB8,PSMC1,PSMD3,RPS27A
Signaling by Hedgehog	1.03E-04	PRKAR2A,PSMA4,PSMB5,PSMB7,PSMB8,PSMC1,PSMD3,RPS27A,KIF3A,ADCY10
Interleukin-1 signaling	1.03E-04	IL1A,PSMA4,PSMB5,PSMB7,PSMB8,PSMC1,PSMD3,RPS27A,IKBKG
Hedgehog 'on' state	1.07E-04	PSMA4,PSMB5,PSMB7,PSMB8,PSMC1,PSMD3,RPS27A,KIF3A

Table 2A.3. Pathway analysis of all proteins found to be present in the co-IP of PTGFRN with 8C7 monoclonal antibody in A431 cells, continued

Signaling by Interleukins	1.08E-04	CREB1,CRK,IL1A,ITGB1,MSN,PSMA4,PSMB5,PSMB7,PSMB8,PSMC1,PSMD3,RPLP0,RPS27A,FSCN1,STAT6,HSP90B1,IKBKG
Hh mutants abrogate ligand secretion	1.08E-04	PSMA4,PSMB5,PSMB7,PSMB8,PSMC1,PSMD3,RPS27A
NIK-->noncanonical NF-kB signaling	1.08E-04	PSMA4,PSMB5,PSMB7,PSMB8,PSMC1,PSMD3,RPS27A
SCF(Skp2)-mediated degradation of p27/p21	1.17E-04	PSMA4,PSMB5,PSMB7,PSMB8,PSMC1,PSMD3,RPS27A
Dectin-1 mediated noncanonical NF-kB signaling	1.17E-04	PSMA4,PSMB5,PSMB7,PSMB8,PSMC1,PSMD3,RPS27A
Degradation of GLI1 by the proteasome	1.17E-04	PSMA4,PSMB5,PSMB7,PSMB8,PSMC1,PSMD3,RPS27A
Degradation of GLI2 by the proteasome	1.17E-04	PSMA4,PSMB5,PSMB7,PSMB8,PSMC1,PSMD3,RPS27A
GLI3 is processed to GLI3R by the proteasome	1.17E-04	PSMA4,PSMB5,PSMB7,PSMB8,PSMC1,PSMD3,RPS27A
Defective CFTR causes cystic fibrosis	1.28E-04	PSMA4,PSMB5,PSMB7,PSMB8,PSMC1,PSMD3,RPS27A
TCR signaling	1.32E-04	PLCG1,PSMA4,PSMB5,PSMB7,PSMB8,PSMC1,PSMD3,RPS27A,IKBKG
Synthesis of DNA	1.38E-04	FEN1,POLE,PSMA4,PSMB5,PSMB7,PSMB8,PSMC1,PSMD3,RPS27A
Autodegradation of Cdh1 by Cdh1:APC/C	1.69E-04	PSMA4,PSMB5,PSMB7,PSMB8,PSMC1,PSMD3,RPS27A
Hedgehog ligand biogenesis	1.86E-04	PSMA4,PSMB5,PSMB7,PSMB8,PSMC1,PSMD3,RPS27A

Table 2A.3. Pathway analysis of all proteins found to be present in the co-IP of PTGFRN with 8C7 monoclonal antibody in A431 cells, continued

Oxygen-dependent proline hydroxylation of Hypoxia-inducible Factor Alpha	2.03E-04	PSMA4,PSMB5,PSMB7,PSMB8,PSMC1,PSMD3,RPS27A
p53-Dependent G1 DNA Damage Response	2.03E-04	PSMA4,PSMB5,PSMB7,PSMB8,PSMC1,PSMD3,RPS27A
p53-Dependent G1/S DNA damage checkpoint	2.03E-04	PSMA4,PSMB5,PSMB7,PSMB8,PSMC1,PSMD3,RPS27A
Transcriptional regulation by RUNX3	2.25E-04	PSMA4,PSMB5,PSMB7,PSMB8,PSMC1,PSMD3,RPS27A,SRC
APC/C:Cdc20 mediated degradation of Securin	2.39E-04	PSMA4,PSMB5,PSMB7,PSMB8,PSMC1,PSMD3,RPS27A
Regulation of RAS by GAPs	2.39E-04	PSMA4,PSMB5,PSMB7,PSMB8,PSMC1,PSMD3,RPS27A
G1/S DNA Damage Checkpoints	2.39E-04	PSMA4,PSMB5,PSMB7,PSMB8,PSMC1,PSMD3,RPS27A
Downstream TCR signaling	2.55E-04	PSMA4,PSMB5,PSMB7,PSMB8,PSMC1,PSMD3,RPS27A,IKBKG
Regulation of PTEN stability and activity	2.61E-04	PSMA4,PSMB5,PSMB7,PSMB8,PSMC1,PSMD3,RPS27A
Orc1 removal from chromatin	3.12E-04	PSMA4,PSMB5,PSMB7,PSMB8,PSMC1,PSMD3,RPS27A
Proteasome	3.15E-04	PSMA4,PSMB5,PSMB7,PSMB8,PSMC1,PSMD3
UCH proteinases	3.28E-04	PSMA4,PSMB5,PSMB7,PSMB8,PSMC1,PSMD3,RPS27A,RUVBL1
ABC-family proteins mediated transport	3.49E-04	EIF2S3,PSMA4,PSMB5,PSMB7,PSMB8,PSMC1,PSMD3,RPS27A
Cdc20:Phospho-APC/C mediated degradation of Cyclin A	3.57E-04	PSMA4,PSMB5,PSMB7,PSMB8,PSMC1,PSMD3,RPS27A

Table 2A.3. Pathway analysis of all proteins found to be present in the co-IP of PTGFRN with 8C7 monoclonal antibody in A431 cells, continued

CDK-mediated phosphorylation and removal of Cdc6	3.57E-04	PSMA4,PSMB5,PSMB7,PSMB8,PSMC1,PSMD3,RPS27A
Regulation of RUNX2 expression and activity	3.57E-04	PSMA4,PSMB5,PSMB7,PSMB8,PSMC1,PSMD3,RPS27A
Amyotrophic lateral sclerosis	3.65E-04	ATP5F1D,HSPA5,NCBP1,NDUFS3,PPP3CA,PSMA4,PSMB5,PSMB7,PSMC1,PSMD3,SRSF3,MATR3,NUP58,UBQLN1
APC/C:Cdh1 mediated degradation of Cdc20 and other APC/C:Cdh1 targeted proteins in late mitosis/early G1	3.80E-04	PSMA4,PSMB5,PSMB7,PSMB8,PSMC1,PSMD3,RPS27A
APC:Cdc20 mediated degradation of cell cycle proteins prior to satisfation of the cell cycle checkpoint	3.80E-04	PSMA4,PSMB5,PSMB7,PSMB8,PSMC1,PSMD3,RPS27A
PTEN Regulation	3.80E-04	PSMA4,PSMB5,PSMB7,PSMB8,PSMC1,PSMD3,RHEB,RPS27A,MBD3
Cellular response to hypoxia	4.09E-04	PSMA4,PSMB5,PSMB7,PSMB8,PSMC1,PSMD3,RPS27A
Cross-presentation of soluble exogenous antigens (endosomes)	4.20E-04	PSMA4,PSMB5,PSMB7,PSMB8,PSMC1,PSMD3
APC/C:Cdc20 mediated degradation of mitotic proteins	4.40E-04	PSMA4,PSMB5,PSMB7,PSMB8,PSMC1,PSMD3,RPS27A
Prion disease	4.55E-04	ATP5F1D,CREB1,HSPA5,IL1A,LAMC1,NDUFS3,PPP3CA,PSMA4,PSMB5,PSMB7,PSMC1,PSMD3

Table 2A.3. Pathway analysis of all proteins found to be present in the co-IP of PTGFRN with 8C7 monoclonal antibody in A431 cells, continued

Activation of APC/C and APC/C:Cdc20 mediated degradation of mitotic proteins	4.63E-04	PSMA4,PSMB5,PSMB7,PSMB8,PSMC1,PSMD3,RPS27A
The role of GTSE1 in G2/M progression after G2 checkpoint	4.63E-04	PSMA4,PSMB5,PSMB7,PSMB8,PSMC1,PSMD3,RPS27A
ABC transporter disorders	4.98E-04	PSMA4,PSMB5,PSMB7,PSMB8,PSMC1,PSMD3,RPS27A
Regulation of ornithine decarboxylase (ODC)	4.98E-04	PSMA4,PSMB5,PSMB7,PSMB8,PSMC1,PSMD3
Class I MHC mediated antigen processing & presentation	5.50E-04	HSPA5,PSMA4,PSMB5,PSMB7,PSMB8,PSMC1,PSMD3,RPS27A,UBE3A,IKBKG,SEC22B,BCAP31,FBXO7,ERAP1
Regulation of APC/C activators between G1/S and early anaphase	6.25E-04	PSMA4,PSMB5,PSMB7,PSMB8,PSMC1,PSMD3,RPS27A
Interleukin-1 family signaling	6.99E-04	IL1A,PSMA4,PSMB5,PSMB7,PSMB8,PSMC1,PSMD3,RPS27A,IKBKG
Degradation of beta-catenin by the destruction complex	7.10E-04	PSMA4,PSMB5,PSMB7,PSMB8,PSMC1,PSMD3,RPS27A
Cyclin E associated events during G1/S transition	7.10E-04	PSMA4,PSMB5,PSMB7,PSMB8,PSMC1,PSMD3,RPS27A
Cyclin A:Cdk2-associated events at S phase entry	8.24E-04	PSMA4,PSMB5,PSMB7,PSMB8,PSMC1,PSMD3,RPS27A
Transcriptional regulation by RUNX2	9.29E-04	PSMA4,PSMB5,PSMB7,PSMB8,PSMC1,PSMD3,RPS27A,SRC

Table 2A.3. Pathway analysis of all proteins found to be present in the co-IP of PTGFRN with 8C7 monoclonal antibody in A431 cells, continued

APC/C-mediated degradation of cell cycle proteins	9.99E-04	PSMA4,PSMB5,PSMB7,PSMB8,PSMC1,PSMD3,RPS27A
Regulation of mitotic cell cycle	9.99E-04	PSMA4,PSMB5,PSMB7,PSMB8,PSMC1,PSMD3,RPS27A
Metabolism of polyamines	1.06E-03	PSMA4,PSMB5,PSMB7,PSMB8,PSMC1,PSMD3
MAPK6/MAPK4 signaling	1.07E-03	PSMA4,PSMB5,PSMB7,PSMB8,PSMC1,PSMD3,RPS27A
S Phase	1.07E-03	FEN1,POLE,PSMA4,PSMB5,PSMB7,PSMB8,PSMC1,PSMD3,RPS27A
Huntington disease	1.22E-03	ATP5F1D,AP2M1,CLTC,CREB1,NDUFS3,POLR2H,PSMA4,PSMB5,PSMB7,PSMC1,PSMD3,TGM2
PA700-20S-PA28 complex	1.22E-03	PSMA4,PSMB5,PSMB7,PSMC1,PSMD3
Switching of origins to a post-replicative state	1.28E-03	PSMA4,PSMB5,PSMB7,PSMB8,PSMC1,PSMD3,RPS27A
Proteasome degradation	1.33E-03	PSMA4,PSMB5,PSMB7,PSMB8,PSMC1,PSMD3
G1/S Transition	1.49E-03	POLE,PSMA4,PSMB5,PSMB7,PSMB8,PSMC1,PSMD3,RPS27A
Parkinson disease	1.59E-03	ATP5F1D,HSPA5,NDUFS3,PLCG1,PSMA4,PSMB5,PSMB7,PSMC1,PSMD3,RPS27A,TXN2
PIP3 activates AKT signaling	1.64E-03	CREB1,PSMA4,PSMB5,PSMB7,PSMB8,PSMC1,PSMD3,RHEB,RPS27A,SRC,MBD3
TNFR2 non-canonical NF-kB pathway	2.24E-03	PSMA4,PSMB5,PSMB7,PSMB8,PSMC1,PSMD3,RPS27A
Signaling by WNT	2.31E-03	AP2M1,CLTC,PPP3CA,PSMA4,PSMB5,PSMB7,PSMB8,PSMC1,PSMD3,RPS27A,RUVBL1,SCRIB
protein catabolic process	2.53E-03	ADAM10,GUSB,HSPA5,PSMA4,PSMB5,PSMB7,PSMB8,PSMC1,PSMD3,RAD23A,RAD23B,RPS27A,HSP90B1,UBE3A,PDCD6IP,MAEA,FBXO7,UBQLN1,PCSK9
DNA Replication	2.64E-03	FEN1,POLE,PSMA4,PSMB5,PSMB7,PSMB8,PSMC1,PSMD3,RPS27A
26S proteasome	2.66E-03	PSMA4,PSMB5,PSMB7,PSMC1
Mitotic Anaphase	2.82E-03	PPP2R2A,PSMA4,PSMB5,PSMB7,PSMB8,PSMC1,PSMD3,RPS27A,NUP58,NUDC

Table 2A.3. Pathway analysis of all proteins found to be present in the co-IP of PTGFRN with 8C7 monoclonal antibody in A431 cells, continued

Mitotic Metaphase and Anaphase	2.91E-03	PPP2R2A,PSMA4,PSMB5,PSMB7,PSMB8,PSMC1, PSMD3,RPS27A,NUP58,NUDC
proteasome-mediated ubiquitin-dependent protein catabolic process	2.91E-03	HSPA5,PSMA4,PSMB5,PSMB7,PSMC1,PSMD3,RAD23A,RAD23B,HSP90B1,MAEA,FBXO7,UBQLN1
Deubiquitination	3.83E-03	PSMA4,PSMB5,PSMB7,PSMB8,PSMC1,PSMD3,RAD23A,RAD23B,RPS27A,IKBKG,RUVBL1
Pathways of neurodegeneration - multiple diseases	4.36E-03	ATP5F1D,BAK1,CAPN1,HSPA5,IL1A,NDUFS3,PLCG1,PPP3CA,PSMA4,PSMB5,PSMB7,PSMC1,PSMD3,RPS27A
DNA Replication Pre-Initiation	4.76E-03	POLE,PSMA4,PSMB5,PSMB7,PSMB8,PSMC1,PSMD3,RPS27A
proteasomal protein catabolic process	5.89E-03	HSPA5,PSMA4,PSMB5,PSMB7,PSMC1,PSMD3,RAD23A,RAD23B,HSP90B1,MAEA,FBXO7,UBQLN1
Cell Cycle	6.14E-03	CDK6,FEN1,POLE,POLR2H,PPP2R2A,PSMA4,PSMB5,PSMB7,PSMB8,PSMC1,PSMD3,RPS27A,SRC,RUVBL1,NUP58,SMC4,NUDC
Cell Cycle, Mitotic	6.33E-03	CDK6,FEN1,POLE,PPP2R2A,PSMA4,PSMB5,PSMB7,PSMB8,PSMC1,PSMD3,RPS27A,SRC,NUP58,SMC4,NUDC
Ub-specific processing proteases	7.50E-03	PSMA4,PSMB5,PSMB7,PSMB8,PSMC1,PSMD3,RPS27A,IKBKG,RUVBL1
Alzheimer disease	7.50E-03	ADAM10,ATP5F1D,CAPN1,IL1A,NDUFS3,PPP3CA,PSMA4,PSMB5,PSMB7,PSMC1,PSMD3,IKBKG
RUNX1 regulates transcription of genes involved in differentiation of HSCs	7.65E-03	PSMA4,PSMB5,PSMB7,PSMB8,PSMC1,PSMD3,RPS27A
Disorders of transmembrane transporters	8.44E-03	PSMA4,PSMB5,PSMB7,PSMB8,PSMC1,PSMD3,RPS27A,NUP58
proteolysis involved in protein catabolic process	8.86E-03	HSPA5,PSMA4,PSMB5,PSMB7,PSMB8,PSMC1,PSMD3,RAD23A,RAD23B,RPS27A,HSP90B1,UBE3A,PDCD6IP,MAEA,FBXO7,UBQLN1

Table 2A.3. Pathway analysis of all proteins found to be present in the co-IP of PTGFRN with 8C7 monoclonal antibody in A431 cells, continued

RAF/MAP kinase cascade	9.00E-03	PEBP1,PSMA4,PSMB5,PSMB7,PSMB8,PSMC1,PSMD3,RGL2,RPS27A,SRC
MAPK1/MAPK3 signaling	1.03E-02	PEBP1,PSMA4,PSMB5,PSMB7,PSMB8,PSMC1,PSMD3,RGL2,RPS27A,SRC
Signaling by NOTCH	1.09E-02	ADAM10,CREB1,PSMA4,PSMB5,PSMB7,PSMB8,PSMC1,PSMD3,RPS27A
Transcriptional regulation by RUNX1	1.15E-02	CDK6,PSMA4,PSMB5,PSMB7,PSMB8,PSMC1,PSMD3,RPS27A,SRC
20S proteasome	1.18E-02	PSMA4,PSMB5,PSMB7
Assembly of the pre-replicative complex	1.22E-02	PSMA4,PSMB5,PSMB7,PSMB8,PSMC1,PSMD3,RPS27A
Separation of Sister Chromatids	1.31E-02	PSMA4,PSMB5,PSMB7,PSMB8,PSMC1,PSMD3,RPS27A,NUDC
Neddylation	1.40E-02	PSMA4,PSMB5,PSMB7,PSMB8,PSMC1,PSMD3,RPS27A,FBXO7,DCAF8
PA28gamma-20S proteasome	1.41E-02	PSMA4,PSMB5,PSMB7
G2/M Transition	1.49E-02	PPP2R2A,PSMA4,PSMB5,PSMB7,PSMB8,PSMC1,PSMD3,RPS27A
Mitotic G2-G2/M phases	1.57E-02	PPP2R2A,PSMA4,PSMB5,PSMB7,PSMB8,PSMC1,PSMD3,RPS27A
PA28-20S proteasome	1.65E-02	PSMA4,PSMB5,PSMB7
Alzheimer's disease	2.13E-02	ADAM10,CAPN1,IL1A,PPP3CA,PSMA4,PSMB5,PSMB7,PSMC1,PSMD3
MAPK family signaling cascades	2.31E-02	PEBP1,PSMA4,PSMB5,PSMB7,PSMB8,PSMC1,PSMD3,RGL2,RPS27A,SRC
Transport of small molecules	2.39E-02	AP2M1,CLTC,EIF2S3,PRKAR2A,PSMA4,PSMB5,PSMB7,PSMB8,PSMC1,PSMD3,RPS27A,AKAP1,GLRX3,LSR,SLC44A2,PCSK9
modification-dependent protein catabolic process	2.41E-02	HSPA5,PSMA4,PSMB5,PSMB7,PSMC1,PSMD3,RAD23A,RAD23B,RPS27A,HSP90B1,UBE3A,MAEA,FBXO7,UBQLN1
G2/M Checkpoints	2.64E-02	PSMA4,PSMB5,PSMB7,PSMB8,PSMC1,PSMD3,RPS27A
modification-dependent macromolecule catabolic process	2.81E-02	HSPA5,PSMA4,PSMB5,PSMB7,PSMC1,PSMD3,RAD23A,RAD23B,RPS27A,HSP90B1,UBE3A,MAEA,FBXO7,UBQLN1

Table 2A.3. Pathway analysis of all proteins found to be present in the co-IP of PTGFRN with 8C7 monoclonal antibody in A431 cells, continued

TCF dependent signaling in response to WNT	3.62E-02	PSMA4,PSMB5,PSMB7,PSMB8,PSMC1,PSMD3,RPS27A,RUVBL1
M Phase	3.83E-02	PPP2R2A,PSMA4,PSMB5,PSMB7,PSMB8,PSMC1,PSMD3,RPS27A,NUP58,SMC4,NUDC
Antigen processing: Ubiquitination & Proteasome degradation	5.23E-02	PSMA4,PSMB5,PSMB7,PSMB8,PSMC1,PSMD3,RPS27A,UBE3A,FBXO7
ubiquitin-dependent protein catabolic process	5.23E-02	HSPA5,PSMA4,PSMB5,PSMB7,PSMC1,PSMD3,RAD23A,RAD23B,HSP90B1,UBE3A,MAEA,FBXO7,UBQLN1
Alzheimer's disease and miRNA effects	7.29E-02	ADAM10,CAPN1,IL1A,PPP3CA,PSMA4,PSMB5,PSMB7,PSMC1,PSMD3
Cell Cycle Checkpoints	1.14E-01	PSMA4,PSMB5,PSMB7,PSMB8,PSMC1,PSMD3,RPS27A,NUDC
Spinocerebellar ataxia	2.06E-01	PSMA4,PSMB5,PSMB7,PSMC1,PSMD3
actin filament organization	2.76E-06	ALDOA,DIAPH1,MYO5A,MYO6,PLEC,FSCN1,SRC,TPM3,HSP90B1,EZR,TAGLN2,CORO1C,CORO1B,INF2,CORO7
actin cytoskeleton organization	4.42E-05	ALDOA,CRK,DIAPH1,ITGB1,MYO5A,MYO6,PLEC,FSCN1,SRC,TPM3,HSP90B1,EZR,TAGLN2,ARHGEF10,PDCD6IP,CORO1C,CORO1B,INF2,CORO7
actin filament-based process	4.94E-05	ALDOA,CRK,DIAPH1,ITGB1,MYL6,MYO5A,MYO6,PLEC,FSCN1,SRC,TPM3,HSP90B1,EZR,TAGLN2,ARHGEF10,PDCD6IP,CORO1C,CORO1B,INF2,CORO7
positive regulation of lamellipodium organization	1.35E-03	FSCN1,SRC,CYFIP1,CORO1C,CORO1B
positive regulation of lamellipodium morphogenesis	1.82E-03	SRC,CORO1C,CORO1B
supramolecular fiber organization	2.47E-03	ALDOA,DIAPH1,ITGB1,MYO5A,MYO6,PLEC,FSCN1,SRC,TPM3,HSP90B1,EZR,TAGLN2,CORO1C,CORO1B,INF2,CORO7

Table 2A.3. Pathway analysis of all proteins found to be present in the co-IP of PTGFRN with 8C7 monoclonal antibody in A431 cells, continued

regulation of lamellipodium organization	6.44E-03	FSCN1,SRC,CYFIP1,CORO1C,CORO1B
regulation of lamellipodium morphogenesis	6.47E-03	SRC,CORO1C,CORO1B
actin filament bundle assembly	7.90E-03	FSCN1,SRC,HSP90B1,EZR,CORO1B
actin filament bundle organization	1.02E-02	FSCN1,SRC,HSP90B1,EZR,CORO1B
mRNA metabolic process	3.12E-06	CLNS1A,CREB1,GSPT1,HNRNPU,NCBP1,UPF1,SRSF3,SNRPB2,SNRPE,PRPF4,SYNCRIP,AHCYL1,NUDT21,CNOT1,PABPC1,GPKOW,TRA2A,DDX41,RBM28,RBM25,THOC3,EXOSC6,TRUB1
Spliceosome	1.12E-05	NCBP1,SRSF3,SNRPB2,SNRPE,PRPF4,IGF2BP3,NUDT21,PABPC1,DDX41,RBM25,THOC3
Processing of Capped Intron-Containing Pre-mRNA	4.24E-05	HNRNPU,NCBP1,POLR2H,SRSF3,SNRPB2,SNRPE,PRPF4,NUP58,CHERP,NUDT21,GPKOW,DDX41,RBM25,THOC3
mRNA processing	5.07E-05	CLNS1A,HNRNPU,NCBP1,SRSF3,SNRPB2,SNRPE,PRPF4,SYNCRIP,AHCYL1,NUDT21,PABPC1,GPKOW,TRA2A,DDX41,RBM28,RBM25,THOC3,TRUB1
Spliceosome	1.35E-04	HNRNPU,NCBP1,SRSF3,SNRPB2,SNRPE,PRPF4,CHERP,TRA2A,RBM25,THOC3
mRNA Splicing - Major Pathway	2.28E-04	HNRNPU,NCBP1,POLR2H,SRSF3,SNRPB2,SNRPE,PRPF4,CHERP,GPKOW,DDX41,RBM25
RNA splicing	2.93E-04	CLNS1A,HNRNPU,NCBP1,SRSF3,SNRPB2,SNRPE,PRPF4,SYNCRIP,PABPC1,GPKOW,TRA2A,DDX41,RBM28,RBM25,THOC3
mRNA Splicing	3.12E-04	HNRNPU,NCBP1,POLR2H,SRSF3,SNRPB2,SNRPE,PRPF4,CHERP,GPKOW,DDX41,RBM25
regulation of mRNA processing	3.65E-04	CLNS1A,HNRNPU,NCBP1,NCL,SRSF3,AHCYL1,NUDT21,TRA2A,RBM25
RNA splicing, via transesterification reactions with bulged adenosine as nucleophile	4.46E-04	CLNS1A,HNRNPU,NCBP1,SRSF3,SNRPB2,SNRPE,PRPF4,SYNCRIP,PABPC1,GPKOW,TRA2A,DDX41

Table 2A.3. Pathway analysis of all proteins found to be present in the co-IP of PTGFRN with 8C7 monoclonal antibody in A431 cells, continued

mRNA splicing, via spliceosome	4.46E-04	CLNS1A,HNRNPU,NCBP1,SRSF3,SNRPB2,SNRPE,PRPF4,SYNCRIP,PABPC1,GPKOW,TRA2A,DDX41
RNA splicing, via transesterification reactions	4.98E-04	CLNS1A,HNRNPU,NCBP1,SRSF3,SNRPB2,SNRPE,PRPF4,SYNCRIP,PABPC1,GPKOW,TRA2A,DDX41
positive regulation of mRNA processing	2.09E-03	CLNS1A,NCBP1,NCL,NUDT21,TRA2A
regulation of mRNA splicing, via spliceosome	3.02E-03	CLNS1A,HNRNPU,NCBP1,NCL,SRSF3,TRA2A,RBM25
mRNA processing	6.86E-03	HNRNPU,NCBP1,SRSF3,SNRPB2,SNRPE,PRPF4,NUDT21
positive regulation of mRNA metabolic process	8.93E-03	CLNS1A,NCBP1,NCL,UPF1,NUDT21,CNOT1,PABPC1,TRA2A
positive regulation of mRNA splicing, via spliceosome	9.21E-03	CLNS1A,NCBP1,NCL,TRA2A
regulation of RNA splicing	1.03E-02	CLNS1A,HNRNPU,NCBP1,NCL,SRSF3,TRA2A,RBM25,AHNAK
positive regulation of RNA splicing	2.83E-02	CLNS1A,NCBP1,NCL,TRA2A
Protein processing in endoplasmic reticulum	8.79E-06	BAK1,CAPN1,HSPA5,LMAN1,RAD23A,RAD23B,HSP90B1,BAG2,PREB,BCAP31,HSPBP1,UBQLN1
positive regulation of protein catabolic process	2.77E-04	MSN,PSMC1,RAD23A,SUMO2,EZR,BAG2,SEC22B,BCAP31,HSPBP1,UBQLN1,PCSK9
regulation of protein catabolic process	1.37E-03	MSN,PSMC1,PSMD3,RAD23A,RAD23B,SUMO2,EZR,BAG2,SEC22B,BCAP31,HSPBP1,UBQLN1,PCSK9

Table 2A.3. Pathway analysis of all proteins found to be present in the co-IP of PTGFRN with 8C7 monoclonal antibody in A431 cells, continued

regulation of proteolysis involved in protein catabolic process	2.45E-03	PSMC1,RAD23A,RAD23B,SUMO2,UBE3A,RPL23,BAG2,BCAP31,HSPBP1,UBQLN1
positive regulation of catabolic process	2.47E-03	MSN,PSMC1,RAD23A,UPF1,SUMO2,EZR,IKBKG,BAG2,SEC22B,BCAP31,CNOT1,HSPBP1,FBXO7,PABPC1,UBQLN1,PCSK9
positive regulation of proteasomal protein catabolic process	4.85E-03	PSMC1,RAD23A,SUMO2,BAG2,BCAP31,HSPBP1,UBQLN1
regulation of ubiquitin-dependent protein catabolic process	7.65E-03	RAD23A,RAD23B,SUMO2,UBE3A,RPL23,BCAP31,HSPBP1,UBQLN1
positive regulation of proteolysis involved in protein catabolic process	1.03E-02	PSMC1,RAD23A,SUMO2,BAG2,BCAP31,HSPBP1,UBQLN1
regulation of proteasomal protein catabolic process	1.46E-02	PSMC1,RAD23A,RAD23B,SUMO2,BAG2,BCAP31,HSPBP1,UBQLN1
regulation of proteolysis	2.16E-02	SERPINC1,BAK1,MMP14,PEBP1,PSMB8,PSMC1,RAD23A,RAD23B,SUMO2,SRC,UBE3A,RPL23,BAG2,BCAP31,HSPBP1,UBQLN1
positive regulation of proteolysis	4.57E-02	BAK1,MMP14,PSMC1,RAD23A,SUMO2,SRC,BAG2,BCAP31,HSPBP1,UBQLN1
positive regulation of proteasomal ubiquitin-dependent protein catabolic process	4.84E-02	RAD23A,SUMO2,BCAP31,HSPBP1,UBQLN1

Table 2A.3. Pathway analysis of all proteins found to be present in the co-IP of PTGFRN with 8C7 monoclonal antibody in A431 cells, continued

regulation of proteasomal ubiquitin-dependent protein catabolic process	5.18E-02	RAD23A,RAD23B,SUMO2,BCAP31,HSPBP1,UBQLN1
positive regulation of ubiquitin-dependent protein catabolic process	8.61E-02	RAD23A,SUMO2,BCAP31,HSPBP1,UBQLN1
RHO GTPase cycle	1.74E-05	ALDH3A2,CCT6A,CLTC,DIAPH1,NIPSNAP2,ITGB1,LMAN1,MYO6,NDUFS3,SRC,TPM3,ARHGAP29,ARHGEF10,BCAP31,NUDC,CYFIP1,SCRIB,LRRC1
Signaling by Rho GTPases	3.42E-04	ALDH3A2,CCT6A,CLTC,DIAPH1,NIPSNAP2,ITGB1,LMAN1,MYL6,MYO6,NDUFS3,SRC,TPM3,ARHGAP29,ARHGEF10,BCAP31,NUDC,CYFIP1,SCRIB,TAX1BP3,LRRC1
Signaling by Rho GTPases, Miro GTPases and RHOBTB3	4.40E-04	ALDH3A2,CCT6A,CLTC,DIAPH1,NIPSNAP2,ITGB1,LMAN1,MYL6,MYO6,NDUFS3,SRC,TPM3,ARHGAP29,ARHGEF10,BCAP31,NUDC,CYFIP1,SCRIB,TAX1BP3,LRRC1
RHOA GTPase cycle	2.25E-01	DIAPH1,LMAN1,ARHGAP29,ARHGEF10,BCAP31
Fragile X syndrome	2.52E-05	ALDH3A2,AP2M1,CLTC,CREB1,EIF4G1,PLCG1,PPP3CA,RHEB,SRC,CYFIP1
FCGR3A-mediated IL10 synthesis	1.88E-03	CREB1,PLCG1,PRKAR2A,SRC,AHCYL1
Signaling by EGFR	4.75E-03	AAMP,ADAM10,PLCG1,RPS27A,SRC
Downstream signal transduction	6.86E-03	CRK,PLCG1,SRC,STAT6
Signaling by NTRK1 (TRKA)	2.20E-02	AP2M1,CLTC,CREB1,CRK,PLCG1,SRC
DAG and IP3 signaling	2.32E-02	CREB1,PLCG1,PRKAR2A,AHCYL1

Table 2A.3. Pathway analysis of all proteins found to be present in the co-IP of PTGFRN with 8C7 monoclonal antibody in A431 cells, continued

Anti-inflammatory response favouring Leishmania parasite infection	2.63E-02	CREB1,PLCG1,PRKAR2A,SRC,AHCYL1
Leishmania parasite growth and survival	2.63E-02	CREB1,PLCG1,PRKAR2A,SRC,AHCYL1
VEGFR2 mediated cell proliferation	3.21E-02	PLCG1,SRC,AHCYL1
Signaling by ERBB2	3.66E-02	DIAPH1,PLCG1,RPS27A,SRC
Signaling by NTRKs	4.24E-02	AP2M1,CLTC,CREB1,CRK,PLCG1,SRC
T-cell receptor signaling pathway	4.30E-02	CREB1,CRK,IL1A,PLCG1,IKBKG
B cell receptor signaling pathway	5.54E-02	CREB1,CRK,ILF2,PLCG1,IKBKG
Signaling by PDGF	5.78E-02	CRK,PLCG1,SRC,STAT6
Follicle stimulating hormone (FSH) signaling pathway	5.86E-02	CREB1,RHEB,SRC
Human immunodeficiency virus 1 infection	8.07E-02	BAK1,CRK,PLCG1,PPP3CA,IKBKG,APOBEC3B,AP1M2
PID AR NONGENOMIC PATHWAY	8.09E-02	CREB1,PLCG1,SRC
EGF/EGFR signaling pathway	9.00E-02	AP2M1,CREB1,CRK,PEBP1,PLCG1,SRC
FCERI mediated Ca+2 mobilization	9.15E-02	PLCG1,PPP3CA,AHCYL1

Table 2A.3. Pathway analysis of all proteins found to be present in the co-IP of PTGFRN with 8C7 monoclonal antibody in A431 cells, continued

BDNF-TrkB signaling	9.15E-02	CREB1,PLCG1,RHEB
Epithelial cell signaling in Helicobacter pylori infection	9.81E-02	ADAM10,PLCG1,SRC,IKBKG
PID EPHA FWDPATHWAY	9.81E-02	CRK,PLCG1,SRC
PID PI3K PLC TRK PATHWAY	1.11E-01	CREB1,PLCG1,SRC
Leptin signaling pathway	1.24E-01	CREB1,PLCG1,SRC,IKBKG
Signaling by FGFR3	1.42E-01	PLCG1,RPS27A,SRC
Signaling by FGFR4	1.49E-01	PLCG1,RPS27A,SRC
Brain-derived neurotrophic factor (BDNF) signaling pathway	2.11E-01	CREB1,PLCG1,SRC,IKBKG,CYFIP1
Opioid Signalling	2.13E-01	CREB1,PPP3CA,PRKAR2A,AHCYL1
Th1 and Th2 cell differentiation	2.13E-01	PLCG1,PPP3CA,STAT6,IKBKG
Netrin-1 signaling	2.34E-01	PLCG1,SRC,EZR
Signaling by FGFR1	2.34E-01	PLCG1,RPS27A,SRC
PLC beta mediated events	2.45E-01	CREB1,PRKAR2A,AHCYL1
PID PTP1B PATHWAY	2.55E-01	CAPN1,CRK,SRC
Lipid and atherosclerosis	2.62E-01	HSPA5,PLCG1,PPP3CA,SRC,HSP90B1,IKBKG
mRNA transport	3.34E-05	NCBP1,UPF1,SRSF3,NUP58,G3BP2,LRPPRC,NUTF2,IGF2BP3,IGF2BP2,THOC3
RNA localization	6.21E-05	HNRNPU,NCBP1,UPF1,SRSF3,NUP58,G3BP2,LRPPRC,NUTF2,IGF2BP3,IGF2BP2,THOC3
nucleic acid transport	1.25E-04	NCBP1,UPF1,SRSF3,NUP58,G3BP2,LRPPRC,NUTF2,IGF2BP3,IGF2BP2,THOC3

Table 2A.3. Pathway analysis of all proteins found to be present in the co-IP of PTGFRN with 8C7 monoclonal antibody in A431 cells, continued

RNA transport	1.25E-04	NCBP1,UPF1,SRSF3,NUP58,G3BP2,LRPPRC,NUTF2,IGF2BP3,IGF2BP2,THOC3
establishment of RNA localization	1.35E-04	NCBP1,UPF1,SRSF3,NUP58,G3BP2,LRPPRC,NUTF2,IGF2BP3,IGF2BP2,THOC3
nucleobase-containing compound transport	1.32E-03	NCBP1,UPF1,SRSF3,NUP58,G3BP2,LRPPRC,NUTF2,IGF2BP3,IGF2BP2,THOC3
nucleocytoplasmic transport	3.89E-03	NCBP1,PPP3CA,UPF1,RPS15,SRSF3,RPL23,NUP58,NUTF2,AHCYL1,THOC3
nuclear transport	3.89E-03	NCBP1,PPP3CA,UPF1,RPS15,SRSF3,RPL23,NUP58,NUTF2,AHCYL1,THOC3
nuclear export	8.53E-03	NCBP1,UPF1,RPS15,SRSF3,NUTF2,AHCYL1,THOC3
RNA Polymerase II Transcription Termination	1.50E-02	NCBP1,SRSF3,SNRPE,NUDT21,THOC3
mRNA 3'-end processing	6.02E-02	NCBP1,SRSF3,NUDT21,THOC3
mRNA export from nucleus	8.09E-02	NCBP1,UPF1,SRSF3,THOC3
Nucleocytoplasmic transport	8.09E-02	NCBP1,UPF1,SUMO2,NUP58,THOC3
Transport of Mature mRNA derived from an Intron-Containing Transcript	1.19E-01	NCBP1,SRSF3,NUP58,THOC3
RNA export from nucleus	1.58E-01	NCBP1,UPF1,SRSF3,THOC3
Transport of Mature Transcript to Cytoplasm	1.64E-01	NCBP1,SRSF3,NUP58,THOC3
nucleobase-containing small molecule metabolic process	6.21E-05	ACAT1,ADK,ALDOA,ATP5F1D,CTPS1,DLST,DTYMK,G6PD,GARS1,GMDS,HPRT1,MDH2,NDUFS3,PGD,APOBEC3B,RAB23,CMPK1,ADCY10,FAR1
nucleotide metabolic process	1.18E-04	ACAT1,ADK,ALDOA,ATP5F1D,CTPS1,DLST,DTYMK,G6PD,GARS1,HPRT1,MDH2,NDUFS3,PGD,RAB23,CMPK1,ADCY10,FAR1
nucleoside phosphate metabolic process	1.43E-04	ACAT1,ADK,ALDOA,ATP5F1D,CTPS1,DLST,DTYMK,G6PD,GARS1,HPRT1,MDH2,NDUFS3,PGD,RAB23,CMPK1,ADCY10,FAR1

Table 2A.3. Pathway analysis of all proteins found to be present in the co-IP of PTGFRN with 8C7 monoclonal antibody in A431 cells, continued

organophosphate biosynthetic process	4.55E-04	ACAT1,ADK,ALDOA,ATP5F1D,CTPS1,DTYMK,G6PD,GARS1,HEXB,HPRT1,NDUFS3,SORD,HDHD5,CMPK1,ADCY10,SLC44A2,FAR1
ribose phosphate biosynthetic process	1.46E-03	ACAT1,ADK,ALDOA,ATP5F1D,CTPS1,G6PD,HPRT1,NDUFS3,CMPK1,ADCY10
nucleotide biosynthetic process	1.48E-03	ACAT1,ADK,ALDOA,ATP5F1D,CTPS1,DTYMK,GARS1,HPRT1,NDUFS3,CMPK1,ADCY10
ribose phosphate metabolic process	1.56E-03	ACAT1,ADK,ALDOA,ATP5F1D,CTPS1,DLST,G6PD,HPRT1,NDUFS3,RAB23,CMPK1,ADCY10,FAR1
nucleoside phosphate biosynthetic process	1.57E-03	ACAT1,ADK,ALDOA,ATP5F1D,CTPS1,DTYMK,GARS1,HPRT1,NDUFS3,CMPK1,ADCY10
ribonucleotide metabolic process	4.55E-03	ACAT1,ADK,ALDOA,ATP5F1D,CTPS1,DLST,HPRT1,NDUFS3,RAB23,CMPK1,ADCY10,FAR1
purine nucleotide metabolic process	4.75E-03	ACAT1,ADK,ALDOA,ATP5F1D,DLST,G6PD,HPRT1,MDH2,NDUFS3,PGD,RAB23,ADCY10,FAR1
ribonucleotide biosynthetic process	5.26E-03	ACAT1,ADK,ALDOA,ATP5F1D,CTPS1,HPRT1,NDUFS3,CMPK1,ADCY10
purine-containing compound metabolic process	8.23E-03	ACAT1,ADK,ALDOA,ATP5F1D,DLST,G6PD,HPRT1,MDH2,NDUFS3,PGD,RAB23,ADCY10,FAR1
nucleoside triphosphate biosynthetic process	2.14E-02	ADK,ALDOA,ATP5F1D,CTPS1,DTYMK,NDUFS3
carbohydrate derivative biosynthetic process	2.64E-02	ACAT1,ADK,ALDOA,ATP5F1D,CTPS1,DTYMK,G6PD,GMDS,HPRT1,NDUFS3,SORD,LCMT2,CMPK1,ADCY10
nucleoside triphosphate metabolic process	2.64E-02	ADK,ALDOA,ATP5F1D,CTPS1,DTYMK,NDUFS3,RAB23
purine ribonucleotide metabolic process	3.09E-02	ACAT1,ADK,ALDOA,ATP5F1D,DLST,HPRT1,NDUFS3,RAB23,ADCY10,FAR1
purine ribonucleotide biosynthetic process	5.32E-02	ACAT1,ADK,ALDOA,ATP5F1D,HPRT1,NDUFS3,ADCY10

Table 2A.3. Pathway analysis of all proteins found to be present in the co-IP of PTGFRN with 8C7 monoclonal antibody in A431 cells, continued

purine nucleotide biosynthetic process	1.10E-01	ACAT1,ADK,ALDOA,ATP5F1D,HPRT1,NDUFS3, ADCY10
purine-containing compound biosynthetic process	1.30E-01	ACAT1,ADK,ALDOA,ATP5F1D,HPRT1,NDUFS3, ADCY10
purine nucleoside triphosphate metabolic process	2.30E-01	ADK,ALDOA,ATP5F1D,NDUFS3,RAB23
ribonucleoside triphosphate metabolic process	2.41E-01	ALDOA,ATP5F1D,CTPS1,NDUFS3,RAB23
purine nucleoside triphosphate biosynthetic process	2.55E-01	ADK,ALDOA,ATP5F1D,NDUFS3
positive regulation of organelle organization	7.31E-05	BAK1,CCT6A,FEN1,IL1A,LMAN1,MSN,FSCN1,SRC,RUVBL1,MACROH2A1,ARHGEF10,G3BP2,PDCD6IP,SMC4,TRIM28,CNOT1,CYFIP1,FBXO7
positive regulation of podosome assembly	4.99E-03	MSN,FSCN1,SRC
positive regulation of organelle assembly	5.32E-03	MSN,FSCN1,SRC,G3BP2,PDCD6IP,CNOT1
regulation of organelle assembly	6.14E-03	HNRNPU,MSN,FSCN1,SRC,EZR,SEC22B,G3BP2,PDCD6IP,CNOT1
regulation of podosome assembly	9.89E-03	MSN,FSCN1,SRC
establishment of apical/basal cell polarity	3.59E-02	MSN,FSCN1,SCRIB
establishment of cell polarity	3.94E-02	CRK,ITGB1,MSN,FSCN1,SCRIB,CORO7
establishment of monopolar cell polarity	4.46E-02	MSN,FSCN1,SCRIB

Table 2A.3. Pathway analysis of all proteins found to be present in the co-IP of PTGFRN with 8C7 monoclonal antibody in A431 cells, continued

establishment or maintenance of monopolar cell polarity	4.89E-02	MSN,FSCN1,SCRIB
establishment or maintenance of apical/basal cell polarity	5.18E-02	MSN,FSCN1,PDCD6IP,SCRIB
establishment or maintenance of bipolar cell polarity	5.18E-02	MSN,FSCN1,PDCD6IP,SCRIB
positive regulation of cellular component biogenesis	5.22E-02	BAK1,EIF4G1,GBP2,MSN,FSCN1,SRC,ARHGEF10 ,G3BP2,PDCD6IP,TRIM28,CNOT1,CYFIP1
establishment or maintenance of cell polarity	6.43E-02	CRK,ITGB1,MSN,FSCN1,PDCD6IP,SCRIB,CORO7
regulation of protein-containing complex assembly	9.71E-02	BAK1,EIF4G1,GBP2,HSPA5,MSN,FSCN1,SRC,PR EB,SEPTIN8,CYFIP1
positive regulation of protein-containing complex assembly	1.94E-01	BAK1,EIF4G1,GBP2,MSN,FSCN1,SRC
establishment or maintenance of epithelial cell apical/basal polarity	2.55E-01	MSN,PDCD6IP,SCRIB
protein folding	7.74E-05	CCT6A,GAK,HSPA5,LMAN1,PFDN4,PPIB,HSP90 B1,BAG2,NUDC,FKBP9,MESD,HSPBP1
chaperone-mediated protein folding	9.39E-02	CCT6A,GAK,HSPA5,PPIB

Table 2A.3. Pathway analysis of all proteins found to be present in the co-IP of PTGFRN with 8C7 monoclonal antibody in A431 cells, continued

negative regulation of transferase activity	9.09E-05	HNRNPU,PLEC,PRKAR2A,SRC,GPRC5A,RPL23,BAG2,MACROH2A1,PRDX3,CORO1C,FBXO7,SMYD3,CEP85
negative regulation of protein modification process	4.55E-04	BAK1,EIF4G1,G6PD,PLEC,PRKAR2A,RPS15,GPRC5A,RPL23,BAG2,MACROH2A1,CORO1C,FBXO7,UBR5,OXR1,SMYD3,CEP85
negative regulation of kinase activity	2.45E-03	HNRNPU,PLEC,PRKAR2A,GPRC5A,MACROH2A1,PRDX3,CORO1C,FBXO7,SMYD3,CEP85
negative regulation of phosphorylation	4.94E-03	BAK1,EIF4G1,HNRNPU,PLEC,PRKAR2A,GPRC5A,MACROH2A1,PRDX3,CORO1C,FBXO7,SMYD3,CEP85
negative regulation of phosphate metabolic process	1.47E-02	BAK1,EIF4G1,HNRNPU,PLEC,PRKAR2A,GPRC5A,MACROH2A1,PRDX3,CORO1C,FBXO7,SMYD3,CEP85
negative regulation of phosphorus metabolic process	1.49E-02	BAK1,EIF4G1,HNRNPU,PLEC,PRKAR2A,GPRC5A,MACROH2A1,PRDX3,CORO1C,FBXO7,SMYD3,CEP85
negative regulation of catalytic activity	2.13E-02	SERPINC1,HNRNPU,PEBP1,PLEC,PRKAR2A,SRC,GPRC5A,RPL23,BAG2,MACROH2A1,PRDX3,CORO1C,FBXO7,SMYD3,CEP85
negative regulation of protein kinase activity	2.13E-02	PLEC,PRKAR2A,GPRC5A,MACROH2A1,CORO1C,FBXO7,SMYD3,CEP85
negative regulation of protein phosphorylation	2.69E-02	BAK1,EIF4G1,PLEC,PRKAR2A,GPRC5A,MACROH2A1,CORO1C,FBXO7,SMYD3,CEP85
Signaling by Receptor Tyrosine Kinases	1.02E-04	AAMP,ADAM10,AP2M1,CLTC,CREB1,CRK,DIAPH1,ITGA3,ITGB1,LAMC1,NCBP1,PLCG1,POLR2H,RPS27A,SRC,STAT6,AHCYL1,CYFIP1
MET promotes cell motility	2.09E-03	CRK,ITGA3,ITGB1,LAMC1,SRC
PID UPA UPAR PATHWAY	2.31E-03	CRK,ITGA3,ITGB1,NCL,SRC
Signaling by MET	4.24E-03	CRK,ITGA3,ITGB1,LAMC1,RPS27A,SRC

Table 2A.3. Pathway analysis of all proteins found to be present in the co-IP of PTGFRN with 8C7 monoclonal antibody in A431 cells, continued

PID FAK PATHWAY	8.94E-03	CRK,ITGB1,MMP14,PLCG1,SRC
Shigellosis	1.46E-02	CAPN1,CRK,DIAPH1,ITGB1,PLCG1,RPS27A,SRC, IKBKG,SEPTIN8
PID TCPTP PATHWAY	2.17E-02	ITGB1,LMAN1,SRC,STAT6
Bacterial invasion of epithelial cells	2.40E-02	CLTC,CRK,ITGB1,SRC,SEPTIN8
TROP2 regulatory signaling	3.46E-02	ADAM10,ITGB1,TACSTD2,SRC
PID INTEGRIN A9B1 PATHWAY	4.89E-02	ITGB1,SRC,TGM2
PID LYMPH ANGIOGENESIS PATHWAY	4.89E-02	CREB1,CRK,ITGB1
PID CXCR4 PATHWAY	6.15E-02	CRK,ITGA3,ITGB1,SRC,UBQLN1
Integrin-mediated cell adhesion	6.62E-02	CAPN1,CRK,ITGA3,ITGB1,SRC
RAC1/PAK1/p38 /MMP2 pathway	9.15E-02	CRK,ITGB1,SRC,IKBKG
PID SYNDECAN 2 PATHWAY	9.15E-02	ITGB1,SRC,EZR
PID INTEGRIN A4B1 PATHWAY	9.15E-02	CRK,ITGB1,SRC
Hepatocyte growth factor receptor signaling	9.81E-02	CRK,ITGB1,SRC
Gastrin signaling pathway	9.87E-02	CREB1,CRK,ITGB1,PLCG1,SRC
positive regulation of cell migration	1.09E-01	AAMP,ADAM10,CRK,DIAPH1,HSPA5,IL1A,ITGA 3,ITGB1,MMP14,PLCG1,PPP3CA,SRC
regulation of small GTPase mediated signal transduction	1.24E-01	CRK,ITGA3,ITGB1,RGL2,SRC,TGM2,ARHGAP29, ARHGEF10
PID RET PATHWAY	1.34E-01	CREB1,CRK,SRC

Table 2A.3. Pathway analysis of all proteins found to be present in the co-IP of PTGFRN with 8C7 monoclonal antibody in A431 cells, continued

leukocyte migration	1.42E-01	CRK,ITGA3,ITGB1,MSN,PLEC,PPIB,SRC
positive regulation of cell motility	1.42E-01	AAMP,ADAM10,CRK,DIAPH1,HSPA5,IL1A,ITGA3,ITGB1,MMP14,PLCG1,PPP3CA,SRC
positive regulation of locomotion	1.66E-01	AAMP,ADAM10,CRK,DIAPH1,HSPA5,IL1A,ITGA3,ITGB1,MMP14,PLCG1,PPP3CA,SRC
Yersinia infection	1.79E-01	CRK,ITGB1,PLCG1,SRC,IKBKG
GPER1 signaling	1.86E-01	ITGB1,PRKAR2A,SRC
Focal adhesion	1.94E-01	CRK,DIAPH1,ITGA3,ITGB1,LAMC1,SRC
regulation of signaling receptor activity	2.11E-01	CAPN1,ITGB1,SRC,GPRC5A,PCSK9
Focal adhesion	2.12E-01	CRK,DIAPH1,ITGA3,ITGB1,LAMC1,SRC
integrin-mediated signaling pathway	2.25E-01	ADAM10,ITGA3,ITGB1,SRC
Carbon metabolism	1.03E-04	ACAT1,ALDOA,ALDOC,CS,DLST,G6PD,GCSH,MDH2,PGD
Glyoxylate and dicarboxylate metabolism	7.59E-03	ACAT1,CS,GCSH,MDH2
generation of precursor metabolites and energy	1.82E-02	ACAT1,ATP5F1D,CS,DLST,FDXR,G6PD,NIPSNAP2,MDH2,NDUFS3,PGD,PLEC
Metabolic reprogramming in colon cancer	2.17E-02	DLST,G6PD,MDH2,PGD
TCA cycle (aka Krebs or citric acid cycle)	2.20E-02	CS,DLST,MDH2
Citric acid cycle (TCA cycle)	3.59E-02	CS,DLST,MDH2
Amino acid metabolism	4.46E-02	ASNS,CS,DLST,MDH2,OAT
cellular respiration	5.46E-02	ATP5F1D,CS,DLST,NIPSNAP2,MDH2,NDUFS3,PLEC
Citrate cycle (TCA cycle)	7.48E-02	CS,DLST,MDH2
aerobic respiration	9.15E-02	ATP5F1D,CS,DLST,NIPSNAP2,MDH2,NDUFS3

Table 2A.3. Pathway analysis of all proteins found to be present in the co-IP of PTGFRN with 8C7 monoclonal antibody in A431 cells, continued

tricarboxylic acid cycle	9.15E-02	CS,DLST,MDH2
The citric acid (TCA) cycle and respiratory electron transport	1.28E-01	ATP5F1D,CS,DLST,MDH2,NDUFS3,LRPPRC
energy derivation by oxidation of organic compounds	2.05E-01	ATP5F1D,CS,DLST,NIPSNAP2,MDH2,NDUFS3,PLEC
response to inorganic substance	1.32E-04	ATP5F1D,BAK1,CREB1,CRK,G6PD,HSPA5,IL1A,LTA4H,PLEC,PPP3CA,SORD,SRC,STAT6,UBE3A,STK24,AHCYL1,PRDX3,ADCY10
response to salt	6.02E-02	G6PD,HSPA5,IL1A,PLEC,PPP2R2A,PPP3CA,TGM2,HSP90B1,UBE3A,AHCYL1
response to metal ion	1.32E-01	ATP5F1D,CREB1,G6PD,HSPA5,IL1A,LTA4H,PPP3CA,SORD,AHCYL1
Human papillomavirus infection	1.43E-04	BAK1,CDK6,CREB1,ITGA3,ITGB1,LAMC1,PPP2R2A,PSMC1,RHEB,UBE3A,IKBKG,OASL,BCAP31,SCRIB
Small cell lung cancer	1.28E-03	BAK1,CDK6,CKS2,ITGA3,ITGB1,LAMC1,IKBKG
Small cell lung cancer	1.59E-03	BAK1,CDK6,CKS2,ITGA3,ITGB1,LAMC1,IKBKG
MET activates PTK2 signaling	7.59E-03	ITGA3,ITGB1,LAMC1,SRC
Pathways in cancer	2.85E-02	BAK1,CDK6,CKS2,CRK,ITGA3,ITGB1,LAMC1,PLCG1,STAT6,TPM3,HSP90B1,CCDC6,IKBKG
Malignant pleural mesothelioma	5.37E-02	BAK1,CREB1,DSC3,EIF4G1,ITGA3,ITGB1,LAMC1,MMP14,RHEB,SRC,BAG2
Laminin interactions	7.48E-02	ITGA3,ITGB1,LAMC1
PID INTEGRIN1 PATHWAY	8.41E-02	ITGA3,ITGB1,LAMC1,TGM2
PI3K-Akt signaling pathway	8.61E-02	CDK6,CREB1,ITGA3,ITGB1,LAMC1,PPP2R2A,RHEB,HSP90B1,IKBKG
Primary focal segmental glomerulosclerosis (FSGS)	1.06E-01	ITGA3,ITGB1,PLCG1,INF2

Table 2A.3. Pathway analysis of all proteins found to be present in the co-IP of PTGFRN with 8C7 monoclonal antibody in A431 cells, continued

PI3K-Akt signaling pathway	1.06E-01	CDK6,CREB1,ITGA3,ITGB1,LAMC1,PPP2R2A,RHEB,HSP90B1,IKBKG
maintenance of blood-brain barrier	1.19E-01	ITGB1,LAMC1,LSR
PID A6B1 A6B4 INTEGRIN PATHWAY	1.95E-01	IL1A,ITGB1,LAMC1
DGCR8 multiprotein complex	2.23E-04	HNRNPU,HSPA5,ILF3,NCL

Appendix 3. Additional Author Contributions

Chapter 1: Overview and Objectives

Jorge Marquez and Ginette Serrero contributed to writing and editing of the chapter.

Chapter 2: PTGFRN and Cancer

Jorge Marquez and Ginette Serrero designed research; Jorge Marquez and Mehari Weldemariam performed research; Jorge Marquez and Mehari Weldemariam analyzed data; Jorge Marquez, Mehari Weldemariam, Maureen Kane, and Ginette Serrero contributed to writing and editing of the chapter.

Chapter 3: PTGFRN as a Target for ADC Development

Jorge Marquez and Ginette Serrero designed research; Jorge Marquez performed research and analyzed data; Jorge Marquez and Ginette Serrero contributed to writing and editing of the chapter.

Chapter 4: Conclusions and Future Discussions

Jorge Marquez and Ginette Serrero contributed to writing and editing of the chapter.

Comprehensive List of References

1. van Middendorp JJ, Sanchez GM, Burridge AL. The Edwin Smith papyrus: a clinical reappraisal of the oldest known document on spinal injuries. Eur Spine J [Internet]. 2010;19(11):1815–23. Available from: https://doi.org/10.1007/s00586-010-1523-6
2. Kaplan HS. Historic milestones in radiobiology and radiation therapy. Semin Oncol. 1979;6 4:479–89.
3. PUSEY WA. REPORT OF CASES TREATED WITH ROENTGEN RAYS. J Am Med Assoc [Internet]. 1902 Apr 12;XXXVIII(15):911–9. Available from: https://doi.org/10.1001/jama.1902.62480150001001
4. Senn N. Case of splenomedullary leukemia successfully treated by the use of rontgen ray. J Med Res. 1903;64(281).
5. Sudhakar A. History of Cancer, Ancient and Modern Treatment Methods. J cancer Sci \& Ther. 2009;1 2:1–4.
6. Iqbal N, Iqbal N. Imatinib: a breakthrough of targeted therapy in cancer. Chemother Res Pract [Internet]. 2014/05/19. 2014;2014:357027. Available from: https://pubmed.ncbi.nlm.nih.gov/24963404
7. Maximiano S, Magalhães P, Guerreiro MP, Morgado M. Trastuzumab in the Treatment of Breast Cancer. BioDrugs [Internet]. 2016;30(2):75–86. Available from: https://doi.org/10.1007/s40259-016-0162-9
8. Garcia J, Hurwitz HI, Sandler AB, Miles D, Coleman RL, Deurloo R, et al. Bevacizumab (Avastin®) in cancer treatment: A review of 15 years of clinical experience and future outlook. Cancer Treat Rev [Internet]. 2020;86(December 2019):102017. Available from: https://doi.org/10.1016/j.ctrv.2020.102017
9. Truitt G, Gittleman H, Leece R, Ostrom QT, Kruchko C, Armstrong TS, et al. Partnership for defining the impact of 12 selected rare CNS tumors: a report from the CBTRUS and the NCI-CONNECT. J Neurooncol [Internet]. 2019;144(1):53–63. Available from: https://doi.org/10.1007/s11060-019-03215-x
10. Bianchi C, Bianchi T. Malignant mesothelioma: Global incidence and relationship with asbestos. Ind Health. 2007;45(3):379–87.
11. Ning N. Malignant peritoneal mesothelioma. Retroperitoneal Tumors Clin Manag. 2017;4(27):263–7.
12. Sekido Y. Molecular pathogenesis of malignant mesothelioma. Carcinogenesis [Internet]. 2013 Jul 1;34(7):1413–9. Available from: https://doi.org/10.1093/carcin/bgt166
13. Beyer HL, Geschwindt RD, Glover CL, Tran L, Hellstrom I, Hellstrom K-E, et al. MESOMARK^{TM}: A Potential Test for Malignant Pleural Mesothelioma. Clin Chem [Internet]. 2007 Apr 1;53(4):666–72. Available from: https://doi.org/10.1373/clinchem.2006.079327
14. Bridda A, Padoan I, Mencarelli R, Frego M. Peritoneal mesothelioma: a review. MedGenMed. 2007 May;9(2):32.

15. Alesawi AM, Mandourah FS, Alesawi HM. Malignant mesothelioma. Mesothelioma Risk Factors, Treat Progn. 2021;51–85.

16. Saint-pierre MD, Pease C, Mithoowani H, Zhang T, Nicholas GA, Laurie SA, et al. Malignant Pleural Mesothelioma Outcomes in the Era of Combined Platinum and Folate Antimetabolite Chemotherapy. 2015;2015.

17. Woodard GA, Jablons DM. Surgery for pleural mesothelioma , when it is indicated and why : arguments against surgery for malignant pleural mesothelioma. Transl Lung Cancer Res. 2020;9(Suppl 1):86–91.

18. Rintoul RC, Ritchie AJ, Edwards JG, Waller DA, Coonar AS, Bennett M, et al. Efficacy and cost of video-assisted thoracoscopic partial pleurectomy versus talc pleurodesis in patients with malignant pleural mesothelioma (MesoVATS): an open-label, randomised, controlled trial. Lancet [Internet]. 2014;384(9948):1118–27. Available from: https://www.sciencedirect.com/science/article/pii/S0140673614604189

19. Sugarbaker DJ, Richards WG, Bueno R. Extrapleural pneumonectomy in the treatment of epithelioid malignant pleural mesothelioma novel prognostic implications of combined N1 and N2 nodal involvement based on experience in 529 patients. Ann Surg. 2014;260(4):577–82.

20. Treasure T, Lang-Lazdunski L, Waller D, Bliss JM, Tan C, Entwisle J, et al. Extra-pleural pneumonectomy versus no extra-pleural pneumonectomy for patients with malignant pleural mesothelioma: clinical outcomes of the Mesothelioma and Radical Surgery (MARS) randomised feasibility study. Lancet Oncol [Internet]. 2011;12(8):763–72. Available from: https://www.sciencedirect.com/science/article/pii/S1470204511701498

21. Janes SM, Alrifai D, Fennell DA. Perspectives on the Treatment of Malignant Pleural Mesothelioma. N Engl J Med [Internet]. 2021 Sep 22;385(13):1207–18. Available from: https://doi.org/10.1056/NEJMra1912719

22. Muers MF, Stephens RJ, Fisher P, Darlison L, Higgs CM, Lowry E, et al. Active symptom control with or without chemotherapy in the treatment of patients with malignant pleural mesothelioma (MS01): a multicentre randomised trial. Lancet. 2008;371(9625):1685–94.

23. Vogelzang NJ, Rusthoven JJ, Symanowski J, Denham C, Kaukel E, Ruffie P, et al. Phase III study of pemetrexed in combination with cisplatin versus cisplatin alone in patients with malignant pleural mesothelioma. J Clin Oncol. 2003;21(14):2636–44.

24. Van Meerbeeck JP, Gaafar R, Manegold C, Van Klaveren RJ, Van Marck EA, Vincent M, et al. Randomized phase III study of cisplatin with or without raltitrexed in patients with malignant pleural mesothelioma: An intergroup study of the European organisation for research and treatment of cancer lung cancer group and the National Cancer Institute . J Clin Oncol. 2005;23(28):6881–9.

25. Zalcman G, Mazieres J, Margery J, Greillier L, Audigier-Valette C, Moro-Sibilot D, et al. Bevacizumab for newly diagnosed pleural mesothelioma in the Mesothelioma Avastin Cisplatin Pemetrexed Study (MAPS): A randomised,

controlled, open-label, phase 3 trial. Lancet. 2016;387(10026):1405–14.

26. R.K. G. Review of pemetrexed in combination with cisplatin for the treatment of malignant pleural mesothelioma. Ther Clin Risk Manag [Internet]. 2008;4(1):205–11. Available from: http://www.embase.com/search/results?subaction=viewrecord&from=export&id=L351460944

27. Milano MT, Zhang H. Malignant pleural mesothelioma: A population-based study of survival. J Thorac Oncol [Internet]. 2010;5(11):1841–8. Available from: http://dx.doi.org/10.1097/JTO.0b013e3181f1cf2b

28. Stahel RA, Riesterer O, Xyrafas A, Opitz I, Beyeler M, Ochsenbein A, et al. Neoadjuvant chemotherapy and extrapleural pneumonectomy of malignant pleural mesothelioma with or without hemithoracic radiotherapy (SAKK 17/04): a randomised, international, multicentre phase 2 trial. Lancet Oncol [Internet]. 2015;16(16):1651–8. Available from: https://www.sciencedirect.com/science/article/pii/S1470204515002089

29. Rimner A, Hu C, Zauderer M, Yorke ED, Simone CB, Gill RR, et al. A Phase III Randomized Trial of Pleurectomy/Decortication Plus Chemotherapy With Or Without Adjuvant Hemithoracic Intensity-Modulated Pleural Radiation Therapy (IMPRINT) For Malignant Pleural Mesothelioma (MPM) (NRG-LU006). Int J Radiat Oncol [Internet]. 2020;108(3, Supplement):e928–9. Available from: https://www.sciencedirect.com/science/article/pii/S0360301620320022

30. Mansha M, Ali N, Ali S, Azam N, Khan A. Malignant Pleural Mesothelioma: A Multi-Disciplinary Approach. Gulf J Oncolog. 2019;1(30):76–80.

31. Hassan R, Kindler HL, Jahan T, Bazhenova L, Reck M, Thomas A, et al. Phase II Clinical Trial of Amatuximab, a Chimeric Antimesothelin Antibody with Pemetrexed and Cisplatin in Advanced Unresectable Pleural Mesothelioma. Clin Cancer Res [Internet]. 2014 Nov 30;20(23):5927–36. Available from: https://doi.org/10.1158/1078-0432.CCR-14-0804

32. Rottey S, Clarke J, Aung K, Machiels J-P, Markman B, Heinhuis KM, et al. Phase I/IIa Trial of BMS-986148, an Anti-mesothelin Antibody–drug Conjugate, Alone or in Combination with Nivolumab in Patients with Advanced Solid Tumors. Clin Cancer Res [Internet]. 2022 Jan 1;28(1):95–105. Available from: https://doi.org/10.1158/1078-0432.CCR-21-1181

33. Faust JR, Hamill D, Kolb EA, Gopalakrishnapillai A, Barwe SP. Mesothelin: An Immunotherapeutic Target beyond Solid Tumors. Vol. 14, Cancers. 2022.

34. Kumar LP, Fayaz S, Deepa AJ, Moinca I, Suresh P, Naidu KVJR. Medulloblastoma : A common pediatric tumor : Prognostic factors and predictors of outcome. 2015;10(1).

35. Becker L, Hinton D. Primitive Neuroectodermal Tumors of the. Hum Pathol. 1983;14(6):538–50.

36. Zeltzer PM, Boyett JM, Finlay JL, Albright AL, Rorke LB, Milstein JM, et al. Metastasis stage, adjuvant treatment, and residual tumor are prognostic factors for

medulloblastoma in children: conclusions from the Children's Cancer Group 921 randomized phase III study. J Clin Oncol. 1999;17(3):832.

37. Kortmann R-D, Kühl J, Timmermann B, Mittler U, Urban C, Budach V, et al. Postoperative neoadjuvant chemotherapy before radiotherapy as compared to immediate radiotherapy followed by maintenance chemotherapy in the treatment of medulloblastoma in childhood: results of the German prospective randomized trial HIT'91. Int J Radiat Oncol Biol Phys. 2000;46(2):269–79.

38. Palmer SL, Goloubeva O, Reddick WE, Glass JO, Gajjar A, Kun L, et al. Patterns of intellectual development among survivors of pediatric medulloblastoma: a longitudinal analysis. J Clin Oncol. 2001;19(8):2302–8.

39. Ris MD, Packer R, Goldwein J, Jones-Wallace D, Boyett JM. Intellectual outcome after reduced-dose radiation therapy plus adjuvant chemotherapy for medulloblastoma: a Children's Cancer Group study. J Clin Oncol. 2001;19(15):3470–6.

40. Heideman RL. Overview of the treatment of infant central nervous system tumors: medulloblastoma as a model. J Pediatr Hematol Oncol. 2001;23(5):268–71.

41. Taylor RE, Bailey CC, Robinson K, Weston CL, Ellison D, Ironside J, et al. Results of a randomized study of preradiation chemotherapy versus radiotherapy alone for nonmetastatic medulloblastoma: The International Society of Paediatric Oncology/United Kingdom Children's Cancer Study Group PNET-3 Study. J Clin Oncol. 2003;21(8):1581–91.

42. Packer RJ, Goldwein J, Nicholson HS, Vezina LG, Allen JC, Ris MD, et al. Treatment of children with medulloblastomas with reduced-dose craniospinal radiation therapy and adjuvant chemotherapy: A Children's Cancer Group Study. J Clin Oncol. 1999;17(7):2127.

43. Strother D, Ashley D, Kellie SJ, Patel A, Jones-Wallace D, Thompson S, et al. Feasibility of four consecutive high-dose chemotherapy cycles with stem-cell rescue for patients with newly diagnosed medulloblastoma or supratentorial primitive neuroectodermal tumor after craniospinal radiotherapy: results of a collaborative study. J Clin Oncol. 2001;19(10):2696–704.

44. Gilbertson RJ. Medulloblastoma: Signalling a change in treatment. Lancet Oncol. 2004;5(4):209–18.

45. Ellison DW, Clifford SC, Gajjar A, Gilbertson RJ. What's new in neuro-oncology? Recent advances in medulloblastoma. Eur J Paediatr Neurol. 2003;7(2):53–66.

46. Tarbell NJ, Friedman H, Polkinghorn WR, Yock T, Zhou T, Chen Z, et al. High-risk medulloblastoma: A pediatric oncology group randomized trial of chemotherapy before or after radiation therapy (POG 9031). J Clin Oncol. 2013;31(23):2936–41.

47. Taylor MD, Northcott PA, Korshunov A, Remke M, Cho Y-J, Clifford SC, et al. Molecular subgroups of medulloblastoma: the current consensus. Acta Neuropathol [Internet]. 2012;123(4):465–72. Available from: https://doi.org/10.1007/s00401-011-0922-z

48. Luzzi S, Giotta Lucifero A, Brambilla I, Semeria Mantelli S, Mosconi M, Foiadelli T, et al. Targeting the medulloblastoma: a molecular-based approach . Acta Biomed Atenei Parm [Internet]. 2020 Jun 30;91(7-S SE-ORIGINAL ARTICLES):79–100. Available from: https://www.mattioli1885journals.com/index.php/actabiomedica/article/view/9958

49. Ganesh K, Massague J. Targeting Metastatic Cancer. Nat Med. 2021;27(1):34–44.

50. Urruticoechea A, Alemany R, Balart J, Villanueva F, Vinals F, Capella G. Recent Advances in Cancer Therapy. Curr Pharm Des. 2010;16:3–10.

51. Hapach LA, Mosier JA, Wang W, Reinhart-King CA. Engineered models to parse apart the metastatic cascade. npj Precis Oncol [Internet]. 2019;3(1):20. Available from: https://doi.org/10.1038/s41698-019-0092-3

52. Chambers AF, Groom AC, MacDonald IC. Dissemination and growth of cancer cells in metastatic sites. Nat Rev Cancer. 2002;2(8):563–72.

53. Chambers AF, Macdonald IC, Schmidt EE, Morris VL, Groom AC. Clinical Targets for Anti-Metastasis Therapy.pdf. Adv Cancer Res. 2000;79:91–121.

54. Haeger A, Krause M, Wolf K, Friedl P. Cell jamming: collective invasion of mesenchymal tumor cells imposed by tissue confinement. Biochim Biophys Acta (BBA)-General Subj. 2014;1840(8):2386–95.

55. Wisdom KM, Adebowale K, Chang J, Lee JY, Nam S, Desai R, et al. Matrix mechanical plasticity regulates cancer cell migration through confining microenvironments. Nat Commun [Internet]. 2018;9(1):4144. Available from: https://doi.org/10.1038/s41467-018-06641-z

56. Folkman J. Role of angiogenesis in tumor growth and metastasis. Semin Oncol [Internet]. 2002;29(6, Supplement 16):15–8. Available from: https://www.sciencedirect.com/science/article/pii/S0093775402700651

57. Carmeliet P, Jain RK. Angiogenesis in cancer and other diseases. Nature. 2000;407(6801):249–57.

58. Chang YS, di Tomaso E, McDonald DM, Jones R, Jain RK, Munn LL. Mosaic blood vessels in tumors: frequency of cancer cells in contact with flowing blood. Proc Natl Acad Sci U S A [Internet]. 2000 Dec 19;97(26):14608–13. Available from: https://pubmed.ncbi.nlm.nih.gov/11121063

59. Helmlinger G, Yuan F, Dellian M, Jain RK. Interstitial pH and pO 2 gradients in solid tumors in vivo: high-resolution measurements reveal a lack of correlation. Nat Med. 1997;3:177–82.

60. Wirtz D, Konstantopoulos K, Searson PC. The physics of cancer: the role of physical interactions and mechanical forces in metastasis. Nat Rev Cancer. 2011;11(7):512–22.

61. Kienast Y, Von Baumgarten L, Fuhrmann M, Klinkert WEF, Goldbrunner R, Herms J, et al. Real-time imaging reveals the single steps of brain metastasis formation. Nat Med. 2010;16(1):116–22.

62. Zhu C, Yago T, Lou J, Zarnitsyna VI, McEver RP. Mechanisms for flow-enhanced

cell adhesion. Ann Biomed Eng. 2008;36:604–21.

63. Chang K-C, Hammer DA. The forward rate of binding of surface-tethered reactants: effect of relative motion between two surfaces. Biophys J. 1999;76(3):1280–92.

64. Rankin EB, Erler J, Giaccia AJ. The Cellular Microenvironment and Metastases. In: Niederhuber JE, Armitage JO, Doroshow JH, Kastan MB, Tepper JEBT-ACO (Fifth E, editors. Abeloff's Clinical Oncology (Fifth Edition) [Internet]. Philadelphia: Churchill Livingstone; 2014. p. 40-51.e4. Available from: https://www.sciencedirect.com/science/article/pii/B9781455728657000035

65. Miles FL, Pruitt FL, van Golen KL, Cooper CR. Stepping out of the flow: capillary extravasation in cancer metastasis. Clin Exp Metastasis [Internet]. 2008;25(4):305–24. Available from: https://doi.org/10.1007/s10585-007-9098-2

66. Lambert AW, Pattabiraman DR, Weinberg RA. EMERGING BIOLOGICAL PRINCIPLES OF METASTASIS. Cell. 2017;168(4):670–91.

67. Balic M, Lin H, Young L, Hawes D, Giuliano A, McNamara G, et al. Most Early Disseminated Cancer Cells Detected in Bone Marrow of Breast Cancer Patients Have a Putative Breast Cancer Stem Cell Phenotype. Clin Cancer Res [Internet]. 2006 Oct 4;12(19):5615–21. Available from: https://doi.org/10.1158/1078-0432.CCR-06-0169

68. Massagué J, Obenauf AC. Metastatic Colonization. Nature. 2016;529(7586):298–306.

69. Boire A, Brastianos PK, Garzia L, Valiente M. Brain metastasis. Nat Rev Cancer [Internet]. 2020;20(1):4–11. Available from: http://dx.doi.org/10.1038/s41568-019-0220-y

70. Koscielny S, Tubiana M. Parallel progression of tumour and metastases. Nat Rev Cancer. 2010;10(2):156.

71. Martin TA, Ye L, Sanders AJ, Lane J, Jiang WG. Cancer Invasion and Metastasis: Molecular and Cellular Perspective. In: Madame Curie Bioscience Database. 2013.

72. Van Den Hoogen C, Van Der Horst G, Cheung H, Buijs JT, Lippitt JM, Guzmán-Ramírez N, et al. High aldehyde dehydrogenase activity identifies tumor-initiating and metastasis-initiating cells in human prostate cancer. Cancer Res. 2010;70(12):5163–73.

73. Karakuş F, Eyol E, Yılmaz K, Ünüvar S. Inhibition of cell proliferation, migration and colony formation of LS174T Cells by carbonic anhydrase inhibitor. Afr Health Sci. 2018;18(4):1303–10.

74. Zhang Q, Yu S, Lam MMT, Poon TCW, Sun L, Jiao Y, et al. Angiotensin II promotes ovarian cancer spheroid formation and metastasis by upregulation of lipid desaturation and suppression of endoplasmic reticulum stress. J Exp Clin Cancer Res. 2019;38(1):1–18.

75. Dean M, Jin V, Bergsten TM, Austin JR, Lantvit DD, Russo A, et al. Loss of PTEN in Fallopian tube epithelium results in multicellular tumor spheroid formation and metastasis to the ovary. Cancers (Basel). 2019;11(6).

76. Jiang X, Zhang J, Huang Y. Tetraspanins in Cell Migration. Cell Adhes Migr. 2015;9(5):406–15.

77. Orlicky DJ, Nordeen SK. Cloning, sequencing and proposed structure for a prostaglandin F2α receptor regulatory protein. Prostaglandins, Leukot Essent Fat Acids [Internet]. 1996;55(4):261–8. Available from: https://www.sciencedirect.com/science/article/pii/S0952327896900071

78. Sala-Valdés M, Ursa Á, Charrin S, Rubinstein E, Hemler ME, Sánchez-Madrid F, et al. EWI-2 and EWI-F link the tetraspanin web to the actin cytoskeleton through their direct association with ezrin-radixin-moesin proteins. J Biol Chem. 2006;281(28):19665–75.

79. Yáñez-Mó M, Barreiro O, Gordon-Alonso M, Sala-Valdés M, Sánchez-Madrid F. Tetraspanin-enriched microdomains: a functional unit in cell plasma membranes. Trends Cell Biol. 2009;19(9):434–46.

80. André M, Chambrion C, Charrin S, Soave S, Chaker J, Boucheix C, et al. In situ chemical cross-linking on living cells reveals CD9P-1 cis-oligomer at cell surface. J Proteomics. 2009;73(1):93–102.

81. Charrin S, Jouannet S, Boucheix C, Rubinstein E. Tetraspanins at a glance. J Cell Sci. 2014;127(17):3641–8.

82. Charrin S, Manié S, Billard M, Ashman L, Gerlier D, Boucheix C, et al. Multiple levels of interactions within the tetraspanin web. Biochem Biophys Res Commun. 2003;304(1):107–12.

83. Glazar AI, Evans JP. Immunoglobulin superfamily member IgSF8 (EWI-2) and CD9 in fertilisation: Evidence of distinct functions for CD9 and a CD9-associated protein in mammalian sperm-egg interaction. Reprod Fertil Dev. 2009;21(2):293–303.

84. Swegen A, Grupen CG, Gibb Z, Baker MA, de Ruijter-Villani M, Smith ND, et al. From Peptide Masses to Pregnancy Maintenance: A Comprehensive Proteomic Analysis of The Early Equine Embryo Secretome, Blastocoel Fluid, and Capsule. Proteomics. 2017;17(17–18):1–13.

85. Dooley K, Mcconnell RE, Xu K, Lewis ND, Haupt S, Youniss MR, et al. A versatile platform for generating engineered extracellular vesicles with defined therapeutic properties. Mol Ther. 2021;29(5):1729–43.

86. Xu J, Wang Y, Hsu CY, Gao Y, Meyers CA, Chang L, et al. Human perivascular stem cell-derived extracellular vesicles mediate bone repair. Elife. 2019;8:1–23.

87. Orlicky DJ, Lieber JG, Morin CL, Evans RM. Synthesis and accumulation of a receptor regulatory protein associated with lipid droplet accumulation in 3T3-L1 cells. J Lipid Res. 1998;39(6):1152–61.

88. Zhang X, Shi G, Gao F, Liu P, Wang H, Tan X. TSPAN1 upregulates MMP2 to promote pancreatic cancer cell migration and invasion via PLCγ. Oncol Rep [Internet]. 2019/01/30. 2019 Apr;41(4):2117–25. Available from: https://pubmed.ncbi.nlm.nih.gov/30720116

89. Zhou C, Liang Y, Zhou L, Yan Y, Liu N, Zhang R, et al. TSPAN1 promotes

autophagy flux and mediates cooperation between WNT-CTNNB1 signaling and autophagy via the MIR454-FAM83A-TSPAN1 axis in pancreatic cancer. Autophagy [Internet]. 2021 Oct 3;17(10):3175–95. Available from: https://doi.org/10.1080/15548627.2020.1826689

90. Otsubo C, Otomo R, Miyazaki M, Matsushima-Hibiya Y, Kohno T, Iwakawa R, et al. TSPAN2 Is Involved in Cell Invasion and Motility during Lung Cancer Progression. Cell Rep [Internet]. 2014 Apr 24;7(2):527–38. Available from: https://doi.org/10.1016/j.celrep.2014.03.027

91. Seipold L, Damme M, Prox J, Rabe B, Kasparek P, Sedlacek R, et al. Tetraspanin 3: A central endocytic membrane component regulating the expression of ADAM10, presenilin and the amyloid precursor protein. Biochim Biophys Acta - Mol Cell Res [Internet]. 2017;1864(1):217–30. Available from: https://www.sciencedirect.com/science/article/pii/S0167488916302890

92. Li Y, Wang L, Qiu J, Da L, Tiollais P, Li Z, et al. Human tetraspanin transmembrane 4 superfamily member 4 or intestinal and liver tetraspan membrane protein is overexpressed in hepatocellular carcinoma and accelerates tumor cell growth. Acta Biochim Biophys Sin (Shanghai) [Internet]. 2012;44(3):224–32. Available from: http://www.sciengine.com/doi/10.1093/abbs/gmr124

93. Schreyer L, Mittermeier C, Franz MJ, Meier MA, Martin DE, Maier KC, et al. Tetraspanin 5 (TSPAN5), a Novel Gatekeeper of the Tumor Suppressor DLC1 and Myocardin-Related Transcription Factors (MRTFs), Controls HCC Growth and Senescence. Vol. 13, Cancers. 2021.

94. Zhou J, Fujiwara T, Ye S, Li X, Zhao H. Downregulation of Notch Modulators, Tetraspanin 5 and 10, Inhibits Osteoclastogenesis in Vitro. Calcif Tissue Int [Internet]. 2014;95(3):209–17. Available from: https://doi.org/10.1007/s00223-014-9883-2

95. Andrijes R, Hejmadi RK, Pugh M, Rajesh S, Novitskaya V, Ibrahim M, et al. Tetraspanin 6 is a regulator of carcinogenesis in colorectal cancer. Proc Natl Acad Sci [Internet]. 2021 Sep 28;118(39):e2011411118. Available from: https://doi.org/10.1073/pnas.2011411118

96. Humbert PO, Pryjda TZ, Pranjic B, Farrell A, Fujikura K, de Matos Simoes R, et al. TSPAN6 is a suppressor of Ras-driven cancer. Oncogene [Internet]. 2022;41(14):2095–105. Available from: https://doi.org/10.1038/s41388-022-02223-y

97. Lee S-A, Suh Y, Lee S, Jeong J, Kim SJ, Kim SJ, et al. Functional expression of dopamine D2 receptor is regulated by tetraspanin 7–mediated postendocytic trafficking. FASEB J [Internet]. 2017 Jun 1;31(6):2301–13. Available from: https://doi.org/10.1096/fj.201600755RR

98. Bassani S, Cingolani LA, Valnegri P, Folci A, Zapata J, Gianfelice A, et al. The X-Linked Intellectual Disability Protein TSPAN7 Regulates Excitatory Synapse Development and AMPAR Trafficking. Neuron [Internet]. 2012;73(6):1143–58. Available from: https://www.sciencedirect.com/science/article/pii/S0896627312001390

99. Heo K, Lee S. TSPAN8 as a Novel Emerging Therapeutic Target in Cancer for Monoclonal Antibody Therapy. Vol. 10, Biomolecules. 2020.

100. Protty MB, Watkins NA, Colombo D, Thomas SG, Heath VL, Herbert JMJ, et al. Identification of Tspan9 as a novel platelet tetraspanin and the collagen receptor GPVI as a component of tetraspanin microdomains. Biochem J [Internet]. 2008 Dec 12;417(1):391–401. Available from: https://doi.org/10.1042/BJ20081126

101. Qi Y, Lv J, Liu S, Sun L, Wang Y, Li H, et al. TSPAN9 and EMILIN1 synergistically inhibit the migration and invasion of gastric cancer cells by increasing TSPAN9 expression. BMC Cancer [Internet]. 2019;19(1):630. Available from: https://doi.org/10.1186/s12885-019-5810-2

102. Dornier E, Coumailleau F, Ottavi J-F, Moretti J, Boucheix C, Mauduit P, et al. TspanC8 tetraspanins regulate ADAM10/Kuzbanian trafficking and promote Notch activation in flies and mammals. J Cell Biol [Internet]. 2012 Oct 22;199(3):481–96. Available from: https://doi.org/10.1083/jcb.201201133

103. Liu J, Jiang C, Xu C, Wang D, Shen Y, Liu Y, et al. Identification and development of a novel invasion-related gene signature for prognosis prediction in colon adenocarcinoma. Cancer Cell Int [Internet]. 2021;21(1):101. Available from: https://doi.org/10.1186/s12935-021-01795-1

104. Ye M, Wei T, Wang Q, Sun Y, Tang R, Guo L, et al. TSPAN12 promotes chemoresistance and proliferation of SCLC under the regulation of miR-495. Biochem Biophys Res Commun [Internet]. 2017;486(2):349–56. Available from: https://www.sciencedirect.com/science/article/pii/S0006291X17305016

105. Knoblich K, Wang H-X, Sharma C, Fletcher AL, Turley SJ, Hemler ME. Tetraspanin TSPAN12 regulates tumor growth and metastasis and inhibits β-catenin degradation. Cell Mol Life Sci [Internet]. 2014;71(7):1305–14. Available from: https://doi.org/10.1007/s00018-013-1444-8

106. Li P, Dong M, Wang Z. Downregulation of TSPAN13 by miR-369-3p inhibits cell proliferation in papillary thyroid cancer (PTC). Biomol Biomed [Internet]. 2019 May 20;19(2 SE-Molecular Biology):146–54. Available from: https://www.bjbms.org/ojs/index.php/bjbms/article/view/2865

107. Huang H, Sossey-Alaoui K, Beachy SH, Geradts J. The tetraspanin superfamily member NET-6 is a new tumor suppressor gene. J Cancer Res Clin Oncol [Internet]. 2007;133(10):761–9. Available from: https://doi.org/10.1007/s00432-007-0221-1

108. Haining EJ, Yang J, Bailey RL, Khan K, Collier R, Tsai S, et al. The TspanC8 Subgroup of Tetraspanins Interacts with A Disintegrin and Metalloprotease 10 (ADAM10) and Regulates Its Maturation and Cell Surface Expression *. J Biol Chem [Internet]. 2012 Nov 16;287(47):39753–65. Available from: https://doi.org/10.1074/jbc.M112.416503

109. Sidahmed-Adrar N, Ottavi J-F, Benzoubir N, Ait Saadi T, Bou Saleh M, Mauduit P, et al. Tspan15 Is a New Stemness-Related Marker in Hepatocellular Carcinoma. Proteomics [Internet]. 2019 Nov 1;19(21–22):1900025. Available from: https://doi.org/10.1002/pmic.201900025

110. Koo CZ, Harrison N, Noy PJ, Szyroka J, Matthews AL, Hsia H-E, et al. The tetraspanin Tspan15 is an essential subunit of an ADAM10 scissor complex. J Biol Chem [Internet]. 2020 Sep 4;295(36):12822–39. Available from: https://doi.org/10.1074/jbc.RA120.012601

111. Puls KL, Ni J, Liu D, Morahan G, Wright MD. The molecular characterisation of a novel tetraspanin protein, TM4-B1Sequence described in this paper, has been deposited in the GenBank database under accession number AF133424.1. Biochim Biophys Acta - Gene Struct Expr [Internet]. 1999;1447(1):93–9. Available from: https://www.sciencedirect.com/science/article/pii/S0167478199001165

112. Reyat JS, Chimen M, Noy PJ, Szyroka J, Rainger GE, Tomlinson MG. ADAM10-Interacting Tetraspanins Tspan5 and Tspan17 Regulate VE-Cadherin Expression and Promote T Lymphocyte Transmigration. J Immunol [Internet]. 2017 Jul 15;199(2):666–76. Available from: https://doi.org/10.4049/jimmunol.1600713

113. Gavin RL, Koo CZ, Tomlinson MG. Tspan18 is a novel regulator of thrombo-inflammation. Med Microbiol Immunol [Internet]. 2020;209(4):553–64. Available from: https://doi.org/10.1007/s00430-020-00678-y

114. Scherer SE, Muzny DM, Buhay CJ, Chen R, Cree A, Ding Y, et al. The finished DNA sequence of human chromosome 12. Nature [Internet]. 2006;440(7082):346–51. Available from: https://doi.org/10.1038/nature04569

115. Wang FH, Ma XJ, Xu D, Luo J. UPK1B promotes the invasion and metastasis of bladder cancer via regulating the Wnt/β-catenin pathway. Eur Rev Med Pharmacol Sci. 2018;22(17):5471–80.

116. Byun Y, Choi Y-C, Jeong Y, Yoon J, Baek K. Long Noncoding RNA Expression Profiling Reveals Upregulation of Uroplakin 1A and Uroplakin 1A Antisense RNA 1 under Hypoxic Conditions in Lung Cancer Cells. Mol Cells [Internet]. 2020/12/31. 2020 Dec;43(12):975–88. Available from: https://molcells.org/journal/view.html?doi=10.14348/molcells.2020.0126

117. Tebbe L, Kakakhel M, Makia MS, Al-Ubaidi MR, Naash MI. The Interplay between Peripherin 2 Complex Formation and Degenerative Retinal Diseases. Vol. 9, Cells. 2020.

118. Strayve D, Makia MS, Kakakhel M, Sakthivel H, Conley SM, Al-Ubaidi MR, et al. ROM1 contributes to phenotypic heterogeneity in PRPH2-associated retinal disease. Hum Mol Genet [Internet]. 2020 Sep 29;29(16):2708–22. Available from: https://doi.org/10.1093/hmg/ddaa160

119. Kumari S, Gayatri Devi V, Badana A, Dasari VR, Malla RR. CD151—A Striking Marker for Cancer Therapy. Biomark Cancer [Internet]. 2015 Jan 1;7:BIC.S21847. Available from: https://doi.org/10.4137/BIC.S21847

120. Dunlock VE. Tetraspanin CD53: an overlooked regulator of immune cell function. Med Microbiol Immunol [Internet]. 2020;209(4):545–52. Available from: https://doi.org/10.1007/s00430-020-00677-z

121. Xu-Monette ZY, Li L, Byrd JC, Jabbar KJ, Manyam GC, Maria de Winde C, et al. Assessment of CD37 B-cell antigen and cell of origin significantly improves risk

prediction in diffuse large B-cell lymphoma. Blood [Internet]. 2016 Dec 29;128(26):3083–100. Available from: https://doi.org/10.1182/blood-2016-05-715094

122. Funakoshi T, Tachibana I, Hoshida Y, Kimura H, Takeda Y, Kijima T, et al. Expression of tetraspanins in human lung cancer cells: Frequent downregulation of CD9 and its contribution to cell motility in small cell lung cancer. Oncogene. 2003;22(5):674–87.

123. Dinsdale NL, Crespi BJ. Endometriosis and polycystic ovary syndrome are diametric disorders. Evol Appl [Internet]. 2021 Jul 1;14(7):1693–715. Available from: https://doi.org/10.1111/eva.13244

124. Signorelli D, Ghidotti P, Proto C, Brambilla M, De Toma A, Ferrara R, et al. Circulating CD81-expressing extracellular vesicles as biomarkers of response for immune-checkpoint inhibitors in advanced NSCLC [Internet]. Vol. 13, Frontiers in Immunology . 2022. Available from: https://www.frontiersin.org/articles/10.3389/fimmu.2022.987639

125. Quast T, Eppler F, Semmling V, Schild C, Homsi Y, Levy S, et al. CD81 is essential for the formation of membrane protrusions and regulates Rac1-activation in adhesion-dependent immune cell migration. Blood [Internet]. 2011 Aug 18;118(7):1818–27. Available from: https://doi.org/10.1182/blood-2010-12-326595

126. Toyo-oka K, Yashiro-Ohtani Y, Park C-S, Tai X-G, Miyake K, Hamaoka T, et al. Association of a tetraspanin CD9 with CD5 on the T cell surface: role of particular transmembrane domains in the association. Int Immunol [Internet]. 1999 Dec 1;11(12):2043–52. Available from: https://doi.org/10.1093/intimm/11.12.2043

127. Brosseau C, Colas L, Magnan A, Brouard S. CD9 Tetraspanin: A New Pathway for the Regulation of Inflammation? [Internet]. Vol. 9, Frontiers in Immunology . 2018. Available from: https://www.frontiersin.org/articles/10.3389/fimmu.2018.02316

128. Tognoli ML, Dancourt J, Bonsergent E, Palmulli R, de Jong OG, Van Niel G, et al. Lack of involvement of CD63 and CD9 tetraspanins in the extracellular vesicle content delivery process. Commun Biol [Internet]. 2023;6(1):532. Available from: https://doi.org/10.1038/s42003-023-04911-1

129. Duch P, Díaz-Valdivia N, Ikemori R, Gabasa M, Radisky ES, Arshakyan M, et al. Aberrant TIMP-1 overexpression in tumor-associated fibroblasts drives tumor progression through CD63 in lung adenocarcinoma. Matrix Biol [Internet]. 2022;111:207–25. Available from: https://www.sciencedirect.com/science/article/pii/S0945053X22000890

130. Ma X, Qiu S, Tang X, Song Q, Wang P, Wang J, et al. TSPAN31 regulates the proliferation, migration, and apoptosis of gastric cancer cells through the METTL1/CCT2 pathway. Transl Oncol [Internet]. 2022;20:101423. Available from: https://www.sciencedirect.com/science/article/pii/S1936523322000821

131. Lombardo SD, Mazzon E, Basile MS, Campo G, Corsico F, Presti M, et al. Modulation of Tetraspanin 32 (TSPAN32) Expression in T Cell-Mediated Immune

Responses and in Multiple Sclerosis. Vol. 20, International Journal of Molecular Sciences. 2019.

132. Navarro-Hernandez IC, López-Ortega O, Acevedo-Ochoa E, Cervantes-Díaz R, Romero-Ramírez S, Sosa-Hernández VA, et al. Tetraspanin 33 (TSPAN33) regulates endocytosis and migration of human B lymphocytes by affecting the tension of the plasma membrane. FEBS J [Internet]. 2020 Aug 1;287(16):3449–71. Available from: https://doi.org/10.1111/febs.15216

133. Witwer KW. On your MARCKS , get set , deliver : Engineering extracellular vesicles. Mol Ther [Internet]. 2021;29(5):1664–5. Available from: https://doi.org/10.1016/j.ymthe.2021.04.013

134. Fabris L, Sato K, Alpini G, Strazzabosco M. The Tumor Microenvironment in Cholangiocarcinoma Progression. Hepatology. 2021;73(S1):75–85.

135. Yekula A, Yekula A, Muralidharan K, Kang K. Extracellular Vesicles in Glioblastoma Tumor Microenvironment. Front Immunol. 2020;10(January):1–12.

136. Arneth B. Tumor Microenvironment. Medicina (B Aires). 2020;56(15):1–21.

137. Balkwill FR, Hagemann T. The tumor microenvironment at a glance. J Cell Sci. 2012;125(23):5591–6.

138. Jang SC, Economides KD, Moniz RJ, Sia CL, Lewis N, McCoy C, et al. ExoSTING, an extracellular vesicle loaded with STING agonists, promotes tumor immune surveillance. Commun Biol [Internet]. 2021;4(1):497. Available from: https://doi.org/10.1038/s42003-021-02004-5

139. Testa JE, Brooks PC, Lin JM, Quigley JP. Eukaryotic expression cloning with an antimetastatic monoclonal antibody identifies a tetraspanin (PETA-3/CD151) as an effector of human tumor cell migration and metastasis. Cancer Res. 1999;59(15):3812–20.

140. Jackson P, Marreiros A, Russell PJ. KAI1 tetraspanin and metastasis suppressor. Int J Biochem Cell Biol. 2005;37(3):530–4.

141. Zheng R, Yano S, Zhang H, Nakataki E, Tachibana I, Kawase I, et al. CD9 Overexpression Suppressed the Liver Metastasis and Malignant Ascites via Inhibition of Proliferation and Motility of Small-Cell Lung Cancer Cells in NK Cell-Depleted SCID Mice. Oncol Res. 2005;15:365–72.

142. Yin M, Soikkeli J, Jahkola T, Virolainen S, Saksela O, Hölttä E. Osteopontin promotes the invasive growth of melanoma cells by activating integrin αvβ3 and down-regulating tetraspanin CD9. Am J Pathol [Internet]. 2014;184(3):842–58. Available from: http://dx.doi.org/10.1016/j.ajpath.2013.11.020

143. Longo N, Yáñez-Mó M, Mittelbrunn M, De La Rosa G, Muñoz ML, Sánchez-Madrid F, et al. Regulatory role of tetraspanin CD9 in tumor-endothelial cell interaction during transendothelial invasion of melanoma cells. Blood. 2001;98(13):3717–26.

144. Castro-Sanchez L, Soto-Guzman A, Navarro-Tito N, Martinez-Orozco R, Salazar EP. Native type IV collagen induces cell migration through a CD9 and DDR1-dependent pathway in MDA-MB-231 breast cancer cells. Eur J Cell Biol

[Internet]. 2010;89(11):843–52. Available from: http://dx.doi.org/10.1016/j.ejcb.2010.07.004

145. Powner D, Kopp PM, Monkley SJ, Critchley DR, Berditchevski F. Tetraspanin CD9 in cell migration. Biochem Soc Trans. 2011;39(2):563–7.

146. Colin S, Guilmain W, Creoff E, Schneider C, Steverlynck C, Bongaerts M, et al. A truncated form of CD9-partner 1 (CD9P-1), GS-168AT2, potently inhibits in vivo tumour-induced angiogenesis and tumour growth. Br J Cancer. 2011;105(7):1002–11.

147. Guilmain W, Colin S, Legrand E, Vannier JP, Steverlynck C, Bongaerts M, et al. CD9P-1 expression correlates with the metastatic status of lung cancer, and a truncated form of CD9P-1, GS-168AT2, inhibits in vivo tumour growth. Br J Cancer. 2011;104(3):496–504.

148. Karhemo PR, Ravela S, Laakso M, Ritamo I, Tatti O, Mäkinen S, et al. An optimized isolation of biotinylated cell surface proteins reveals novel players in cancer metastasis. J Proteomics [Internet]. 2012;77:87–100. Available from: http://dx.doi.org/10.1016/j.jprot.2012.07.009

149. Aguila B, Morris AB, Spina R, Bar E, Schraner J, Vinkler R, et al. The Ig superfamily protein PTGFRN coordinates survival signaling in Glioblastoma multiforme. Cancer Lett. 2019;462(April):33–42.

150. Beck A, Reichert JM. Antibody-drug conjugates present and future. MAbs. 2014;6(1):15–7.

151. Tang H, Liu Y, Yu Z, Sun M, Lin L, Liu W, et al. The Analysis of Key Factors Related to ADCs Structural Design. Front Pharmacol [Internet]. 2019 Apr 24;10:373. Available from: https://pubmed.ncbi.nlm.nih.gov/31068807

152. Edwards PAW. Some properties and applications of monoclonal antibodies. Biochem J. 1981;200(1):1–10.

153. Irani V, Guy AJ, Andrew D, Beeson JG, Ramsland PA, Richards JS. Molecular properties of human IgG subclasses and their implications for designing therapeutic monoclonal antibodies against infectious diseases. Mol Immunol [Internet]. 2015;67(2):171–82. Available from: http://dx.doi.org/10.1016/j.molimm.2015.03.255

154. Casali P, Schettino EW. Structure and Function of Natural Antibodies. Curr Top Microbiol Immunol. 1992;210:167-179-.

155. Padlan EA. Anatomy of the antibody molecule. Mol Immunol. 1994;31(3):169–217.

156. Hughes B. Antibody – drug conjugates for cancer : poised to deliver ? Nat Rev Drug Discov. 2010;9:665–7.

157. Herbener P, Schönfeld K, König M, Germer M, Przyborski JM, Bernöster K, et al. Functional relevance of in vivo half antibody exchange of an IgG4 therapeutic antibody-drug conjugate. PLoS One [Internet]. 2018 Apr 19;13(4):e0195823. Available from: https://doi.org/10.1371/journal.pone.0195823

158. Perez HL, Cardarelli PM, Deshpande S, Gangwar S, Schroeder GM, Vite GD, et al. Antibody–drug conjugates: current status and future directions. Drug Discov Today [Internet]. 2014;19(7):869–81. Available from: https://www.sciencedirect.com/science/article/pii/S135964461300398X

159. Sapra P, Shor B. Monoclonal antibody-based therapies in cancer: Advances and challenges. Pharmacol Ther [Internet]. 2013;138(3):452–69. Available from: https://www.sciencedirect.com/science/article/pii/S0163725813000739

160. Firan M, Bawdon R, Radu C, Ober RJ, Eaken D, Antohe F, et al. The MHC class I-related receptor, FcRn, plays an essential role in the maternofetal transfer of γ-globulin in humans. Int Immunol [Internet]. 2001 Aug 1;13(8):993–1002. Available from: https://doi.org/10.1093/intimm/13.8.993

161. Medesan C, Matesoi D, Radu C, Ghetie V, Ward ES. Delineation of the amino acid residues involved in transcytosis and catabolism of mouse IgG1. J Immunol [Internet]. 1997 Mar 1;158(5):2211–7. Available from: https://doi.org/10.4049/jimmunol.158.5.2211

162. Zheng K, Bantog C, Bayer R. The impact of glycosylation on monoclonal antibody conformation and stability. MAbs [Internet]. 2011/11/01. 2011;3(6):568–76. Available from: https://pubmed.ncbi.nlm.nih.gov/22123061

163. Sau S, Alsaab HO, Kashaw SK, Tatiparti K, Iyer AK. Advances in antibody – drug conjugates : A new era of targeted cancer therapy. Drug Discov Today [Internet]. 2017;22(10):1547–56. Available from: https://doi.org/10.1016/j.drudis.2017.05.011

164. Harding FA, Stickler MM, Razo J, DuBridge RB. The immunogenicity of humanized and fully human antibodies: Residual immunogenicity resides in the CDR regions. MAbs. 2010;2(3):256–65.

165. Ndoja S, Lima H. Monoclonal Antibodies. Current Developments in Biotechnology and Bioengineering: Human and Animal Health Applications. 2017. 71–95 p.

166. Gerber H-P, Senter PD, Grewa IS. Antibody drug-conjugates targeting the tumor vasculature. MAbs [Internet]. 2009;(June):247–53. Available from: www.landesbioscience.com

167. Singh AP, Sharma S, Shah DK. Quantitative characterization of in vitro bystander effect of antibody-drug conjugates. J Pharmacokinet Pharmacodyn [Internet]. 2016/09/26. 2016 Dec;43(6):567–82. Available from: https://pubmed.ncbi.nlm.nih.gov/27670282

168. Wynn C, Patel R, Hillegass WB, Tang S-C. Increased systemic toxicities from antibody-drug conjugates (ADCs) with cleavable versus non-cleavable linkers: A meta-analysis of commercially available ADCs. J Clin Oncol [Internet]. 2022 Jun 1;40(16_suppl):3032. Available from: https://doi.org/10.1200/JCO.2022.40.16_suppl.3032

169. Diamantis N, Banerji U. Antibody-drug conjugates - An emerging class of cancer treatment. Br J Cancer [Internet]. 2016;114(4):362–7. Available from:

http://dx.doi.org/10.1038/bjc.2015.435

170. Tan G, Peng Z, Lu J, Tang F. Cathepsins mediate tumor metastasis. World J Biol Chem. 2013;4(4):91–102.

171. Renoux B, Legigan T, Bensalma S, Chadéneau C, Muller J-M, Papot S. A new cyclopamine glucuronide prodrug with improved kinetics of drug release. Org Biomol Chem. 2011;9(24):8459–64.

172. Jeffrey SC, Andreyka JB, Bernhardt SX, Kissler KM, Kline T, Lenox JS, et al. Development and properties of β-glucuronide linkers for monoclonal antibody− drug conjugates. Bioconjug Chem. 2006;17(3):831–40.

173. Ha SYY, Anami Y, Yamazaki CM, Xiong W, Haase CM, Olson SD, et al. An Enzymatically Cleavable Tripeptide Linker for Maximizing the Therapeutic Index of Antibody – Drug Conjugates. Mol Cancer Ther. 2022;21(9):1449–61.

174. Kobayashi H, Griffiths GL, Choyke PL. Near-Infrared Photoimmunotherapy: Photoactivatable Antibody-Drug Conjugates (ADCs). Bioconjug Chem. 2020;31(1):28–36.

175. Jain N, Smith SW, Ghone S, Tomczuk B. Current ADC Linker Chemistry. Pharm Res. 2015;32(11):3526–40.

176. Behrens CR, Ha EH, Chinn LL, Bowers S, Probst G, Fitch-Bruhns M, et al. Antibody-Drug Conjugates (ADCs) Derived from Interchain Cysteine Cross-Linking Demonstrate Improved Homogeneity and Other Pharmacological Properties over Conventional Heterogeneous ADCs. Mol Pharm. 2015;12(11):3986–98.

177. Ohri R, Bhakta S, Fourie-O'Donohue A, Dela Cruz-Chuh J, Tsai SP, Cook R, et al. High-Throughput Cysteine Scanning to Identify Stable Antibody Conjugation Sites for Maleimide- and Disulfide-Based Linkers. Bioconjug Chem. 2018;29(2):473–85.

178. Yoder NC, Bai C, Tavares D, Widdison WC, Whiteman KR, Wilhelm A, et al. A case study comparing heterogeneous lysine- And site-specific cysteine-conjugated maytansinoid antibody-drug conjugates (ADCs) Illustrates the Benefits of Lysine Conjugation. Mol Pharm. 2019;16(9):3926–37.

179. Shefet-Carasso L, Benhar I. Antibody-targeted drugs and drug resistance - Challenges and solutions. Drug Resist Updat [Internet]. 2015;18:36–46. Available from: http://dx.doi.org/10.1016/j.drup.2014.11.001

180. Teicher BA, Chari RVJ. Antibody conjugate therapeutics: Challenges and potential. Clin Cancer Res. 2011;17(20):6389–97.

181. Rocha DD, Balgi A, Maia AI V., Pessoa OD, Silveira ER, Costa-Lotufo L V., et al. Cell cycle arrest through inhibition of tubulin polymerization by withaphysalin F, a bioactive compound isolated from Acnistus arborescens. Invest New Drugs. 2012;30(3):959–66.

182. Pahl A, Lutz C, Hechler T. Amanitins and their development as a payload for antibody-drug conjugates. Drug Discov Today Technol [Internet]. 2018;30:85–9. Available from:

https://www.sciencedirect.com/science/article/pii/S1740674918300350

183. Piha-Paul S, Simon G, Belani CP, Chao H, Gaspar K, Lee B, et al. A Phase 1, Open-Label, Dose-Escalation Study of L-DOS47 in Combination With Pemetrexed Plus Carboplatin in Patients With Stage IV Recurrent or Metastatic Nonsquamous NSCLC. JTO Clin Res reports [Internet]. 2022 Sep 16;3(11):100408. Available from: https://pubmed.ncbi.nlm.nih.gov/36268537

184. Molinolo A, Miller LS, Colcher D, Molinolo A, Siler K. Therapeutic Advantage of High-Affinity Anticarcinoma Radioimmunoconjugates. Cancer Res. 1992;52(5):1067–72.

185. Lakes AL, An DD, Gauny SS, Ansoborlo C, Liang BH, Rees JA, et al. Evaluating 225Ac and 177Lu radioimmunoconjugates against antibody-drug conjugates for small-cell lung cancer. Mol Pharm. 2020;17(11):4270–9.

186. Mellman I, Plutner H, Ukkonen P. Internalization and rapid recycling of macrophage Fc receptors tagged with monovalent antireceptor antibody: possible role of a prelysosomal compartment. J Cell Biol [Internet]. 1984 Apr 1;98(4):1163–9. Available from: https://doi.org/10.1083/jcb.98.4.1163

187. Kalim M, Chen J, Wang S, Lin C, Ullah S, Liang K, et al. Intracellular trafficking of new anticancer therapeutics: antibody-drug conjugates. Drug Des Devel Ther [Internet]. 2017 Aug 2;11:2265–76. Available from: https://pubmed.ncbi.nlm.nih.gov/28814834

188. Pettinato MC. Introduction to Antibody-Drug Conjugates. Antibodies (Basel, Switzerland) [Internet]. 2021 Oct 27;10(4):42. Available from: https://pubmed.ncbi.nlm.nih.gov/34842621

189. Kohler G, Milstein C. Continuous cultures of fused cells secreting antibody of predefined. Nature. 1975;256(5517):495–7.

190. Sievers EL, Larson RA, Stadtmauer EA, Estey E, Löwenberg B, Dombret H, et al. Efficacy and Safety of Gemtuzumab Ozogamicin in Patients With CD33-Positive Acute Myeloid Leukemia in First Relapse. J Clin Oncol [Internet]. 2001 Jul 1;19(13):3244–54. Available from: https://doi.org/10.1200/JCO.2001.19.13.3244

191. Petersdorf SH, Kopecky KJ, Slovak M, Willman C, Nevill T, Brandwein J, et al. A phase 3 study of gemtuzumab ozogamicin during induction and postconsolidation therapy in younger patients with acute myeloid leukemia. Blood [Internet]. 2013/04/16. 2013 Jun 13;121(24):4854–60. Available from: https://pubmed.ncbi.nlm.nih.gov/23591789

192. Norsworthy KJ, Ko C-W, Lee JE, Liu J, John CS, Przepiorka D, et al. FDA Approval Summary: Mylotarg for Treatment of Patients with Relapsed or Refractory CD33-Positive Acute Myeloid Leukemia. Oncologist [Internet]. 2018/04/12. 2018 Sep;23(9):1103–8. Available from: https://pubmed.ncbi.nlm.nih.gov/29650683

193. Senter PD, Sievers EL. The discovery and development of brentuximab vedotin for use in relapsed Hodgkin lymphoma and systemic anaplastic large cell lymphoma. Nat Biotechnol [Internet]. 2012;30(7):631–7. Available from:

https://doi.org/10.1038/nbt.2289

194. Krop I, Winer EP. Trastuzumab emtansine: A novel antibody-drug conjugate for HER2-positive breast cancer. Clin Cancer Res. 2014;20(1):15–20.

195. Shepard HM, Jin P, Slamon DJ, Pirot Z, Maneval DC. Herceptin. In: Chernajovsky Y, Nissim A, editors. Therapeutic Antibodies [Internet]. Berlin, Heidelberg: Springer Berlin Heidelberg; 2008. p. 183–219. Available from: https://doi.org/10.1007/978-3-540-73259-4_9

196. Yurkiewicz IR, Muffly L, Liedtke M. Inotuzumab ozogamicin: a CD22 mAb-drug conjugate for adult relapsed or refractory B-cell precursor acute lymphoblastic leukemia. Drug Des Devel Ther [Internet]. 2018 Jul 24;12:2293–300. Available from: https://pubmed.ncbi.nlm.nih.gov/30087554

197. Kreitman RJ, Pastan I. Antibody fusion proteins: anti-CD22 recombinant immunotoxin moxetumomab pasudotox. Clin Cancer Res [Internet]. 2011 Oct 15;17(20):6398–405. Available from: https://pubmed.ncbi.nlm.nih.gov/22003067

198. Camus V, Tilly H. Polatuzumab vedotin, an anti-CD79b antibody–drug conjugate for the treatment of relapsed/refractory diffuse large B-cell lymphoma. Futur Oncol [Internet]. 2020 Sep 21;17(2):127–35. Available from: https://doi.org/10.2217/fon-2020-0675

199. Halford Z, Anderson MK, Clark MD. Enfortumab Vedotin-ejfv: A First-in-Class Anti–Nectin-4 Antibody-Drug Conjugate for the Management of Urothelial Carcinoma. Ann Pharmacother [Internet]. 2020 Sep 18;55(6):772–82. Available from: https://doi.org/10.1177/1060028020960402

200. Ogitani Y, Aida T, Hagihara K, Yamaguchi J, Ishii C, Harada N, et al. DS-8201a, A Novel HER2-Targeting ADC with a Novel DNA Topoisomerase I Inhibitor, Demonstrates a Promising Antitumor Efficacy with Differentiation from T-DM1. Clin Cancer Res [Internet]. 2016 Oct 13;22(20):5097–108. Available from: https://doi.org/10.1158/1078-0432.CCR-15-2822

201. Bardia A, Mayer IA, Vahdat LT, Tolaney SM, Isakoff SJ, Diamond JR, et al. Sacituzumab govitecan-hziy in refractory metastatic triple-negative breast cancer. N Engl J Med. 2019;380(8):741–51.

202. Lonial S, Lee HC, Badros A, Trudel S, Nooka AK, Chari A, et al. Belantamab mafodotin for relapsed or refractory multiple myeloma (DREAMM-2): a two-arm, randomised, open-label, phase 2 study. Lancet Oncol [Internet]. 2020 Feb 1;21(2):207–21. Available from: https://doi.org/10.1016/S1470-2045(19)30788-0

203. Weisel K, Hopkins TG, Fecteau D, Bao W, Quigley C, Jewell RC, et al. Dreamm-3: A Phase 3, Open-Label, Randomized Study to Evaluate the Efficacy and Safety of Belantamab Mafodotin (GSK2857916) Monotherapy Compared with Pomalidomide Plus Low-Dose Dexamethasone (Pom/Dex) in Participants with Relapsed/Refractory Multiple Myelo. Blood [Internet]. 2019 Nov 13;134(Supplement_1):1900. Available from: https://doi.org/10.1182/blood-2019-129893

204. Hamadani M, Linhares Y, Gandhi MD, Chung M, Adamis H, Ungar D, et al.

PB2118: PHASE 3 RANDOMIZED STUDY OF LONCASTUXIMAB TESIRINE IN COMBINATION WITH RITUXIMAB (LONCA-R) VERSUS IMMUNOCHEMOTHERAPY IN PATIENTS WITH R/R DLBCL (LOTIS-5). HemaSphere [Internet]. 2022 Jun 23;6(Suppl):1989–90. Available from: https://www.ncbi.nlm.nih.gov/pmc/articles/PMC9431578/

205. Heitz N, Greer SC, Halford Z. A Review of Tisotumab Vedotin-tftv in Recurrent or Metastatic Cervical Cancer. Ann Pharmacother [Internet]. 2022 Aug 12;10600280221118370. Available from: https://doi.org/10.1177/10600280221118370

206. O'Malley DM, Matulonis UA, Birrer MJ, Castro CM, Gilbert L, Vergote I, et al. Phase Ib study of mirvetuximab soravtansine, a folate receptor alpha (FRα)-targeting antibody-drug conjugate (ADC), in combination with bevacizumab in patients with platinum-resistant ovarian cancer. Gynecol Oncol. 2020;157(2):379–85.

207. Weldemariam MM, Sudhir P-R, Woo J, Zhang Q. Effects of multiple stressors on pancreatic human islets proteome reveal new insights into the pathways involved. Proteomics [Internet]. 2023 Jul 24;n/a(n/a):2300022. Available from: https://doi.org/10.1002/pmic.202300022

208. Palomba A, Abbondio M, Fiorito G, Uzzau S, Pagnozzi D, Tanca A. Comparative Evaluation of MaxQuant and Proteome Discoverer MS1-Based Protein Quantification Tools. J Proteome Res [Internet]. 2021/05/26. 2021 Jul 2;20(7):3497–507. Available from: https://pubmed.ncbi.nlm.nih.gov/34038140

209. Tyanova S, Temu T, Sinitcyn P, Carlson A, Hein MY, Geiger T, et al. The Perseus computational platform for comprehensive analysis of (prote)omics data. Nat Methods [Internet]. 2016;13(9):731–40. Available from: https://doi.org/10.1038/nmeth.3901

210. Zhou Y, Zhou B, Pache L, Chang M, Khodabakhshi AH, Tanaseichuk O, et al. Metascape provides a biologist-oriented resource for the analysis of systems-level datasets. Nat Commun [Internet]. 2019;10(1):1523. Available from: https://doi.org/10.1038/s41467-019-09234-6

211. Gheytanchi E, Naseri M, Karimi-Busheri F, Atyabi F, Mirsharif ES, Bozorgmehr M, et al. Morphological and molecular characteristics of spheroid formation in HT-29 and Caco-2 colorectal cancer cell lines. Cancer Cell Int [Internet]. 2021;21(1):204. Available from: https://doi.org/10.1186/s12935-021-01898-9

212. Lin R, Chou LF, Chien C-CM, Chang H-Y. Dynamic analysis of hepatoma spheroid formation: roles of E-cadherin and β 1-integrin. Cell Tissue Res. 2006;324:411–22.

213. Das CK, Banerjee I, Mandal M. Pro-survival autophagy: An emerging candidate of tumor progression through maintaining hallmarks of cancer. Semin Cancer Biol [Internet]. 2020;66:59–74. Available from: https://www.sciencedirect.com/science/article/pii/S1044579X19300203

214. Mala U, Baral TK, Somasundaram K. Integrative analysis of cell adhesion molecules in glioblastoma identified prostaglandin F2 receptor inhibitor

(PTGFRN) as an essential gene. BMC Cancer [Internet]. 2022;22(1):1–12. Available from: https://doi.org/10.1186/s12885-022-09682-2

215. Lazareth H, Henique C, Lenoir O, Puelles VG, Flamant M, Bollée G, et al. The tetraspanin CD9 controls migration and proliferation of parietal epithelial cells and glomerular disease progression. Nat Commun [Internet]. 2019;10(3303). Available from: http://dx.doi.org/10.1038/s41467-019-11013-2

216. Zöller M. Tetraspanins : push and pull in suppressing and promoting metastasis. Nat Rev. 2009;9:45–50.

217. Chambrion C, le Naour F. The tetraspanins CD9 and CD81 regulate CD9P1-induced effects on cell migration. PLoS One. 2010;5(6).

218. Alt-Holland A, Shamis Y, Riley KN, DesRochers TM, Fusenig NE, Herman IM, et al. E-cadherin suppression directs cytoskeletal rearrangement and intraepithelial tumor cell migration in 3D human skin equivalents. J Invest Dermatol [Internet]. 2008;128(10):2498–507. Available from: http://dx.doi.org/10.1038/jid.2008.102

219. Elisha Y, Kalchenko V, Kuznetsov Y, Geiger B. Dual role of E-cadherin in the regulation of invasive collective migration of mammary carcinoma cells. Sci Rep [Internet]. 2018;8(1):1–15. Available from: http://dx.doi.org/10.1038/s41598-018-22940-3

220. Fiebig H., Maier A, Burger A. Clonogenic assay with established human tumour xenografts. Vol. 40, European Journal of Cancer. 2004. p. 802–20.

221. Brix N, Samaga D, Belka C, Lauber K, Zitzelsberger H. Analysis of clonogenic growth in vitro. Nat Protoc. 2021;16:4963–91.

222. Zhang W, Xu Z, Hao X, He T, Li J, Shen Y, et al. Bone Metastasis Initiation Is Coupled with Bone Remodeling through Osteogenic Differentiation of NG2 + Cells. Cancer Discov. 2023;13:1–22.

223. Yang Y, Chen C, Zuo Q, Lu H, Salman S, Lyu Y, et al. NARF is a hypoxia-induced coactivator for OCT4- mediated breast cancer stem cell specification. Sci Adv. 2022;8(49):1–14.

224. Toledo-Guzmán ME, Hernández MI, Gómez-Gallegos ÁA, Ortiz-Sánchez E. ALDH as a Stem Cell Marker in Solid Tumors. Curr Stem Cell Res Ther. 2018;14(5):375–88.

225. Rozenberg JM, Filkov GI, Tro A V, Karpulevich EA, Parshin VD, Royuk V V, et al. Biomedical Applications of Non- Small Cell Lung Cancer Spheroids. Front Oncol. 2021;11:1–13.

226. Lazova R, Camp RL, Klump V, Siddiqui SF, Amaravadi RK, Pawelek JM. Punctate LC3B Expression Is a Common Feature of Solid Tumors and Associated with Proliferation , Metastasis , and Poor Outcome. Hum Cancer Biol. 2012;18(2):370–9.

227. Levine B, Kroemer G, Roussy IG. Autophagy in the Pathogenesis of Disease. Cell. 2008;132(1):27–42.

228. Mizushima N. The role of the Atg1 / ULK1 complex in autophagy regulation. Cell

Biol [Internet]. 2010;22(2):132–9. Available from: http://dx.doi.org/10.1016/j.ceb.2009.12.004

229. Lin P, Chu M, Liu H. Autophagy and metabolism. Kaohsiung J Med Sci. 2020;37(1):12–9.

230. Yue Z, Jin S, Yang C, Levine AJ, Heintz N. Beclin 1 , an autophagy gene essential for early embryonic development , is a haploinsufficient tumor suppressor. Proc Natl Acad Sci U S A. 2003;100(25).

231. Qu X, Yu J, Bhagat G, Furuya N, Hibshoosh H, Troxel A, et al. Promotion of tumorigenesis by heterozygous disruption of the beclin 1 autophagy gene. J Clin Invest. 2003;112(12):1809–20.

232. Degenhardt K, Mathew R, Beaudoin B, Bray K, Anderson D, Chen G, et al. Autophagy promotes tumor cell survival and restricts necrosis , inflammation , and tumorigenesis. Cancer Cell. 2006;10:51–64.

233. Marsh T, Kenific CM, Suresh D, Woo K, Werb Z, Debnath J, et al. Autophagic Degradation of NBR1 Restricts Metastatic Outgrowth during Mammary Tumor Article Autophagic Degradation of NBR1 Restricts Metastatic Outgrowth during Mammary Tumor Progression. Dev Cell [Internet]. 2020;52(5):591-604.e6. Available from: https://doi.org/10.1016/j.devcel.2020.01.025

234. Zhou W, Liu W, Zhou D, Li A. ITGB1 Suppresses Autophagy Through Inhibiting The mTORC2/AKT Signaling Pathway In H9C2 Cells. Pharmazie. 2022;77(5):137–40.

235. Barrow-McGee R, Kishi N, Joffre C, Ménard L, Hervieu A, Bakhouche BA, et al. Beta 1-integrin–c-Met cooperation reveals an inside-in survival signalling on autophagy-related endomembranes. Nat Commun [Internet]. 2016;7(1):11942. Available from: https://doi.org/10.1038/ncomms11942

236. Frisch SM, Screaton RA. Anoikis mechanisms. Curr Opin Cell Biol [Internet]. 2001;13(5):555–62. Available from: https://www.sciencedirect.com/science/article/pii/S0955067400002519

237. Vlahakis A, Debnath J. The Interconnections between Autophagy and Integrin-Mediated Cell Adhesion. J Mol Biol [Internet]. 2017;429(4):515–30. Available from: https://www.sciencedirect.com/science/article/pii/S0022283616305228

238. Damiano V, Spessotto P, Vanin G, Perin T, Maestro R, Santarosa M. The autophagy machinery contributes to E-cadherin turnover in breast cancer. Front cell Dev Biol. 2020;8:545.

239. Xu W, Chen B, Ke D, Chen X. TRIM29 mediates lung squamous cell carcinoma cell metastasis by regulating autophagic degradation of E-cadherin. Aging (Albany NY). 2020;12(13):13488.

240. Vera-Ramirez L. Cell-intrinsic survival signals. The role of autophagy in metastatic dissemination and tumor cell dormancy. In: Seminars in Cancer Biology. Elsevier; 2020. p. 28–40.

241. Ou Q, Ma N, Yu Z, Wang R, Hou Y, Wang Z, et al. Nudix hydrolase 1 is a prognostic biomarker in hepatocellular carcinoma. Aging (Albany NY) [Internet].

2020/04/27. 2020 Apr 27;12(8):7363–79. Available from: https://pubmed.ncbi.nlm.nih.gov/32341205

242. Miao F, Chu K, Chen H, Zhang M, Shi P, Bai J, et al. Increased DKC1 expression in glioma and its significance in tumor cell proliferation, migration and invasion. Invest New Drugs [Internet]. 2019;37(6):1177–86. Available from: https://doi.org/10.1007/s10637-019-00748-w

243. Yu N, Zhang P, Wang L, He X, Yang S, Lu H. RBBP7 is a prognostic biomarker in patients with esophageal squamous cell carcinoma. Oncol Lett [Internet]. 2018/10/03. 2018 Dec;16(6):7204–11. Available from: https://pubmed.ncbi.nlm.nih.gov/30546458

244. Zhang X, Fu L, Xue D, Zhang X, Hao F, Xie L, et al. Overexpression of Rsf-1 correlates with poor survival and promotes invasion in non-small cell lung cancer. Virchows Arch [Internet]. 2017;470(5):553–60. Available from: https://doi.org/10.1007/s00428-017-2102-6

245. Li D, Xing Y, Tian T, Guo Y, Qian J. Overexpression of LRRC59 Is Associated with Poor Prognosis and Promotes Cell Proliferation and Invasion in Lung Adenocarcinoma. Onco Targets Ther [Internet]. 2020 Jul 3;13:6453–63. Available from: https://pubmed.ncbi.nlm.nih.gov/32753886

246. Peng L, Xiong Y, Wang R, Xiang L, Zhou H, Fu Z. The critical role of peroxiredoxin-2 in colon cancer stem cells. Aging (Albany NY) [Internet]. 2021/03/26. 2021 Mar 26;13(8):11170–87. Available from: https://pubmed.ncbi.nlm.nih.gov/33819194

247. Kanwar SS, Yu Y, Nautiyal J, Patel BB, Majumdar APN. The Wnt/beta-catenin pathway regulates growth and maintenance of colonospheres. Mol Cancer [Internet]. 2010 Aug 6;9:212. Available from: https://pubmed.ncbi.nlm.nih.gov/20691072

248. Mizuta K, Matsubara T, Goto A, Addison WN, Nakatomi M, Matsuo K, et al. Plectin promotes tumor formation by B16 mouse melanoma cells via regulation of Rous sarcoma oncogene activity. BMC Cancer [Internet]. 2022;22(1):936. Available from: https://doi.org/10.1186/s12885-022-10033-4

249. Khobrekar N V, Quintremil S, Dantas TJ, Vallee RB. The Dynein Adaptor RILP Controls Neuronal Autophagosome Biogenesis, Transport, and Clearance. Dev Cell [Internet]. 2020/04/09. 2020 Apr 20;53(2):141-153.e4. Available from: https://pubmed.ncbi.nlm.nih.gov/32275887

250. Pan X, Chen Y, Shen Y, Tantai J. Knockdown of TRIM65 inhibits autophagy and cisplatin resistance in A549/DDP cells by regulating miR-138-5p/ATG7. Cell Death Dis [Internet]. 2019 Jun 3;10(6):429. Available from: https://pubmed.ncbi.nlm.nih.gov/31160576

251. Reid DW, Nicchitta C V. Primary role for endoplasmic reticulum-bound ribosomes in cellular translation identified by ribosome profiling. J Biol Chem [Internet]. 2011/12/23. 2012 Feb 17;287(8):5518–27. Available from: https://pubmed.ncbi.nlm.nih.gov/22199352

252. Kuroda K, Liu H, Kim S, Guo M, Navarro V, Bander NH. SaporinToxin-conjugated monoclonal antibody targeting prostate-specific membrane antigen has potent anticancer activity. Prostate. 2010;70(12):1286–94.

253. Flavell D. Saporin Immunotoxins. Curr Top Microbiol Immunol. 1998;234:57–61.

254. Hanka LJ, Dietz A, Gerphiede SA, Kuentzel SL, Martin DG. CC-1065 (NSC-298223), a new antitumor antibiotic. Production, in vitro biological activity, microbiological assays and taxonomy of the producing microorganism. J Antibiot (Tokyo). 1978;31(12):1211–7.

255. Jukes Z, Morais GR, Loadman PM, Pors K. How can the potential of the duocarmycins be unlocked for cancer therapy? Drug Discov Today [Internet]. 2021;26(2):577–84. Available from: https://www.sciencedirect.com/science/article/pii/S1359644620304852

256. Patil CP, Satam V, Lee M. A Short Review on the Synthetic Strategies of Duocarmycin Analogs that are Powerful DNA Alkylating Agents [Internet]. Vol. 15, Anti-Cancer Agents in Medicinal Chemistry. 2015. p. 616–30. Available from: http://www.eurekaselect.com/article/64019

257. Kim S, Kim H, Jo DH, Kim JH, Kim SR, Kang D, et al. Bispecific anti-mPDGFRβ x cotinine scFv-Cκ-scFv fusion protein and cotinine-duocarmycin can form antibody-drug conjugate-like complexes that exert cytotoxicity against mPDGFRβ expressing cells. Methods [Internet]. 2019;154:125–35. Available from: https://www.sciencedirect.com/science/article/pii/S1046202318301610

258. Takauchi A, Kobayashi T, Tahara T, Nakazawa K, Hayakawa M, Shibata Y, et al. The Trans-Chromosomic Mouse-Derived Human Monoclonal Antibody Promotes Phagocytosis of Porphyromonas gingivalis by Neutrophils. J Periodontol [Internet]. 2005 May 1;76(5):680–5. Available from: https://doi.org/10.1902/jop.2005.76.5.680

259. Baah S, Laws M, Rahman KM. Antibody–drug conjugates—a tutorial review. Molecules. 2021;26(10).

260. Marquez J, Dong J, Dong C, Tian C. Identification of Prostaglandin F2 Receptor Negative Regulator (PTGFRN) as an internalizable target in cancer cells for antibody-drug conjugate development. PLoS One [Internet]. 2021;1–18. Available from: http://dx.doi.org/10.1371/journal.pone.0246197

261. Ritchie M, Tchistiakova L, Scott N. Implications of receptor-mediated endocytosis and intracellular trafficking dynamics in the development of antibody drug conjugates. MAbs. 2013;5(1):13–21.

262. Durbin KR, Phipps C, Liao X. Mechanistic modeling of antibody–drug conjugate internalization at the cellular level reveals inefficient processing steps. Mol Cancer Ther. 2018;17(6):1341–51.

263. Chen HW, Lin MC, Wu PR, Chang YC, Weng SS, Tsai WC. Prostaglandin F2 receptor inhibitor overexpression predicts advanced who grades and adverse prognosis in human glioma tissue. Chin J Physiol. 2022;65(2):93–102.

264. Tsuruo T, Fidler IJ. Differences in Drug Sensitivity among Tumor Cells from

Parental Tumors, Selected Variants, and Spontaneous Metastases. Cancer Res. 1981;41(8):3058–64.

265. Yao HP, Zhao H, Hudson R, Tong XM, Wang MH. Duocarmycin-based antibody–drug conjugates as an emerging biotherapeutic entity for targeted cancer therapy: Pharmaceutical strategy and clinical progress. Vol. 26, Drug Discovery Today. 2021. p. 1857–74.

266. Patil PC, Satam V, Lee M. A Short Review on the Synthetic Strategies of Duocarmycin Analogs that are Powerful DNA Alkylating Agents. Anticancer Agents Med Chem. 2015;15(5):616–30.

267. Shen BQ, Xu K, Liu L, Raab H, Bhakta S, Kenrick M, et al. Conjugation site modulates the in vivo stability and therapeutic activity of antibody-drug conjugates. Nat Biotechnol. 2012;30(2):184–9.

268. Walsh SJ, Bargh JD, Dannheim FM, Hanby AR, Seki H, Counsell AJ, et al. Site-selective modification strategies in antibody-drug conjugates. Chem Soc Rev. 2021;50(2):1305–53.

269. Engelman JA, Jänne PA. Mechanisms of Acquired Resistance to Epidermal Growth Factor Receptor Tyrosine Kinase Inhibitors in Non–Small Cell Lung Cancer. Clin Cancer Res [Internet]. 2008 May 15;14(10):2895–9. Available from: https://doi.org/10.1158/1078-0432.CCR-07-2248

270. Turcotte S, Giaccia AJ. Targeting cancer cells through autophagy for anticancer therapy. Curr Opin Cell Biol [Internet]. 2010;22(2):246–51. Available from: https://www.sciencedirect.com/science/article/pii/S0955067409002361

271. Muenst S, Läubli H, Soysal SD, Zippelius A, Tzankov A, Hoeller S. The immune system and cancer evasion strategies: Therapeutic concepts. J Intern Med. 2016;279(6):541–62.

272. Wee P, Wang Z. Epidermal Growth Factor Receptor Cell Proliferation Signaling Pathways. Vol. 9, Cancers. 2017.

273. Duffy MJ, McGowan PM, Gallagher WM. Cancer invasion and metastasis: Changing views. J Pathol. 2008;214(3):283–93.